SAPIENZA
UNIVERSITÀ DI ROMA

FACULTY OF PHARMACY AND MEDICINE

Ph.D. Thesis in Pharmaceutical Sciences

XXXV Cycle

Innovative strategies for the development of biopolymer-based materials with suitable properties for biomedical and pharmaceutical applications

Ph.D. student

Dott.ssa Chiara Brandelli

Tutor

Prof.ssa Patrizia Paolicelli

Academic year 2021-2022

TABLE OF CONTENTS

INTRODUCTION

Since ancient times, human beings had always used exogenous materials to facilitate wound healing and try to restore damaged tissues and organs [1]. For example, it is known that Egyptians employed linen threads to suture wounds, while Aztecs implanted resinous woods into the medullary canal of long bones, practicing a kind of "osteosynthesis". At that time, there was no knowledge of the problems and limitations related to the implantation of exogenous materials inside the body, which showed, however, an impressive ability to adapt itself to foreign materials, ensuring the success of these original surgical procedures. The subsequent study of the interactions between implanted materials and living tissues, as well as the increased knowledge of inflammatory and immunogenic responses, has allowed to introduce the concept of biomaterials and to investigate their potential applications in the biomedical and pharmaceutical field [1,2].

Biomaterials can be broadly defined as materials designed to interface with biological systems without causing any toxic reaction, and this ability to come into close contact with human body tissues without inducing an undesirable degree of response represents the single most crucial aspect that distinguishes a biomaterial from any other material [3,4]. Based on the above, biocompatibility can be considered the most relevant hallmark of biomaterials. However, it is important to underline that the concept of biocompatibility should not be limited only to the biological safety of the material and its degradation products, since it also includes the ability of materials to correctly carry out their intended function when in contact with (or inserted into) the biological environment [1].

In recent years, biomaterials field has grown consistently, becoming an integral component in the modern-day improvement of human condition and quality of life [3]. A wide variety of biomaterials products are commercially available today, and many others are under investigation to meet new emerging clinical needs. Therefore, biomaterials field is constantly expanding and involve the synergistic integration of knowledge and ideas from different disciplines (e.g., chemistry, chemical engineering, materials science, mechanics, surface science, bioengineering, biology, medicine and so on), thus defining the multidisciplinary nature of this intricate field [1,3,4]. Referring to

the commercially available biomaterials products, biopolymer-based materials are found to cover a considerable portion of today's products, especially in the medical, agricultural and goods packaging sectors [3]. Biomedical and pharmaceutical applications have posed to draw remarkable attention for biopolymer materials utilization in comparison to other areas, due to the wide range of properties that they possess, which includes not only biocompatibility but also biodegradability, low toxicity, low cost, and ease of processability. They also exhibit a high degree of versatility, which is demonstrated by the possibility to produce them in a wide range of shapes with various properties, making them suitable for a variety of applications, as well as the ability to modulate and modify their mechanical, chemical, and physical properties depending on the application they are intended for. Among the numerous biopolymer-based materials developed over the years, polymer thin films and hydrogels have distinguished themselves as outstanding candidates for biomedical and pharmaceutical applications, thanks to their countless features that make them suitable as drug delivery systems, innovative dressings for wound healing, and scaffolds for cell growth and proliferation. However, despite the advantages usually associated with their use in the above-mentioned areas, thin films and hydrogels are still suffering from significant drawbacks that prevent their effective application. In light of this, the aim of this research work was to investigate some of the key issues found in the development of these polymer matrices and to suggest alternative and innovative strategies that could be used to increase their usefulness in the fields under consideration. In the specific, the work is structured into two sections, one of which is dedicated to polymer thin films employed as formulations for oral drug delivery and wound healing, while the other one is focused on hydrogels and their use as scaffolds for tissue engineering. It is important to underline that the development of the matrices provided for the use of natural biopolymers (polysaccharides and proteins) and their semi-synthetic derivatives, obtained through the chemical modification of natural polymers backbone. This choice is due to the advantages related to such polymers, which certainly include biocompatibility, biodegradability and non-toxicity, as well as inherent bioactivity which ensures the perfect integration of films and hydrogels with the surrounding living tissues, limiting the occurrence of inflammatory and immunogenic reactions.

~SECTION I~

POLYMER THIN FILMS AS ORAL DRUG DELIVERY SYSTEMS AND WOUND DRESSINGS

Films are generally defined as thin flexible layer containing one or more polymers with or without a plasticizer [5], which usually help to increase the flexibility and the mechanical strength of the polymer matrices, thus reducing their friability [6].

Polymer thin films are gaining an ever-growing popularity in the biomedical and pharmaceutical field, due to their unique properties that make them suitable for a wide range of applications, among which drug delivery and wound healing stand out for importance.

Polymer thin films meet many requirements for being used efficiently as drug delivery systems [7]. They allow to target sensitive site that may not be possible with other dosage forms [8] and show the capabilities to improve the bioavailability of drugs, also reducing their side effects and the administration frequency, thus increasing the patient's compliance and the adherence to the therapeutic treatment [7,9]. Several efforts have been made to formulate polymer thin films usually administered via buccal, sublingual, ocular and skin routes [10,11]. In this scenario, oral thin films (OTFs) have drawn remarkable interest as platforms for the delivery of bioactive molecules [12], being considered a convenient alternative to the conventional oral dosage forms for the treatment of both local and systemic diseases also in pediatric or geriatric patients, for which the assumption of conventional drug formulations would not result in a positive outcome [13].

The flexible nature of thin films which enables an easy conformation to different anatomic regions, their ability to absorb exudates and provide a protective physical barrier, as well as the ease of application and removal are just some of the advantages that make polymer films also attractive materials for the development of dressings to promote the healing of wounds and burns [14].

1.1 Manufacturing methods of thin films

Manufacturing processes usually involved in the production of thin films include solvent and semi-solid casting, hot melt extrusion, solid dispersion extrusion and rolling [15]. However, an innovative technique like 3D printing has evolved in the past few years [16]. Here, an overview of these manufacturing methods is presented.

Solvent and semi-solid casting. Based on the literature, solvent casting technique is surely the most explored and frequently used for manufacturing polymer thin films. This is mainly due to the effortless steps involved in the process and the inexpensive system setup that incurs at the research on a laboratory scale. [17-19]. The whole procedure for the development of thin films by using solvent casting can be summarized as shown in Figure 1, where the quality control parameters characteristic of each step is also reported [9].

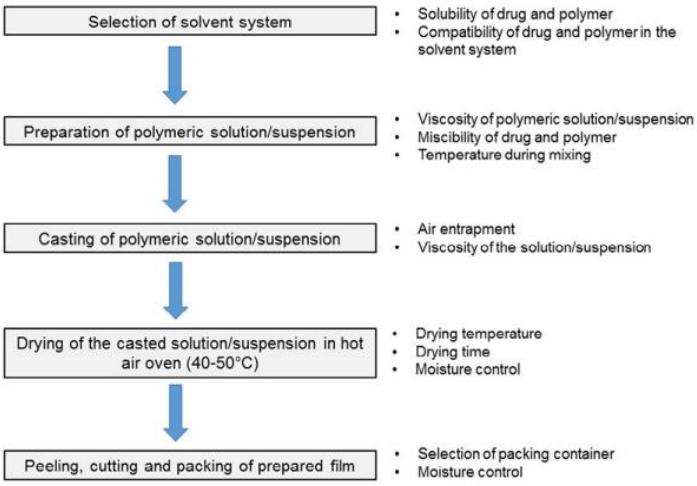

Figure 1. Solvent casting method for film preparation along with quality control parameters of each step [9].

The first step implies the preparation of the starting polymeric solution or suspension by mixing the film-forming components, such as polymer, plasticizers, filling materials, and active pharmaceutical ingredients (APIs) in a suitable solvent or solvents system [16,20]. The choice of the solvent is essentially based on the nature of the film-forming components. However, as it should be easily removed during the drying phase, the selected solvent should be volatile as well as compatible with the materials used for the film production [21]. One of the most critical aspects of this preliminary phase is

represented by the possible entrapment of air bubbles into the polymeric mixture, which leads to the production of uneven film. Therefore, deaeration is essential to obtain a homogeneous product with uniform thickness. The starting solution/suspension is subjected to continuous mixing by magnetic stirring, to keep the viscosity and concentration unchanged. To promote the complete dissolution of the various film-forming components, heating is often required [20]. However, temperature conditions should be finely controlled to achieve the desired viscosity of the material, which is of fundamental importance when polymer films are prepared by using solvent casting. In fact, inadequate viscosity and viscoelasticity of the starting polymer mixture may affect the final outcome, impacting on the casting and spreadability of the material in the selected support, thus leading to barely uniform and homogenous film. Therefore, the rheological properties of the mixture should be considered and evaluated, as they also affect the drying rate, films' thickness, and morphology as well as their content uniformity [22]. Once the solution is prepared, the casting process is performed. Thus, the polymer mixture is casted into suitable supports, and subsequently dried at room temperature or in hot air oven (40°C-50°C) to allow solvent evaporation. Then, the obtained film is carefully separated from the support and cut into pieces of the desired shape and size before being packed [6]. The packaging of films is also particularly important: it should be robust enough to give mechanical protection to the final product and should act as a moisture barrier to ensure the stability of the film while maintaining its properties unchanged during the storage [20]. Several advantages such as better physical properties, easy and low-cost processing, and excellent thickness uniformity are observed with the film prepared by solvent casting [23,24]. Moreover, unlike hot melt extrusion, high temperatures are not required, neither for the preparation of the starting mixture nor for the drying of the casted solution, thus preserving the integrity of the film-forming components during the film production. For this reason, it is the technique of choice when thermolabile drugs are present in the formulation. Despite the just mentioned advantages, this manufacturing process suffers from some limitations. For example, films prepared by solvent casting method generally become brittle during storage, as evidenced by the decrease in percent elongation due to evaporation or loss of the residual solvent over time [25]. Furthermore, a significative challenge is encountered when the formulation is scaled up from the bench scale to the production scale, where

the optimization of various parameters such as casting speed, drying time, and final thickness of the dried strip can severely affect the quality of the final product [9,20].

In the semi-solid casting, a homogenous viscous solution is firstly prepared by mixing a solution of water-soluble film-forming polymer with a solution of an acid insoluble polymer (e.g., cellulose acetate phthalate and cellulose acetate butyrate). Then, the gel mass is casted into films. The ratio of the acid insoluble polymer to film-forming polymer should be 1:4 [26-28].

Hot-Melt Extrusion (HME). Hot-melt extrusion is generally adopted for the manufacture of granules, tablets and pellets [29], but it can be considered a substitute to solvent casting technique for the preparation of thin films [25,30-32]. To this end, appropriate amounts of polymer, plasticizer, drug and additives are mixed into powders or granules blend without using any solvent. Then, the solid mass is melted and forced through an orifice (the die) under controlled temperature and pressure to obtain homogeneous matrices [5,33,34]. Several advantages are offered by HME, including increased solubility and bioavailability of water-insoluble compounds and better content uniformity of the final product [5,25]. Furthermore, the absence of solvent leads to the production of denser formulations, allowing the development of sustained release dosage form without the need of insoluble polymers [19]. However, the thermal process to which the film-forming components are subjected strongly limits the use of HME. The high temperatures can cause the degradation of heat sensitive APIs, which can also undergo a subsequent recrystallization when the temperature drop, thus affecting the stability of the formulations over time [9]. The equipment for HME process is shown in Figure 2 [35].

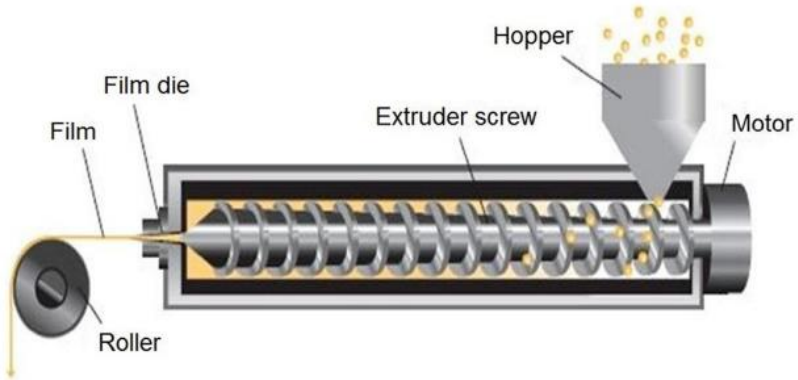

Figure 2. Hot melt extrusion system [35].

Solid dispersion extrusion. A solid dispersion is firstly prepared by extruding immiscible components with drug and then shaped into films by means of dies [36,37].

Rolling method. By means of high shear processor, active agent and other ingredients are dissolved in small portion of aqueous solvent. Water soluble hydrocolloids are dissolved in water to form homogenous viscous solution. Then, the resulting solution or suspension is rolled on a carrier and dried. Finally, the obtained film is cut into the desired shapes and sizes [27,36,37].

3D printing. 3D printing could be employed for manufacturing polymer thin films. The main ideas in the use of this type of technology revolve around the fact that printing technologies would allow to develop and fabricate pharmaceuticals in a tailored manner to meet some of the envisaged personalization needs of patients. This means on-demand fabrication and custom-made medications. This approach could create platforms to support the realization of tailored treatments. This can benefit the individual patient and give solutions to the pharmaceutical industry and pharmacies to meet the future needs of making customized medicines optimally at point of care [38]. These technologies are gaining popularity for its high flexibility and cost-effectiveness. From the pharmaceutical industry point of view, printing technologies are commonly used for identifying or labeling the pharmaceutical dosage forms, thus optimizing the product to be readily identified and to prevent any counterfeit production. This approach has been recently used for the drug loading of pharmaceutical dosage forms. A combination of both inkjet and flexographic technologies has been practiced as well [38]. The inkjet printing is used for printing of API on a different substrate, and the flexographic printing is employed for coating the drug loaded substrate with a polymeric thin film [39]. All these techniques contribute to produce films with high homogeneous distribution and accurate dosage of the drug. Furthermore, when printing is combined with different film fabrication technologies, such as solvent casting and other deposition techniques, multifunctional structures can be created in a new way to permit further complexity and high level of sophistication. This approach creates a possibility to fabricate multilayer, multi-component and multi-compartment systems.

To summarize, printing a drug on dosage form is the latest breakthrough in film development and proved to be a powerful tool to manufacture dosage form with

excellent uniformity, unique speed-ability, and high stability [38]. Figure 3 shows a schematic representation of flexography technology for the preparation of thin films.

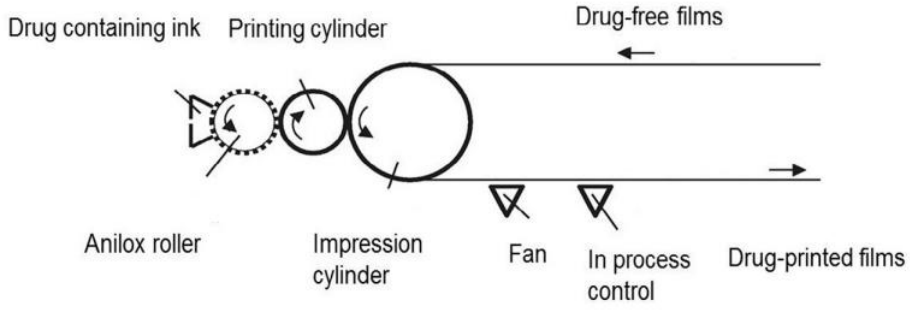

Figure 3. Schematic overview of flexography technology for the preparation of films [9].

1.2 Composition of thin films

The general composition of thin films can be summarized as shown in Table 1. However, it may vary depending on the type of application the film is designed for.

Table 1. General composition of OTFs

Ingredient	Amount (w/w)
Film-forming polymer	40-50%
API	5-30%
Plasticizer	0-20%
Coloring, flavoring and sweeting agents	Q.S

Regardless of the application, polymers represent the backbone of film formulations and should not be viewed as simple excipients since they are essential components of these matrices. They can be natural or synthetic and can be used alone or in combination with other polymers to achieve the desired film properties. Stiffness and other notable features of the final product strongly depend on the type and the amount of polymer present in the formulation [40]. However, since it represents the most essential and major component of these matrices, at least 45% w/w of polymer should generally be present based on the total weight of the dry films [41]. Polymer selection is one of the most crucial and important aspects affecting the successful preparation of thin films for oral drug delivery and wound healing. In general, film-forming polymers should be biocompatible, non-toxic and non-irritating to the surrounding tissues, and the absence

of impurities is also required. They should have good wettability and spreadability properties, as well as exhibit sufficient peel, shear and tensile strengths. Furthermore, they should be easily accessible and not very expensive [20,23,42]. Oral film-forming polymers should also have good shelf-life and should not cause secondary infections in the oral mucosa or dental regions. Even more, it would be ideal to have polymers with a local enzymatic inhibiting action along with penetration enhancing properties [23]. Naturally, polymer choice is directly dependent on the type of application the film is intended for. Given their importance in thin film preparation, polymers commonly used in the development of films as oral drug delivery systems and wound dressings will be discussed in greater detail in the following paragraphs, along with the criteria that guide the polymer selection for a specific application.

The polymer by itself is not usually sufficient for the development of thin films with suitable properties for pharmaceutical applications, thus calling for the inclusion of a plasticizer to the initial polymer mixture. The selection of plasticizer depends upon its compatibility with the polymer and the type of solvent employed in the casting of the film. In general, the plasticizer is a vital ingredient of thin films because it helps to improve the flow properties of the starting polymeric solution, which are fundamental for obtaining homogeneous matrices through the solvent casting technique, as well as the mechanical properties of the resulting films [20]. Typically, plasticizers are used in the concentration of 0–20% w/w of dry polymer weight. However, an inappropriate use can cause films to peel, split and crack. Additionally, it has been suggested that some plasticizers may have an impact on the absorption rate of drugs [43-46]. Among all the plasticizers, glycerol is one of the most commonly used mainly due to its biocompatibility and hydrophilic nature.

The therapeutic impact, especially of OTFs, depends on the loading of an active ingredient, which serves as the core component of the formulation. Anticancer, antiasthmatic, antitussives, antihistamine, antiepileptic, antianginal, antiemetic, cardiovascular, antiulcer, neuroleptic, analgesic, anxiolytic, antiallergic, hypnotic, sedative, antibacterial, anti-parkinsonism, anti-Alzheimer's, diuretics, expectorants, and erectile dysfunction drugs are the most suitable APIs for OTFs [6,28]. They are mainly potent drugs used at low dosage (less than 20 mg/day), small in size, with a moderate molecular weight, stable and soluble in the saliva and, at the same time, able to permeate

the oral mucosa [6,28]. These characteristics are required to make sure that the pharmaceuticals are well absorbed by passive diffusion, which is the main absorption mechanism through the oral mucosa. However, if the drug has poor permeability properties, its bioavailability can be increased by the addition of permeation enhancers, which effectiveness depends on the physicochemical properties of the drug, administration site, nature of the vehicle, and whether enhancer is used alone or in combination [47,48]. On the other hand, to promote the healing of wounds, film dressings usually required to be loaded with antimicrobial drugs, including organic or inorganic nano-sized materials able to prevent and eradicate infections while offering better control over the concentration and stability of the drug at the wound site [49]. In this regard, metal-based nanoparticles (NPs) demonstrated great effectiveness both as nano-biocides, due to their intrinsic and broad-spectrum antimicrobial activity, and as nano-carriers for the delivery of antimicrobial drugs [50,51]. Among all the investigated metal-based NPs, silver nanoparticles (AgNPs) have aroused great interest due to their excellent antimicrobial and antioxidant properties, promoting the development of Ag-nanocomposite films for the treatment of poorly healing and infected wounds [52].

1.2.1 Polymers for the preparation of thin films as oral drug delivery systems

Various polymers are available for the preparation of OTFs. A summary is shown in Table 2, where the general information and key findings of polymers commonly used in oral film formulation are also reported. A single polymer is not always sufficient to ensure films' suitable properties for oral administration of therapeutic agents. Many times, blends of different polymers are needed to improve the hydrophilicity, flexibility, mouthfeel and solubility of the final product [53-55]. The choice of polymers is of fundamental importance to modulate the disintegration rate of oral thin films. Orodispersible films should rapidly disintegrate and dissolve in the oral cavity, so film-forming polymers must be water-soluble [6]. On the other hand, if a sustained release of drugs is required, it is possible to intervene by varying the polymer molecular weight or by developing films with mucoadhesive properties. Mucoadhesive films are thin and flexible retentive dosage forms, which facilitate the extension of the residence time at the application site, thus leading to prolonged therapeutic effects [56]. Polymers implied in

the development of mucoadhesive films must be characterized by certain physicochemical properties, including hydrophilicity, large numbers of groups able to form hydrogen bonds, and sufficient chain mobility to allow diffusion through both mucus and epithelial tissue [57-61]. The ability of these films to absorb water from the mucosal surface in the dry state leads to a strong initial interaction. The subsequent wetting of mucoadhesive polymers allows the formation of a viscous fluid, which improves the duration of the adhesion to mucous surface and promotes the formation of further adhesive interactions, including mechanical and physical interactions (e.g. tangling of the flexible polymer and mucin chains), hydrogen bonds, hydrophobic interactions, van der Waals interactions, electrostatic interactions, covalent bonding, and recognition of specific ligands [57,59,61-63]. The development of mucoadhesive systems forming contacts with surfaces by van der Waals interactions and hydrogen bonds have aroused great interest among researchers. Although these forces are weak, quite strong adhesion can be achieved by formation of large numbers of interaction sites. Therefore, polymers with high molecular weight and high polar group contents (such as COOH, OH and NH_2) may be characterized by stronger mucoadhesion with a minimum of toxic effects [61]. According to adhesion theories, the mucoadhesive property of a polymer can be tailored by changing the parameters which has the capacity to alter the interaction between the polymer and the mucosal layer. Physiochemical properties of film-forming polymers as well as environmental and physiological factors play a key role in determining mucoadhesion, so they must be considered and finely evaluated for the development of films with proper mucoadhesive features. A focus on the theories proposed to explain the mucoadhesion mechanism and factors affecting oral thin films mucoadhesion will be presented below.

There are several polymers that are continuously being explored to develop these matrices for oral drug delivery. The innumerous types of polymers, the different polymer grades, and the several possible polymer-polymer blend ratios result in an exponential number of possible formulations and a wide range of final product characteristics. Therefore, it is crucial to have a deep understanding of the system under development to avoid undesired and unexpected product profiles. Although, polymers are the main oral films component, additional excipients may be required to tailor the

target product profile. These excipients include plasticizers, sweeteners, flavor, colorants, stabilizers, fillers, saliva stimulating agents, buffer systems and others [7].

Table 2. Properties and key findings of representative polymers used in the development of OTFs.

Polymer	General information	Key findings	Ref
Pullulan	• White, odorless, and tasteless powder • Non-ionic and non-hygroscopic exopolysaccharide obtained by fermentation (Aureobasidium pullulans) • Linear glucan with repeating units of maltotriose (modified starch) • Soluble in hot as well as cold water and dilute alkali	• Good film forming properties • It forms flexible films in 5-25% (w/w) solution • Films prepared at low temperatures are stiffer and more flexible than films prepared at higher temperatures that are brittle and do not have a clear plastic deformation • Usually blended with synthetic, semi-synthetic, and natural polymers (HPMC, pectin, maltodextrin, PVP, alginate, CMC) to decrease cost and improve other properties.	[7] [9] [64-68]
Sodium alginate	• White or buff powder, odorless and tasteless • Anionic polysaccharide extracted from brown seaweed using dilute alkali • Copolymer of β-D-mannuronic acid (M) and α-L-glucuronic acid (G) • Different block configurations give rise to different materials properties • Soluble in water (pH > 3) and insoluble in organic solvents • It forms gels in presence of divalent cations (Ca^{2+} and Mg^{2+}) • **High mucoadhesive properties**	• Used as immobilization matrices for cells and enzymes, controlled release of bioactive substances • Excellent gel and film forming properties • Compatible with most water-soluble thickeners and resins • Blended with HPMC, xanthan gum, maltodextrin, PVA and PEG400	[9] [69-71]
Pectin	• Yellowish white, odorless powder with mucilaginous taste • Anionic polysaccharide seen in primary cell walls • Classified as high methoxyl pectin (HMP) and low methoxyl pectin (LMP) • HMP forms gels in acidic media in the presence of sugars, while LMP forms gels in the presence of multivalent ions • Soluble in water but insoluble in most of the organic solvents • **Strong mucoadhesive properties**	• Not particularly useful for fast dissolving films, but modified pectins yielded films with fast dissolution rates • Good film forming capacity at low temperature • Brittle and do not have a clear plastic deformation • Films' properties depend on the pectin's source and the concentration of the filmogenic solution	[9] [64]
Chitosan	• White or creamy powder or flakes, and odorless • Cationic polysaccharide obtained by partial deacetylation of chitin • Sparingly soluble in water (1% acetic acid solution; pH < 6.5); insoluble in ethanol (95%) and other organic solvents • **Mucoadhesive and antimicrobial properties**	• Excellent film forming ability • Films produced using low molecular weight chitosan presented better physical-chemical properties • All films presented fast disintegration, but when chitosan concentration increased, disintegration time also increased • It enhances the transport of polar drugs across epithelial surfaces • Possesses cell-binding activity due to cationic charge which allows the binding to the negative charge of the cell surface	[9] [64] [72]
Carrageenan	• White or tiny yellow powder, free of smell or taste. • Anionic polysaccharide extracted from the red seaweed Chondrus crispus • Three structural types: Iota, Kappa, and Lambda, differing in solubility and rheological properties • All the types are dissolvable in heated water. In chilled water, just lambda-carrageenan and the sodium salts of	• Potential to act as protein/peptide stabilizer by steric stabilization • It is compatible with most nonionic and anionic water-soluble thickeners • Solutions are susceptible to shear and heat degradation	[9] [64] [73]

	kappa and particle carrageenan are dissolvable. • **Moderate mucoadhesive properties**		
Starch	• Odorless, tasteless, fine, white powder • Reserve polysaccharide in plants tubes and seed endosperm plants (granules) • Mixture of amylose and amylopectin (10-20% water soluble amylose and 80-90 % water insoluble amylopectin depending on the source) • Insoluble in cold water and ethanol. • It fit to shape a **mucoadhesive gel-like framework.** • It decomposes at 250 °C	• Amylose is responsible for starch's film forming ability • Pure starch films are brittle and tacky • Modified or pre-gelatinized starches are more suitable, forming homogeneous and hydrophilic films, besides presenting good mechanical properties, fast disintegration, and high mucoadhesiveness. • Often combined with gelatin, HPMC and pullulan.	[7] [64] [74,75]
Maltodextrin	• White hygroscopic powder or granules • Produced by partial enzymatic hydrolysis of starch • Soluble in water, and poorly soluble or even insoluble in anhydrous alcohol • Classified according to the dextrose equivalent (DE), ranging from 3 to 20.	• Good film forming properties • Maltodextrin films generally exhibit high flexibility and rapid disintegration due to their hydrophilic nature • It can be used alone or blended with HPMC, pullulan, dextran, karaya gum and xanthan gum	[64] [76,77]
Gellan gum	• Bland, odorless, white-beige fine powder • Linear anionic exopolysaccharide produced by microbial fermentation of the bacterium Sphingomonas (Pseudomonas) elodea • Two forms available: acetylated form (native or high acyl gellan gum) and deacetylated form (low acyl gellan gum) • The acetylation degree affects its gelling properties • It forms thermoreversible gels (low acyl gellan gum requires the presence of divalent cation for gelling) • Soluble in water (basic pH and high temperature) • **High mucoadhesion properties**	• Good film forming properties • Solution of 2% w/v leads to brittle films requiring the addition of a plasticizer (mainly glycerol) • It can be used alone on in combination with other polymers, such as pectin or cellulose derivatives.	[78-82]
Gelatin	• Light amber to faintly yellow colored powder • Polyelectrolytic polypeptide obtain through thermal denaturation and acidic (type A) or alkaline (type B) hydrolysis of collagen • Extracted from bovine, pigskin, bones, and fish skin • Practically insoluble in acetone, chloroform, ethanol (95%), ether, and methanol. Soluble in glycerine, acids, and alkalis, although strong acids or alkalis cause precipitation • **High mucoadhesion properties**	• It has an exceptionally good film forming ability • Gelatin-based films presented high tensile strength and mucoadhesiveness • Useable for preparation of sterile film, ophthalmic film, and sterile sponge • Blended with HC, starch, CMC and HPMC	[9] [64] [83,84]
Hydroxypropyl methylcellulose (HPMC)	• White, creamy, odorless, and tasteless powder • Non-ionic polymer obtained by partial O-methylation and O-(hydroxypropylation) of cellulose • Soluble in cold water, but insoluble in chloroform and ethanol • Two types of HPMC used in oral film formulation (K and E) • **Moderate mucoadhesive properties**	• Film forming ability at 2–20% concentrations • The substitution degree strongly affects the film-forming ability, drug release and mechanical/thermal properties • Generally used for controlled and/or delayed release of the drug substance (HPMC K) • Initial burst drug release followed by slow or sustained drug release diffusion observed in buccal bioadhesive system of nicotine hydrogen tartrate • Blended with maltodextrin, pullulan, alginate, chitosan, PVA, PVP	[7] [9] [85-87]
Carboxymethyl cellulose (CMC)	• White, odorless powder • Anionic linear polysaccharide produced by reacting cellulose with sodium	• The substitution degree strongly affects the film-forming • Improved the residence time of HPC and sodium alginate buccal mucoadhesive films	[7] [9] [88,89]

	monochloroacetate under controlled conditions • Easily dispersed in water to form a clear or colloidal solution • High swelling properties • **Good bioadhesive strength**	• Good compatibility with starch forming single-phase polymeric matrix films with improved mechanical and barrier properties • The enzymatically modified CMC has good film forming property	
Hydroxypropyl cellulose (HPC)	• White to slightly yellow colored, odorless, inert and tasteless powder • Cellulose derivative obtained by hydroxypropylation of hydroxyl groups • Soluble in cold and hot polar organic solvents such as absolute ethanol, methanol, isopropyl alcohol and propylene glycol • **Moderate mucoadhesive properties**	• It forms films with proper mechanical properties • Used to replace synthetic polymers or HPMC in a polymer matrix with modified starch to improve solubility • It has a good film forming property and 5% (w/w) solution is generally used for film coating	[7] [9]
Poly (vinyl pyrrolidone) (PVP)	• Wide range of solubility • Non-ionic • High swelling properties • **Used as co-adjuvant to increase mucoadhesion**	• Blending of PVP with PVA and HPMC improves film forming ability • Blended with ethyl cellulose and HPC produces films with increased flexibility, softer and tougher properties • Different ratios of PVP-alginate blends can be used to design drug-controlled release	[7] [9] [90]
Poly (vinyl alcohol) (PVA)	• White to cream-colored granular powder • Water soluble synthetic polymer • Non-ionic polymer • **Moderate mucoadhesive properties**	• Very flexible films • Mainly used in ophthalmic polymeric preparations at concentration of 3–5% • Higher elongation at break values	[7] [9]
Poly (ethylene oxide) (PEO)	• Non-ionic polymer • **High mucoadhesion with high molecular weight**	• It can be used as self-plasticizing polymer matrix • Optimization of tear resistance, dissolution rate, and adhesion tendencies of film by combining low Mw PEO, with a higher Mw PEO and/or with cellulose • Films with good resistance to tearing, minimal or no curling • Pleasant mouth feeling with no sticky or highly viscous gel formation	[7] [9]

1.2.2 Polymers for the preparation of thin films as wound dressings

Wound healing is an orchestrated process that requires an appropriate approach to support the wound at its various stages. Injured skin generally needs to be covered by a wound dressing to minimize the loss of its functions [91]. A favorable dressing should fulfill the following characteristics: it should easily accommodate complex wound contours and volumes, possess mechanical protection, maintain a moist environment, have ideal permeability of gases, be capable of absorbing exudates, protect the wound from infections of opportunistic bacteria, be easily and atraumatically changed and removed, be able to be stored for a long time in extreme environments, be costly/commercially acceptable, be lightweight, nontoxic, nonallergic, biocompatible, biodegradable, and elastic [92-96]. During the preparation of wound dressings, the attention is focused on biocompatibility, hemostatic and antibacterial properties,

adhesion, and proper mechanical strength [97]. To meet these demands, plenty of natural and synthetic biopolymers are extensively utilized, due to their attractive features that make them excellent materials for the development of dressings to promote wounds and burns healing. Despite the advantages of synthetic polymers, including better mechanical properties, greater stability to degradation, high reproducibility and ease of processing, natural biopolymers have established themselves as the material of choice for designing wound dressings. Due to their natural origin, these polymers are extensively biodegradable and biocompatible. Moreover, they are readily reabsorbed by the body without causing an inflammatory response when applied to injured areas. Coupling these features with hydrophilicity and their supporting presence during new tissue formation has generated much attention towards the use of natural polymers in skin tissue engineering, especially in wound care and treatment [98-101]. Natural polymers have been studied in detail for decades and suggested to exhibit numerous beneficial health properties potentially usable in wound treatment. Due to their bioactivities, natural polymers can interact with inflammation, proliferation and remodeling phases of wound healing [100,102]. They can enhance or intervene on cell signaling pathways to increase the rate and effectiveness of differentiation, specialization, and function of significant cell types of wound healing such as fibroblasts, macrophages, and keratinocytes [103-106]. In addition to intracellular interaction, bioactive polymers can also regulate inflammatory response, eliminate infectious threats, and help the ECM building [99]. However, the number of film-forming polymers with intrinsic beneficial properties (antimicrobial, restorative and antioxidant) is limited, therefore bioactive ingredients often need to be load in film formulations, either to provide or enhance a certain desire effect on the wound bed [107]. Table 3 shows the main natural biopolymers employed in the development of thin films for wound healing. Some of the polymers have already been mentioned as major component of thin films for oral drug delivery. In this case, the factors that make them excellent materials for the development of wound dressings are highlighted.

Table 3. Advantages and disadvantages of natural and synthetic polymers in the formulation of thin films as wound dressings

Polymer	Advantages in wound healing	Possible disadvantages	Ref
	• One of the main components of ECM and synovial liquid	• High cost	[99] [108-111]

Hyaluronic acid	• Biocompatible, biodegradable, non-toxic and non-immunogenic • Involved in cell signaling • Anti-inflammatory effect • Stimulation of cell migration and proliferation (e.g., fibroblast) • Promoting the formation of granulation tissue matrix • Regulation of re--epithelialization process	• Presence of protein impurities that can be potentially immunogenic • Poor stability • Requirement of chemical modification to improve mechanical properties • Low bacterial barrier	
Chitosan	• Biocompatible, biodegradable, non-toxic, low immunogenic • Stimulation of cell migration and proliferation • Stimulation of re-epithelization, angiogenesis, tissue and nerve regeneration • Anti-inflammatory effect • Antibacterial and antifungal properties • Good adhesiveness	• High cost • Poor mechanical and strength stability • High viscosity and low solubility at neutral pH • Rapid in vivo degradation rate • Molecular weight-dependent negative effects on cell proliferation	[99] [107] [111,112]
Alginate	• Biocompatible, biodegradable, non-toxic, low immunogenic • Quite effective in absorbing the wound excretion and preventing undesired odor and pain • Maintaining a moist environment, limiting infection and external interference, and stimulating tissue regeneration • Stimulation of IL-6 and TNFα • Ability carrier of beneficial molecules • Good adhesiveness	• Difficult to sterilized • Low cell adhesion • Poor mechanical characteristics	[99] [111] [113,114]
Cellulose	• Biocompatible and non-toxic • The porous structure resembles the ECM of human skin • Wound protection activity • Moist retention and exudate absorption (removal of wound excretions via absorbing the dead tissue molecules and fibers) • Methylated and oxidized cellulose stimulated critical cellular responses such as cell migration and proliferation in injured area with improved hemostasis	• Non-degradable or very slow degradable • Poor antimicrobial activity • Needs often changes due to the dryness • Other than wound protection activities cellulose does not exhibit any beneficial effects in healing process	[99] [111] [115,116]
Gellan gum	• Biocompatible and non-toxic • Wound protection from further damages or infections • Moist retention and exudate absorption (removal of wound excretions via absorbing the dead tissue molecules and fibers) • Inhibition of post-surgical adhesion and prevention of scar formation • Stimulation of skin proper regeneration	• Non-degradable or very slow degradable • No antimicrobial activity	[117-120]
Collagen	• Most abundant protein in mammals • Dominant component of ECM • Biocompatible, biodegradable, non-toxic, low immunogenic • Stimulation of cell migration, adhesion, proliferation and differentiation • Stimulation of ECM components production and secretion	• High cost • Low mechanical strength • Poor stability in physiological condition • Potential for antigenicity through telopeptides	[111] [121-123]
Gelatin	• Biocompatible, biodegradable, non-toxic and non-immunogenic • Prevent fluid loss during exudation • Promotes cell adhesion, epithelialization, contraction, and granulation • Stimulation of cell migration for tissue regeneration • Inhibits proteolysis of EGF and can act as a biodegradable carrier for EGF delivery,	• Low stability in physiological conditions • Need of plasticizers to improve films properties	[108] [111]

	showing double-mode cellular regeneration • Good adhesiveness		
Keratin	• Main structural fibrous protein found in hair, nails, wool, feathers, and horns with a high concentration of cysteine • Essential component of human skin • Biocompatible, biodegradable, non-toxic and low immunogenic • Facilitates cell adhesion and proliferation • Intrinsic cellular recognition	• Poor mechanical properties • Quick loss of mechanical integrity	[107] [111] [124,125]
Silk fibroin	• Fibrous protein composed of glycine, alanine and serine in various proportions • Biocompatible, biodegradable, non-toxic • Good substrate for cell adhesion and proliferation • Good mechanical properties • Anti-inflammatory effect • Induces high cell mobility (fibroblast) and high expression of genes related to wound healing and skin reconstruction	• Prolonged present of silk may induce degradation, which release certain residues or degraded products that may prompt immune response	[107] [111] [126,127]

1.2.3 Gellan Gum

GG, produced by microbial fermentation of the bacterium *Sphingomonas (Pseudomonas) elodea*, is a natural biocompatible exopolysaccharide and food additive approved by the FDA and the European Union (E418). Tetrasaccharide repeating units made up of α-L-rhamnose, β-D-glucose, and β-D-glucuronate in the molar ratios 1:2:1 characterize this linear, anionic, and high molecular weight polymer, which exists in two different forms: its acetylated (native) form, commonly known as high acyl GG, where two acyl groups, O-acetate and L-glycerate, are bound to the same glucose residue next to glucuronic acid (figure 4A), and its deacetylated form (derived from alkaline hydrolysis of native GG), usually referred as low acyl GG, which is the most prevalent and commercially available (Figure 4B) [119,128].

The peculiar properties of both high and low acyl GG have generated a considerable deal of attention, helping to make these polysaccharides interesting materials for a variety of applications, among which those in the biomedical and pharmaceutical fields undoubtedly stand out. Both low and high acyl GG are capable of undergoing physical gelation through the transition from a random coil conformation at high temperature (~90°C) to an ordered double-helix structure when the polymeric solutions are cooled (coil-helix transition) [128]. Then, the aggregation of double helices at particular junctions' sites causes a further packing of the polymer chains, thus leading to the

generation of thermo-reversible gels (sol-gel transition). A schematic representation of this gelation process is shown in Figure 5.

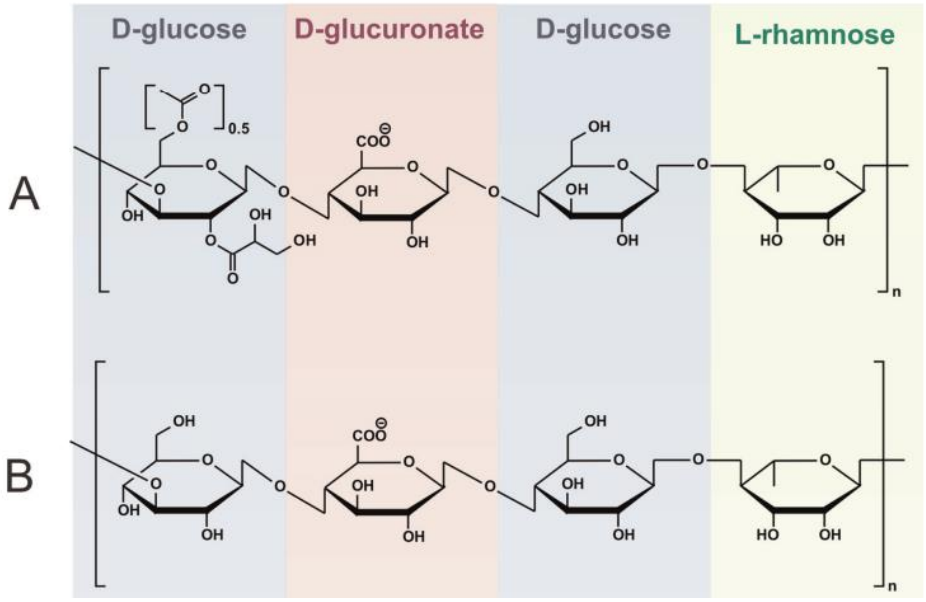

Figure 4. Chemical structure of native (A) and low acyl (B) GG repeating unit [119].

It is well known that several factors, some of them related to the polymer itself, such as deacetylation degree, concentration, and molecular weight, while others related to specific properties of the polymeric solution, such as pH value and ionic strength, strongly influence the gelling behavior of the polymer and the mechanical properties of the obtained gels [119].

The deacetylation degree of GG is a fundamental parameter in determining the gelling temperature, the rate of gel formation as well as the gel strength, texture and clarity. In native GG, acetyl and L-glyceryl groups act as physical barriers that prevent the aggregation of polymer chains, resulting in a less effective packing and, therefore, in soft and elastic gels [128-130]. Furthermore, L-glyceryl groups alter the orientation of the nearby glucoronate residue and its carboxyl groups, disabling those sites for the binding of metal cations which would contribute to the improvement of hydrogels' mechanical properties. On the other hand, the lack of acetyl groups in the repeating units of low acyl GG allows an easier and stronger interaction between the polymer chains, enabling the formation of hard, rigid, transparent gels with higher thermal stability [131].

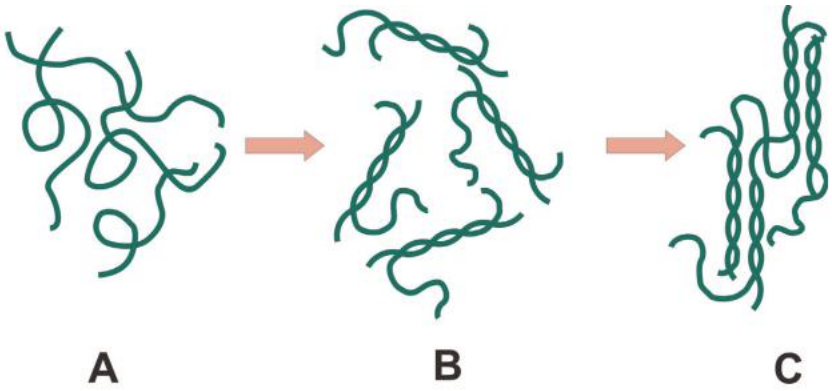

Figure 5. Coil-to-helix (A-B) and sol-gel transition (B-C) of GG [119].

GG gelling is an ionotropic process, which means that the presence of cations is usually required for the formation of stable hydrogel structures. Consequently, the amount and chemical nature of cations present in the polymeric solution greatly influence GG gelation. In the specific, both divalent cations (e.g., Ca^{2+} and Mg^{2+}) and monovalent ones (e.g., Na^{+} and K^{+}) can encourage the packing of polymer chains, resulting in the production of stable 3D structures. However, due to the formation of chemical bonds between the cation and two carboxylate groups of glucuronic acid molecules belonging to neighboring polymer chains, divalent cations lead to a more efficient gelation than monovalent ones. Indeed, monovalent cations are unable to form coordination bonds with multiple carboxylic functions, but they can shield the negative charges of GG carboxylate groups, reducing the electrostatic repulsion between the polymer chains and promoting, therefore, their aggregation through hydrogen bonding [128].

The unique gelling properties of GG combined with its stability in acidic environments and resistance to enzymatic degradation have led to the development of several controlled-release forms based on this polymer for the administration of therapeutic agents by the oral, buccal, ophthalmic, nasal and rectal routes [119]. In particular, the high molecular weight and the abundance of hydroxyl and carboxyl groups capable of forming hydrogen bonds give GG considerable mucoadhesive properties, which can be exploited for the design of transmucosal drug delivery systems. Delivery of therapeutic agents through various transmucosal routes has gained significant attention, owing to their presystemic metabolism or instability in the acidic environment associated with oral administration [132]. Among the various absorptive mucosae, the mucosa of the oral cavity is viewed as a convenient and easily accessible site for the delivery of therapeutic

agents aimed at the treatment of both local and systemic diseases. Although the use of GG in the development of OTFs for the buccal delivery of drugs has not been extensively investigated, its gelling and mucoadhesive properties make this polymer an excellent candidate for the development of platforms that may be used for the buccal administration of various therapeutic agents.

Due to its hydrophilic nature, which allows exudates to be absorbed while maintaining a moist environment, and its capacity to serve as a physical barrier to prevent further damage and infection by opportunistic bacteria, GG is also widely used as wound dressing material in various forms, such as hydrogel, scaffolds, and injectable dressing, even if the most GG-based dressings are produced in the form of films [120]. It is well recognized that GG-based materials can inhibit post-surgical adhesion, prevent scar formation, and contribute to the proper regeneration of skin [119]. In this context, GG is often combined with metals or metal oxides in different shapes, such as nanoparticles, nanotubes, and nanorods, to increase the mechanical and antimicrobial properties of these systems, thus leading to an overall improvement of their *in vivo* performance [120,133-136].

GG-based hydrogels have also been investigated in the field of tissue engineering, mostly as materials for cartilage reconstruction and bone regeneration as well as for the treatment of intervertebral disc disorders related to the disfunction and deformation of nucleus pulposus, the central part of the intervertebral disc. Furthermore, they are currently explored as injectable carriers for various autologous cells and the results are very promising [119].

However, it must be taken into account that physical GG hydrogels are vulnerable to a significant loss of stability *in vivo*, which is typically brought on by the substitution of divalent cations with monovalent ones that are found in larger concentrations in the physiological environment. In addition, the harsh conditions for GG gelling are often unsuitable for its use in the pharmaceutical and biomedical fields [119,128]. These restrictions are typically addressed through the chemical modification of the several hydroxyl and carboxylic free groups present in GG backbone. For instance, one of the most common chemical modifications of GG involves the introduction of methacrylic groups on the polymer by the reaction of its primary hydroxyl groups with methacrylic anhydride. The presence of methacrylic groups with double conjugated bonds makes

the methacrylate derivative of GG (GG-MA) susceptible to chemical crosslinking by light irradiation. The photo-crosslinking reaction involves the presence of a photo-initiator compound and irradiation by UV light to start a free radical polymerization reaction that propagate through carbon-carbon double bonds to create covalent crosslinks between polymer chains. The photocuring of GG-MA solutions leads to the production of chemical hydrogels which have been demonstrated to exhibit improved mechanical properties and higher Young's modulus when compared to those of the unmodified GG hydrogels [128]. Another common modification of the polymeric backbone involves the amination of GG carboxyl groups using carbodiimides chemistry. For example, this method has been exploited to functionalize GG with the RGD peptide, enabling the creation of scaffolds with improved cellular adhesion [137]. Alternative methods are based on the polymer functionalization with catechol-containing molecules, such as dopamine (DA) [138].

1.3 Thin films as drug delivery systems: Oral Thin Films (OTFs)

As mentioned before, polymeric thin films successfully fulfill numerous conditions to be used as platforms for drug delivery. They allow to target sensitive site that may not be possible with conventional dosage forms and show the ability to improve the onset of therapeutic action, reduce dose frequency and enhance drug efficacy. Compared to existing traditional dosage forms, they appear to be superior in terms of improved bioavailability, high patient compliance, and API patent extension. Additionally, thin films offer several benefits, including the development of cost-effective formulation, convenient administration of several therapeutic agents through non-invasive routes and ease of handling during manufacturing and shipping [9,139].

OTFs are polymeric films with reduced thickness and an area of 5–20 cm^2, which can be rapidly dispersed/dissolved in the oral cavity (orodispersible films) or applied directly on the oral mucosa (buccal films) [6,7,13]. Orodispersible films work like conventional orodispersible dosage forms. They are non-adhesive films designed to dissolve instantly after being placed on the tongue and the drug substance is ingested along with the saliva taking the same path as a tablet [6,7]. Buccal films, on the other hand, are intended to release drug substances through the oral mucosa, which has been identified as an

attractive option for the administration of bioactive molecules, especially in pediatric and geriatric patients who have trouble chewing or swallowing solid pharmaceutical forms or patients suffering from pathological conditions commonly known as dysphagia [6,7,140]. The oral mucosa is easily accessible, allowing for simple application of pharmaceutical dosage forms as well as quick removal in case of need [141]. Furthermore, it has a relatively low enzyme activity, which prevents the degradation of labile drugs, and can be used to achieve both local and systemic therapeutic effects. Drugs administered through the buccal mucosa reach high plasma concentrations because the internal jugular vein allows direct access to the systemic circulation. This prevents the pre-systemic elimination of therapeutic agents, protecting them from the acid pH of the stomach and the action of liver metabolizing enzymes, responsible for the first-pass hepatic effect [132,141]. However, it should be considered that a number of environmental parameters, such as fluid volume, pH value, enzymatic activity, and mucosal permeability, have a significant impact on how a drug will be absorbed by the oral mucosa. For example, excessive salivation prevents the medicine from remaining at the point of delivery since it washes the drug out. Similarly, drugs may be swallowed before they are absorbed through the mucus membrane of the mouth. Therefore, thoughtful considerations should be made when creating an oral formulation, such as polymeric thin films, to increase the bioavailability and ensure patient adherence to therapeutic treatment [140,142].

However, despite the clear advantages of polymer thin films, their use as drug delivery systems is often limited. Both the reduced size and thickness as well as the considerable number of excipients used in the film formulation can have a serious impact on the drug loading capacity of the dosage form, where non-uniform distribution, aggregation and crystallization of therapeutic agents are also commonly observed [78]. Furthermore, the composition of the formulation and the method used for its preparation are found to play a key role in determining the mechanical and adhesive properties of thin films, also affecting the homogeneous distribution of the drug in the final product and, therefore, its application as drug delivery platform.

1.3.1 Drug-loading capacity, phase separation and drug crystallization in OTFs

As briefly discussed above, OTFs represent excellent systems for the administration of potent drugs typically taken in small doses. However, they fail when it comes to delivering less potent medications which must be administered in larger quantities to have an acceptable therapeutic effect. This is mainly due to the low drug-loading capacity of these dosage forms which is a direct consequence of their small size and reduced thickness [9,143]. Moreover, the combination of multiple drugs is a particularly challenging task in the formulation of thin films, not only because of their poor loading capacity, but also because both the dissolution rate and the disintegration time are hindered by the co-administration of different therapeutic agents [144].

Due to the hydrophilic nature of film-forming polymers, physical instability upon exposure to a humid environment is a major drawback of thin films and compromise their anticipated advantage as drug delivery systems. One of the direct effects of the physical instability of thin films is phase separation, usually followed by drug crystallization. The phase separation behavior of thin films is significantly affected by many factors which include their thickness, external environment, as well as the miscibility and chemical compatibility of the film-forming components [145]. For example, it seems to be favored when low water-soluble and/or amorphous drug molecules are present in the formulation, while can be minimized if the drug is highly chemically similar to the film-forming polymer, since the formation of drug-polymer interactions lead to a decrease in the molecular mobility, thus reducing the driving force for drug crystallization [146,147]. However, also environmental conditions, such as humidity and temperature, can affect the stability of film formulations especially during storage. Since water molecules can compete with the drug for hydrogen bonding sites on the polymers, moisture can alter the driving force for crystallization, thus promoting the separation of polymer and drug into domains [10].

Understanding phase separation/drug crystallization in polymer thin films is crucial because it has a direct impact on *in vivo* performance of these delivery systems. The formation of phase-separated drug crystals on the surface or inside the film can significantly affect how the drug is released. Furthermore, high levels of crystal growth

on a solid dispersion's surface can significantly reduce the wettability of the formulation and cause a decrease in dissolution [145,148].

Drug crystallization is a heterogeneous process, and crystals formation is frequently advantageous at the free surface, which not only offers a favorable site for crystal nucleation, but also accelerates their growth rate. This is mainly due to the gain in molecular mobility that is recorded at the surface of the polymer matrix, which enhances crystallization through upward crystal growth. Although it has been observed that crystallization is more rapid at free surfaces, other elements, such as the properties of the solid surface as well as its density and roughness, can also influence the crystallization process [10]. Based on the above, the most widely used approaches to prevent and inhibit drug crystallization mainly involve the stabilization of the formulation using polymers capable of interacting with the loaded drug [149], the coating of thin films with an additional polymer layer that extinguishes drug molecular mobility reducing the crystallization driving force [150,151], and modification of substrates' surfaces [152].

We studied an alternative and innovative strategy for avoiding fluconazole crystallization in GG-based OTFs. Although fluconazole is a highly water-soluble drug (BCS I), it shown a certain inclination to crystallization, especially during the storage of film formulations. In particular, a correlation between the amount of glycerol used as plasticizer and the crystallization of the active molecule was discovered. In practice, fluconazole crystallization can be avoided only in the presence of extremely high concentrations of glycerol. However, the increase in the amount of plasticizer has a negative impact on both the mechanical and mucoadhesive properties of GG-based OTFs, thus precluding their use for the buccal administration of drugs [78]. This issue was resolved by the addition of hydroxypropyl-β-cyclodextrin (HP-β-CD) in the formulations, either directly or after the development of the inclusion complex with the drug by the kneading method. This made it possible to prevent fluconazole crystallization, leading to the production of films with good mechanical properties and excellent mucoadhesion allowing, at the same time, a modified release of the drug.

pharmaceutics

MDPI

Article

Enhanced Loading Efficiency and Mucoadhesion Properties of Gellan Gum Thin Films by Complexation with Hydroxypropyl-β-Cyclodextrin

Alessandra Adrover [1,*], Laura di Muzio [2], Jordan Trilli [2], Chiara Brandelli [2], Patrizia Paolicelli [2,*], Stefania Petralito [2] and Maria Antonietta Casadei [2]

1 Dipartimento di Ingegneria Chimica, Materiali e Ambiente, Sapienza Universitá di Roma, Via Eudossiana 18, 00184 Rome, Italy

2 Dipartimento di Chimica e Tecnologia del Farmaco, Sapienza Universitá di Roma, Piazzale Aldo Moro 5, 00185 Rome, Italy; laura.dimuzio@uniroma1.it (L.d.M.); jordan.trilli@uniroma1.it (J.T.); chiara.brandelli@uniroma1.it (C.B.); stefania.petralito@uniroma1.it (S.P.); mariaantonietta.casadei@uniroma1.it (M.A.C.)

* Correspondence: alessandra.adrover@uniroma1.it (A.A.); patrizia.paolicelli@uniroma1.it (P.P.)

Received: 26 July 2020; Accepted: 25 August 2020; Published: 28 August 2020

Abstract: Polymeric oral thin films (OTFs) were prepared by the casting method, combining gellan gum (GG), a water-soluble polysaccharide, and glycerol (Gly) as a plasticizing agent. GG-Gly films were investigated as potential systems for buccal drug delivery using fluconazole (Class I of the Biopharmaceutical Classification System) as a model drug. At a low concentration of Gly drug precipitation occurred while, for higher concentrations of Gly, a significant deterioration of mucoadhesive and mechanical properties was observed. One possible way to overcome all these problems could be the addition of hydroxypropyl-β-cyclodextrin (HP-β-CD) to the GG-Gly formulation as a drug-precipitation inhibitor. In this work the effect of cyclodextrin addition on the mechanical, mucoadhesive, swelling and release properties of GG-Gly films was investigated. In-vitro drug release studies were carried out using the paddle type dissolution apparatus (USP II) and the millifluidic flow-through device (MFTD). A moving-boundary model for swelling dynamics and release in USP II is proposed to estimate the effective diffusivity of the solvent, HP-β-CD, fluconazole and complex fluconazole/HP-β-CD in the swelling film. Experimental results, supported by theoretical modeling, confirmed that gellan gum-low glycerol thin films including HP-β-CD represent a suitable formulation for fluconazole drug delivery. A sustained release was observed when GG-Gly film is loaded with a preformed complex fluconazole/HP-β-CD.

Keywords: thin films; drug delivery; gellan gum; cyclodextrins; USP II; millifluidic flow-through device; mathematical modeling

1. Introduction

The oral dosage form for GI-tract delivery represents the preferred way for drug administration as it is the most convenient, practical and easily accessible way for the assumption of biological active agents. However, some unfavorable conditions, such as degradation through the gastrointestinal tract or first-pass metabolism, can decrease the bioavailability of therapeutic molecules administered by this route [1,2]. For this reason, over the last years, research in the pharmaceutical technology field has been looking for effective and well-accepted alternatives to the oral route.

The oral mucosa has been identified as an interesting option for the administration of bioactive molecules [3]. It is easily accessible and offers ease of application of pharmaceutical dosage forms, but also their prompt removal in case of need [4]. Furthermore, oral mucosa presents a relatively low

enzyme activity, thus enabling the preservation of labile drugs from degradation and it can be used to obtain both local and systemic therapeutic effects. In the latter case, a therapeutic molecule can directly access the systemic circulation through the internal jugular vein, avoiding first-pass hepatic metabolism, and therefore reaching high plasma concentrations [4]. All these advantages stimulated the design of innovative buccal dosage forms such as oral thin films (OTFs) that attracted increasing attention and attained a preeminent position over other formulations.

OTFs are polymeric films with reduced thickness and an area of 5–20 cm^2, which can be applied directly on the oral mucosa [5–7]. OTFs can be formulated as fast-acting or prolonged drug delivery systems and can be used to treat a wide range of diseases and disorders, both local, such as candidiasis and gingivitis, and systemic, such as migraine, schizophrenia, pain, nausea and vomiting [6]. OTFs can also be used for the effective treatment of oral mucosal lesions as they combine drug delivery capability and mechanical protection to the surface of the wound. The double effect produced by polymeric films contributes to a better outcome in pain relief [8]. The extreme ease of application and removal of OTFs makes them also a valid and convenient alternative to conventional oral dosage forms particularly for pediatric or geriatric patients with swallowing problems or for patients with gastroesophageal disorders, for which the assumption of conventional drug formulations may cause worsening of symptoms of the disease [9].

Despite their potential, there is still the need for extensive studies to optimize the performance of thin films accurately. Major limitations of OTFs are low drug loading capacity, non-uniform drug distribution and precipitation. For these reasons, the phases of formulation, development and manufacturing of polymeric thin films are particularly challenging [10–12]. In order to expand the capabilities of OTFs, scientists are exploring novel techniques and formulation approaches to increase their loading efficiency. In this scenario, we have recently investigated the effect of glycerol, employed as a plasticizer, on the characteristics of OTFs made of gellan gum loaded with fluconazole [13]. Indeed, we chose fluconazole as a model drug to show that drug precipitation can occur in OTFs even for highly water soluble molecules (Class I of the Biopharmaceutical Classification System). We observed that only high concentrations of glycerol (6% w/v) were capable to avoid drug precipitation during the preparation and the subsequent storage of the film. However, high concentrations of the plasticizer significantly worsened mechanical and mucoadhesive properties of the film.

We proposed, as an alternative, the addition to the formulation of hydroxypropyl-β-cyclodextrin (HP-β-CD) to avoid fluconazole precipitation. Cyclodextrins are classified as GRAS (Generally Recognized as Safe) expicipients by the U.S. Food and Drug Administration and those with high water solubility, such as HP-β-CD, have been proposed as effective precipitation inhibitors [14,15] and frequently used to improve solubility and bioavailability of drugs [15]. Despite the fact that cyclodextrins have been widely applied for drug delivery from OTFs [16], hydrogels [17,18], nanofibers [19], vesicles [20], only few reports have investigated the feasibility of enhancing loading efficiency of drugs in OTFs using this functional excipient. Therefore, the analysis of how cyclodextrin affects the mechanical, mucoadhesive, swelling and release properties of the OTF formulations was deepened in this work. All these features were investigated considering that an ideal film should be soft, elastic, flexible and resistant in order to withstand without breakage all the mechanical stresses produced during manufacturing, storage and application [11,21]. Moreover, it should be retained in the mouth with adequate bioadhesive strength to produce the desired pharmacological effect, but avoiding too extensive swelling of the film in order to prevent patient discomfort.

The produced OTF formulations were characterized for their drug release profiles, which were obtained by employing two different types of apparatus for in-vitro release studies, namely the official paddle type dissolution apparatus (USP II) and the millifluidic flow-through device (MFTD) [22]. The MFTD has been designed to mimic mouth physiological conditions, i.e., a low hold-up volume (order of 1 mL) and laminar tangential solvent flow rates comparable with salivary flow rates, Q = 2–4 mL/min.

A moving-boundary model for swelling dynamics and release in USP II is proposed to estimate the effective diffusivity of solvent, HP-β-CD and fluconazole (free and complexed form) in the swelling film. The estimate of all these diffusivities led us to a clear interpretation of release data in MFTD and to a quantification of the amounts of fluconazole (free form) and complex fluconazole/HP-β-CD actually present in the dry film.

Experimental results, supported by theoretical modeling, confirmed that gellan gum-low glycerol thin films including HP-β-CD represent a suitable formulation for fluconazole drug delivery. A sustained release was obtained when the film is loaded with a preformed complex fluconazole/HP-β-CD.

2. Materials and Methods

2.1. Materials

All the used reagents were of analytical purity grade. Gellan gum (GG, Gelzan^{TM} CM, CP Kelco U.S., Inc., Atlanta, GA, USA), fluconazole, glycerol (Gly), ethanol, mucin type III from porcine stomach were purchased from Sigma Aldrich. Methanol, glacial acetic acid, distilled water, potassium di-hydrogen phosphate, di-sodium hydrogen phosphate, sodium chloride and hydrochloric acid were purchased from Carlo Erba. Parenteral grade hydroxypropyl-β-cyclodextrin (HP-β-CD, Kleptose®) was provided by Roquette Italia S.P.A (Cassano Spinola AL, Italy). Simulated salivary fluid (pH 6.7) consisted of 16.8 mM $NaHPO_4$, 1.4 mM KH_2PO_4 and 136.9 mM NaCl.

2.2. Film Production

Films with different GG:Gly weight ratios (from 1:0.25 to 1:3 *w*/*w*) were prepared using the solvent casting technique. Gellan gum (GG, 120 mg) and different amounts of glycerol (Gly, 30, 60, 120, 180, 300 and 360 mg) were solubilized in 6 mL of distilled water (Gly 0.5, 1, 2, 3, 5, 6 % *w*/*v*) and maintained at the temperature of 60.0 ± 0.5 °C for 5 h under magnetic stirring and for further 30 min without shaking, in order to eliminate air bubbles formed during the solubilization process. At the end of the solubilization process, the polymeric solutions were poured into an inert silicone tray mold (5.6 cm diameter), leveled and oven-dried at 40.0 ± 2 °C for 15 h. Medicated films were obtained by adding fluconazole (17 mg, 14% *w*/*w* with respect to GG) to the polymeric mixture; films containing cyclodextrin were prepared adding HP-β-CD (78 mg) to the initial polymeric mixture. Further OTF samples were obtained by adding the preformed Flu/HP-β-CD inclusion complex (98 mg, see Section 2.4) to the GG-Gly 2% mixture.

2.3. Phase Solubility Studies of Fluconazole with Hydroxypropyl-β-Cyclodextrin (HP-β-CD)

Phase solubility studies were carried out according to the method reported by Higuchi and Connors [23]. Excess amounts of fluconazole were added to 10 mL of distilled water containing increasing concentrations of HP-β-CD, specifically 0.071, 1.43, 2.14, 2.86, 5.72 and 9.23 mM of cyclodextrin. The resulting dispersions were maintained under magnetic stirring at 37.0 ± 0.1 °C for 72 h. After this time, the suspensions were left to settle, then 1 mL of supernatant was taken and appropriately diluted with distilled water (1:10), taking care to not alter temperature. Fluconazole concentration was determined by measuring the UV absorption at 260 nm and 37.0 ± 0.1 °C with a Perkin Elmer Lambda 40 UV-Vis spectrophotometer. Calibration curve for fluconazole reference standard was obtained by measuring the UV absorption (λ = 260 nm) in an ethanol/water 50:50 (*v*/*v*) solution at 37.0 ± 0.1 °C. The linearity of the calibration curve was confirmed in the range 0.066–1.32 mg/mL with a regression coefficient (R^2) value of 0.995 [24–26].

2.4. Preparation of Drug-Cyclodextrin Inclusion Complex

The inclusion complex between fluconazole and HP-β-CD was prepared with 1:1 molar ratio by the kneading method [27]. Equimolar amounts of the two components were ground in a mortar

until a homogeneous mixture was obtained. Then, the mixture was thoroughly kneaded for further 30 min with 0.5 mL of an ethanol/water 50:50 (*v*/*v*) solution to obtain a paste, which was subsequently oven-dried for 24 h at 70 °C. The dried inclusion complex was then reduced to powder and stored in a sealed container at room temperature until its use for film preparation.

2.5. Mechanical and Mucoadhesion Properties of Films

Mechanical properties of the produced thin films were investigated using a traction machine to evaluate elastic modulus, stress and strain at break. Traction studies were carried out with the ZWICK-ROELL-Z010 instrument (Zwick GmbH & Co., Ulm, Germany) loaded with 1 kN and setting a deformation speed of 1 mm/min. For each film, ten standard-sized samples of rectangular sections were prepared and each sample was fixed to the two machine clamps in a vertical position. The measurements were conducted in three different directions (0°, 45° and 90°) to verify the isotropy of the films. Each analysis was conducted in triplicate and the results were reported as mean values ± standard deviation. The mucoadhesion properties of the films were evaluated in-vitro measuring the force required for detaching the films from a mucin tablet. The method, based on a water counterweight system, has already been described in our previous study [13].

2.6. Fluconazole Content Uniformity

To determine the drug content uniformity, films were cut into square pieces (2 × 2 cm). Each sample was extracted exhaustively with 10 mL of simulated saliva at a temperature of 37 °C. The quantity of fluconazole was determined by HPLC analysis with a Perkin Elmer system (Waltham, MA, USA) consisting of a Series 200 LC pump, a 235 Diode Array Detector, a Total Chrom data processor and an RP-18 column (250–4.5 µm) Merck Hibar LiChrocart, monitoring the drug at λ = 260 nm. The analyses were carried out under isocratic conditions, using as mobile phase a mixture methanol/bidistilled water/acetic acid 50:48:2 in volume, with a flow rate of 0.7 mL/min. The linearity of the calibration curve was confirmed in the range 10–500 µg/mL with a regression coefficient (R^2) value of 0.998. The analyses were repeated on 6 different samples of each OTF and the results were reported as mean values ± standard deviation.

2.7. Swelling Tests

To evaluate the swelling behavior, OTFs were cut into square pieces (2 cm × 2 cm), weighted and immersed in simulated salivary fluid at 37.0 ± 0.1 °C. At regular time intervals, wet films were drained to remove excess water and weighed. The solvent-uptake capacity (Q) was evaluated as

$$Q(t) = (W(t) - W_0)/W_0 \quad (1)$$

where W_0 is the weight of the dry film and $W(t)$ the weight of the swelling film at time t. Each test was repeated in triplicate and the results were reported as mean values ± standard deviation.

2.8. In-Vitro Release Studies with Paddle Type Dissolution Apparatus (Usp II)

The release studies were performed in a USP rotating paddle dissolution apparatus (USP II Sotax Smart AT7 Dissolution Tester) at 37 °C and 50 rpm. OTFs were kept floating in the bottom of the vessel (hold in place by an inert lead retina) filled with 500 mL of preheated simulated saliva (pH 6.7). Aliquots (2 mL) of the release medium were withdrawn at fixed time intervals and replaced with equal volumes of fresh simulated saliva. Tests were repeated in triplicate.

2.9. In-Vitro Release Studies with the Millifluidic Flow-Through Device (MFTD)

Drug release studies from OTFs were also performed using a continuous millifluidic flow-through device [16,22,28,29], henceforth referred to with the acronym MFTD. The MFTD has been designed to

mimic mouth physiological conditions because of the low hold-up volume (less than 1 mL), the laminar tangential solvent flow and flow rates comparable to salivary flow rates.

A schematic representation of the millifluidic flow-through device is shown in Figure 1.

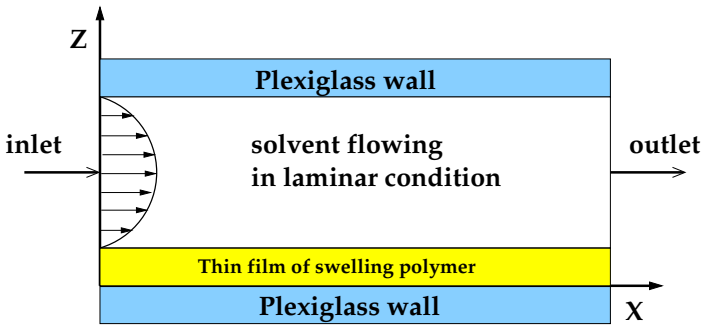

Figure 1. Schematic representation of the flow-through cell.

In the MFTD, thin film strip was placed on the bottom plate of a dissolution cell with dimensions 2 × 9 × 30 mm. These dimensions of the dissolution cell were chosen to assure a laminar regular flow through the device also after complete film swelling. The surface area of the OTF exposed to the solvent tangential laminar flow was 9 × 30 mm. Only one side of the film was exposed to the tangential solvent flow. As soon as wetted, strips adhered firmly to the plate, and there was no need to make use of a double-sided tape, thus avoiding unpredictable and ruinous detachments or floating problems often encountered with other existing devices (USP I, USP II).

The dissolution medium (simulated saliva) was kept in a reservoir at 37 ± 1 °C and circulated through the dissolution cell in open loop by means of a volumetric pump. Flow rates investigated in this work were in the range $Q \in$ [1–5] mL/min, comparable with salivary flow rates Q = 2–4 mL/min and corresponding to laminar flow conditions with Reynolds numbers $Re = \rho < v > d_e/\mu \in$ [1–20], d_e being the hydraulic radius $d_e = 4 \times$ cross section area/wetted perimeter = 3.27 mm.

In order to quantify the amount of drug released from the swelling film, the solution coming out the cell was sent to the UV/Vis spectrophotometer (UV-2401 PC, Shimadzu Corporation, Kyoto, Japan, continuous flow cell, optical path 1 mm). Drug concentration values $c_s(t)$ mg/mL were recorded every 2–4 s. The amount of drug released was calculated with a calibration curve. Calibration curve for fluconazole reference standard (RS) was obtained by measuring the UV absorption (λ = 260 nm) in simulated saliva. The linearity of the calibration curves was confirmed in the range 1–300 µg/mL with a regression coefficient (R^2) value of 0.997. Limits of detection and quantification were 0.2 µg/mL. Tests were repeated in triplicate.

The differential $F(t)$ and integral $M(t)$ release curves were computed from the experimental concentration data $c_s(t)$ by evaluating

$$F(t) = Q\, c_s(t)\ , \quad M_t = \int_0^t Q c_s(t')dt' = \int_0^t F(t')dt' \tag{2}$$

where t_f is a final time for the experimental test. The final time t_f, sufficiently long to ensure the complete drug release, was changed according to the flow rate Q. Specifically, longer time intervals were chosen for smaller flow rates Q.

3. Transport Models

In this section we present the mathematical models adopted for the analysis of experimental data of swelling tests and drug release in the USP II apparatus from which we evaluated the solvent diffusivity D_s, the fluconazole diffusivity D_F and the HP-β-CD diffusivity D_{CD} in the swelling films.

3.1. Swelling Modeling of Thin Films

Swelling of thin films can be modeled as a one-dimensional moving-boundary problem along the z direction, orthogonal to the x–y plane representing the flat surface of the OTF. When only the solvent and the polymer are involved in the swelling process, the pointwise swelling velocity $v_s(z)$ is assumed equal (and opposite in sign) to the volumetric solvent flux [29–33]

$$v_{sw}(z) = D_s \frac{\partial \phi_s}{\partial z} \tag{3}$$

where ϕ_s is the solvent volume fraction and D_s the solvent effective diffusivity in the swelling film.

For thin films under investigation, this well established approach must be modified in order to account for the presence of glycerol and cyclodextrin (when present). While solvent is penetrating the film, glycerol and cyclodextrins are simultaneously released by the swelling film and therefore contribute to the pointwise swelling velocity that can be rewritten as

$$v_{sw}(z) = D_s \frac{\partial \phi_s}{\partial z} + D_G \frac{\partial \phi_G}{\partial z} + D_{CD} \frac{\partial \phi_{CD}}{\partial z} \tag{4}$$

where ϕ_G and ϕ_{CD} are the glycerol and cyclodextrin volume fractions, D_G and D_{CD} the corresponding effective diffusivities in the swelling film.

The advection–diffusion transport equations for solvent, glycerol and cyclodextrin read as

$$\frac{\partial \phi_s}{\partial t} = -\frac{\partial J_s}{\partial z} = -\frac{\partial}{\partial z}\left(-D_s \frac{\partial \phi_s}{\partial z} + v_{sw}\, \phi_s\right) \tag{5}$$

$$\frac{\partial \phi_G}{\partial t} = -\frac{\partial J_G}{\partial z} = -\frac{\partial}{\partial z}\left(-D_G \frac{\partial \phi_G}{\partial z} + v_{sw}\, \phi_G\right) \qquad R(t) < z < S(t), \quad t > 0 \tag{6}$$

$$\frac{\partial \phi_{CD}}{\partial t} = -\frac{\partial J_{CD}}{\partial z} = -\frac{\partial}{\partial z}\left(-D_{CD} \frac{\partial \phi_{CD}}{\partial z} + v_{sw}\, \phi_{CD}\right) \tag{7}$$

where $S(t)$ and $R(t)$ are the positions of the erosion front (gel–solvent interface) and of the swelling front (glassy–rubbery interface), both evolving in time.

On the gel-solvent interface $z = S(t)$, solvent/polymer thermodynamic equilibrium $\phi_s = \phi_{eq}$ is assumed for the solvent, consistent with the perfect sink boundary conditions $\phi_G = \phi_{CD} = 0$ adopted for glycerol and cyclodextrins. The temporal evolution of $S(t)$ is described by the Stefan condition [31]

$$\phi_s = \phi_{eq}, \;\; \phi_G = 0, \; \phi_{CD} = 0, \quad \frac{dS}{dt} = v_{sw}|_{S(t)} \quad at \quad z = S(t). \tag{8}$$

On the glassy-rubbery front $R(t)$, a threshold concentration to initiate swelling $\phi_s = \phi_{\text{glass}} > \phi_s^0$ is assumed for the solvent [34], while for glycerol and cyclodextrin the Stefan conditions apply

$$\phi_s = \phi_{\text{glass}} \tag{9}$$

$$(\phi_G - \phi_G^0)\frac{dR}{dt} = J_G \qquad at \quad z = R(t) \tag{10}$$

$$(\phi_{CD} - \phi_{CD}^0)\frac{dR}{dt} = J_{CD} \tag{11}$$

where ϕ_s^0, ϕ_G^0 and ϕ_{CD}^0 are the initial volume fractions of solvent, glycerol and cyclodextrin in the dry film. Correspondingly, the temporal evolution of $R(t)$ reads as

$$\left((\phi_s - \phi_{\text{glass}}) + (\phi_G - \phi_G^0) + (\phi_{CD} - \phi_{CD}^0)\right)\frac{dR}{dt} = J_s + J_G + J_{CD} \qquad at \quad z = R(t) \tag{12}$$

When $R(t)$ reaches $z = 0$, the glassy phase disappears and the zero-flux boundary condition applies to all the components

$$\frac{\partial \phi_s}{\partial z} = \frac{\partial \phi_G}{\partial z} = \frac{\partial \phi_{CD}}{\partial z} = 0 \Longrightarrow J_s = J_G = J_{CD} = 0 \quad at \quad z = 0. \tag{13}$$

The zero-flux boundary condition at $z = 0$, Equation (13), represents a symmetry boundary condition when both film surfaces are exposed to the solvent like in a swelling test or in a release experiment in USP apparatuses. In these two cases, the initial conditions for the two moving fronts are $R(0) = S(0) = L_0/2$, L_0 being the half-thickness of the dry film. Equation (13) represents an impermeability condition when film swelling occurs in the millifluidic device. Indeed, the thin film adheres firmly on the bottom wall of the device and no solvent permeation is allowed. Consequently, in the MFTD, the initial conditions for the two moving fronts are $R(0) = S(0) = L_0$.

The diffusivity of glycerol in simulated saliva has been estimated from the correlation proposed by D'Errico et al. [35] for the diffusivity of Gly in water at 25 °C

$$D_{Gly}\,[\mathrm{m}^2/\mathrm{s}] = \frac{1.024 - 0.91 x_{Gly}}{1 + 7.5 x_{Gly}} \times 10^{-9} \tag{14}$$

where x_{Gly} is the glycerol molar fraction, approximated as

$$x_{Gly} = \frac{\phi_{Gly}\tilde{\rho}_{Gly}}{\phi_{Gly}\tilde{\rho}_{Gly} + \phi_s\tilde{\rho}_s} \tag{15}$$

due to the very low values of the molar densities [moL/cm^3] of gellan gum and HP-β-CD with respect to that of glycerol $\tilde{\rho}_{Gly}$ and solvent (water) $\tilde{\rho}_s$.

3.2. Drug Release Modeling in the Usp II Apparatus

The fluconazole release process from the OTFs in the USP II apparatus can be simply modeled by a one dimensional advection-diffusion equation describing drug transport in the swelling film along the preferential swelling direction z (orthogonal to the flat surface of the thin film)

$$\frac{\partial c_F}{\partial t} = -\frac{\partial J_F}{\partial z} = -\frac{\partial}{\partial z}\left(-D_F \frac{\partial c_F}{\partial z} + v_{sw}\, c_F\right), \quad R(t) < z < S(t). \tag{16}$$

where $c_F(z,t)$ is the fluconazole concentration and D_F the effective diffusivity of fluconazole in the swelling film. Equation (16) must be solved simultaneously with the equations describing the swelling-erosion dynamics (presented in Section 3.1) because they furnish, at each time instant, all the necessary information regarding the pointwise swelling velocity v_{sw} and the position of the gel-solvent $S(t)$ and the glassy-rubbery $R(t)$ interfaces (moving boundaries).

The boundary condition for the fluconazole concentration c_F at the glassy-rubbery interface $z = R(t)$ is the Stefan condition

$$(c_F - c_{Ff}^0)\frac{dR(t)}{dt} = J_F \qquad at \quad z = R(t) \tag{17}$$

where c_{Ff}^0 is the fluconazole concentration in its free form (not complexed), supposed uniform in the dry film. Moreover, a perfect sink condition $c_F = 0$ is assumed at $z = S(t)$, supported by the large volume of solvent solution (500 mL) and the good mixing induced by paddle rotation.

The total amount of drug M_t, released up to time t, is evaluated as

$$M_t = A\int_0^t D_F \frac{\partial c_F}{\partial z}\Big|_{S(t'),t'} dt' = A\left(c_{Ff}^0 L_0 - 2\int_{R(t)}^{S(t)} c_F(z',t)dz'\right) \tag{18}$$

A and L_0 being the thin dry film surface area and initial thickness, respectively.

In the case when the fluconazole is included in the film as the complex Flu/HP-β-CD, we assume that a small amount of fluconazole $AL_0c^0_{Ff}$ is initially present in the film in its free form, while a larger amount $AL_0c^0_{Fc}$ is present as a complex Flu/HP-β-CD. The fluconazole in its free form is released according to the model equations Equations (16) and (17), with initial concentration $c^0_{Ff} = \epsilon c^0_F$ and diffusivity D_F. The parameter $\epsilon < 1$ represents the partition coefficient between the free and the complexed forms. The larger amount of fluconazole $AL_0c^0_{Fc} = AL_0(1-\epsilon)c^0_F$ is released as a complex and therefore its release kinetics is controlled by the same transport equation and the same diffusivity $D_{Fc} = D_{CD}$ adopted for cyclodextrin in the swelling film, presented in Section 3.1.

In this case, the total amount of drug released up to time t must be evaluated as

$$M_t = A\int_0^t D_F \frac{\partial c_F}{\partial z}\Big|_{S(t'),t'} dt' + A\,\rho_{CD}(1-\epsilon)\frac{MW_F}{MW_{CD}}\int_0^t D_{CD}\frac{\partial \phi_{CD}}{\partial z}\Big|_{S(t'),t'} dt' \tag{19}$$

where $\rho_{CD} \simeq 1.41$ g/cm^3 is the density of HP-β-CD, $MW_F = 306.27$ g/mol and $MW_{CD} = 1541.5$ g/mol are the molecular weights of Flu and HP-β-CD, respectively.

4. Results and Discussion

4.1. Rheological, Mechanical and Mucus-Adhesion Properties

OTFs were produced by the solvent casting technique. This technique requires the initial deposition and successive spreading of the polymeric solution on a solid support. As a consequence, the viscosity of the starting polymeric solution strongly influences the quality and properties of the final product.

Rheological properties of GG-Gly films were already investigated in our previous study [13] and briefly reviewed here. To avoid casting defects within the dried products, 2% w/v gellan gum was selected as the optimal polymer concentration for the film preparation, as it could be freely and homogeneously spread and leveled in the silicone tray molds. However, after drying, GG solutions at 2% w/v formed very brittle films, difficult to remove from the silicone molds. For this reason, different amounts of glycerol, ranging from 0.5% to 6% w/v, were added to 2% w/v GG solutions. It was observed that, irrespective of the amount of plasticizer used, all the investigated GG-Gly mixtures showed almost the same flow curves as the pure GG 2% w/v solution, i.e., a viscosity ranging from 1 to 0.1 Pa·s in the range of shear stresses $[10^{-2} \div 10^3]$ s^{-1}. The effect of the plasticizer on the gelation process of the polymer was also studied. It was observed that the gelation temperature slightly shifted from 50 to 52 °C when glycerol was added to GG solutions, from 0.5% to 6% w/v.

In the present study, the influence of the addition of HP-β-CD to the GG-Gly mixture and on the resulting thin films was addressed in detail. No significant differences were observed on the viscosity as well as on the gelation temperature when 1.3 % w/v of HP-β-CD was added to the GG-Gly mixture. Film thickness resulted in a monotonically increasing function of the glycerol content, with an increase of about 20% when HP-β-CD are included, as shown in Figure 2, where data from the previous experimental campaign on GG-Gly films without cyclodextrins [13] are reported together with new data for GG-Gly films including HP-β-CD.

Films were also subjected to tensile tests, in order to evaluate the influence of HP-β-CD on mechanical properties [36], i.e., elastic modulus, stress and deformation at break, shown in Figure 3A–C for increasing values of % Gly. Indeed, Figure 3A–C report data from the previous experimental campaign on GG-Gly films without cyclodextrins [13] together with new data for GG-Gly films including HP-β-CD.

Experimental results show that the addition of 1.3% w/v of HP-β-CD in the formulation slightly influences the mechanical properties, in terms of a small decrease in the stress (less than 10% for 3% Gly films) and deformation at break (less than 25% for 3% Gly films). This can be due to the formation of interactions, such as hydrogen bonds, between the cyclodextrin and the gellan gum that reduce

the mobility of the polymer chains, causing an increase in the elastic modulus and a decrease in the capacity of deformation, thus leading to the formation of a more rigid and less resistant material.

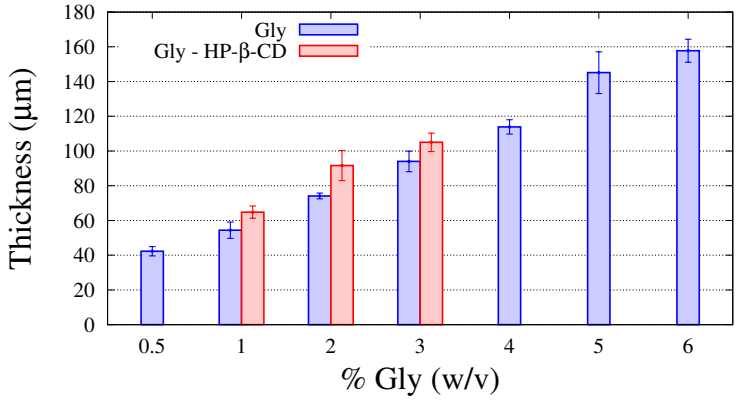

Figure 2. Film thickness for increasing amounts of glycerol, % Gly (w/v), with and without hydroxypropyl-β-cyclodextrin (HP-β-CD).

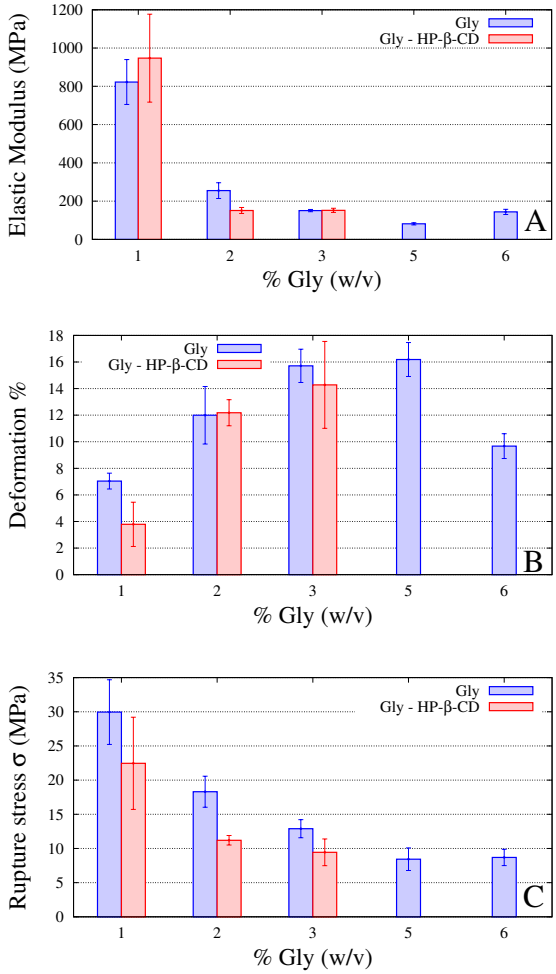

Figure 3. Elastic modulus (**A**), deformation (**B**) and stress (**C**) at break of films for increasing amounts of glycerol, % Gly (w/v), with and without HP-β-CD.

The histograms in Figure 3A–C also show data for film without HP-β-CD and higher Gly content, namely Gly 5% w/v and Gly 6% w/v. This is to show that films with 2%Gly and 3%Gly including HP-β-CD exhibit mechanical properties slightly better than that of 6%Gly film, especially for the

deformation at break, for example, greater than 45 % for 3% Gly+HP-β-CD with respect to that for 6% Gly.

The presence of HP-β-CD has a very relevant influence on the mucoadhesion properties of the gel. A film suitable for buccal drug administration has to remain at the application site for a time long enough to perform the therapeutic effect, so that the mucus adhesiveness of the formulation is a fundamental property for this type of formulation. The average values of the mucoadhesion strength were obtained by measuring the force necessary to detach the film from a mucin tablet and shown in Table 1.

Table 1. Mucoadhesion strength (N).

Film	GG-1%Gly	GG-2%Gly	GG-2% Gly-HP-β-CD	GG-6%Gly
Strength (N)	0.5782 ± 0.0014	0.1274 ± 0.0016	0.6762 ± 0.0012	0.0052 ± 0.0014

Mucoadhesion is due to the formation of hydrogen bonds between the carboxyl of glucuronic acid and the hydroxyl groups of the gellan gum and the appropriate H-group donor/acceptor groups of the mucin [37]. The mucoadhesion decreases progressively as the amount of plasticizer increases. Considering the formation of hydrogen bonds as the most relevant adhesion mechanism, the decrease in mucoadhesion strength as the plasticizer concentration increases is probably due to the onset of weak interactions between glycerol and gellan gum, which causes a progressive decrease in the interactions between gellan gum and mucin, with consequent loss of mucoadhesive strength. In the formulations containing cyclodextrin, a net increase of the mucoadhesive strength is observed with respect to the film with the same glycerol concentration. It is likely that cyclodextrin, having free hydrophilic groups in its external structure, is able to establish hydrogen bonds with mucin, increasing the mucoadhesive characteristics of the formulation.

4.2. Fluconazole Content Uniformity

The fluconazole content uniformity has been investigated for GG-2%Gly films including HP-β-CD and for GG-6%Gly films without HP-β-CD, i.e., for two formulations for which no drug precipitation occurs. Experimental results are 0.482 ± 0.005 mg/cm^2 for GG-6%Gly film and 0.488 ± 0.024 mg/cm^2 for GG-2%Gly films including HP-β-CD. The drug content uniformity is quite satisfactory as well as the loading capacity for both formulations.

4.3. Analysis of Phase Solubility of Fluconazole with HP-β-CD

Figure 4 shows the phase solubility plot, i.e., fluconazole concentration at saturation c_F [mol/L] vs. cyclodextrin concentration c_{CD} [mol/L]. The system exhibits an AL type solubility curve [23] characterized by the linear behavior.

$$c_F = \alpha + \beta\, c_{CD}\,, \quad \alpha = 0.02821 \pm 0.0001841\ [\text{mol/L}]\,, \quad \beta = 0.5911 \pm 0.04201\ [\text{ad}] \tag{20}$$

with a slope β lower than unity. This indicates the formation of a 1:1 complex fluconazole/HP-β-CD. Indeed, the cyclodextrin cavity has selectivity for the two triazole rings and for the di-fluoro-phenyl ring, while the three sp^3 hybridized carbon atoms that connect the triazole groups guarantee good flexibility to the molecule [38]. According to this hypothesis, a complexation equilibrium constant $K_{1:1}$

$$K_{1:1} = \frac{\beta}{\alpha(1-\beta)} = 51.237\,[(\text{mol/L})^{-1}] \tag{21}$$

has been estimated as in Brewster and Loftsson [39].

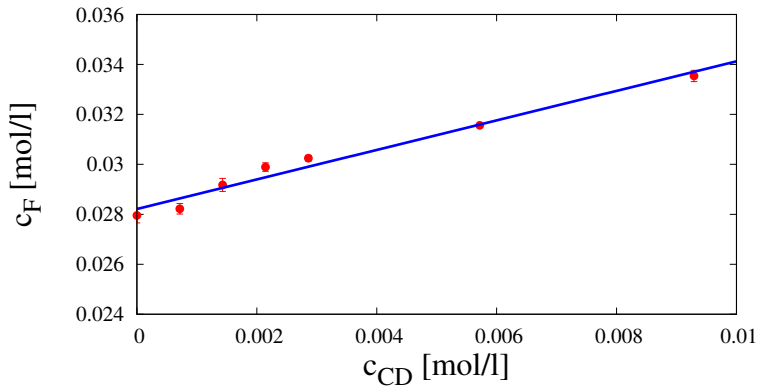

Figure 4. Phase solubility diagram of fluconazole with HP-β-CD in distilled water at T = 37 °C.

4.4. Analysis of Swelling Tests

Figure 5A shows the results of dynamic swelling tests in simulated saliva (pH 6.7) for films with and without HP-β-CD. The arrow indicates increasing content of Gly in the film. In agreement with what was already observed in our previous work [13], the equilibrium value $Q_{eq} = Q(\infty)$ is reached within 20 min and decreases for increasing amount of Gly. A further decrease of Q_{eq} is observed when HP-β-CD is included in the formulation. However, it should be taken into account that both Gly and HP-β-CD can diffuse out from the film, towards the swelling medium, during the course of the swelling process.

Since no degradation or erosion occurred, one can assume that, when the swelling equilibrium is reached, the swollen film is composed exclusively by solvent (absorbed plus that initially present in the dry film) and polymer. Starting from this assumption, the film weight at equilibrium $W_{eq} = W(\infty)$ can be expressed as

$$\frac{W_{eq}}{W_0} = 1 + Q_{eq} = \frac{W_{as}(\infty) + W_s^0 + W_{GG}}{W_0} \tag{22}$$

where $W_{as}(\infty)$ is the weight of the absorbed solvent at equilibrium, W_s^0 and W_{GG} are the amounts of solvent and gellan gum in the dry film. Since no erosion occurs, W_{GG} is constant during the swelling process. Equation (22) can be further rearranged to obtain the following expression for the amount of absorbed solvent $W_{as}(\infty)$ at equilibrium, rescaled onto the polymer weight W_{GG}

$$\frac{W_{as}(\infty)}{W_{GG}} = (Q_{eq} + 1 - \alpha)\left(\frac{W_0}{W_{GG}}\right) - 1 = (Q_{eq} + 1 - \alpha)\frac{(1 + \beta + \gamma)}{(1 - \alpha)} - 1 \tag{23}$$

$$\alpha = \frac{W_s^0}{W_0} = 0.12, \quad \beta = \frac{W_{Gly}^0}{W_{GG}} \in [0.25 \div 3], \quad \gamma = \frac{W_{CD}^0}{W_{GG}} = 0.65 \tag{24}$$

where W_{Gly}^0 and W_{CD}^0 are the amounts of Gly and HP-β-CD in the dry film, respectively. The value of $\alpha = 0.12 \pm 0.02$ has been estimated from thermogravimetric curves as reported in our previous study [13] and is almost independent of the amount of Gly in the formulation. The parameter β is the weight ratio Gly:GG ranging from 0.25:1 to 3:1 (w/w). The parameter γ is the weight ratio HP-β-CD:GG, equal to 78:120 (w/w) when HP-β-CD is included in the formulation.

Points in Figure 5B show experimental data for $W_{as}(\infty)/W_{GG}$, evaluated from Equation (23) for OTFs with and without HP-β-CD. The arrow indicates increasing content of Gly, i.e., increasing values of β. It can be observed that the amount of absorbed solvent increases for increasing values of β and a further increase is observed when HP-β-CD is included in the formulation.

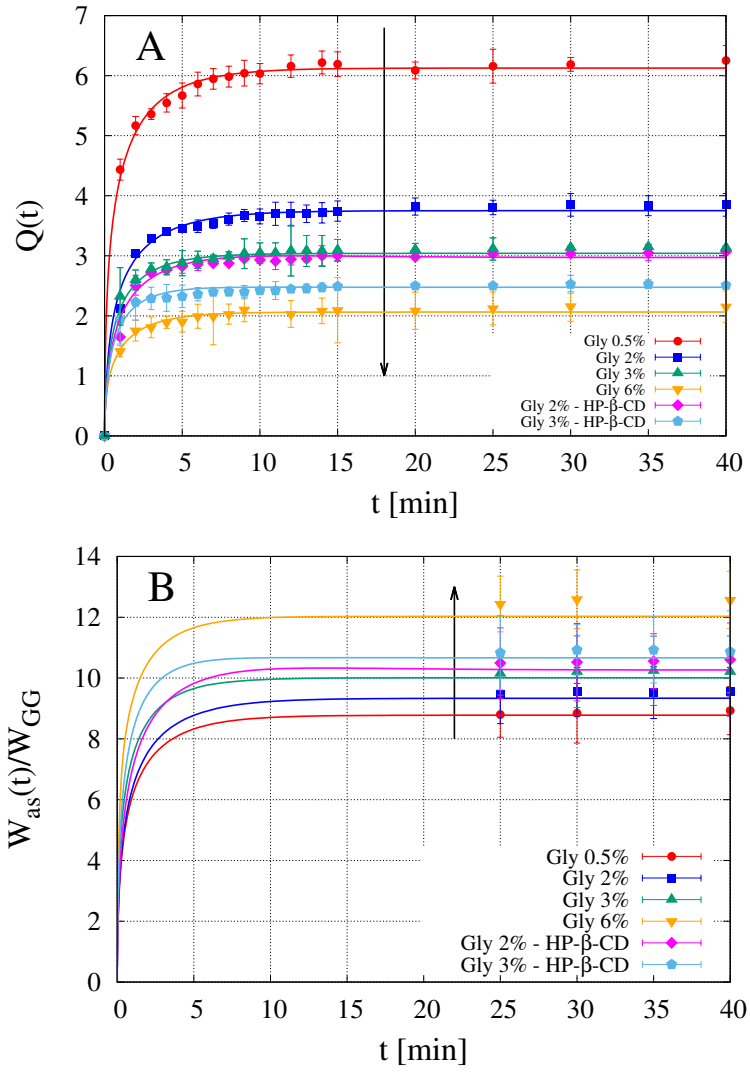

Figure 5. Dynamic swelling data in simulated saliva (pH = 6.7) at T = 37 °C for GG-Gly films with and without HP-β-CD. Continuous lines represent model predictions. The corresponding diffusivity values D_s and D_{CD} are reported in Table 2. (**A**) $Q(t) = (W(t) - W_0)/W_0$ vs. t; (**B**) rescaled amount of absorbed water as a function of time. Points represent the asymptotic experimental values evaluated from Equation (23).

A higher capability of absorbing solvent corresponds to a higher solvent diffusivity D_s in the swelling film. This can be assessed through the application of the swelling model described in Section 3.1. Indeed, the simple visual inspection of the rate of growth of the solvent uptake $Q(t)$ could be misleading, being it related not only to D_s but also to the initial film thickness L_0 (different for different OTF compositions) and to release rates of Gly and HP-β-CD (if present).

The swelling model for GG-Gly films not including HP-β-CD requires the estimate of three parameters, i.e., equilibrium solvent volume fraction ϕ_{eq}, the glassy-rubbery transition solvent volume fraction ϕ_{glassy} and the effective solvent diffusivity D_s. For films including HP-β-CD, the model also requires the estimate of the HP-β-CD effective diffusivity D_{CD}.

The equilibrium solvent volume fraction ϕ_{eq} can be directly estimated from the experimental asymptotic values of Q_{eq}. Indeed, by assuming that the fully swollen film is exclusively made by solvent and polymer, the film volume V_{eq} and weight W_{eq} at equilibrium can be expressed as

$$V_{eq} = \frac{W_{GG}}{\rho_{GG}\,(1 - \phi_{eq})} \tag{25}$$

$$W_{eq} = W_0(1 + Q_{eq}) = W_0(\rho_s \phi_{eq} V_{eq} + W_{GG}) \quad (26)$$

By replacing Equation (25) into Equation (26), one arrives to the following expression for ϕ_{eq}

$$\phi_{eq} = \frac{1}{1+\delta}, \quad \delta = \frac{\rho_{GG}}{\rho_s}\left((1+Q_{eq})(\frac{W_0}{W_{GG}}) - 1\right) = \frac{\rho_{GG}}{\rho_s}\left((1+Q_{eq})\frac{(1+\beta+\gamma)}{(1-\alpha)} - 1\right) \quad (27)$$

where $\rho_s = 0.998\ \mathrm{g/cm^3}$ and $\rho_{GG} = 0.55\ \mathrm{g/cm^3}$ are the densities of solvent and gellan gum, respectively. The resulting value of ϕ_{eq}, evaluated from Equation (27) and from the experimental values of Q_{eq}, is $\phi_{eq} = 0.85 \pm 0.02$ for films with and without HP-β-CD and is independent of the amount of Gly, thus confirming the basic assumptions.

The glassy-rubbery transition solvent volume fraction ϕ_{glassy} has been set to $\phi_{\mathrm{glassy}} = 0.3$ significantly larger than $\phi_0 \in [0.07 \div 0.1]$ for all the different formulations. Moreover, model results exhibit very low sensitivity to ϕ_{glassy} because this parameter mainly controls the time required for the disappearance of the glassy phase, a phenomenon that is very fast (less than one minute) if compared to the time scale (20 min) for complete swelling.

Continuous lines in Figure 5A show model results for $Q(t)$ in excellent agreement with experimental data (points). Continuous lines in Figure 5B show model results for the temporal evolution of the amount of absorbed solvent $W_{as}(t)/W_{GG}$ in agreement with asymptotic experimental data (points) evaluated from Equation (23).

The values of solvent diffusivities D_s adopted in the swelling model are reported in Table 2 and plotted in Figure 6 as a function of the glycerol volume fraction ϕ^0_{Gly} in the dry film.

Table 2. Solvent diffusivity $D_s \times 10^{10}$ [$\mathrm{m^2/s}$] and HP-β-CD diffusivity $D_{CD} \times 10^{10}$ [$\mathrm{m^2/s}$] in oral thin films (OTFs) with and without HP-β-CD.

	0.5% Gly	2%Gly	2%Gly-HP-β-CD	3%GLy	3%Gly-HP-β-CD	6%Gly
D_s	1.35 ± 0.05	3.3 ± 0.5	3.4 ± 0.2	5.2 ± 0.5	5.3 ± 0.4	11.5 ± 0.8
D_{CD}	-	-	0.45 ± 0.06	-	0.69 ± 0.05	-
D_F	-	0.92 ± 0.08				3.02 ± 0.25

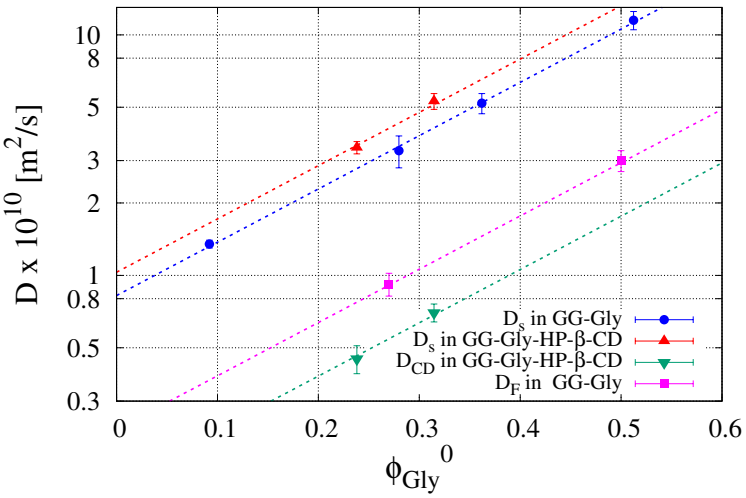

Figure 6. Log-normal plot of solvent diffusivity $D_s \times 10^{10}$ [$\mathrm{m^2/s}$], HP-β-CD diffusivity $D_{CD} \times 10^{10}$ [$\mathrm{m^2/s}$] and fluconazole diffusivity $D_F \times 10^{10}$ [$\mathrm{m^2/s}$] vs. glycerol volume fraction ϕ^0_{Gly} in the dry film. Dashed lines represent the exponential behavior $D \sim \exp(5.1\,\phi^0_{Gly})$.

It can be observed that the solvent diffusivity D_s is an increasing function of the Gly content. The presence of HP-β-CD is responsible for a very small further increase of D_s. HP-β-CD diffusivity in the swelling film is one order of magnitude smaller than D_s and even smaller than glycerol diffusivity, Equation (14). Therefore, the glycerol is released very rapidly from the swelling film, as expected for a small molecule highly soluble in water, while HP-β-CD release occurs during the entire course of the swelling process.

The solvent diffusivity D_s and the HP-β-CD diffusivity exhibit a well defined exponential behavior as a function of ϕ^0_{Gly}

$$D_s[\mathrm{m}^2/\mathrm{s}] = 8.24 \times 10^{-11} \exp\left(5.1\,\phi^0_{Gly}\right), \quad D_{CD}[\mathrm{m}^2/\mathrm{s}] = 1.37 \times 10^{-11} \exp\left(5.1\,\phi^0_{Gly}\right) \tag{28}$$

characterized by the same dimensionless exponent ($\simeq 5.1$), as shown in Figure 6. This is reasonably due to the fast loss of the plasticizer that facilitates the solvent penetration as well as the HP-β-CD diffusion.

The results of the swelling model represent the starting point for the subsequent analysis of release data in USP II apparatus. The estimated value of HP-β-CD diffusivity in GG-2%Gly-HP-β-CD film is assumed as the effective diffusivity D_{Fc} of the complex Flu/HP-β-CD in the swelling film.

4.5. Analysis of Release Kinetics in Usp II (Paddle) Apparatus

Figure 7A shows experimental release data of fluconazole from different OTFs. The first two experiments (red squares and blue triangles) refer to fluconazole release from GG-6%Gly and GG-2%Gly films. Orange diamonds refer to GG-2%Gly films in which the mixture made by fluconazole and HP-β-CD is added to the casting solution and not the preformed complex Flu/HP-β-CD as in the fourth set of release data (magenta circles). Different formulations correspond to different initial thicknesses L_0 of the dry films and therefore to different diffusional pathways for fluconazole to be released from the swelling film. For this reason, for a better comprehension of the release kinetics, experimental release data are shown in Figure 7B as a function of the rescaled dimensionless time $\tau = tD^0_F/L^2_0$ where $D^0_F = 5.89^{-10}$ [m^2/s] is the fluconazole diffusivity in water at 37 °C [40] that is assumed as a reference diffusivity.

Figure 7B clearly shows that drug release is significantly faster for GG-6%Gly film, as expected from the larger solvent diffusivity and swelling rate. Slower and almost overlapping release curves are obtained from GG-2%Gly film without HP-β-CD and that including the mixture fluconazole/HP-β-CD. Indeed, the phase-solubility study highlighted that the complexation equilibrium is reached in 72 h whereas only 5.5 h are used to solubilize the solution before casting. This time could not be sufficient to achieve the complexation equilibrium and therefore the fluconazole is included in its free form in both formulations, characterized by almost the same solvent diffusivity (see Table 2). The real difference between the two formulations was that the presence of HP-β-CD prevented the precipitation of fluconazole, which instead occurred in the first few hours after the preparation of the GG-2%Gly film without HP-β-CD. A significant slow down of the release kinetics is observed for GG-2%Gly film including the complex Flu/HP-β-CD, it being controlled by the release kinetics of HP-β-CD, in turn controlled by the low HP-β-CD diffusivity in the swelling film. Indeed, the 80% release is attained after 5 min, while it takes less than two minutes in the GG-6%Gly film.

Continuous lines in Figure 7A,B represent model predictions as obtained from the numerical integration of the release model developed in Section 3.2. The model was preliminarily applied to fluconazole release data from GG-6%Gly and GG-2%Gly films to estimate the effective diffusivity of fluconazole in its free form (not complexed). Indeed, this is the only parameter of the model since solvent diffusivity D_s was preliminarily estimated from dynamic swelling experiments.

Fluconazole diffusivities are reported in Table 2 and plotted in Figure 6 in order to show that they exhibit the same exponential dependence on the glycerol volume fraction ϕ^0_{Gly} as D_s and D_{CD}. Fluconazole diffusivity in GG-6%Gly swelling films is about half of that in the pure solvent solution D^0_F while it reduces to $D^0_F/6$ in GG-2%Gly films. In GG-2%Gly films, the effective diffusivity of fluconazole

in its free form is significantly higher (almost double) than HP-β-CD diffusivity D_{CD} in the same film. The diffusivity D_{Fc} of the complex fluconazole/HP-β-CD in GG-2%Gly films was assumed equal to D_{CD} and the two diffusivities D_F and D_{CD} were adopted to predict the release curve of fluconazole in GG-2%Gly films (magenta filled circles and continuous line). The only assumption made was that 25% of fluconazole is in its free form ($\epsilon = 0.25$ in Equation (19)) and diffuses out from the swelling film with diffusivity D_F while the complementary 75% is complexed and diffuses with diffusivity D_{CD}. This assumption is supported by the analysis of release data from the MFTD, where the release kinetics are significantly slower and can be monitored in detail with time due to the fast acquisition method adopted.

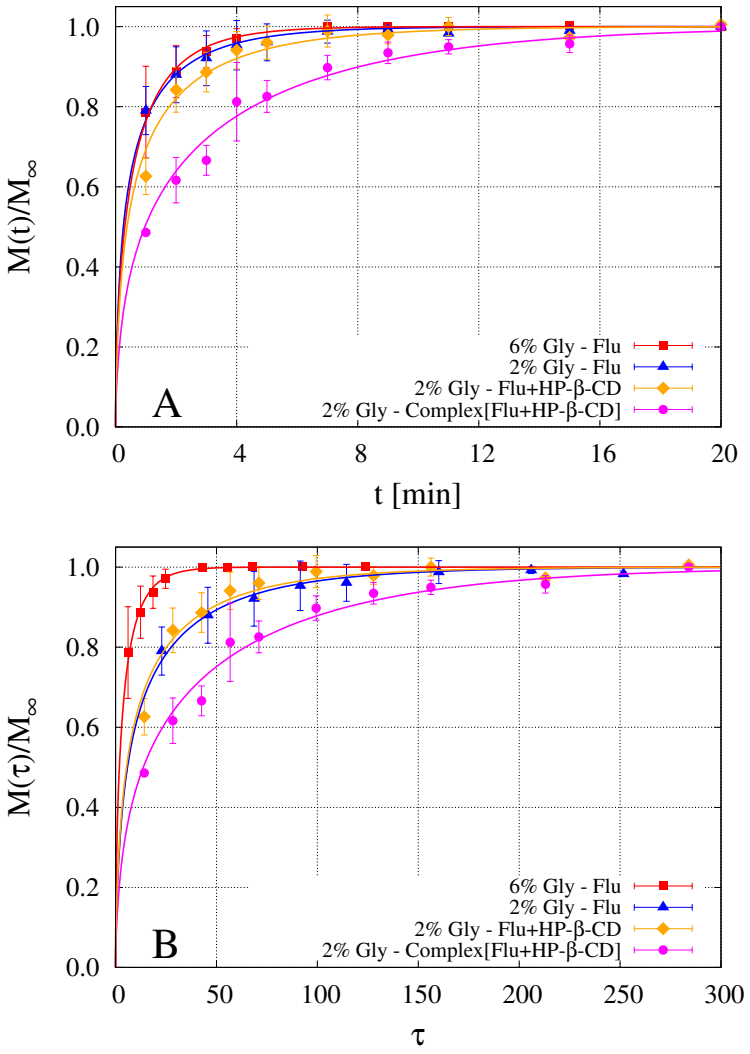

Figure 7. Release data of fluconazole from OTFs in USP II apparatus. Red squares: GG-6%Gly; blue triangles: GG-2%Gly; orange diamonds: GG-2%Gly including the mixture fluconazole/HP-β-CD; magenta circles: GG-2%Gly including the preformed inclusion complex Flu/HP-β-CD. Continuous lines represent model predictions. The corresponding diffusivity values D_F and D_{CD} are reported in Table 2. (**A**) $M(t)/M_\infty$ vs. time t [min]; (**B**) $M(\tau)/M_\infty$ vs. rescaled dimensionless time $\tau = tD_F^o/L_0^2$.

4.6. Analysis of Release Data from MFTD

Drug release tests of commercially available melatonin strips [22] and furosemide-loaded HPMC OTFs [16] were recently performed in the millifluidic flow-through device and compared with release curves obtained with the official USP XXXVII basket (USP I) and paddle (USP II) apparatuses. For flow rates comparable to salivary flow rates Q = 2–4 mL/min, the MFTD furnished release profiles were

significantly slower (approximately 10–15 min of delay) than that obtained with the other two methods. Also in the present case, we observed that the official method (USP II) significantly overestimated the release kinetics, and therefore underestimated the time for complete drug release, when compared to the millifluidic device.

Figure 8A,B show rescaled integral release curves M_t/M_∞ vs. t [min] as obtained with the USP II apparatus and with the MFTD with flow rates Q = 1–5 mL/min. Figure 8A shows release curves for GG-2%Gly films including the complex Flu/HP-β-CD while Figure 8B shows fluconazole release curves from GG-6%Gly films without HP-β-CD. Drug precipitation manifests itself in the form of dendritic aggregates within a few hours after the drying process is complete. The lower the Gly content, the faster the appearance of drug aggregates, in the absence of HP-β-CD. Fluconazole release in the MFTD occurs on time scales significantly longer than that required in the USP II apparatus. For this reason, we chose to compare release data from MFTD for 2% Gly films including HP-β-CD with 6% Gly films without HP-β-CD, in order to assure that release data were not affected, in any way, by drug precipitation on the time scales of the release process.

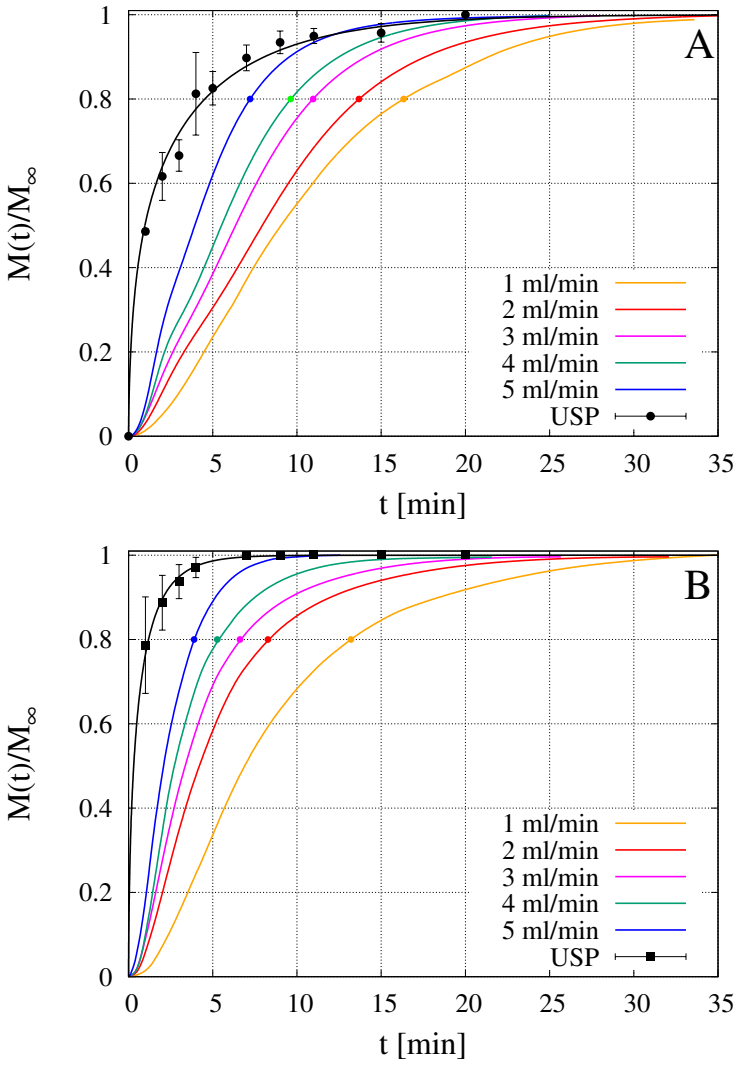

Figure 8. Rescaled integral release curves $M(t)/M_\infty$ vs. time t [min] of fluconazole in millifluidic flow-through device (MFTD) and USP II device. (**A**) GG-2%Gly films loaded with the preformed inclusion complex Flu/HP-β-CD; (**B**) GG-6%Gly films loaded with not complexed fluconazole.

For both formulations, release curves from the MFTD are extremely sensitive to the solvent flow rate Q and significantly slower than that from USP II apparatus. Indeed, the smaller is Q, the slower

is the release because the higher is the mass-transfer resistance at the gel-solvent interface. The time $t_{80\%}$ required for attaining the 80% release is reported in Table 3. For $Q = 2$ mL/min the time $t_{80\%}$ in MFTD is more than three times larger than that in USP II device for both formulations.

Table 3. Time $t_{80\%}$ [min] required for attaining the 80% release in the MFTD (Q = 1–5 mL/min) and USP II apparatus for two different film formulations: complex Flu/HP-β-CD in GG-2%Gly and Flu in GG-6%Gly.

Film	USP II	5 mL/min	4 mL/min	3 mL/min	2 mL/min	1 mL/min
complex in GG-2%Gly	4.58	7.21	9.62	10.96	13.67	16.33
Flu in GG-6%Gly	1.22	3.89	5.26	6.62	8.27	13.2

By comparing the two formulations, it can be observed that, despite the larger thickness of GG-6%Gly films, fluconazole release from GG-6%Gly films is faster than that from GG-2%Gly films including the complex Flu/HP-β-CD. This can be explained by considering two factors: (1) the higher solvent diffusivity D_s in GG-6%Gly films, corresponding to a higher swelling rate and (2) the higher diffusivity D_F of fluconazole in its free form with respect to the diffusivity D_{Fc} of the complex Flu/HP-β-CD.

The slightly wigging behavior of the integral release curves shown in Figure 8A is due to the coexistence, in the dry film, of fluconazole in its free and complexed form. This can be readily verified by analyzing the behavior of the corresponding differential release curves $F(t)$ shown in Figure 9A. The presence of two peaks is indicative of two different time scales for the release of fluconazole. The first peak corresponds to the faster release of the fluconazole in its free form, while the second peak is associated to the slower release of the complex Flu/HP-β-CD. As a confirmation, the double peak disappears in the differential release curves from GG-6%Gly films (Figure 9B), where the entire amount of fluconazole is included in the dry film in its free form.

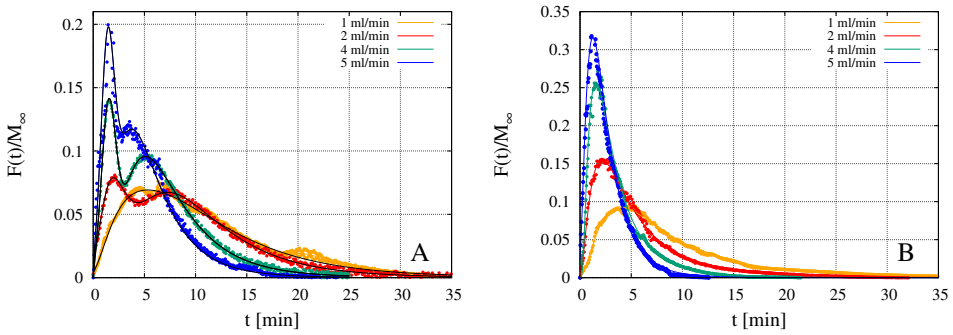

Figure 9. Rescaled differential release curves $F(t)/M_\infty$ vs. time t [min] of fluconazole in MFTD. (**A**) GG-2%Gly films loaded with the complex Flu/HP-β-CD. (**B**) GG-6%Gly films loaded with not complexed fluconazole. Continuous black lines in Figure A show the best-fitted bimodal function, Equation (29).

From the differential release curves shown in Figure 9A it is possible to estimate the fraction of fluconazole in its free (ϵ) and complexed form ($1 - \epsilon$). To this end, the differential release curves have been fitted with the following bimodal function

$$\frac{F(t)}{M_\infty} = \frac{F_F(t)}{M_\infty} + \frac{F_{Fc}(t)}{M_\infty} \tag{29}$$

linear superposition of two log-normal distribution functions

$$\frac{F_F(t)}{M_\infty} = \frac{\epsilon}{t\,\sigma_F\sqrt{2\pi}} \exp\left(-\frac{(\ln t - \mu_F)^2}{2\,\sigma_F^2}\right) \tag{30}$$

$$\frac{F_{Fc}(t)}{M_\infty} = \frac{(1-\epsilon)}{(t-\nu_{Fc})\,\sigma_{Fc}\sqrt{2\pi}} \exp\left(-\frac{(\ln(t-\nu_{Fc}) - \mu_{Fc})^2}{2\,\sigma_{Fc}^2}\right) \tag{31}$$

Continuous black lines in Figure 9A show the excellent capability of the bimodal function Equation (29) to describe the two peaks and the long exponential tails of the differential release curves. The asymptotic exponential behavior $F(t)/M_\infty \sim \exp(-\lambda t)$ is highlighted in Figure 10A where the differential release curves for $Q = 2, 4, 5$ mL/min are plotted on a log-normal scale. It should be observed how the parameter λ, characterizing the exponential decay, is an increasing function of Q, being controlled by the mass-transfer resistance at the gel-solvent interface.

Figure 10B shows the behavior of the two contributions $F_F(t)/M_\infty$ (continuous lines) and $F_{Fc}(t)/M_\infty$ (dashed lines) separately, for $Q = 2, 4, 5$. Data for $Q = 3$ mL/min are not reported for the sake of clarity of the picture but actually analyzed. By observing that

$$\epsilon = \int_0^\infty \frac{F_F(t')}{M_\infty} dt' \tag{32}$$

the following values of the partition coefficient $\epsilon = 0.2857, 0.265, 0.248, 0.2876$ have been evaluated for $Q = 2, 3, 4, 5$ mL/min, respectively. Therefore an average value of 27.15% $\pm$ 1.87 is estimated as the fraction of fluconazole in its free form, in perfect agreement with the 25% assumed in Section 4.4 to obtain an excellent agreement between model prediction and the experimental release curve in USP II apparatus.

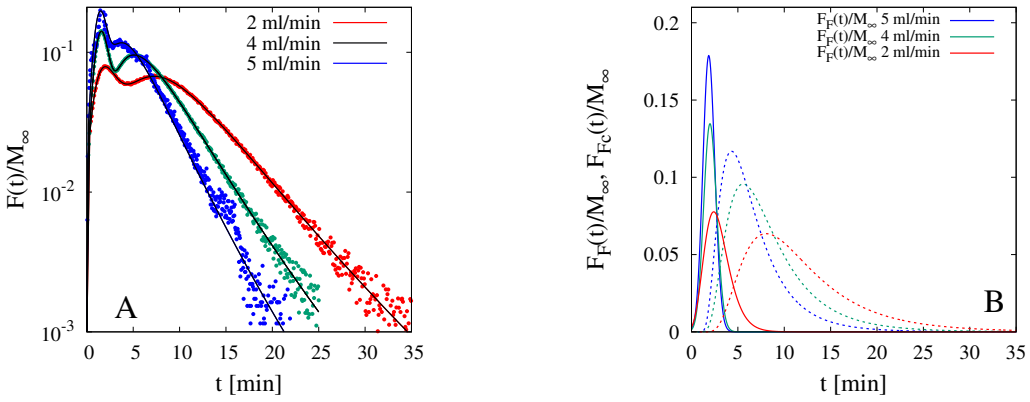

Figure 10. Analysis of rescaled differential release curves in MFTD for GG-6%Gly films loaded with the complex Flu/HP-β-CD. (**A**) Log-normal plot of $F(t)/M_\infty$ vs. t for $Q = 2, 4, 5$ mL/min. (**B**) $F_F(t)/M_\infty$ and $F_{Fc}(t)/M_\infty$ vs. t [min], Equation (29), for $Q = 2, 4, 5$ mL/min.

5. Conclusions

In this work gellan gum thin films containing low amounts of glycerol and hydroxypropyl-β-cyclodextrin are proposed as a suitable formulation for fluconazole buccal drug delivery. The inclusion of HP-β-CD prevents drug precipitation and significantly increases the mucoadhesive property of the film.

Dynamic swelling studies allowed us to estimate the effective solvent diffusivity D_s as well as the HP-β-CD diffusivity in the swelling film. Swelling data confirm that the small amount of HP-β-CD included in the formulation does not influence the solvent penetration. This result is in agreement with in-vitro drug release tests performed in the USP II apparatus, showing comparable release kinetics of fluconazole in GG-2%Gly films and GG-2%Gly films including an equimolar mixture of fluconazole

and HP-β-CD. On the contrary, the release kinetics significantly slows down when the preformed inclusion complex Flu/HP-β-CD is included in the GG-2%Gly formulation. This phenomenon is due to the low diffusivity of the complex in the swelling film, comparable to the HP-β-CD diffusivity, and perfectly predicted by the swelling-release model developed.

A more reliable estimate of fluconazole release kinetics from GG-Gly films is obtained from in-vitro release tests performed in a millifluidic flow-through device, which mimics mouth physiological conditions thanks to the laminar tangential solvent flow and flow rates comparable to salivary flow rates Q = 2–4 mL/min. Indeed, the time $t_{80\%}$ required for attaining the 80% of release, for Q = 2 mL/min, is more than three times larger than that in the USP II device for the two films, namely GG-6%Gly and GG-2%Gly including the complex Flu/HP-β-CD.

The high sampling rate of the drug outlet concentration in the MFTD allows us to have a very detailed description of the temporal evolution of the differential and integral release curves. Specifically, the differential release curve of fluconazole from GG-2%Gly including the complex Flu/HP-β-CD exhibits a peculiar double-peak behavior due to the coexistence, in the dry film, of the fluconazole in its free and complexed forms, characterized by very different effective diffusivities in the swelling film. The amount of fluconazole in its free (not-complexed) form has been estimated as about 27.15% of the total amount of drug initially loaded in the film.

Experimental results, supported by theoretical modeling, confirm that gellan gum-low glycerol thin films including HP-β-CD represent a suitable and interesting strategy to enhance the loading efficiency of OTF formulations for fluconazole buccal drug delivery, still keeping excellent physical properties. A sustained release is observed when GG-Gly film is loaded with a preformed complex fluconazole/HP-β-CD.

Author Contributions: Conceptualization, A.A., P.P., S.P. and M.A.C.; methodology, L.d.M., P.P., S.P. and M.A.C.; software, validation, L.d.M., J.T., C.B., P.P., S.P. and M.A.C.; formal analysis, A.A., P.P., S.P. and M.A.C.; investigation, A.A., L.d.M., J.T., C.B., P.P., S.P. and M.A.C.; resources, A.A. and P.P.; data curation, A.A. and L.D.M.; writing—original draft preparation, A.A., P.P., M.A.C.; writing—review and editing, A.A. and P.P.; visualization, A.A and S.P.; supervision, A.A. and P.P.; project administration, M.A.C.; funding acquisition, A.A., P.P. and M.A.C. All authors have read and agreed to the published version of the manuscript.

Funding: This research received no external funding.

Conflicts of Interest: The authors declare no conflict of interest.

References

1. Rouge, N.; Buri, P.; Doelker, E. Drug absorption sites in the gastro-intestinal tract and dosage forms for site-specific delivery. *Int. J. Pharm.* **1996**, *136*, 117–139. [CrossRef]
2. Pinto, J. F. Site-specific drug delivery systems within the gastro-intestinal tract: From the mouth to the colon. *Int. J. Pharm.* **2010**, *395*, 44–52. [CrossRef] [PubMed]
3. Patel, V.F.; Liu, F.; Brow, M.B. Advances in oral transmucosal drug delivery. *J. Control. Release* **2011**, *153*, 106–116. [CrossRef] [PubMed]
4. Madhav, N.V.S.; Shakya, A.K.; Singh, K. Oro-transmucosal drug delivery system: A review. *J. Control. Release* **2009**, *140*, 2–11. [CrossRef] [PubMed]
5. Dixit, R.P.; Puthli, S.P. Oral strip technology: Overview and future potential. *J. Control. Release* **2009**, *139*, 94–107. [CrossRef]
6. Hearnden, V.; Sankar, V.; Hull, K.; Jaras, D.V.; Greenberg, M.; Kerr, A.R.; Lockhart, P.B.; Patton, L.L.; Porter, S.; Thornhill, M.H. New developments and opportunities in oral mucosal drug delivery for local and systemic disease. *Adv. Drug Deliv. Rev.* **2012**, *64*, 16–28. [CrossRef]
7. Kathpalia, H.; Gupte, A. An introduction to fast dissolving oral thin film drug delivery systems: A review. *Curr. Drug Deliv.* **2013**, *10*, 667–684. [CrossRef]
8. Gilhotra, R.M.; Ikram, M.; Srivastava, S.; Gilhotra, N. A clinical perspective on mucoadhesive buccal drug delivery systems. *J. Biomed. Res.* **2014**, *28*, 81–97. [CrossRef]

9. Walsh, J.; Cram, A.; Woertz, K.; Breitkreutz, J.; Winzenburg, G.; Turner, R.; Tuleu, C. Playing hide and seek with poorly tasting pediatric medicines: Do not forget the excipients. *Adv. Drug Deliv. Rev.* **2014**, *73*, 14–33. [CrossRef]
10. Karkia, S.; Kim, H.; Na, S.J.; Shina, D.; Jo, K.; Lee, J. Thin films as an emerging platform for drug delivery. *Asian J. Pharm. Sci.* **2016**, *11*, 559–574. [CrossRef]
11. Borges, A.F.; Silva, C.; Coelho, J.F.J.; Simoes, S. Oral films: Current status and future perspectives: I-Galenical development and quality attributes. *J. Control. Release* **2015**, *206*, 1–19. [CrossRef] [PubMed]
12. Lee, Y.; Kim, K.; Kim, M.; Choi, D.H.; Jeong, S.H. Orally disintegrating films focusing on formulation, manufacturing process, and characterization. *J. Pharm. Investig.* **2017**, *47*, 183–201. [CrossRef]
13. Paolicelli, P.; Petralito, S.; Varani, G.; Nardoni, M.; Pacelli S.; Di Muzio, L.; Tirilló, J.; Bartuli, C.; Cesa, S.; Casadei, M.A.; et al. Effect of glycerol on the physical and mechanical properties of thin gellan gum films for oral drug delivery. *Int. J. Pharm.* **2018**, *547*, 226–234. [CrossRef] [PubMed]
14. Price, D.J.; Ditzinger, F.; Koehl, N.J.; Jankovic, S.; Tsakiridou, G.; Nair, A.; Holm, R.; Kuentz, M.; Dressman, J.B.; Saal, C. Approaches to Increase Mechanistic Understanding and Aid in the Selection of Precipitation Inhibitors for Supersaturating Formulations—A PEARRL Review. *J. Pharm. Pharmacol.* **2019**, *71*, 483–509. [CrossRef]
15. Kurkov, S.V., Loftsson, T. Cyclodextrins. *Int. J. Pharm.* **2013**, *453*, 167–180. [CrossRef]
16. Adrover, A.; Varani, G.; Paolicelli, P.; Petralito, S.; Di Muzio, L.; Casadei, M.A.; Tho, I. Experimental and Modeling Study of Drug Release from HPMC-Based Erodible Oral Thin Films. *Pharmaceutics* **2018**, *10*, 222. [CrossRef]
17. Quaglia, F.; Varricchio, G.; Miro, A.; La Rotonda, M.I.; Larobina, D.; Mensitieri, G. Modulation of drug release from hydrogels by using cyclodextrins: The case of nicardipine-β-cyclodextrin system in crosslinked polyethylenglycol. *J. Control. Release* **2001**, *71*, 329–337. [CrossRef]
18. Machín, R.; Ramón Isasi, J.; Vélaz, I. β-Cyclodextrin hydrogels as potential drug delivery systems. *Carbohydr. Polym.* **2012**, *87*, 2024–2030. [CrossRef]
19. Canbolat, M.F.; Celebioglu, A.; Uyar, T. Drug delivery system based on cyclodextrin-naproxen inclusion complex incorporated in electrospun polycaprolactone nanofibers. *Colloids Surfaces B Biointerfaces* **2014**, *115*, 15–21. [CrossRef]
20. Milcovich, G.; Antunes, F.E.; Grassi, M.; Asaro, F. Stabilization of unilamellar catanionic vesicles induced by β-cyclodextrins: A strategy for a tunable drug delivery depot. *Int. J. Pharm.* **2018**, *548*, 474–479. [CrossRef]
21. Peh, K.K.; Wong, C.F. Polymeric films as vehicle for buccal delivery: Swelling, mechanical, and bioadhesive properties. *J. Pharm. Pharm. Sci.* **1999**, *2*, 53–61.
22. Adrover, A.; Pedacchia, A.; Petralito, S.; Spera, R. In vitro dissolution testing of oral thin films: A comparison between USP 1, USP 2 apparatuses and a new millifluidic flow-through device. *Chem. Eng. Res. Des.* **2015**, *95*, 173–178. [CrossRef]
23. Higuchi, T.; Connors, K.A. Phase solubility techniques. *Adv. Anal. Chem. Instr.* **1965**, *4*, 117–122.
24. Petralito, S.; Zanardi, I.; Memoli, A.; Annesini, M.C.; Travagli, V. Solubility, spectroscopic properties and photostability of Rhein/cyclodextrin inclusion complex. *Spectrochim. Acta. Part Mol. Biomol. Spectrosc.* **2009**, *74*, 1254–1259. [CrossRef] [PubMed]
25. Sunil, S.; Jambhekar; Breen, P. Cyclodextrins in pharmaceutical formulations I, structure and physiochemical properties, formation of complexes, and types of complex. *Drug Deliv. Today* **2016**, *21*, 356–362.
26. Sunil, S.; Jambhekar; Breen, P. Cyclodextrins in pharmaceutical formulations II, solubilization, binding costant, and complexation efficiency. *Drug Deliv. Today* **2016**, *21*, 363–368.
27. Petralito, S.; Zanardi, I.; Spera, R.; Memoli, A.; Travagli, V. Spectroscopic characterization of both aqueous and solid-state Diacerhein/hydroxypropyl-β-cyclodextrin inclusion complexes. *Spectrochim. Acta Part A Mol. Biomol. Spectrosc.* **2014**, *127*, 355–360. [CrossRef]
28. Pedacchia, A.; Adrover, A. Study of release kinetics and diffusion coefficients in swellable cellulosic thin films by means of a simple spectrophotometric technique. *Chem. Eng. Res. Des.* **2014**, *92*, 2550–2556. [CrossRef]
29. Adrover, A.; Nobili, M. Release kinetics from oral thin films: Theory and experiments. *Chem. Eng. Res. Des.* **2015**, *98*, 188–211. [CrossRef]
30. Siepmann, J.; Peppas, N.A. Modeling of drug release from delivery systems based on hydroxypropyl methylcellulose (HPMC). *Adv. Drug Deliv. Rev.* **2001**, *48*, 139–157. [CrossRef]

31. Papanu, J.S.; Soane, D.S.; Bell, A.T.; Hess, D.M. Transport Models for swelling and dissolution of thin polymer films. *J. Appl. Polym. Sci.* **1989**, *38*, 859–885. [CrossRef]
32. Tu,Y.-O.; Ouano, A.C. Model for the Kinematics of Polymer Dissolution. *IBM J. Res. Dev.* **1977**, *21*, 131–142. [CrossRef]
33. Ranade, V.V.; Mashelkar, R.A., Convective Diffusion from a dissolving Polymeric Particle. *AIChE J.* **1995**, *41*, 666–676. [CrossRef]
34. Narasimhan, B.; Peppas, N.A. Molecular Analysis of Drug Delivery Systems Controlled by Dissolution of the Polymer Carrier. *J. Pharm. Sci.* **1997**, *86*, 297–304. [CrossRef]
35. D'Errico, G.; Ortona, O.; Capuano, F.; Vitagliano, V. Diffusion Coefficients for the Binary System Glycerol + Water at 25 °C. A Velocity Correlation Study. *J. Chem. Eng. Data* **2004**, *49*, 1665–1670. [CrossRef]
36. Preis, M.; Knop, K.; Breitkreutz, J. Mechanical strength test for orodispersible and buccal films. *Int. J. Pharm.* **2014**, *461*, 22–29. [CrossRef]
37. John, D.S. The basics and underlying mechanisms of mucoadhesion. *Adv. Drug Deliv. Rev.* **2005**, *57*, 1556–1568. [CrossRef]
38. Li, J.; Zhang, S.; Zhou, Y.; Guan, S.; Zhang, L. Inclusion complexes of fluconazole with β-cyclodextrin and 2-hydroxypropyl-β-cyclodextrin in aqueous solution: Preparation, characterization and a structural insight. *J. Incl. Phenom. Macrocycl. Chem.* **2016**, *84*, 209–217. [CrossRef]
39. Brewster, M.E.; Loftsson, T. Cyclodextrins as pharmaceutical solubilizers. *Adv. Drug Deliv. Rev.* **2007**, *59*, 645–666. [CrossRef]
40. Paolicelli, P.; Varani, G.; Pacelli, S.; Ogliani, E.; Nardoni, M.; Petralito, S.; Adrover, A.; Casadei, M.A. Design and characterization of a biocompatible physical hydrogel based on scleroglucan for topical drug delivery. *Carbohydr. Polym.* **2017**, *174*, 960–969. [CrossRef]

1.3.2 Mucoadhesive properties of OTFs and factors affecting mucoadhesion

Mucoadhesion is a critical parameter to consider during the formulation and production of buccal thin films. There are several theories that may explain the mucoadhesion process, but none is able to explain the overall mechanism. The wetting theory is one of the oldest theories and involves notions of thermodynamic work and contact angle. In this approach, bioadhesion is defined as the surface tension of the two adherent phases subtracted by their apparent interfacial tensions. On the other hand, the diffusion theory is associated with the possible relation between the polymeric chains and the glycoprotein mucin chains. According to this theory, semi-permanent bonds between the substrate and polymer adhesive chains may occur depending on the depth of the contact. Therefore, the molecular weight and crosslinking density of the polymer may have an impact on the diffusion coefficient. Other theories are associated with attractive forces mediated by electrons transference (electrostatic theory) or by chemisorption due to the formation of van der Waal's, hydrogen, and hydrophobic bonding (adsorption theory) and/or fracture strength (fracture theory) [7,132].

In general, mucoadhesion process can be divided into two stages. The first stage, also referred as contact stage, begins with the wetting of the mucoadhesive polymer by the mucus membrane followed by the establishment of several interactions between the polymeric chains and the mucus, including mechanical and physical interactions, hydrogen bonds, hydrophobic interactions, van der Waals interactions, electrostatic interactions, covalent bonding, and recognition of ligands. The created contacts are stabilized, and further interactions are encouraged in the second step, also known as consolidation stage [153].

The buccal adhesive strength of polymer thin films is affected by the nature of the polymer and surrounding media. The factors that influence mucoadhesion strength are summarized in Table 4 [61,132].

Table 4. Factors affecting muchoadesion

Polymer properties	
Hydrophilicity (Ability to form hydrogen bonds)	Presence of hydrophilic functional groups able to form hydrogen bond (COOH, OH, NH_2, etc.)
Molecular weight	Low-molecular-weight polymers penetrate the mucus layer better [59]. High molecular weight promotes physical entangling [57]. The optimum molecular weight is between 10^4

	and $4x10^6$ Daltons. Polymers with higher molecular weights will not moisten quickly to expose free groups for interaction with the substrate, while polymers with low molecular weights will form loose gels or will dissolve quickly [154]. For linear polymers, the mucoadhesion strength increases with increases in molecular weight. However, the effect of the molecular conformation should also be considered [155].
Concentration	Strong adhesive bond can be explained by the polymer chain length available for penetration into the mucus layer. When the concentration of the polymer is too low, the number of penetrating polymer chains per unit volume of the mucus is small, and the interaction between polymer and mucus is unstable. In general, the more concentrated polymer would result in a longer penetrating chain length and better adhesion. However, for each polymer, there is a critical concentration above which the polymer produces an "unperturbed" state due to a significantly coiled structure. As a result, the accessibility of the solvent to the polymer decreases, and chain penetration of the polymer is drastically reduced. Therefore, higher concentrations of polymers do not necessarily improve and, in some cases, diminish mucoadhesive properties [156].
Charge	Polymers with carboxyl groups show much stronger mucoadhesion than that of those with neutral groups [156]. Nonionic polymers appear to undergo less adhesion compared to anionic polymers. Peppas and Buri have demonstrated that strong anionic charge on the polymer is one of the required characteristics for mucoadhesion. It has been shown that some cationic polymers, such as chitosan, exhibit superior mucoadhesive properties, especially in a neutral or alkaline medium [157].
Flexibility of polymer chains and crosslinking density	Chain flexibility is critical for interpretation and entanglement of mucoadhesive polymers [59]. As water-soluble polymers become cross-linked, mobility of individual polymer chains decreases and thus the effective length of the chain that can penetrate the mucous layer decreases, which reduces bioadhesive strength [61].
Swelling	Hydration is required for a mucoadhesive polymer to expand and create a proper "macromolecular mesh" of sufficient size, and to induce mobility in the polymer chains in order to enhance the interpenetration process between polymer and mucin. Polymer swelling permits a mechanical entanglement by exposing the bioadhesive sites for hydrogen bonding and/or electrostatic interaction between the polymer and the mucous network. However, a critical degree of hydration of the mucoadhesive polymer exists where optimum swelling and bioadhesion occur [153,158,159].
	Environmental factors
pH	The pH of the microenvironment surrounding the mucoadhesive polymer can alter the ionization state and, therefore, the adhesion properties of a polymer. Mucus has a different charge density depending on pH due to difference in dissociation of functional groups on the carbohydrate moiety and the amino acids of the polypeptide backbone [59,155].
Applied strength	Pressure applied to the system for attachment affects the depth of diffusion of chains. It cannot be controlled for systems used in the GIT [154].
Initial contact time	Contact time between the bioadhesive and mucus layer determines the extent of swelling and interpenetration of the polymer chains. Moreover, bioadhesive strength increases as the initial contact time increases [160].
Presence of metal ions	Interaction with charged groups of polymers andor mucus can decrease the number of interaction sites and the tightness of mucoadhesive bonding [161].
	Physiological factors
Mucin turnover rate	Estimation of mucin turnover varies widely, depending on location and method of measurement. Values ranging from a few hours to a day have been reported. However, residence times of bioadhesives that are thought to attach to mucin are typically longer than the reported mucin turnover, suggesting that the presence of bioadhesive polymer on mucin may alter the turnover of this biopolymer. The residence time of dosage forms is limited by the mucin turnover time, which has been calculated to range between 47 and 270 min in rats and between 12 and 24 h in humans [162].
Disease state	Concomitant diseases can alter the physicochemical properties of mucus or its quantity (for example, hypo- and hyper-secretion of gastric juice), increases in body temperature, ulcer disease, colitis, tissue fibrosis, allergic rhinitis, bacterial or fungal infection, and inflammation [161].
Tissue movements	On consumption of liquid and food, speaking, peristalsis in the GIT [57,154].

However, even the excipients used for the formulation of buccal films might have an impact on their mucoadhesive properties. Our previous work, which investigated the effect of glycerol employed as plasticizer on GG-based OTFs, revealed the existence of a correlation between the amount of glycerol used in films' production and the mechanical and mucoadhesive properties of the obtained formulations. In the specific, these properties, which are of fundamental importance for the use of thin films as buccal delivery systems, were observed to undergo deterioration as a consequence of the plasticizer content increase. It was supposed that the worsening of OTFs mucoadhesive properties was due to the onset of weak interactions between glycerol and GG, which causes a progressive decrease in the contact between the film-forming polymer and mucin, thus leading to a loss in the mucoadhesive strength of the formulations [78].

It is widely believed that the adhesive qualities of polymeric materials undergo general weakening in wet environments such as the oral cavity, because the hydrophilic nature of polymers enables them to interact with water molecules, thus resulting in the formation of a weak boundary layer around the matrices which can prevent their direct contact with surfaces [163]. According to collision theory, the amount of adhesion junctions created depends on both the likelihood that two surface functional groups will come into contact with one another and the likelihood that those groups will connect once they do. However, polar and partially dissociated water molecules may shield the functional groups of polymers through van der Waals and Coulomb interactions making it difficult to form chemical bonds at the surface of the materials [164,165]. In other words, water can reduce the contact between functional groups, thus hindering the development of adhesive junctions which require more molecular collisions for the purpose of their formation. To improve the possibility of functional groups colliding and forming stable adhesion junctions, many physical techniques have been devised [164]. However, as is frequently the case, the solution to this issue has been revealed by the observation of phenomena that occur in nature. In particular, the adhesion mechanism of mussels, as marine organisms able to remain attached to any type of surface even in turbulent ocean environments and in extreme conditions, has aroused great interest among scientists, inspiring them in the design of novel bio-inspired materials with advanced adhesive properties. Although the exact mechanism underlying mussel adhesion is still not entirely understood, it is generally acknowledged that it relies on

the production of certain proteins, called Mussel foot proteins (Mfps), which are well known for curing rapidly leading to the production of sticky plaques with excellent interfacial binding strength, hardness, and durability. One of the key components of Mfps is 3,4-dihydroxyphenylalanine (L-Dopa), a catechol-based aminoacid obtained by post-translational hydroxylation of tyrosine. Dopa's catechol side chain can engage in a variety of chemical interactions and crosslinking processes, which gives Mfps the capacity to solidify *in situ* and adhere securely to a range of surface substrates [166]. To develop strong adhesive materials, natural Mfps from various species of mussels have been isolated and examined [167,168]. However, the direct use of these proteins for commercial applications is extremely difficult because it takes thousands of mussel specimens to extract only one gram of them [169], thus emphasizing the importance of designing synthetic and semi-synthetic polymers able to mimic their unique feature.

1.3.2.1 Catechol chemistry and the role of dopamine (DA) in the design of adhesive materials

Catechol groups feature a unique combination of hydroxyl groups and benzene ring which enable it to participate in various non-covalent (reversible) and covalent (irreversible) interfacial interactions (Figure 6) [163,170]. Catechol's dihydroxy functionality causes the formation of hydrogen bonds with hydrophilic surfaces promoting the absorption of catechol-containing materials into mucosal tissues [166], as well as coordination bonds with metal ions to generate strong and reversible complexes that have been exploited in the design of self-healing hydrogels [171-173], pH-responsive drug carrier [174], soft actuators [175,176], and mechanically reinforced polymeric fibers [177,178]. Catechol is also a perfect anchoring group for surface modification due to its ability to form strong and reversible interfacial connections also with metal oxide surfaces. However, this ability of binding to metal substrates is strongly influenced by the oxidation state of catechol, in fact when it is oxidized the binding strength drastically drop. On the other hand, the benzene ring is able to interact with other aromatic rings through π–π electron interaction, enhancing the cohesiveness of catechol-containing polymers and making it possible for them to adhere to surfaces that are rich in aromatic compounds [166]. Furthermore, they can establish cation–π interactions with positively charged ions, giving rise to one of the strongest non-covalent interactions found in wet

environments. This type of binding enhances absorption of catechol to charged surfaces and contributes to the cohesive properties of materials rich in both aromatic and cationic functional groups [179-181]. To form covalent bonds, catechol must first undergo oxidation, and this can happen both in the presence of molecular oxygen (auto-oxidation) or by the addition of chemical (e.g., sodium periodate) or enzymatic (e.g., tyrosinase, peroxidase) oxidants, thus resulting in the generation of highly reactive species such as semiquinones and quinones [166]. Semiquinone radicals have two possible fates: they can undergo radical aril-aril coupling causing the dimerization of catechol groups and resulting in the curing of catechol-containing polymers, or they can decay rapidly to form catechols and quinones [182]. The latter should be subjected to nucleophilic substitution reactions by amino and thiol groups widely expressed in biological surfaces, forming interfacial covalent bond, and ensuring a strong adhesion of catechol-materials to natural living tissues. The oxidative crosslinking of catechol is heavily dependent on multiple factors, including the type and concentration of oxidant as well as the pH value of the solution [166]. In the last case, it is well known that the increase in pH promotes the dissociation of the hydroxyl groups of catechols and, therefore, their conversion to quinones. Based on the above, it is evident that the adhesion of catechol-containing materials is strongly dependent on the oxidation state of the catechol moieties, which is a direct consequence of the pH conditions.

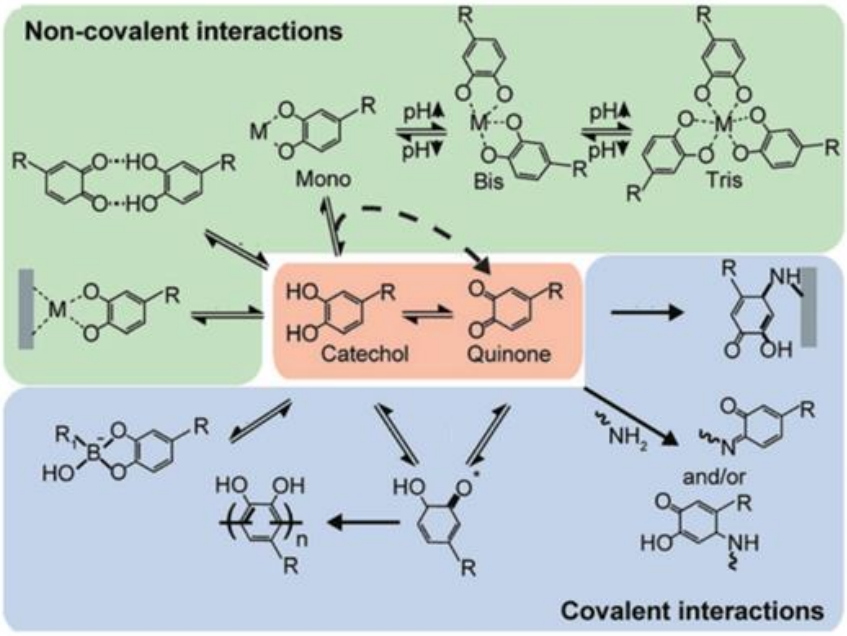

Figure 6. Schematic representation of non-covalent and covalent interactions of catechol groups [169].

Catechol polymers are generally designed using two major approaches: one of which involves the polymerization of catechol-containing monomers, while the other entails the derivatization of both natural and synthetic polymers with catechol-containing molecules [183]. Dopamine (DA), one of the most prevalent catecholamines in the human body, has played a significant role in the development of polymers with outstanding adhesive properties, due to the possibility of being exploited as a source of catechol groups in both aforementioned synthetic strategies. DA is subjected to oxidative polymerization under mildly alkaline conditions resulting in the formation of polydopamine (pDA), nowadays recognized as one of the main coating agents of a large variety of substrates, imparting them considerable adhesive strength and allowing their further functionalization through the immobilization of several biomolecules which can react with catechol and quinone moieties found in its chemical structure [184-186]. The primary amino group of DA, however, is also easily conjugated with the electrophilic groups present in the backbone of both natural and synthetic polymers.

DA-modified polymers are typically used as biological glues for both internal and external application, exhibiting superior biocompatibility and a higher adhesion strength than cyanoacrylates and fibrin glue, which is often regarded as the gold standard of tissue adhesives [187]. Additionally, GG-DA based injectable scaffolds have found a promising application for the release of cells in the treatment of retinal pigmented epithelium atrophy, which causes the macular degeneration responsible for visual disorders and, in the worst cases, permanent blindness [138]. In contrast to other natural polymers, however, the literature contains very limited information about the derivatization of GG with DA and its use for biological and pharmaceutical applications. To create a polymeric conjugate with potential adhesive capabilities, we decided to further explore the idea of chemically modifying the carboxyl groups of GG with DA.

Dopamine-modified gellan gum: from synthesis to the development of chemical hydrogels via catechol autoxidation

Chiara Brandelli[1,], Arianna Tarquini[1], Laura Di Muzio[1], Vito Cosimo Carriero[1], Jordan Trilli[1], Barbara Bigi[1], Claudia Sergi[2], Jacopo Tirillò[2], Stefania Petralito[1], Stefania Cesa[1], Maria Antonietta Casadei[1], Patrizia Paolicelli[1,*].*

[1] Department of Drug Chemistry and Technologies, Sapienza University of Rome, 00185 Rome, Italy

[2] Department of Chemical Engineering Materials Environment, Sapienza University of Rome, 00184 Rome, Italy

Correspondence: chiara.brandelli@uniroma1.it (C.B.); patrizia.paolicelli@uniro1.it (P.P.). Tel.: +39-06-4991-3173 (P.P.)

Abstract

The chemical modification of natural biopolymers with dopamine has aroused great interest as an alternative semi-synthetic approach for mimicking marine-inspired bioadhesion processes, providing substantial improvement over the adhesive and cohesive properties of the parent polymers. Among natural polymers, gellan gum (GG) has proven to be a promising material for biomedical applications due to its biocompatibility, interesting physicochemical properties, and availability of a large number of reactive groups that can be exploited for the production of semi-synthetic derivatives. However, the tissue adhesiveness of native and semi-synthetic GG and its networks remains problematic. In this work, the possibility to functionalize GG carboxyl groups with dopamine (DA) using the EDC and NHS chemistry was investigated. In specific, the effect of different parameters, such as the molar ratio COOH:EDC:NHS:DA, the reaction solvent and the purifying strategy applied, on the derivatization degree of the synthesized derivative (GGDA) was studied. Furthermore, the experimental conditions to promote oxidative cross-linking of GGDA chains without using additional oxidizing agents were identified and successfully exploited for the development of polymeric thin films with suitable properties for biomedical applications.

1. Introduction

Hydrogels are three-dimensional networks of hydrophilic polymer chains capable of absorbing and retaining large amounts of water and biological fluids [1-3]. They can swell significantly without dissolving due to the presence of chemical and/or physical cross-links that provide network structure and maintain macroscopic integrity. Depending on the functional groups available on the backbone of network-forming polymers and the cross-linking mechanism, hydrogels can be designed to have a variety of porous structures and mechanical resistance [4]. Furthermore, because of their high-water content, they also exhibit excellent biocompatibility and a high degree of elasticity and flexibility, which make them more closely resemble natural living tissues than most synthetic biomaterials [5-6]. Despite an impressive increase in the number of hydrogel formulations developed for biomedical and pharmaceutical applications, the achievement of strong and robust adhesion between hydrogels and solid materials in wet conditions, which is highly desirable for their integration and performance in medical devices and pharmaceutical systems, remains an ongoing challenge [4], severely limiting the full exploitation of hydrogel potential for biomedical purposes. To address this main drawback of traditional hydrogels, much work has been done in an effort to develop hydrogels with outstanding adhesion properties under wet conditions. As often happens, the most appealing approach to reach this goal derives from nature. Building on the impressive adhesive capacity of certain organisms in a wet environment, the development of more surface-adherent biomaterials has focused on biomimetic approaches. Particular focus has been paid to the molecular mechanisms mediating the adhesion of marine mussels to slippery surfaces. Their remarkable capacity to establish stable long-term attachment has been attributed to the production of adhesive proteins in adhesive pads, containing high levels of the catecholamine-rich amino acid 3,4-dihydroxy-L-phenylalanine (L-DOPA) [7]. Based on this observation, the premise of mimicking natural adhesion mechanisms has been explored using dopamine (DA) to improve the adhesive properties of hydrogels. Indeed, dopamine can easily polymerize to polydopamine (PDA) under mild conditions and this ability can be exploited using polydopamine as coating agent of bulk materials [8]. PDA coatings exhibit great adhesion onto a wide variety of surfaces [9] and the availability of numerous functional moieties in PDA structure enable further surface modifications by immobilization of

biomolecules and drugs [10,11]. PDA coatings have shown promising results in promoting the biointegration of medical implants [12], also representing an alternative approach to improve the biological properties of hydrogels with potential application in the tissue engineering field [13-15]. In recent years the use of DA as a source of catechol groups for the chemical modification of natural biopolymers has aroused a growing interest as an alternative semi-synthetic approach for mimicking marine-inspired bioadhesion processes, providing substantial improvement over the adhesive and cohesive properties of the parent polymers [7]. Indeed, the amino group of DA has been successfully attached to the carboxyl functions available on the backbone of natural polymers, including both polysaccharides [16-19] and polypeptides [20-23], via straightforward carbodiimides chemistry [24], resulting in the formation of stable amide bonds without affecting the gelling kinetics and mechanical properties of the resulting hydrogels [7]. Combining the advantages of natural polymers, such as biocompatibility, biodegradability, and intrinsic bioactivity along with the strong underwater adhesion mediated by catechol moieties, DA-modified natural polymers have established themselves as an attractive tool for the design of adhesive hydrogels, extending their potential in a variety of biomedical applications including tissue repair and regeneration [25-29], drug delivery [30-31], and cell encapsulation [32-33]. Among the naturally sourced polymers described in the literature for biomedical applications, gellan gum (GG), a *Sphingomonas elodea*-derived anionic polysaccharide, with a linear structure consisting of repeats of the tetra-saccharide D-glucose–D-glucuronic acid–D-glucose–L-rhamnose, has been presented as a promising biomaterial. Indeed, GG presents interesting physicochemical properties, biocompatibility and a versatile backbone that includes multiple reactive hydroxyl and carboxyl groups. Nevertheless, unmodified GG is severely limited by low aqueous solubility, inconvenient thermo-reversible gelation, and limited adhesiveness to biological structures. For this reason, GG has been modified to optimize its physicochemical and biological properties. However, the tissue adhesiveness of native and semi-synthetic GG hydrogels remains problematic, especially for applications that require integration of the hydrogels with surrounding structures [7]. Based on these findings, the possibility of chemically modifying the carboxyl groups of this natural polysaccharide with DA molecules via EDC/NHS coupling reaction has been investigated, paying particular attention to the effect of the

reaction solvent, such as double distilled water or DMSO, on the yield of GG derivation and on the properties of the synthesized derivatives (GGDA), and underlining the critical role of the purification strategy adopted in defining the amount of catechol groups covalently bonded to the polymer backbone. The obtained derivatives have been investigated for the possibility of developing GGDA-based hydrogels through oxidative cross-linking of catechol groups without using chemical oxidants. Covalent cross-linking induced by catechol oxidation is one of the often-applied catechol chemistry in designing adhesive hydrogels. Indeed, catechol can be easily oxidized in its reactive form resulting in the curing of catechol-containing polymers [34], while leading to strong adhesion to natural tissues through reaction with available nucleophile groups (e.g., -NH_2, -SH, imidazole) on tissues surfaces, resulting in the establishment of strong interfacial covalent bonds [34,35]. However, oxidative cross-linking is usually accomplished in the presence of chemical oxidants, such as sodium periodate, which could cause detrimental effects on normal cellular process, representing a problem for hydrogel implantation in the human body [36]. Although it is widely known that catechols spontaneously oxidize in the presence of oxygen [37], the data available on the polymerization of DA-modified natural polymers driven by catechol autoxidation are still very limited [36,38]. For this reason, we have studied the effect of variables such as the temperature and the solubilization time of GGDA, as well as the pH and concentration of the buffer used, on the oxidation of polymer-bound catechols, identifying the appropriate experimental conditions for the development of GGDA-based chemical hydrogels in the absence of additional oxidizing agents. The obtained hydrogels have been investigated for the formulation of GGDA-based thin films with suitable properties for biomedical and pharmaceutical applications.

2. Materials and Methods

2.1. Materials

All used reagents were of analytical grade. Low acetyl gellan gum (GG) Mn 1×10^6 Da, N-(3-dimethylaminopropyl)-N′-ethylcarbodiimide hydrochloride (EDC), N-hydroxysuccinimide (NHS), dopamine hydrochloride (DA), hydrochlorid acid (HCl), anhydrous dimethylsulfoxide (DMSO), dimethyl sulfoxide-d6 (DMSO-d6), deuterium

oxide (D_2O), tris-(hydroxymethyl)-aminomethan (TRIS base) and dialysis membranes (cut-off 12,000-14,000) were purchased from Sigma.

Double distilled water, potassium dihydrogen phosphate (KH_2PO_4) and sodium phosphate dibasic (Na_2HPO_4) were obtained from Carlo Erba Reagents.

2.2. Synthesis and characterization of GGDA derivatives

GG was functionalized with DA through EDC/NHS coupling reaction performed under N_2 atmosphere. In specific, 50 mL of double distilled water were used to dissolve 500 mg of GG (0.77 mmol of repetitive units) at 80.0±0.5°C for 1 h. Then, the temperature of the polymeric solution was lowered to 50.0±0.5°C and EDC and NHS were added and allowed to react for 10 min to enable the activation of GG carboxyl groups. After that, DA was added to the reaction mixture and the pH was adjusted to 5 by HCl 1N. Then, the solution was kept reacting under magnetic stirring at 50.0±0.5°C for 24 h. Two different molar ratios GG:EDC:NHS:DA were tested. In specific, a first attempt was performed using EDC (0.77 mmol, 148.2 mg), NHS (0.77 mmol, 89.0 mg) and DA (0.77 mmol, 146.7 mg) in an equimolar ratio to the GG carboxyl groups. Subsequently, maintaining constant COOH mmoles, the mmoles of reagents were doubled (EDC 1.54 mmol, 295.2 mg; NHS 1.54 mmol, 117.2 mg; DA 1.54 mmol, 292.1 mg).

The same synthetic procedure was carried out using DMSO as the reaction solvent. In this case, the solubilization of GG was performed at 80.0±0.5°C for 3 h and, following the addition of DA, the reaction mixture was kept reacting under magnetic stirring at 50.0±0.5°C per 24 h. The procedure was performed using a molar ratio COOH:EDC:NHS:DA equal to 1:2:2:2.

All the experimental applied conditions are summarized in Table 1.

Table 1. Experimental conditions of GG-DA synthesis.

	Molar ratio GG:EDC:NHS:DA	Solvent	Solubilization conditions	Activation time of COOH (min)	Reaction time (h)
$GGDA_1$	1:1:1:1	H_2O	80°C for 1 h	10	24
$GGDA_2$	1:2:2:2	H_2O	80°C for 1 h	10	24
$GGDA_3$	1:2:2:2	DMSO	80°C for 3 h	10	24

All synthesized polymers were purified by dialysis. To identify the most suitable purification method, GGDA derivatives were subjected to different dialysis procedure as shown in Table 2.

Table 2. Procedures applied to purify GGDA derivatives through dialysis.

GGDA$_1$	2 days against distilled water at 4°C
	7 days against distilled water at 4°C
	1 day against NaCl aqueous solution (0.5 M) and 6 days against distilled water at 4°C
GGDA$_2$	1 day against NaCl aqueous solution (0.5 M) and 6 days against distilled water at 4°C
GGDA$_3$	7 days against distilled water at 4°C
	1 day against NaCl aqueous solution (0.5 M) and 6 days against distilled water at 4°C
	6 days against distilled water (pH 5) and 1 day against distilled water at 4°C

The resulting solutions were frozen and then freeze-dried employing a LIO 5P freeze-dryer (5 Pascal, Italy) equipped with a vacuum pump Adixen (France). GGDA derivatives were stored in a calcium chloride desiccator protected from light with aluminum foil for further characterization.

2.3. Characterization of GGDA derivatives

UV-Vis spectroscopy and proton nuclear magnetic resonance (^{1}H-NMR) were used to evaluate the success of derivatization and purification of GGDA derivatives and to quantify the DA catechol groups grafted onto the polymeric backbone.

UV-Vis absorption spectra were recorded with a Perkin Elmer Lambda 40 UV-Vis spectrophotometer in the wavelength range 200-600 nm. The analyzed samples were prepared by solubilizing GGDA derivatives in a mixture H_2O/DMSO 1:4 *v*/*v*, used as reference, to obtain solutions with a concentration of about 0.5 mg/mL. The conjugation efficiency of DA to GG backbone was determined by measuring the absorbance of the resulting solutions at 280 nm, because the aromatic ring structure of conjugated catechol group exhibits absorption peak at this wavelength. For this regard, a DA calibration curve was generated by recording the absorbance values at 280 nm of standard DA solutions in the concentration range from 0.1 to 0.004 mg/mL, which were obtained by dilution from a 0.5 mg/mL DA stock solution.

^{1}H-NMR spectra were recorded with a Bruker AC-400 instrument (Germany) on samples prepared by dissolving proper quantities of GGDA conjugates in DMSO-d_6 supplemented with a specific amount of a nicotinamide solution in D_2O (1 mg/mL), used as an internal standard for determining the polymers derivatization degree (DD%), defined as the number of catechol groups every 100 repetitive units of GG.

2.4. Optimization of oxidative cross-linking conditions of GGDA derivative

$GGDA_3$ was chosen to identify the conditions required to promote an oxidative cross-linking of DA catechol groups in the absence of oxidizing chemicals. For this purpose, the polymeric derivative (2% *w*/*v*) was solubilized in TRIS buffer by varying the temperature and solubilization time as well as the pH and concentration of the buffer used. Table 3 provides a summary of the experiments performed.

The gelling capacity of the resulting polymer solutions was assessed by the vial tilting method. Then, the polymeric solutions were poured into suitable glass supports and stored at room temperature for 24 h.

Table 3. Optimization of $GGDA_3$ oxidative crosslinking conditions carried out on 2% *w*/*v* GGDA solutions.

Solubilization temperature (°C)	Solubilization time	TRIS buffer pH	TRIS buffer concentration (M)
50	Form 30 min to 6 h	7.4	0.01
70			
50	From 30 min to 2 h	8.5	0.01
70			
70	2 h	8.5	0.1

2.5. Rheological measurements

The rheological measurements were conducted using a Discovery TA HR-1 stress-control rheometer (TA Instruments, New Castle, DE, USA). A cone-plate geometry with a diameter of 40 mm (α 1.005°, gap 27 μm) was used for all the experiments [39].

Solutions of GG and $GGDA_3$ (2.0% *w*/*v*) were prepared solubilizing the polymers in TRIS buffer (pH 7.4 - 0.01M and pH 8.5 - 0.1M) at 70.0±0.1°C for 20 min under magnetic stirring. Then, the temperature of the polymeric solutions was decreased to 60.0±0.1°C for GG samples and 50.0±0.1°C for $GGDA_3$ samples. A small amount of the resulting solutions (0.5 mL) was promptly transferred on the Peltier plate of the rheometer, pre-

heated at 60°C or 50°C, and homogenized by pre-shearing at 1 rad/s for 1 min. Oscillatory temperature-sweep analysis were carried out by decreasing the temperature from 60.0 to 30.0°C for GG samples and from 50.0 to 25.0°C for $GGDA_3$ samples (cooling rate 3.0 ± 0.1 °C/min), maintaining a constant frequency of 1 Hz and a deformation of 1%, which was previously determined using oscillatory strain-sweep tests to assess the linear viscoelastic region of the polymers.

The crossover of the G' and G'' moduli was used to determine the gelation temperature of the polymers.

2.6. Thin films preparation

Thin films were produced using the solvent casting technique by solubilizing $GGDA_3$ (2% *w*/*v*) alone or in combination with glycerol (2% *w*/*v*), which was chosen as plasticizer [39-41], in 0.1 M TRIS buffer (pH 8.5) at 70.0±0.5°C for 2 h. After the removal of air bubbles, the resulting polymeric solutions were poured into suitable silicon supports (diameter 5.6 cm) and stored at room temperature for 24 h to allow the oxidative cross-linking of the polymer chains. Then, the obtained hydrogels were dried at a constant temperature of 40.0±0.5°C.

First attempts were performed using 6 mL of TRIS buffer and a drying time of 13 or 15 h. Subsequently, solutions of 8 mL were prepared and dried for 24 h.

2.7. Measurement of film thickness

The thickness of all the prepared films was measured by using the thickness gauge Mitutoyo Digimatic Micrometer (Mitutoyo Corporation, Lainate, Italy). The measurements were carried out in six different points of the same film to evaluate the homogeneity of the prepared samples. The results were reported as mean values ± standard deviation.

2.8. Mechanical characterization of thin films: tensile tests

The mechanical performance of the films was evaluated through tensile testing [40]. The tests were performed with a Zwick/Roell Z010 (Zwick/Roell Srl, Genova, Italy) equipped with a 100 N load cell. A test speed of 2 mm/min was used. Specimen length was slightly variable due to the circular nature of the produced films, but a fixed grip-to-grip

separation of 15 mm was used, whereas specimen width was 3.5 mm ± 0.3 mm. The experiments were carried out at least in triplicate, and the results were reported as mean values ± standard deviation.

2.9. Swelling Studies

The films were characterized through dynamic swelling measurements [39]. For this purpose, each film was divided into three portions of comparable size, weighed and immersed in 20 mL of PB (pH 7.4, ionic strength *I*=0.1) at 37.0±1.0°C. At predetermined time points, the samples were extracted from the medium, gently wiped to remove the liquid in excess and weighed. The degree of swelling (Q) was calculated as follows [41]:

$$Q = \frac{Ws}{Wd}$$

where Ws and Wd are the weight of the swollen sample at time t and that of the dry sample, respectively.

Alternatively, the degree of swelling was expressed as water uptake (WU) and calculated as follows [41]:

$$WU = \frac{(Ws - We)}{We}$$

where Ws and We are, respectively, the weight of the swollen film after 2 h in PB at 37.0±0.5°C and the weight of the sample recovered at the end of the swelling study and heat dried at 40.0±0.5°C until constant weight.

Each test was repeated in triplicate and the results reported as mean values ± standard deviation.

3. Results and Discussion

3.1. Synthesis and characterization of GGDA derivatives

DA was conjugated to GG according to the synthetic scheme shown in Figure 1. Specifically, the amino group of DA was covalently bound to GG carboxyl groups by an amination reaction performed in the presence of EDC and NHS, used as coupling agents. According to the literature [42], a first attempt of synthesis was carried out dissolving GG in double distilled water before adding coupling agents (EDC/NHS) and catechol-containing molecule (DA) to the polymeric solution in an equimolar ratio to GG carboxyl groups. The reaction was carried out under nitrogen atmosphere and in mild acidic

conditions to avoid possible collateral reactions (e.g., DA autoxidation and polymerization), which would strongly influence the yield of polymer derivatization.

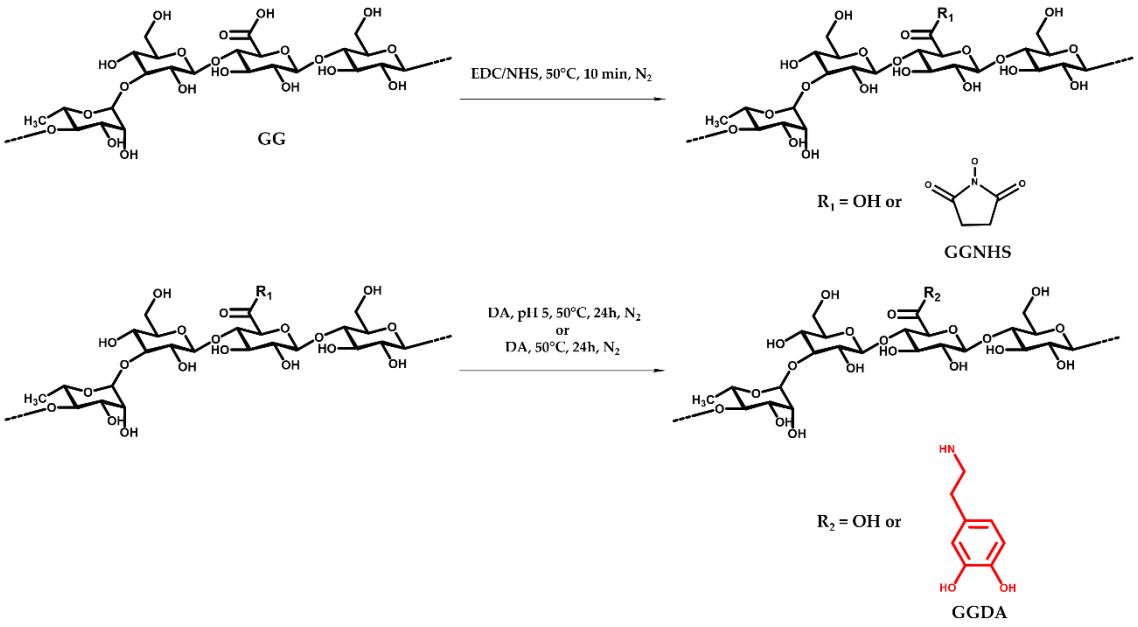

Figure 1. Schematic representation of GGDA synthesis.

With the aim of identifying the most suitable purifying strategy, the resultant reaction mixture was subjected to three different dialysis procedures. Each purification procedure was performed at a temperature of 4°C for a limited period of time (2 or 7 days), in order to slow down any possible oxidation of catechol groups which could occur during the purification phase of the synthesized derivative. Regardless of the purifying strategy adopted, a gelation of the polymer solution was observed as a consequence of the temperature lowering. The polymer derivative ($GGDA_1$) produced following the three purification procedures was first characterized using UV-Vis spectroscopy. The peak at 280 nm in the absorption spectra of $GGDA_1$, absent in that of non-derivatized GG, confirmed the presence of catechol groups in the analyzed samples, whereas the absence of additional bands around 400 nm, usually related to catechol oxidized forms, indicated that no DA oxidation occurred during synthesis and purification of $GGDA_1$, underlining the suitability of the experimental conditions adopted (Figure 2) [43,44].

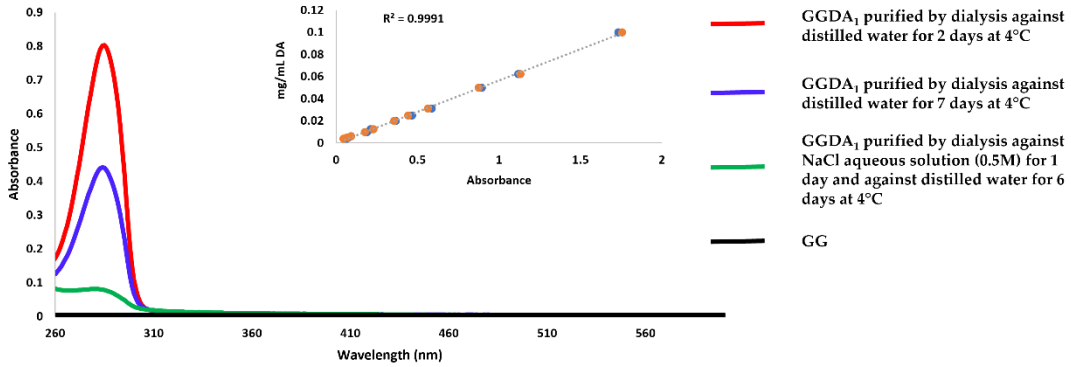

Figure 2. Absorption spectra of GGDA1 following the different purification procedures. The calibration curve of DA used for the determination of the DD is reported.

Table 4. Effect of the purification method applied on GGDA1 DD determined by UV-Vis spectroscopy.	
Purification procedures (dialysis)	**DD (%)**
2 days against distilled water at 4°C	**34.0±1.0**
7 days against distilled water at 4°C	**18.0±1.0**
1 day against NaCl aqueous solution (0.5 M) and 6 days against distilled water at 4°C	**3.0±1.0**

The DD of the polymer conjugate, evaluated by monitoring the absorbance of the analyzed samples at 280 nm, showed significant changes depending on the dialysis method applied, decreasing as a result of the extension of the purification period and undergoing a further reduction for the polymer derivative purified by the procedure involving one day of dialysis against NaCl aqueous solution (Table 4). The results obtained suggested the presence of DA molecules not covalently bound to GG carboxyl groups in the analyzed samples. To further investigate the effect of the purifying strategy and acquire more information on the chemical structure of the synthesized derivative, GGDA1 was subjected to ^{1}H-NMR analysis and the resulting spectra were compared to that of non-derivatized GG (Figure 3). Besides the typical signals of the polysaccharide chain and the three characteristic peaks related to the methine groups located on the benzene ring of DA (from δ 6 ppm to δ 7 ppm) [5], several additional multiplets can be observed. The extra signals detected in the spectra of GGDA1 purified by dialysis against distilled water along with the peaks of DA's aromatic protons undergo a variation of intensity as a function of the dialysis conditions, confirming the data previously collected by UV-Vis spectroscopy.

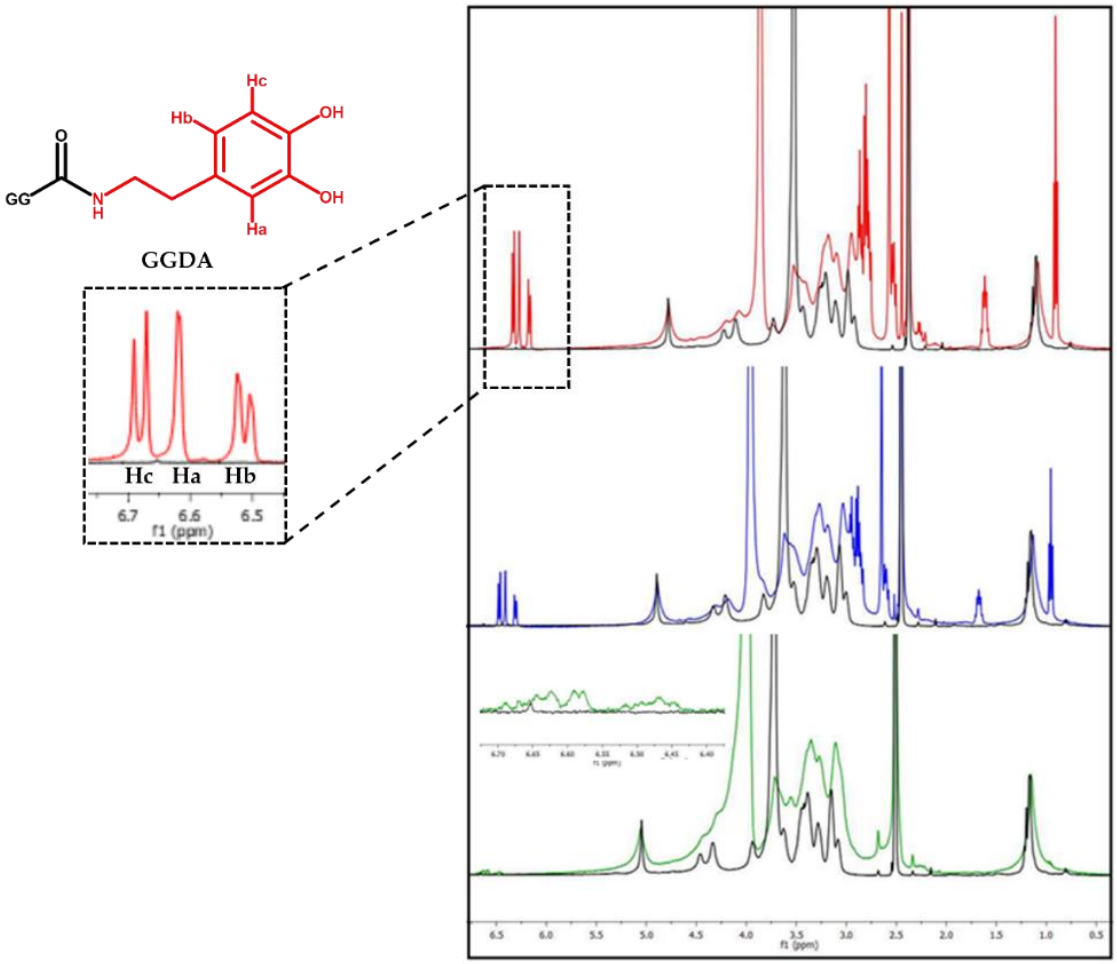

Figure 3. Evaluation of the purification procedures by ^{1}H-NMR. The spectra of GGDA$_1$ purified by dialysis against distilled water for 2 days (red) and 7 days (blue), and for 1 day against NaCl aqueous solution (0.5M) and 6 days against distilled water (green) are overlap to that of non-derivatized GG (black).

The experimental findings, therefore, highlighted the ineffectiveness of the purification procedures applied, emphasizing the presence of excess reagents not properly removed during dialysis, probably because of the gelation of the polymer solution that hindered the diffusion of these molecules. Although gelation was also observed for the polymer solution purified against NaCl, this procedure was found to be the most suitable one, allowing to completely remove the excess reagents and, therefore, to identify the actual amount of catechol groups covalently bound to GG backbone. This effect may be due to an ion exchange between Na ions and DA and EDC molecules which, being provided with protonable amino groups, could interact with GG carboxylic functions by forming a stable electrostatic interaction that would further impede the diffusion of such chemicals during dialysis. The yield of GG derivatization was found to be particularly low (3.0±1.0%), justifying the gelling of the polymer solution at low temperatures.

Indeed, it is widely accepted that GG carboxyl groups play a key role in the formation of intermolecular interactions leading to the development of thermoreversible hydrogels. Since the derivation is very limited, its impact on the ability of polymer chains to physically gel is negligible, and the synthesized derivative showed a comparable behavior to the natural polymer.

The effect of the molar ratio COOH:EDC:NHS:DA on GG derivatization yield was also investigated. For this purpose, the same synthetic procedure was performed by doubling EDC, NHS and DA mmoles while keeping constant those of GG carboxyl groups. The resulting polymer solution was then purified by dialysis carried out under the conditions previously identified and, again, a gelation of the polymer solution was observed during purification at low temperature. The absence of additional multiplets in $GGDA_2$ ^{1}H-NMR spectrum further confirmed the effectiveness of the selected purification procedure, while showing an increase in the intensity of DA's aromatic protons peaks when compared to that of $GGDA_1$ (Figure 4). Supporting this, $GGDA_2$ DD estimated using UV-Vis spectroscopy grew proportionally to the amount of reagents used (Table 5). However, the conjugation efficiency of DA molecule to GG backbone was still extremely low (6.0±1.0%).

The same synthetic procedure performed in aqueous solution was repeated, this time using DMSO as the reaction solvent. Obviously, the use of organic solvent provided a longer time for GG dissolution, while resulting in several advantages. First, using an organic solvent avoided the need to monitor and adjust the pH of the polymeric solution after adding DA to the reaction mixture. When the reaction takes place in water, the pH is a crucial variable affecting the yield of polymer derivatization, because it must be such as to prevent the oxidation and polymerization of DA molecules while enabling the formation of amide bonds, both of which are favored in a basic environment [45,46].

Table 5. Effect of the molar ratio COOH:EDC:NHS:DA on the DD of GGDA conjugates synthesized using water as the reaction solvent.

	Molar ratio COOH:EDC:NHS:DA	**DD (%)**
$GGDA_1$	1:1:1:1	**3.0±1.0**
$GGDA_2$	1:2:2:2	**6.0±1.0**

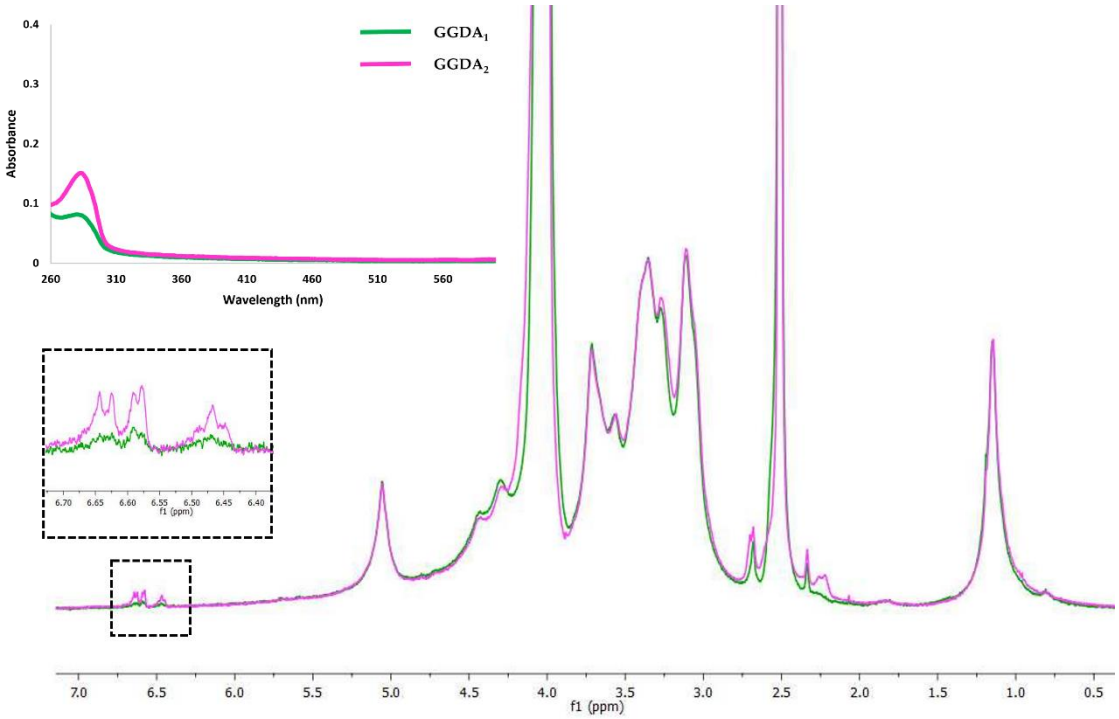

Figure 4. Effect of the molar ratio COOH:EDC:NHS:DA. Characterization of GGDA1 (green) and GGDA2 (pink) by ^{1}H-NMR and UV-Vis spectroscopy.

Furthermore, the procedure performed in DMSO resulted in a significant improvement in the catechol content of GGDA3 (Figure 5), which was evaluated using both UV-Vis and ^{1}H-NMR spectroscopy (Table 6). For this achievement, GGDA3 ^{1}H-NMR spectrum was recorded in the presence of a specific amount of nicotinamide (Figure 6), which was chosen as an internal standard according to previous works [47,48]. The DD was then calculated by comparing the area of a specific standard signal (H_3) within the average area of DA's aromatic protons peaks. The effect on the yield of GG derivatization is probably due to the increased stability of activated intermediates (GGEDC and GGNHS), which are highly susceptible to hydrolysis in the presence of water, causing the sudden inactivation of GG carboxyl groups and preventing their subsequent reaction with DA molecules, as well as the effect that the organic solvent exerts on the polymer chains. DMSO is a highly polar and aprotic solvent capable of dispersing a variety of polymers, including polysaccharides and polypeptides, acting as a destroyer of intra- and intermolecular hydrogen bonds, while favoring the establishment of DMSO-polymer interactions [49], which promotes the relaxation of polymer chains, making GG carboxyl groups more accessible and, therefore, more prone to reaction with DA molecules.

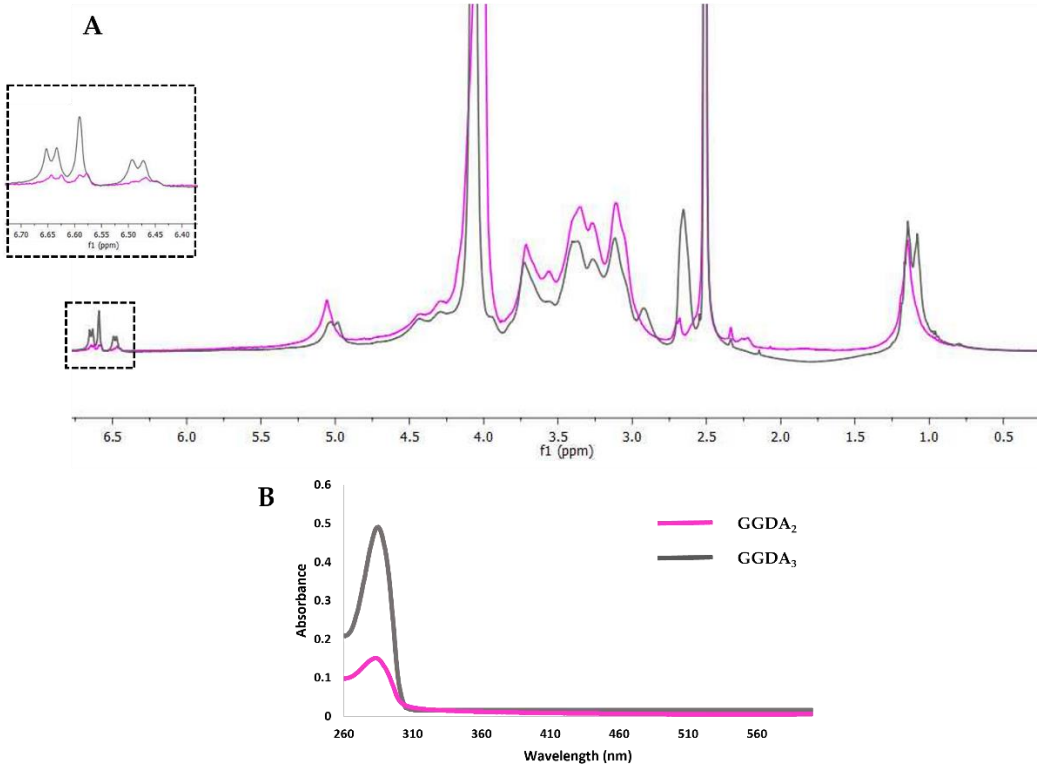

Figure 5. Effect of the reaction solvent. Characterization of GGDA$_2$ (pink) and GGDA$_3$ (Grey) by ^{1}H-NMR (A) and UV-Vis spectroscopy (B).

Table 6. Effect of the solvent on the DD of GGDA derivatives.				
	Molar ratio COOH:EDC:NHS:DA	**Reaction solvent**	**UV-Vis DD (%)**	**^{1}H-NMR DD (%)**
GGDA$_2$	1:2:2:2	H_2O	**6.0±1.0**	**Not evaluable due to low intensity of DA's protons signals**
GGDA$_3$	1:2:2:2	DMSO	**18.0±1.0**	**13.0±1.0**

The DMSO treatment and increased functionalization of GG carboxyl groups caused a different behavior of the resulting polymer solution at low temperatures. In fact, unlike GGDA derivatives synthesized in water, no gelation was observed during the purification of GGDA$_3$ performed at 4°C. As a result, GGDA$_3$ DD determined by both ^{1}H-NMR and UV-Vis spectroscopy remains constant regardless of the purifying strategy applied (Table 7). On the other hand, the lack of gelation during dialysis would appear to facilitate the autoxidation of DA catechol groups grafted onto GG backbone, as evidenced by the appearance of a slightly pronounced brown color during the purification of the synthesized derivative. However, DA oxidation was only mildly

present because it could not be detected by any of the analytical methods employed to characterize $GGDA_3$ and was readily avoided by the moderate acidification of dialysis (pH 4-5).

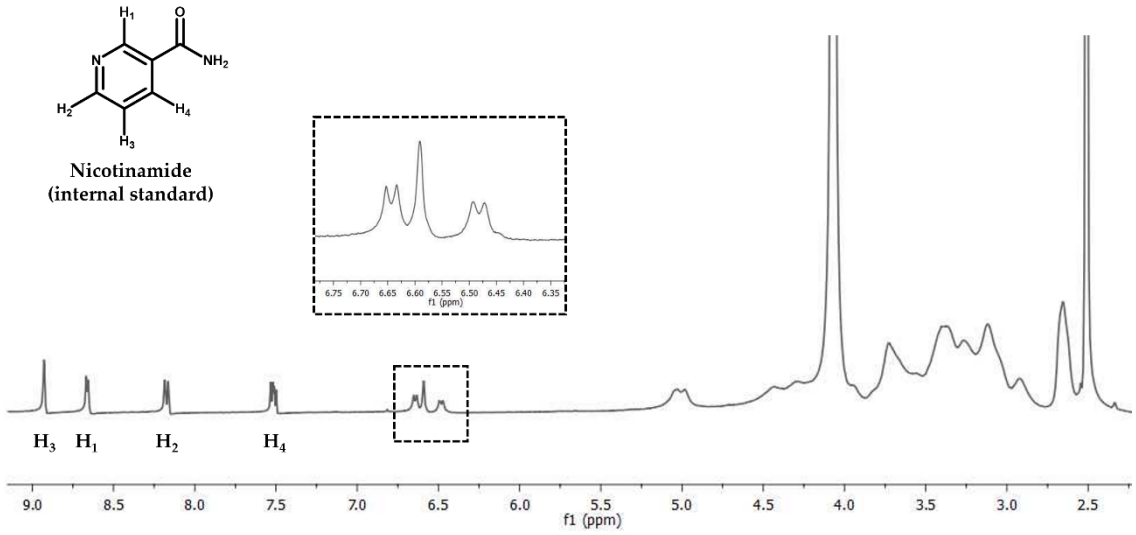

Figure 6. ^{1}H-NMR spectrum of $GGDA_3$ in DMSO-d_6 recorded in the presence of the internal standard nicotinamide in D_2O.

Table 7. Effect of the purification method applied on $GGDA_3$ DD determined by ^{1}H-NMR and UV-Vis spectroscopy.

Purification procedures (dialysis)	Uv-Vis DD (%)	^{1}H-NMR DD (%)
7 days against distilled water at 4°C	18.0±1.0	13.0±1.0
1 day against NaCl aqueous solution (0.5 M) and 6 days against distilled water at 4°C	18.0±1.0	13.0±1.0
6 days against distilled water (pH 5) and 1 day against distilled water at 4°C	18.0±1.0	13.0±1.0

3.2. Optimization of oxidative cross-linking conditions of GGDA derivative

Based on the particular behavior shown by $GGDA_3$, it was selected to investigate the possibility of developing GGDA-based hydrogels through oxidative cross-linking of catechol groups available on the polymer backbone.

Catechol-modified polymers are commonly cross-linked through oxidation of catechol groups which usually takes place in the presence of enzymes (e.g., tyrosinase, horseradish peroxidase) or chemical oxidants (e.g., sodium periodate) [50]. However, chemical oxidants can be responsible for cellular toxicity and oxidative damage to polysaccharide chains, affecting hydrogels stability, and limiting their effective application in biomedical and pharmaceutical fields.

Based on the ability of catechols to spontaneously oxidize in the presence of oxygen (autoxidation) and in a mildly basic environment [37], the effect of variables such as temperature and solubilization time of $GGDA_3$ derivative, as well as pH and concentration of the buffer used, on catechol oxidation was investigated, with the purpose of identifying the most suitable conditions to promote an oxidative cross-linking of polymer chains without using any additional chemical agent (Figure 7). Considering that catechol oxidation and polymerization leads to the development of a characteristic brown color [38], whose intensity is proportional to the oxidation rate of catechol groups, the color change of the polymeric solutions was used as a qualitative index to evaluate the impact of the above-mentioned parameters on $GGDA_3$ oxidation.

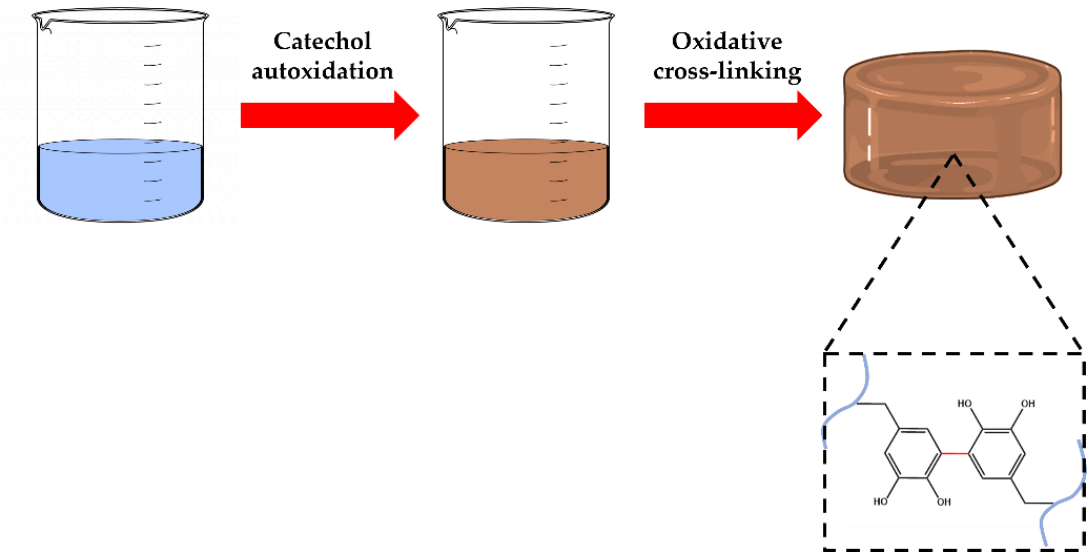

Figure 7. Schematic representation of $GGDA_3$ gelation due to the oxidative cross-linking of catechol groups.

According to the pioneering work of Lee et all [51], who demonstrated the spontaneous deposition of thin polydopamine coatings via oxidative polymerization of DA solution prepared using 0.01M TRIS buffer (pH 8.5), preliminary tests were performed solubilizing $GGDA_3$ in the same buffer conditions, in order to obtain a solution with a concentration of 2% *w/v*. The temperature was set at 50°C and the solubilization time of the polymeric derivative was varied from 30 min to 2 h, to compensate for the absence of chemical oxidizing agents. At the same time, to evaluate the effect of the pH value on the oxidation rate of catechol groups, $GGDA_3$ was dissolved under the same

experimental conditions, this time using 0.01M TRIS buffer (pH 7.4), in order to mimic the physiological environment.

Despite a color change was observed in both cases during the dissolution of $GGDA_3$, the browning of the solution, and thus the oxidation rate of catechol groups, was discovered to be directly dependent on the pH value of the buffer used. According to literature data [52], a basic pH was found to promote DA's catechol oxidation more than a physiological pH value, resulting in a more pronounced browning of the polymeric solution, whose intensity increases by prolonging the exposure time of $GGDA_3$ at 50°C from 30 min to 1 h, after which no further color changes were detected. Because of the higher oxidation degree achieved, only the solution prepared at pH 8.5 was able to gel during 24 h of storage at room temperature, emphasizing the key role of pH in promoting the oxidative cross-linking of $GGDA_3$, visibly hampered at lower pH values. However, while the vial tilting method demonstrated that gelation occurred, the degree of cross-linking achieved was insufficient to allow the development of a stable hydrogel after pouring the resulting solution into a suitable glass support and storing for 24 h at room temperature. Thus, to increase the amount of catechol groups involved in the oxidative cross-linking, $GGDA_3$ was dissolved in the aforementioned buffers, this time at a temperature of 70°C. Temperature was discovered to be an important parameter affecting catechol oxidation, causing a more rapid and intense browning of the solution prepared at pH 8.5, which resulted, after 24 hours of storage at room temperature, in the formation of a hydrogel. The temperature increase, on the other hand, had no effect on the solution buffered at pH 7.4, which showed no color change regardless of the solubilization time of $GGDA_3$ derivative and did not undergo gelation, further highlighting the critical role of pH in encouraging the oxidative cross-linking of polymer chains (Figure 8).

The results of the experiments performed enabled the identification of the pH and solubilization temperature conditions required to promote the chemical gelation of $GGDA_3$ solution. However, despite a higher degree of catechol oxidation was reached, the resulting hydrogel lacked the properties required for biomedical and pharmaceutical applications. As a result, the effect of buffer concentration on $GGDA_3$ oxidation was investigated as well. Therefore, the concentration of TRIS buffer was raised from 0.01M to 0.1M while keeping constant the temperature, solubilization time, and pH value of the

polymeric solution. Table 8 provides an overview of all the experimental applied conditions.

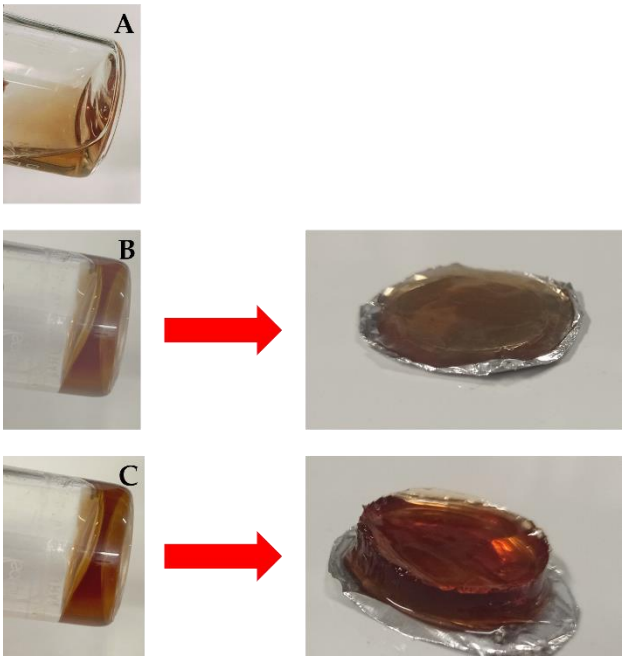

Figure 8. Effect of pH value and temperature on oxidation of catechol groups. GGDA$_3$ in (A) 0.01M TRIS buffer (pH 7.4) at 70°C, (B) 0.01M TRIS buffer (pH 8.5) at 50°C, (C) 0.01M TRIS buffer (pH 8.5) at 70°C after 24 h of storage at room temperature.

The increase in buffer concentration resulted in the formation of a stable hydrogel with the distinctive brown color of catechol oxidation and polymerization (Figure 9). The effect of buffer concentration on the oxidation rate of catechol residues is most likely related to an improvement in buffering capacity, which allows to minimize pH changes that can be recorded during the oxidation process of catechol groups and have a negative impact on the reaction yield.

Although the absence of GGDA$_3$ gelling at pH 7.4 is clear evidence of oxidative cross-linking observed at higher pH value, the physical behavior of the solutions prepared by dissolving the polymer derivative in 0.01M TRIS buffer (pH 7.4) and 0.1M TRIS buffer (pH 8.5) at 70°C was further investigated using oscillatory temperature sweep analysis and compared with that of GG solutions obtained under the same experimental conditions. While GG solutions undergo physical gelling as the temperature decreases from 60°C to 30°C, as evidenced by the crossover of G' and G" moduli, which occurred at different temperatures due to changes in the ionic strength of the buffer used, GGDA$_3$

solutions exhibited completely different behavior, and the crossover of G' and G'' moduli was not detected in the temperature range considered. However, for $GGDA_3$ sample prepared at pH 8.5, an increase in G' modulus can be observed, which is most likely due to the formation of an adhesive layer on the upper cone geometry during the analysis which could affect the final outcome (Figure 10).

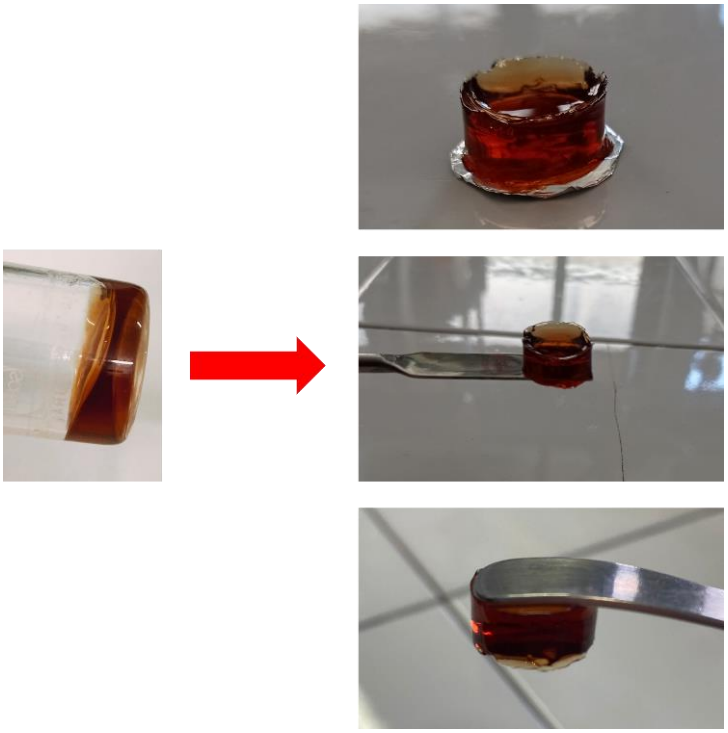

Figure 9. Effect of buffer concentration on catechol oxidation. $GGDA_3$ in 0.01M TRIS buffer (pH 8.5) after 24 h of storage at room temperature.

Table 8. Optimization of $GGDA_3$ oxidative crosslinking conditions.

GG-DA (% w/v)	Solubilization temperature (°C)	Solubilization time	TRIS buffer pH	TRIS buffer concentration (M)	Result
2	50	Form 30 min to 6 h	7.4	0.01	No gelation
	70				No gelation
	50	From 30 min to 2 h	8.5	0.01	Mild gelation
	70				Formation of a hydrogel
	70	2 h	8.5	0.1	Formation of a hydrogel

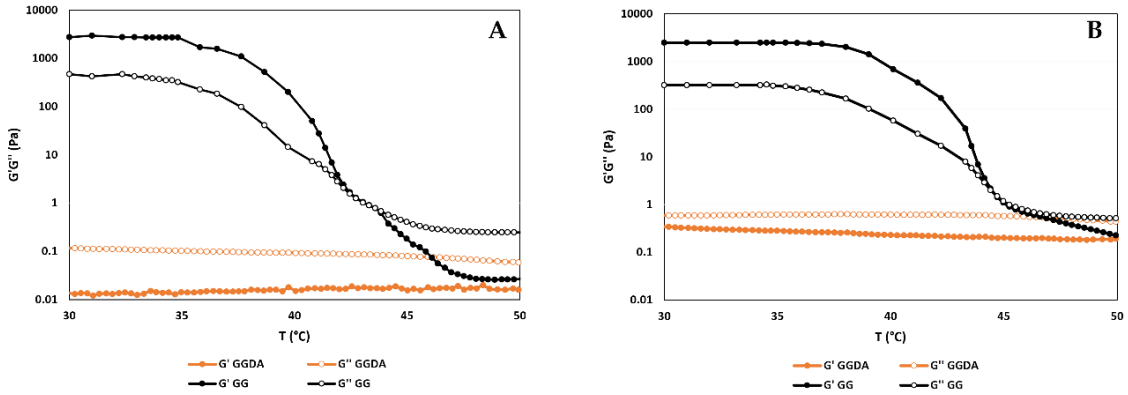

Figure 10. Oscillatory temperature sweep analysis of GG and GGDA solutions (2% w/v) prepared in (A) 0.01M TRIS buffer (pH 7.4) and (B) 0.1M TRIS buffer (pH 8.5).

The collected data demonstrated the potential for developing GGDA-based hydrogels through oxidative cross-linking of catechol groups without the use of any additional oxidants, while directly acting on variables that significantly affect the autoxidation rate of DA molecules. Additionally, the lack of physical gelling provides partially support for the unique behavior of $GGDA_3$ derivative seen during purification performed at low temperature, emphasizing the impact of derivatization carried out using DMSO as the reaction solvent on the gelling properties of the synthesized derivative.

Since physical gelation is not present in the temperature range under investigation, the temperature of the polymer solution can be lowered after reaching the proper rate of catechol oxidation enabling the loading of any active ingredients and leading to the development of hydrogels with potential application in the drug delivery field.

3.3. Fabrication of GGDA-based thin films

Based on these findings and taking into account the film-forming properties of GG, the potential for producing GGDA-based thin films using the solvent casting technique was explored.

The solvent casting technique involves the initial deposition of a liquid polymeric film on the surface of a solid support followed by the evaporation of the solvent with the conversion of the polymeric solution into a solid film [39].

An initial attempt was made by solubilizing $GGDA_3$ (2% *w/v*) under the experimental conditions identified for the purpose of oxidative crosslinking of polymer chains. The obtained solution was poured into a suitable silicon support, which was chosen to

promote film detachment at the end of the drying process, and stored at room temperature for 24 h to allow the curing of $GGDA_3$ chains. The resulting hydrogel was then heat-dried at a constant temperature of 40°C to allow the solvent to evaporate and the polymer film to form. In accordance with literature data, the polymer derivative alone led to the production of extremely brittle film, thus requiring the addition of a plasticizer to the starting polymer solution to improve the elasticity, flexibility, and strength of the resulting product [39]. Since previous research conducted on GG-based films showed that using glycerol (Gly) as a plasticizer induces a significant improvement in the mechanical properties of the resulting films, without affecting the rheological behavior of the polymer solution, which was found to be suitable for the solvent casting method [39,41], Gly was chosen as plasticizer and added to the starting polymer solution at a concentration of 2% *w*/*v*. The total volume of the casted solution was first fixed at 6 mL in order to obtain a film with suitable thickness following the drying process, carried out at 40°C for 15 h. The elasticity of the resulting film significantly improved following the addition of plasticizer; however, excessive shrinkage of the final product was also observed after the drying step. Therefore, the drying time was decreased to 13 h while maintaining the entire volume of the polymer solution, but again, a considerable shrinkage was experienced, resulting in the formation of non-homogeneous film. To overcome this problem, the total volume of the polymer solution was increased to 8 mL. Naturally, by increasing the final volume of the film-forming solution, it was necessary to further optimize the duration of the drying step. In particular, the drying time was prolonged to 24 h, thus resulting in the development of a film with appropriate thickness and ideal residual moisture content, which is fundamental for proper film handling (Figure 11). Therefore, GGDA-based film was characterized in terms of thickness, swelling capacity and mechanical strength. The results obtained are summarized in Table 9.

To evaluate homogeneity and uniformity of the produced film, the thickness was measured at six distinct points of the final product. The acquired results demonstrated the development of nearly uniform-thick film, confirming the suitability of the setup parameters chosen for the casting and drying processes.

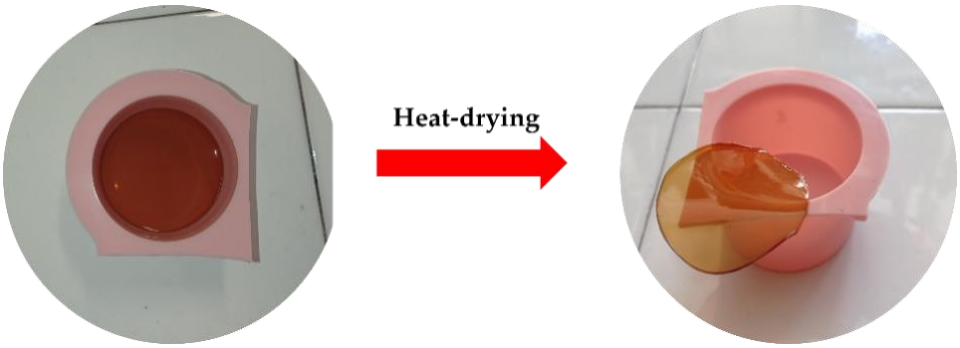

Figure 11. GGDA-based film prepared using the solvent casting technique.

The film ability to swell when in contact with biological fluids was assessed by dynamic swelling studies performed under physiological conditions. The swelling degree (Q) was determined by the ratio between the swollen and dry weight of the film, as typically reported [41]. Figure 12 illustrates the trend of the Q value over time. However, previous observations suggested that a possible diffusion of the formulation components, such as plasticizer and TRIS buffer components, through the polymer matrix occurred during the swelling process [39-41]. Consequently, the Q value was considered not ideal for describing the swelling capabilities of GGDA-based film and it was corrected by considering the loss of the formulation components. To this end, the film was recovered at the end of the swelling study and dried up to constant weight (We). The measured We value was found to be inferior to the initial weight of the dried film, confirming the actual release of the excipients used for film formulation. Consequently, the swelling degree was corrected expressed as water uptake (WU) [41].

Table 9. GGDA-based film characterization: thickness, swelling capacity and mechanical properties.

Thickness (μm)	Swelling capacity		Mechanical properties		
154.00±0.01	Q	WU	Tensile modulus [MPa]	Tensile strength [MPa]	Strain at break [%]
	6.53±0.11	18.28±1.17	13.36±1.12	2.70±0.37	52.83±9.96

Comparing mechanical test data with those available in the literature on films formulated using GG and Gly [39-41], GGDA-based film showed promising results, also exhibiting a great ability to adapt to different anatomical regions (Figure 13). Based on

these observations, a possible application of this formulation in areas such as drug delivery and wound healing can be hypothesized.

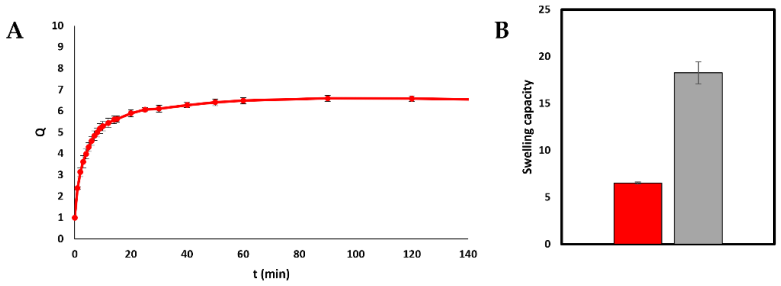

Figure 12. Swelling capacity of GGDA film measured in PB (pH = 7.4) at 37.0 ± 0.1 ◦C. (A) Dynamic swelling over time. (B) Comparison between the swelling degree (red bar) and water uptake capacity (grey bar).

Figure 13. Qualitative evaluation of GGDA-based film adhesive properties.

4. Conclusions

The possibility of derivatizing GG carboxyl groups with DA molecules through EDC/NHS coupling chemistry was investigated and the effect of two different reaction solvents, such as double-distilled water and DMSO, on the derivatization yield and on properties of the resultant polymeric solutions was evaluated. Different dialysis procedures were compared with the aim of identifying the most suitable purification strategy, highlighting the crucial role of the purification step in determining the amount of catechol groups covalently bound to GG backbone, and stressing how an inadequate removal of excess reagents may lead to a significant error in the evaluation of the derivatization degree. The use of DMSO as the reaction solvent resulted in significant advantages mostly related to GG derivatization yield, leading to an improvement in the DD of the synthesized derivative, which lost the ability to undergo a sol-gel transition with temperature. This polymer derivative was chosen to develop GGDA-based hydrogels through oxidative crosslinking of catechol groups performed in the absence

of oxidizing chemicals, which could cause cellular toxicity and oxidative damage to polymer chains, affecting hydrogels stability and limiting their effective application in biomedical and pharmaceutical fields. Specific variables, including temperature and solubilization time of GGDA, as well as the pH and concentration of the TRIS buffer used, resulted critical for the catechol autoxidation rate. The experimental conditions required to promote oxidative crosslinking of polymer chains without using any additional chemical agent were then used to produce GGDA-based thin film with suitable properties for biomedical and pharmaceutical applications.

References

1. Yuk, H., Lu, B., Zhao, X. Hydrogel bioelectronics. Chem. Soc. Rev. 2019, 48:1642-1667. DOI: 10.1039/C8CS00595H
2. Zhang, Y.S., Khademhosseini, A. Advances in engineering hydrogels. *Science*. 2017, 356(6337):eaaf3627. doi: 10.1126/science.aaf3627.
3. Caccavo, D., Cascone, S., Lamberti, G., Barba, A.A. Hydrogels: experimental characterization and mathematical modelling of their mechanical and diffusive behaviour *Chem.Soc. Rev. 2018*, 47:2357–2373. https://doi.org/10.1039/C7CS00638A.
4. Zhang, W., Wang, R., Sun, Z.M., Zhu, X., Zhao, Q., Zhang, T., Cholewinski, A., Yang, F.K., Zhao, B., Pinnaratip, R., Forooshanie, P.K., Lee, B.P. Catechol-functionalized hydrogels: biomimetic design, adhesion mechanism, and biomedical applications. *Chem.Soc. Rev*. 2020, 49:433-464. https://doi.org/10.1039/C9CS00285E.
5. Zhu, W., Iqbal, J., Wang, D.A. A DOPA-functionalized chondroitin sulfate-based adhesive hydrogel as a promising multi-functional bioadhesive. *J. Mater. Chem. B*. 2019, 7:1741-1752. https://doi.org/10.1039/C8TB01990H.
6. Hoffman, A.S. Hydrogels for biomedical applications. *Adv Drug Deliv Rev*. 2002, 54(1):3-12. doi: 10.1016/s0169-409x(01)00239-3.
7. Costa, P.M., Learmonth, D.A., Gomes, D.B., Cautela, M.P., Oliveira, A.C.N., Andrade, R., Espregueira-Mendes, J., Veloso, T.R., Cunha, C.B., Sousa, R.A. Mussel-Inspired Catechol Functionalisation as a Strategy to Enhance Biomaterial Adhesion: A Systematic Review. *Polymers (Basel)*. 2021, 13(19):3317. doi: 10.3390/polym13193317.
8. Hauser, D., Septiadi, D., Turner, J., Petri-Fink, A., Rothen-Rutishauser, B. From Bioinspired Glue to Medicine: Polydopamine as a Biomedical Material. *Materials*. 2020, 13(7): 1730. https://doi.org/10.3390/ma13071730.
9. Fredi, G., Simon, F., Sychev, D., Melnyk, I., Janke, A., Scheffler, C., Zimmerer, C. Bioinspired Polydopamine Coating as an Adhesion Enhancer Between Paraffin Microcapsules and an Epoxy Matrix. *ACS Omega*. 2020, 5(31):19639-19653. doi: 10.1021/acsomega.0c02271.
10. Khan, Z., Shanker, R., Um, D., Jaiswal, A., Ko, H. Bioinspired Polydopamine and Composites for Biomedical Applications. 2018, 1-29. https://doi.org/10.1002/9783527807918.ch1.
11. Davidsen, M.B., Teixeira, F.J.L., Dehli, J., Karlsoon, C., Kraft, D., Souza, P.P.C., Foss, M. Post-treatments of polydopamine coatings influence cellular response. *Colloids and Surfaces B: Biointerfaces*. 2021, 207:111972. https://doi.org/10.1016/j.colsurfb.2021.111972
12. Dinh, T.N., Hou, S., Park, S., Shalek, B.A., Jeong, K.J. Gelatin Hydrogel Combined with Polydopamine Coating to Enhance Tissue Integration of Medical Implants. *ACS Biomater Sci Eng*. 2018, 4(10):3471-3477. doi: 10.1021/acsbiomaterials.8b00886.
13. Tang, Y., Tan, Y., Lin, K., Zhu, M. Research Progress on Polydopamine Nanoparticles for Tissue Engineering. *Front Chem.* 2021, 9:727123. doi: 10.3389/fchem.2021.727123.
14. Pacelli, S., Paolicelli, P., Petralito, S., Subham, S., Gilmore, D., Varani, G., Yang, G., Lin, D., Casadei, M.A., Paul A. Investigating the Role of Polydopamine to Modulate Stem Cell Adhesion and Proliferation on Gellan Gum-Based Hydrogels. ACS Appl. Bio Mater. 2020, 3, 2, 945–951. https://doi.org/10.1021/acsabm.9b00989.

15. Ding, Y. H.; Floren, M.; Tan, W. Mussel-inspired polydopamine for bio-surface functionalization. Biosurface and Biotribology. 2016, 2(4):121−136. doi: 10.1016/j.bsbt.2016.11.001.
16. Lee, S., Kim, S., Park, J., Lee, J.Y. Universal surface modification using dopamine-hyaluronic acid conjugates for anti-biofouling. International Journal of Biological Macromolecules. 2020, 151:1314-1321. https://doi.org/10.1016/j.ijbiomac.2019.10.177.
17. Lih, E., Choi, S.G., Ahn, D.J., Joung, Y.K., Han, D.K. Optimal conjugation of catechol group onto hyaluronic acid in coronary stent substrate coating for the prevention of restenosis. *J Tissue Eng*. 2016, 7:2041731416683745. doi: 10.1177/2041731416683745.
18. Alegre-Requena, J.V., Häring, M., Herrera, R.P., Díaz, D.D. Regulatory parameters of self-healing alginate hydrogel networks prepared via mussel-inspired dynamic chemistry. *New J. Chem*. 2016, 40:8493-8501. DOI: 10.1039/C6NJ02367C.
19. Lee, C., Shin, J., Lee, J.S., Byun, E., Ryu, J.H., Um, S.H., Kim, D.I., Lee, H., Cho, S.W. Bioinspired, calcium-free alginate hydrogels with tunable physical and mechanical properties and improved biocompatibility. *Biomacromolecules*. 2013, 14(6):2004-13. doi: 10.1021/bm400352d.
20. Gowda, A.H.J., Bu, Y., Kudina, O., Krishna, K.V., Bohara, R.A., Eglin, D., Pandit, A. Design of tunable gelatin-dopamine based bioadhesives. International Journal of Biological Macromolecules. 164:1384-1391. https://doi.org/10.1016/j.ijbiomac.2020.07.195.
21. Han, K., Bai, Q., Wu, W., Sun, N., Cui, N., Lu, T. Gelatin-based adhesive hydrogel with self-healing, hemostasis, and electrical conductivity. *Int J Biol Macromol*. 2021, 183:2142-2151. doi: 10.1016/j.ijbiomac.2021.05.147.
22. Fu, J., Quek, K.Y., Chuah, Y.J., Lim, C.S., Fana, C., Wang, D. The effects of gelatin–dopamine coating on polydimethylsiloxane substrates on pluripotency maintenance and myocardial differentiation of cultured mouse embryonic stem cells. *Journal of Material Chemistry B*. 2016, 48. https://doi.org/10.1039/C6TB02631A.
23. Liu, H., Yuan, M., Sonamuthu, J., Yan, S., Huang, W., Cai, Y., Yao, J. A dopamine-functionalized aqueous-based silk protein hydrogel bioadhesive for biomedical wound closure. *New Journal of Chemistry*. 2020, 3. https://doi.org/10.1039/C9NJ04545G.
24. Kord Forooshani, P., Lee B.P. Recent approaches in designing bioadhesive materials inspired by mussel adhesive protein. *J Polym Sci A Polym Chem*. 2017, 55(1):9-33. doi: 10.1002/pola.28368.
25. Koivusalo, L., Kauppila, M., Samanta, S., Parihar, V.S., Ilmarinen, T., Miettinen, S., Oommen, O.P., Skottman, H. Tissue adhesive hyaluronic acid hydrogels for sutureless stem cell delivery and regeneration of corneal epithelium and stroma. *Biomaterials.* 2019, 225, 119516. https://doi.org/10.1016/j.biomaterials.2019.119516.
26. Sousa, M.P., Neto, A.I., Correia, T.R., Miguel, S.P., Matsusaki, M., Correia, I.J., Mano, J.F. Bioinspired multilayer membranes as potential adhesive patches for skin wound healing. *Biomater. Sci*. 2018, 6:1962–1975. https://doi.org/10.1039/C8BM00319J.
27. Zhong, Y., Wang, J., Yuan, Z., Wang, Y., Xi, Z., Li, L., Liu, Z., Guo, X. A mussel-inspired carboxymethyl cellulose hydrogel with enhanced adhesiveness through enzymatic crosslinking. *Colloids Surf. Biointerfaces* 2019, 179:462–469. https://doi.org/10.1016/j.colsurfb.2019.03.044.
28. Wu, T., Cui, C., Huang, Y., Liu, Y., Fan, C., Han, X., Yang, Y., Xu, Z., Liu, B., Fan, G., Liu, W. Coadministration of an adhesive conductive hydrogel patch and an injectable hydrogel to treat myocardial infarction. ACS Appl. Mater. Interfaces 2019, 12, 2039– 2048. https://doi.org/10.1021/acsami.9b17907.
29. Shin, J., Kang, E.H., Choi, S., Jeon, E.J., Cho, J.H., Kang, D., Lee, H., Yun, I.S., Cho, S.W. Tissue-adhesive chondroitin sulfate hydrogel for cartilage reconstruction. *ACS Biomater. Sci. Eng*. 2021, 7, 4230–4243. https://doi.org/10.1021/acsbiomaterials.0c01414.
30. Pornpitchanarong, C., Rojanarata, T., Opanasopit, P., Ngawhirunpat, T., Patrojanasophon, P. Catechol-modified chitosan/hyaluronic acid nanoparticles as a new avenue for local delivery of doxorubicin to oral cancer cells. *Colloids Surf. Biointerfaces.* 2020, 196, 111279. https://doi.org/10.1016/j.colsurfb.2020.111279.
31. Zhang, K.; Wei, Z.; Xu, X.; Feng, Q.; Xu, J.; Bian, L. Efficient catechol functionalization of biopolymeric hydrogels for effective multiscale bioadhesion. Mater. Sci. Eng. C 2019, 103, 109835. https://doi.org/10.1016/j.msec.2019.109835.
32. Shin, J., Lee, J.S., Lee, C., Park, H.J., Yang, K., Jin, Y., Ryu, J.H., Hong, K.S., Moon, S.H., Chung, H.M., Yang, H.S., Um, S.H., Oh, J.W., Kim, D.I., Lee, H., Cho, S.W. Tissue adhesive catechol-modified hyaluronic acid hydrogel for effective, minimally invasive cell therapy. Advanced Functional Material. 2015, 25(25):3814-3824. https://doi.org/10.1002/adfm.201500006.

33. Learmonth, D.A., Costa, P.M., Veloso, T.R., Cunha, C.B., Cautela, M.P., Correia, C., Vallejo, M.C., Sousa, R.A. Synthesis and biological evaluation of a bioinspired, tissue-adhesive gellan gum-based hydrogel designed for minimally invasive delivery and retention of chondrogenic cells. *Biomater. Sci*. 2020, 8, 3697–3711. https://doi.org/10.1039/D0BM00286K.
34. Pinnataip, R., Lee, B.P. Oxidation Chemistry of Catechol Utilized in Designing Stimuli-Responsive Adhesives and Antipathogenic Biomaterials. *ACS Omega.* 2021, 6(8):5113-5118. doi: 10.1021/acsomega.1c00006.
35. Fan, C., Fu, J., Zhu, W., Wang, DA. A mussel-inspired double-crosslinked tissue adhesive intended for internal medical use. *Acta Biomater*. 2016, 33:51-63. doi: 10.1016/j.actbio.2016.02.003.
36. Sato, T., Aoyagi, T., Ebara, M., Auzély-Velty, R. Catechol-modified hyaluronic acid: in situ-forming hydrogels by auto-oxidation of catechol or photo-oxidation using visible light. *Polymer Bulletin*. 2017, 74:4069–4085. DOI:10.1007/s00289-017-1937-y.
37. Yang, J., Cohen Stuart, M.A., Kamperman, M. Jack of all trades: versatile catechol crosslinking mechanisms. Chemical Society Reviews. 2014, 24. https://doi.org/10.1039/C4CS00185K.
38. Conejo-Cuevas, G., Ruiz-Rubio, L., Sáez-Martínez, V., Pérez-González, R., Gartziandia, O., Huguet-Casquero, A., Pérez-Álvarez, L. Spontaneous Gelation of Adhesive Catechol Modified Hyaluronic Acid and Chitosan. *Polymers (Basel).* 2022, 14(6):1209. doi: 10.3390/polym14061209.
39. Paolicelli, P.; Petralito, S.; Varani, G.; Nardoni, M.; Pacelli, S.; Di Muzio, L.; Tirillò, J.; Bartuli, C.; Cesa, S.; Casadei, M.A. Effect of glycerol on the physical and mechanical properties of thin gellan gum films for oral drug delivery. *Int. J. Pharm*. 2018, 547, 226–234. doi: 10.1016/j.ijpharm.2018.05.046.
40. Adrover, A., Di Muzio, L., Trilli, J., Brandelli, C., Paolicelli, P., Petralito, S., Casadei, M.A. Enhanced Loading Efficiency and Mucoadhesion Properties of Gellan Gum Thin Films by Complexation with Hydroxypropyl-β-Cyclodextrin. *Pharmaceutics.* 2020, 12:819. doi: 10.3390/pharmaceutics12090819.
41. Di Muzio, L., Simonetti, P., Carriero, V.C., Brandelli, C., Trilli, J., Sergi, C., Tirillò, J., Cairone, F., Cesa, S., Radocchia, G., Schippa, S., Petralito, S., Paolicelli, P., Casadei, M.A. Solvent Casting and UV Photocuring for Easy and Safe Fabrication of Nanocomposite Film Dressings. *Molecules*. 2022, 27(9):2959. doi: 10.3390/molecules27092959.
42. Lee, W., Choi, J.H., Lee, J., Youn, J., Kim, W., Jeon, G., Lee, S.W., Song, J.E., Khang G. Dopamine-Functionalized Gellan Gum Hydrogel as a Candidate Biomaterial for a Retinal Pigment Epithelium Cell Delivery System. *ACS Appl Bio Mater*. 2021, 4(2):1771-1782. doi: 10.1021/acsabm.0c01516.
43. Hong, S., Yang, K., Kang, B., Lee, C., Song, I.T., Byun, E., Park, K.I., Cho, S.W., Lee, H. Hyaluronic Acid Catechol: A Biopolymer Exhibiting a pH-Dependent Adhesive or Cohesive Property for Human Neural Stem Cell Engineering. *Advanced Functional Materials*. 2012. https://doi.org/10.1002/adfm.201202365.
44. Ye, H., Xia, Y., Liu, Z., Huang, R., Su,R., Qi, W., Wang, L., He, Z. Dopamine-assisted deposition and zwitteration of hyaluronic acid for the nanoscale fabrication of low-fouling surfaces. *Journal of Material Chemistry B*. 2016, 23. https://doi.org/10.1039/C6TB01022A.
45. Lakshminarayanan, R., Madhavi, S., Sim, C.P.C. Oxidative Polymerization of Dopamine: A High-Definition Multifunctional Coatings for Electrospun Nanofibers - An Overview. 2018. DOI: 10.5772/intechopen.81036.
46. Madison, S.A., Carnali, J.O. pH Optimization of Amidation via Carbodiimides. Ind. *Eng. Chem. Res*. 2013, 52(38):13547–13555. https://doi.org/10.1021/ie401724m.
47. Di Muzio, L., Cienzo, F., Paolicelli, P., Petralito, S., Garzoli, S., Brandelli, C., Trilli, J., Casadei, M.A. A convenient strategy to synthesize highly tunable gelatin methacryloyl with very low gelation temperature. European Polymer Journal. 2021, 154:110538. https://doi.org/10.1016/j.eurpolymj.2021.110538.
48. Di Muzio, L., Paolicelli, P., Brandelli, C., Cesa, S., Trilli, J., Petralito, S., Casadei, M.A. Injectable and In Situ Gelling Dextran Derivatives Containing Hydrolyzable Groups for the Delivery of Large Molecules. Gels. 2021, 7(4):150. doi: 10.3390/gels7040150.
49. Kang, D., Cai, Z., Wei, Y., Zhang, H. Structure and chain conformation characteristics of high acyl gellan gum polysaccharide in DMSO with sodium nitrate. Polymer. 2017, 128:147-158. https://doi.org/10.1016/j.polymer.2017.09.035.
50. Quan, W.Y., Hu, Z., Liu, H.Z., Ouyang, Q.Q., Zhang, D.Y., Li, S.D., Li, P.W., Yang, Z.M. Mussel-Inspired Catechol-Functionalized Hydrogels and Their Medical Applications. *Molecules*. 2019, 24(14):2586. doi: 10.3390/molecules24142586.
51. Lee, H., Dellatore, S.M., Miller, W.M., Messersmith, P.B. Mussel-inspired surface chemistry for multifunctional coatings. *Science*. 2007, 318(5849):426-30. doi: 10.1126/science.1147241.
52. Maier, G.P., Bernta, C.M., Butler, A. Catechol oxidation: considerations in the design of wet adhesive materials. *Biomaterial Science*. 2018, 2. https://doi.org/10.1039/C7BM00884H.

1.4 Thin films as wound dressings

Wound healing is a complex biological process that progresses through a series of interdependent and overlapping stages in which a variety of cells (immune and non-immune), soluble mediators and extracellular matrix components act together with the aim of restoring the integrity of damaged tissue and replacing lost tissue. As the skin is the first line of defense against external agents, it is continuously exposed to multiple injuries that should cause the disruption of its normal anatomical structure, thus altering its protective, thermoregulatory, and immunological functions [188,189]. Based on the duration and nature of the healing process, skin wounds can be divided into two main classes: acute and chronic wounds. Acute wounds are lesions that fully recover within a short period, typically 8 to 12 weeks. They mainly include both mechanical injuries, which are produced by external physical factors such as abrasions from frictional contact between the skin and rough surfaces, and chemical injuries brought on by radiation and corrosive chemicals. On the other hand, chronic wounds heal slower over an extended period of time and fail to achieve complete reepithelialization in the appropriate chronological order of tissue repair [188]. The production of excessive exudate is the main characteristic of chronic wounds and results in the maceration of healthy skin tissue surrounding the lesion and in the reduction of lymphocyte mobility [188,190]. This interrupts the sequence of events that characterizes the wound healing process, which is further hampered by inadequate blood supply, necrosis, infections, and persistent trauma [191]. It is evident that the generation of a favorable environment is essential to getting rid of the barriers hindering wound healing, enabling proper and rapid regeneration of injured tissues. This goal is typically met by following standard management guidelines, which include cleaning the wound site, removing necrotic tissue, administering antibiotics to prevent infection, applying compression, receiving hyperbaric oxygen therapy, and using the appropriate wound dressings [191]. The selection of the right dressing for a specific wound is critical to ensure optimal healing and a better quality of life for the patient. Conventional dressings like gauzes and bandages are still widely used in clinical practice. Nonetheless, they have an unsatisfactory hemostatic performance for arterial ruptures and wounds with irregular, deep, narrow shapes. In addition, they need long-term treatment, are unsuitable for

inherently complicated procedures, adhere easily to dried wound surfaces, and must be surgically and mechanically removed from the injured area, often causing substantial secondary harm to patients [97]. An ideal wound care product should be biocompatible and non-irritating to the surrounding tissues. Furthermore, it should be able to absorb excess exudate and toxins, maintain a moist environment, protect the wound from external infection sources, prevent excessive heat at the wound, have good gas permeability, and be simple to remove without causing additional damage [192]. Polymeric materials, especially when produced in the form of films, fulfill several of the aforementioned requirements, establishing themselves as excellent candidates for the development of innovative dressings to promote wound healing and tissue regeneration. The hydrophilic properties of film-forming polymers allow them to absorb exudates while holding onto a reasonable amount of moisture, which is necessary to accelerate the healing process by encouraging keratinocyte migration to the wound site [14,193]. They are simple to apply and remove, and due to their flexible nature, thin films may easily adjust to various anatomical regions, even in awkward places such around joints. They also act as a protective barrier against opportunistic bacteria and further damage caused by thermal and physical factors, reduce pain, encourage gas exchange, and allow for wound inspection without the need of dressing removal [14,194]. Furthermore, films may be loaded with therapeutic agents in order to prevent the onset of underlying infections. One of the primary causes impeding wound healing and aggravating structural and functional tissue damage is the colonization of contaminating microorganisms at the site of skin injury [195]. However, traditional antibiotics (quinolones, tetracyclines, cephalosporins, neomycin, and polymyxin B) often fail to effectively treat infected and poorly healing wounds, as their over-prescription and improper use have resulted in the development of numerous multi-resistant bacteria [189,195]. In the current scenario, nanomaterial-based approaches have emerged as successful tools for the treatment of infected wounds. The reason underlying the increased use of nanomaterials can be attributed to their physiochemical properties including nano-size, large surface area, and high surface area-to-volume ratios [195]. Moreover, their size and shape are crucial to their use in wound healing because they play an important role in active drug delivery, penetrability, and cellular responses [195,196]. Two types of nanomaterials are commonly used in wound therapy: (1)

nanomaterials with intrinsic properties that typically promote wound treatment, and (2) nanomaterials as vehicles for the delivery of therapeutic agents [196]. In this regard, metal-based nanoparticles (NPs) demonstrated great effectiveness both as nano-biocides, due to their intrinsic and broad-spectrum antimicrobial activity, and as nano-carriers for the delivery of antimicrobial drugs [197]. Among all the investigated metal-based NPs, those made of silver are the most widely studied nowadays.

1.4.1 Silver nanoparticles (AgNPs)

Silver and its compounds have been used for therapeutic and antibacterial purposes for thousands of years, being considered one of the most potent weapons for eradicating a wide range of infections. Then, their use in medicine was replaced by the clinical introduction of antibiotics but, when bacterial resistance became a worldwide problem as a result of antibiotic abuse, silver began to arouse interest again, especially with the advent of nanotechnology in the early years of the century [198]. The broad-spectrum antibacterial activity of AgNPs is widely known and has been demonstrated to be higher than that of Ag^+ ions [199]. They can effectively kill various pathogens, including bacteria (*Escherichia coli*, *Klebsiella pneumonia*, *Staphylococcus aureus*), fungi (*Candida albicans* and *Aspergillus niger*), and viruses (*HBV* and *HIV*) even at extremely low doses. Furthermore, some studies have shown nematocidal and anthelmintic activity as well as anticancer efficacy associated to the use of AgNPs [198,200,201]. Although their antibacterial effect has been carefully studied, their action mechanism is still unclear, most likely because it is the result of several processes in which NPs participate. The most widely accepted mechanism concerns the accumulation of NPs on the bacterial cell wall, which compromises the double layer's integrity, increasing its permeability and leading to membrane dissolution. Increased permeability could also allow AgNPs to easily penetrate the cytoplasm and damage the intracellular organisms, including mitochondria and ribosomes, and to disrupt biomolecules, such as proteins and DNA. This would cause cellular toxicity and oxidative stress by the generation of reactive oxygen species (ROS) and free radicals [202,203]. The antimicrobial action of AgNPs is further attributed to a complex interplay of size, shape, and concentrations [203]. Particle size is a fundamental parameter in determining the effectiveness of AgNPs as antimicrobial agents. Smaller particles can penetrate more easily the cytoplasm,

accumulate in higher concentrations, and have a larger surface for interacting with both microbial cells and its components and organelles [202]. However, spontaneous aggregation resulting in the formation of larger and less efficient particles easily occurs, in order to decrease the available surface area and minimize the interfacial free energy of NPs [197]. In this regard, their loading in polymeric matrices, such as hydrogels or films, is a valid approach to maintain a high antibacterial activity since the crosslinking of polymer chains allows to limit the aggregation process of NPs [204]. Besides the ease of aggregation, also the use of strong reducing chemicals, such as hydrazine and sodium borohydride, could limit their medical applications due to their potential cellular toxicity [197]. An intriguing alternative to the traditional methods employed to produce AgNPs provided for the use of light irradiation. This technique can be applied to allow the generation of nanocomposite polymer matrices in only one manufacturing step [205,206]. Photopolymerization is a fast, economic and energy saving technique allowing the realization of coating or free-standing films by light irradiation, typically UV light. When photocurable polymer-based formulations containing metal salts are exposed to irradiation, a polymer network forms, and metal NPs are produced at the same time. Inorganic and organic phases simultaneously forming permits an excellent distribution of metal NPs in the polymeric network, avoiding agglomeration and limiting their size, thus realizing a polymer-metal nanocomposite material with suitable properties for biomedical and pharmaceutical applications in a very short time [205,207]. Since the methacrylate derivative of GG (GG-MA) is well known to undergo chemical crosslinking when subjected to UV irradiation forming biocompatible hydrogels, it was chosen as starting material for the design of AgNPs-loaded thin films potentially usable as innovative dressings to promote the healing of infected wounds. For this purpose, the solvent casting method was coupled with UV photocuring in order to allow the formation of the nanocomposite films in a single step.

molecules

MDPI

Article

Solvent Casting and UV Photocuring for Easy and Safe Fabrication of Nanocomposite Film Dressings

Laura Di Muzio [1,*], Prisca Simonetti [1], Vito Cosimo Carriero [1], Chiara Brandelli [1], Jordan Trilli [1], Claudia Sergi [2], Jacopo Tirillò [2], Francesco Cairone [1], Stefania Cesa [1], Giulia Radocchia [3], Serena Schippa [3], Stefania Petralito [1], Patrizia Paolicelli [1,*] and Maria Antonietta Casadei [1]

[1] Department of Drug Chemistry and Technologies, Sapienza University of Rome, 00185 Rome, Italy; simonetti.1748558@studenti.uniroma1.it (P.S.); vitocosimo.carriero@uniroma1.it (V.C.C.); chiara.brandelli@uniroma1.it (C.B.); jordan.trilli@uniroma1.it (J.T.); francesco.cairone@uniroma1.it (F.C.); claudia.sergi@uniroma1.it (S.C.); stefania.petralito@uniroma1.it (S.P.); mariaantonietta.casadei@uniroma1.it (M.A.C.)

[2] Department of Chemical Engineering Materials Environment, Sapienza University of Rome, 00184 Rome, Italy; stefania.cesa@uniroma1.it (C.S.); jacopo.tirillo@uniroma1.it (J.T.)

[3] Department of Public Health and Infection Disease, Microbiology Section, Sapienza University of Rome, 00185 Rome, Italy; giulia.radocchia@uniroma1.it (G.R.); serena.schippa@uniroma1.it (S.S.)

* Correspondence: laura.dimuzio@uniroma1.it (L.D.M.); patrizia.paolicelli@uniroma1.it (P.P.); Tel.: +39-06-4991-3173 (P.P.)

Abstract: The aim of this work was to optimize and characterize nanocomposite films based on gellan gum methacrylate (GG-MA) and silver nanoparticles (AgNPs) for application in the field of wound dressing. The films were produced using the solvent casting technique coupled with a photocuring process. The UV irradiation of GG-MA solutions containing glycerol as a plasticizer and different amounts of silver nitrate resulted in the concurrent crosslinking of the photocurable polymer and a reduction of Ag ions with consequent in situ generation of AgNPs. In the first part of the work, the composition of the films was optimized, varying the concentration of the different components, the GG-MA/glycerol and GG-MA/silver nitrate weight ratios as well as the volume of the film-forming mixture. Rheological analyses were performed on the starting solutions, whereas the obtained films were characterized for their mechanical properties. Colorimetric analyses and swelling studies were also performed in order to determine the AgNPs release and the water uptake capacity of the films. Finally, microbiological tests were carried out to evaluate the antimicrobial efficacy of the optimized films, in order to demonstrate their possible application as dressings for the treatment of infected hard-to-heal wounds, which is a demanding task for public healthcare.

Keywords: thin film; silver nanoparticles; gellan gum methacrylate; solvent casting; photocuring; antimicrobial activity; colorimetry; wound dressings

Citation: Di Muzio, L.; Simonetti, P.; Carriero, V.C.; Brandelli, C.; Trilli, J.; Sergi, C.; Tirillò, J.; Cairone, F.; Cesa, S.; Radocchia, G.; et al. Solvent Casting and UV Photocuring for Easy and Safe Fabrication of Nanocomposite Film Dressings. *Molecules* **2022**, *27*, 2959. https://doi.org/10.3390/molecules27092959

Academic Editor: Giuseppe De Rosa

Received: 3 April 2022
Accepted: 1 May 2022
Published: 5 May 2022

1. Introduction

Human skin, working as a boundary with the external environment, is continuously exposed to multiple injuries [1]. Physical or thermal damage can cause defects or interruptions in the epidermis of the skin, forming a wound. The healing process of a wound is influenced by several factors, including size, depth, degree of injury [2] and its eventual contamination. For these reasons, skin lesions heal at different times and with different outcomes [3,4]. In particular, acute wounds usually recover in a short period of time, restoring normal anatomical structure and function. On the contrary, the repair of chronic wounds is challenging, particularly when it is complicated by the appearance of infections during the healing process [5,6]. The onset of chronic wounds can lead to a net decrease in patients' quality of life and also produces a considerable expense for the health system.

The most common wound infections are those arising from abrasions and surgical wounds (one of the most common causes of health-care-related infections that can occur

after an invasive surgical procedure) and are caused by bacteria [7]. Among the main microorganisms responsible for wound infections are cocci, gram-positive bacteria such as *Staphylococcus aureus*, coagulase-negative Staphylococci and Enterococci including the most dangerous methicillin-resistant *S. aureus* (MRSA) and vancomycin-resistant *S. aureus* (VRSA). The presence of antibiotic resistant bacteria, often biofilm producers, makes the healing of infected wounds more difficult and challenging and compromises patients' lives [8]. Therefore, the search for new effective treatments that prevent and counteract infections, in addition to promoting the wound healing process, has increased in recent years [9,10]. Wound dressings are generally curative materials easily adaptable to different anatomical regions and endowed with high strength and elasticity [11–13]. In this scenario, systems based on hydrogels have received attention in recent years in therapeutically advanced wound care management, since they are particularly effective for the scope [14–16]. Hydrogels can be defined as highly hydrated polymeric materials whose structural integrity is ensured by physical or chemical inter- and intramolecular crosslinks between polymer chains. This feature makes these polymer networks capable of absorbing wound exudate and maintaining a moist environment, allowing gas exchange and thermal insulation, which are essential characteristics that support hydrogels in promoting repair and reversing chronic wounds. They are generally safe and can be easily and painlessly removed from the injury surface. Moreover, hydrogels possess adequate biomechanical and viscoelastic properties for suturing to the wound surface or applying to it. Globally, hydrogels meet most of the criteria for modern wound dressings, especially when produced in the form of films [17,18]. Wound dressing films are particularly convenient for wound care management because they are flexible, easy to apply, provide a physical barrier to prevent external opportunistic bacteria's entry and enable easy inspection of the injured site, without the need for dressing removal. They also allow for the regulation of gas exchange and the uptake of the exudate through the swelling process. Furthermore, the components of the films can actively participate in promoting the healing process [19,20]. Even more, wound dressing films can be loaded with active substances, including organic or inorganic nano-sized materials, capable of preventing and eradicating infections and offering better control over drug concentration for long times and improved drug stability at the wound site [21]. The wide application of nanomaterials in pharmaceutical and biomedical fields stems from the dramatic improvements of their chemical, physical, mechanical and optical properties in comparison to bulk materials. In this regard, metal-based nanoparticles (NPs) demonstrated great effectiveness both as nano-biocides, due to their intrinsic and broad-spectrum antimicrobial activity [22], and as nano-carriers for the delivery of antimicrobial drugs [23]. The research on metal-based NPs has heavily increased in recent years, and it is not expected to decrease due to their well-described antimicrobial activity against both gram-positive and gram-negative bacteria. Among all the investigated metal-based NPs, those made of silver (silver nanoparticles, AgNPs) are the most widely studied nowadays. The antibacterial and antioxidant activity, as well as the efficacy of silver in the treatment of wounds, have been well-known for a long time, and even though its use was abandoned when antibiotics were discovered, nowadays, silver is once again receiving significant attention as an alternative to traditional antibiotics to overcome bacteria resistance issues [24,25]. In this scenario, silver nanotechnology has led to increased demand for its medical application, including the control of infections in wound dressings. Indeed, AgNPs are some of the most intriguing and extensively employed materials for wound healing because of their excellent antimicrobial properties. Although the mechanism of action has not been fully understood, many articles highlight the therapeutic potential of AgNPs embedded in polymeric networks and their role in controlling wound contamination and biofilm formation [26–31]. AgNPs loaded wound dressings can overcome the problems of silver ions and silver sufadiazine (SSD) containing wound dressings, such as their rapid inactivation, unsustainable antibacterial nature, low biocompatibility and poor stability [30]. Moreover, the incorporation of AgNPs within polymer networks can improve their therapeutic potential [32]. Indeed, AgNPs generally tend to aggregate into larger particles to

decrease the available surface area, thus minimizing their interfacial free energy. In this way, the surface area to volume ratio decreases, and, consequently, their antimicrobial activity reduces, because the smaller specific surface area decreases the binding ability of AgNPs to the bacterial cell. Furthermore, AgNPs aggregation brings about a slower release rate of silver ions, which are conducive to the antimicrobial activity [33,34]. Therefore, nano-silver wound dressings show great prospects in wound repair treatment and are already widely used in the treatment of chronic wounds, such as bacterial infected and purulent wounds. Although nano-silver containing dressings show clear advantages when applied to infected wounds, some problems have been identified that seriously inhibit their wide applications, such as the easy agglomeration of AgNPs and the toxicity during preparation. Generally, there are two ways to load AgNPs into wound dressings. The first one consists of directly blending or soaking preformed AgNPs into dressings. In the second way, the dressing is generally first fabricated, while, in a second step, the matrix material is soaked with silver ions. Silver is then reduced in situ to obtain the final nano-silver dressing. In both cases, AgNPs are chemically synthesized, using strong reducing reagents, such as hydrazine and sodium borohydride, which are toxic for cells. The synthesis of high purity AgNPs is still a challenge, and there is a continuous demand for improved and safe synthetic techniques [35,36]. In this scenario, UV irradiation of silver salts solutions is considered one of the most rapid, safe and efficient methods [37,38]. Starting from this evidence, the aim of this work was the optimization and characterization of nanocomposite thin films containing colloidal silver (AgNPs) for application in the field of wound dressings. The nanocomposite films were produced using the solvent casting technique coupled with UV photocuring. The starting materials used for the preparation of the films were gellan gum (GG), a natural and biocompatible polysaccharide, and glycerol (Gly) employed as a plasticizer. Despite the well-known film-forming features of GG, its application for the development of antimicrobial wound dressings has barely been investigated [39]. GG and Gly were chosen based on recently reported results, demonstrating that they can be successfully combined to produce polymeric thin films with adequate physical and mechanical properties [40]. Considering that we decided to use UV irradiation for AgNPs synthesis, GG was chemically modified by the reaction with methacrylic anhydride to produce a methacrylate derivative of GG (GG-MA), due to its ability to form chemical and biocompatible hydrogels under UV irradiation [41,42]. Therefore, the solvent casting technique was coupled with UV photocuring to allow for the one-step production of nanocomposites films. Indeed, the photocuring of GG-MA solutions, containing the plasticizer and different concentrations of $AgNO_3$, should result in the simultaneous formation of the polymeric matrix and the in situ generation of AgNPs through the reduction of Ag^+ ions to Ag^0. At first, the composition of the films was optimized, varying the concentration and weight ratio of GG-MA and Gly, as well as the volume of the casted solution. Rheological analyses were performed on the different film-forming mixtures in order to evaluate their suitability for the solvent casting process. The dried films were subjected to physical and mechanical characterization, including thickness measurements, tensile studies and swelling evaluations. Colorimetric analyses were performed in order to verify the correlation between color change and the reduction of Ag^+ ions to Ag^0 and to assess the release of AgNPs. Finally, biological tests allowed for the assessment of the antimicrobial efficacy of AgNPs-loaded films in order to verify their possible application as dressing materials for the management of infected wounds. The proposed procedure can represent an interesting approach for the facile and safe fabrication of nanocomposite film dressings.

2. Materials and Methods

2.1. Materials

Gellan gum (Gelzan), glycerol (Gly), methacrylic anhydride (MAA), triethylamine (TEA), anhydrous dimethyl sulfoxide (DMSO), deuterated water (D_2O), 4-dimethylamin opyridine (4-DMAP), phosphate buffer saline (10 mM phosphate and 150 mM NaCl, pH = 7.4, which was labelled PBS), polyethylenglycole (PEG 20,000 Da), 2-hydroxy-4-

(2-hydroxyethoxy)-2-methyl-propiophenone (Irgacure 2959) and dialysis tubes (cut-off 12–14 kDa) were purchased from Sigma Aldrich (Milan, Italy). Silver nitrate ($AgNO_3$), monobasic potassium phosphate (KH_2PO_4, used to prepare 40 mM phosphate buffer, pH = 7.4, which was labelled PB), sodium hydroxide (NaOH) and hydrochloric acid (HCl) were purchased from Carlo Erba (Milan, Italy). Finally, 1-methyl-2-pyrrolidinone from Fluka (St. Louis, MO, USA). Triptone Soy Agar (TSA) and Brain Heart Infusion broth (BHI) were purchased from Oxoid (Basingstoke, UK).

2.2. Synthesis of Gellan Gum Methacrylate (GG-MA)

The functionalization of GG was performed as reported in the literature [41]. The procedure was slightly modified to allow for faster and easier dissolution of the polymer. Specifically, GG (1 g) was solubilized in anhydrous DMSO (65 mL) at 90 °C for 3 h under magnetic stirring. After complete solubilization, the temperature of the polymer solution was brought to 60 °C, and, subsequently, 4-DMAP (0.04 g), TEA (0.5 mL) and MAA (0.5 mL) were added. The reaction mixture was kept under magnetic stirring at 60 °C for 24 h. The synthesized polymer was purified by dialysis against distilled water and freeze-dried, employing a freeze-drier LIO5P (5 Pascal, Trezzano sul Naviglio, Italy). The polymeric derivative was characterized by ^{1}H-NMR analysis in D_2O and recorded with a Bruker AC-400 spectrometer (Bruker Corporation, Billerica, MA, USA). The degree of derivatization (DD%) was calculated as the ratio of the area of the protons of the methyl signal of the methacrylic group (at 1.9 ppm) and the methyl signal of rhamnose of the repetitive unit of GG (at 1.3 ppm), multiplied by 100. In this way, a DD% of 100 ± 1 was obtained. The small changes made to the synthesis protocol allowed for the obtention of a more efficient and reproducible methacrylation degree of GG-MA.

2.3. Rheological Characterization

The rheological measurements were conducted using a Discovery TA HR-1 stress-control rheometer (TA Instruments, New Castle, DE, USA). A cone-plate geometry with a diameter of 40 mm (α 1.005°, gap 27 μm) was used for all the experiments [40]. Solutions of GG (2.0% *w/v*) and of GG-MA containing different concentrations of Gly (2.0 and 4.0% *w/v*) were prepared, solubilizing both the components in distilled water at 50 ± 0.1 °C for 30 min under magnetic stirring. Then, 0.5 mL of the obtained solutions were poured on the Peltier plate of the rheometer, pre-heated at 50 °C. Oscillatory temperature-sweep analysis was carried out by decreasing the temperature from 50.0 to 30.0 ± 0.1 °C (cooling rate 3.0 ± 0.1 °C/min), keeping a constant frequency of 1 Hz and a deformation of 1%, which was previously determined using oscillatory strain-sweep tests. In addition, flow-sweep measurements were carried out on GG-MA solutions (2.0% *w/v*) containing or not containing different concentrations of Gly (2.0, 3.0 and 4.0% *w/v*). In particular, the viscosity as a function of the shear rate was measured, applying shear stresses in the range of 0.0005–500 Pa. The flow-sweep measurements were carried out at 40.0 ± 0.1 °C, the same temperature employed during the casting process. All the experiments were carried out at least in triplicate.

2.4. Film Preparation

GG-MA based films were produced using the solvent casting technique [40] coupled with a photo-polymerization process induced by UV light in the presence of the photoinitiator irgacure 2959. The films were prepared by dissolving the opportune amount of GG-MA and Gly in distilled water at 50 °C for 1 h under magnetic stirring. After complete solubilization, the temperature was decreased to 40 ± 1 °C, and appropriate volumes of $AgNO_3$ solution (30% *w/v*) and 7.5 μL/mL of irgacure 2959 (20% *w/v* solution in *N*-methylpyrrolidone) were added. Then, the film-forming mixture was poured onto a glass support (diameter of 4.5 cm) previously coated with a solution of PEG 20,000 (30% *w/v*) and subjected to irradiation with a UV lamp G.R.E (Helios Italquartz Srl, Cambiago, Italy). 125 W for 20 min. The first film samples were prepared with 6 mL of aqueous

mixtures containing 2.0% *w/v* of GG-MA and 3.0% *w/v* of Gly, as already reported in the literature for the preparation of GG-based thin films [40,43]. Different volumes of $AgNO_3$ aqueous solution (30% *w/v*) were used in order to produce films containing increasing quantities of AgNPs. At the end of the photocuring step, the samples were heat dried in an oven for 15 h at 40 ± 1 °C. In order to produce films with improved mechanical and physical properties, further samples were prepared by varying the concentration of Gly and GG-MA in the precursor solution or increasing the volume of the casted polymer solution from 6 to 12 mL. In the last case, the drying step was extended to 18 h. All the prepared films and their composition are reported in Table 1. The film samples obtained from film-forming mixtures containing different concentrations of GG-MA and Gly were labelled with different letters, whereas a subscript was used to specify the amount of silver salt included in the formulation.

Table 1. Composition of the film-forming mixtures for film preparation. Film samples were labelled with letters (the same letter was used for samples obtained from film-forming mixtures with the same concentrations of GG-MA and Gly) and a subscript, which was used to specify the amount of silver salt included in the formulation.

Sample	GG-MA (% *w/v*)	Gly (% *w/v*)	$AgNO_3$ (mg/mL)	Casted Volume (mL)
A_5	2.0	3.0	5	6
A_{10}	2.0	3.0	10	6
A_{20}	2.0	3.0	20	6
A_{30}	2.0	3.0	30	6
A_{40}	2.0	3.0	40	6
A_{50}	2.0	3.0	50	6
B_{40}	2.0	4.0	40	6
C_{40}	2.0	2.0	40	6
D_{40}	1.5	2.0	40	6
E_{40}	1.5	1.0	40	6
F_5	1.5	1.0	5	12
F_{10}	1.5	1.0	10	12
F_{20}	1.5	1.0	20	12
F_{30}	1.5	1.0	30	12
F_{40}	1.5	1.0	40	12

2.5. Film Characterization

Films F_5, F_{10}, F_{20}, F_{30} and F_{40} were characterized for their physical and mechanical properties, as described in the following sections.

2.5.1. Measurement of Film Thickness

The thickness of all the prepared films was measured by using the thickness gauge Mitutoyo Digimatic Micrometer (Mitutoyo Corporation, Lainate, Italy). The measurements were carried out in six different points of the same film in order to evaluate the homogeneity of the prepared samples. The results were reported as mean values ± standard deviation.

2.5.2. Scanning Electron Microscopy (SEM) and Energy Dispersive Spectroscopy (EDS)

The films were submerged in 30 mL of phosphate buffer (PB, pH = 7.4) for 5 min to eliminate Gly present in the formulations and then freeze-dried. The resulting samples were morphologically characterized through a field-emission scanning electron microscope (FE-SEM) MIRA 3 (Tescan, Brno, Czech Republic). The morphological characterization was supported by an elemental analysis through the EDS Octane Elect (Edax, Leicester, UK). Samples sputter coating with gold or other conductive materials was intentionally avoided to prevent EDS analysis alterations.

2.5.3. Mechanical Characterization: Tensile Tests

The mechanical performance of the films was evaluated through tensile testing [40]. The tests were performed with a Zwick/Roell Z010 (Zwick/Roell Srl, Genova, Italy) equipped with a 100 N load cell. A test speed of 2 mm/min was used. Specimen length was slightly variable due to the circular nature of the produced films, but a fixed grip-to-grip separation of 15 mm was used, whereas specimen width was 3.5 mm ± 0.3 mm. The experiments were carried out at least in triplicate, and the results were reported as mean values ± standard deviation.

2.5.4. Colorimetric Analysis

The films were subjected to colorimetric analysis using a MetaVue X-Rite TM colorimeter (X-Rite, Grand Rapids, MI, USA), featuring an LED illuminant/45-0°. The L* (luminance), a* (redness-greenness), b* (yellowness-blueness), C^*_{ab} (chroma) and h° (hue angle) values were calculated using the iColor software (X-Rite, Grand Rapids, MI, USA). The CIEL*a*b* parameters were used to describe the chromatic properties of the heat dried films characterized by a progressively increasing content of AgNPs (F_5, F_{10}, F_{20}, F_{30} and F_{40}).

2.6. Swelling Studies

The films were characterized through dynamic swelling measurements [40]. Each film was divided into three portions of comparable size, weighed and immersed in 15 mL of PB (pH = 7.4) at 37.0 ± 1.0 °C. At predetermined time points, the samples were extracted from the medium, gently wiped to remove the liquid in excess and weighed. The degree of swelling (Q) was calculated as follows:

$$Q = \frac{W_s}{W_d}$$

where W_s and W_d represent, respectively, the weight of the swollen sample at time t and that of the dry sample. The measurements were continued up to 24 h. However, after 15 min, some specimens of each sample were recovered and heat dried at 40 ± 1 °C until constant weight (W_e). These samples were used to evaluate the contribution to weight loss due to the outward diffusion of Gly and AgNPs. In this case, the degree of swelling was expressed as water uptake (WU) and calculated as follows:

$$WU = \frac{W_s - W_e}{W_e}$$

The experiments were carried out at least in triplicate, and the results were reported as mean values ± standard deviation.

2.7. Release Studies

Silver release was qualitatively monitored by colorimetric analysis and DLS measurements. To this end, F_{40} films were selected for the investigation because they were characterized by the highest silver loading and allowed for a more evident chromatic variation of the release medium. Colorimetric analysis was carried out as reported in Section 2.5.4, whereas dynamic light scattering (DLS) measurements were performed with a Zetasizer Pro (Malvern Panalytical, Malvern, UK) analyzer. The release studies were carried out by immersing the films in 100 mL of PB (pH = 7.4) at 37.0 ± 0.1 °C without stirring. At defined time points, from 1 min to 4 h, aliquots of 1 mL of the release medium were withdrawn and analyzed to evaluate the presence of AgNPs by color evaluation and DLS measurements. At the end of the analyses, the samples taken from the release medium were immediately placed back into the release solution to restore the initial volume. The experiments were carried out in triplicate.

2.8. Antimicrobial Activity of Films Loaded with AgNPs

2.8.1. Antimicrobial Activity in Liquid Culture Media

The antimicrobial activity of films loaded with different quantities of AgNPs was tested on two collection strains, *Staphylococcus aureus* ATCC 6538 (American Type Culture Collection, Manassas, VA, USA) and *Escherichia coli* MG1655 (ATCC 700926) (American Type Culture Collection, Manassas, VA, USA). These strains were conserved at −80 °C in glycerol stocks. For the experiments, the strains were cultured directly from glycerol stock on a TSA plate and incubated aerobically overnight at 37 °C. A colony grown on a TSA plate was inoculated in BHI and incubated overnight at 37 °C with agitation (180 rpm). The bacterial suspension concentration was then measured spectrophotometrically at 600 nm (OD600) (BioPhotometer, Eppendorf, Hamburg, Germany). For the assay, both for *E. coli* MG1655 and *S. aureus* ATCC 6538, a bacterial suspension 1×10^8 CFU/mL was seeded in a 24-well plate (500 µL/well) containing a disk of film for each well. The films had all the same dimension (1 cm of diameter) and weight (10 mg c.a.) but were loaded with different concentrations of AgNPs (5, 10, 20, 30, 40 mg/mL). A higher concentration of AgNPs (80 mg/mL) was also tested using two samples of the F_{40} film loaded with 40 mg/mL of AgNPs. For each bacterial strain, a well without the film was used as the positive control of bacterial growth. The plate was then incubated at 37 °C for 24 h. After the incubation, the contents of each well were collected, and serial 10-fold dilutions were prepared in PBS and seeded on TSA plates in order to count the CFU/mL. Each concentration was tested three times. Furthermore, the maintenance of the activity over time was evaluated by performing antimicrobial assays for four days using the same disks of F_{40} nanocomposite film. Briefly, the disk was added to a bacterial suspension 1×10^8 CFU/mL of *E. coli* MG*1655* or *S. aureus* ATCC *6538*, as described above. Every 24 h (time points were 24, 48, 72 and 96 h), the medium was collected and replaced with a fresh bacterial suspension (1×10^8 CFU/mL). The collected media were then used to estimate the bacterial load by seeding on a TSA plate, as described before.

All the experiments were performed in triplicate, and the results were reported as mean values ± standard deviation.

2.8.2. Antimicrobial Activity in Solid Culture Media (Diffusion Test)

To create a more hydrated/humid environment necessary for the diffusion of AgNPs, from the films inside the media, we decided to perform the diffusion tests using double layer plates. A bottom layer was prepared with TSA 1% of agar, and a top layer (a germs agar) was prepared with TSA 0.6% of agar and 1×10^8 CFU/mL of bacteria (*E. coli* MG1655 or *S. aureus* ATCC 6538). Disks of film, all of the same dimension (1 cm of diameter) and weight (10 mg c.a.), loaded with different concentrations of AgNPs (5, 10, 20, 30, 40, 80 mg/mL) were put on plates. Then, the plates were incubated at 37 °C for 24 h. After the incubation, the halos formed around the disks were observed to evaluate if the AgNPs were able to diffuse in the agar medium and inhibit bacterial growth.

2.9. Statistical Analysis

The statistical significance was assessed using the GraphPad Prism 9 statistical software package (GraphPad Software, Inc., San Diego, CA, USA), using the one-way ANOVA test for multiple comparison and Dunnett's multiple comparisons test to compare paired samples. Differences were considered statistically significant when the *p*-value was less than 0.05.

3. Results and Discussion

3.1. Film Preparation and Optimization

A methacrylic derivative of GG (GG-MA) was employed to develop nanocomposite films containing AgNPs. The use of this photocrosslinkable polymer should allow for the production of a long-lasting and stable polymer network and the concurrent reduction of silver ions in a single step UV-based photocuring process. Solvent casting has already been

coupled with UV irradiation for the fabrication of nanocomposite films. UV photocuring has always been used to allow for either polymer crosslinking or silver reduction [44,45]. Instead, in this work, it was used to let the two processes occur in the same fabrication step.

GG-MA was synthesized following a classic and well-established procedure based on the reaction of GG with MAA in anhydrous DMSO [41,42]. The synthesis protocol and the molar ratio of the reagents were optimized to attain a DD% of 100 ± 1, which was calculated by the ^{1}H-NMR spectrum as the ratio of the area of the methyl protons of the methacrylic group (at 1.9 ppm) and the methyl signal of rhamnose of the GG repeating unit (at 1.3 ppm), multiplied by 100. The attained DD% of 100 ± 1 means that an average of one methacrylic group was introduced in every repeating unit of the polymer. This is an unusual way to express the DD%, which is more typically calculated as the fraction of hydroxyl groups per repeating unit that have been methacrylated [46]. Following the classic definition of DD%, the synthesized GG-MA has a derivatization degree of 10 ± 1%, which means that only one hydroxyl group of the repeating unit was modified. However, we found the novel proposed DD% to be a more intuitive and simple way to define the methacrylation degree of GG-MA.

The obtained GG-MA was used to prepare nanocomposite films, adopting a solvent casting procedure coupled with UV photocuring and subsequent heat drying, as schematized in Figure 1A. The film formulation was optimized with a trial-and-error approach. Specifically, the casting and spreadability of the film-forming solutions as well as flexibility, elasticity, peeling and uniformity of the films were the main attributes evaluated for the optimization of the formulations. The first attempts to prepare GG-MA films were made considering our previous studies on GG-based OTFs (Oral Thin Films) [40,43]. For this reason, a 2.0% *w/v* polymer concentration was used in samples A, B and C (Table 1), which show a typical pseudoplastic behavior and viscosity values at 40.0 ± 0.1 °C, suitable for the casting process (Figure 2A). GG-MA films were prepared using Gly as a plasticizer, which is essential to easily peel off film from the support and allow for the formation of films with adequate elasticity, flexibility and strength, as observed with previous GG-based OTFs. Indeed, using Gly as the plasticizing agent, the mechanical properties of GG-based OTFs were significantly improved [40,43]. For these reasons, Gly was added to GG-MA solution, and its influence on the viscosity of the film-forming solution was investigated. Indeed, the plasticizer may affect the flow properties of the polymer solutions, which are of fundamental importance when polymeric films are prepared using the solvent casting technique, since inadequate viscosity and viscoelasticity may affect the final outcome, leading to barely uniform and homogenous films. The flow curves of solutions containing 2.0% *w/v* of GG-MA and different concentrations of Gly, from 2.0% to 4.0% *w/v*, are reported in Figure 2A. Regardless of the amount of plasticizer used, the solutions had almost the same behavior, with viscosity values suitable for casting in all the cases. In addition, further rheological studies were carried out, aimed at evaluating the physical state and internal structure of the polymer system (physical gel or solution) during the casting process. For this reason, temperature sweep tests were recorded in the temperature range from 30.0 to 50.0 °C on GG-MA at 2.0% *w/v*, alone or mixed with 4% *w/v* of Gly (Figure 2B). It was observed that, regardless of the presence of the plasticizer, the cross-over of the G′ and G″ moduli did not occur in the temperature range considered. Therefore, the entire casting process and the following photocuring step could be carried out on polymer solutions, which allows for adequate polymer chain mobility and the formation of homogeneous and uniform films. The early sol-gel transition and the consequent formation of a physical gel would result in the uneven spreading of the mixtures on the surface of the support during the casting process. Moreover, it may reduce the polymer mobility and interfere with the following free radical crosslinking of GG-MA during the UV irradiation step. On the basis of these results, 2.0% and 3.0% *w/v* were selected as the starting concentrations of GG-MA and Gly, respectively, and 40 °C was selected as the casting temperature. The total volume of casted solution was fixed to 6 mL in order to obtain films of suitable thickness after the drying step, carried out at 40 °C for 15 h. Different volumes of $AgNO_3$ (30% *w/v*) were

added to the polymer solution in order to obtain increasing concentrations of silver ions and consequently AgNPs (see samples A_5–A_{50} in Table 1).

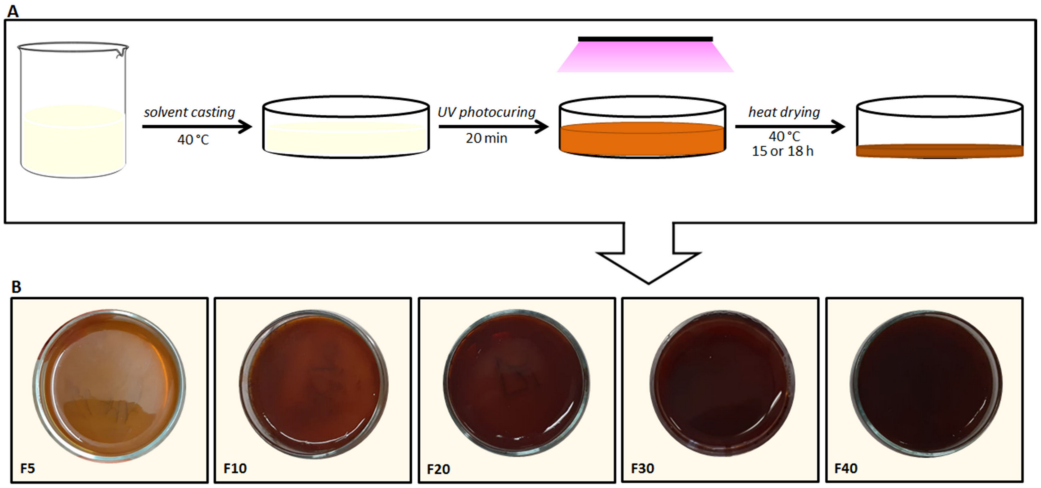

Figure 1. (**A**) Schematic of the procedure followed for the preparation of the nanocomposite films. (**B**) Images of the films obtained after the photocuring step.

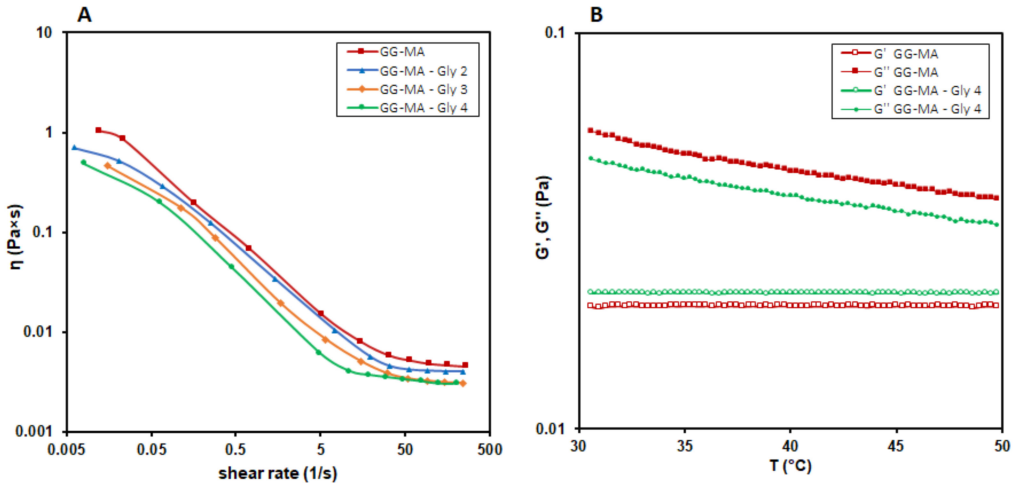

Figure 2. Effect of Gly on (**A**) the flow properties and (**B**) the sol-gel transition of GG-MA solutions (2% *w/v*).

The results showed that the use of $AgNO_3$ concentrations higher than 40 mg/mL gave rise to the formation of a polymer mixture unsuitable for solvent casting, owing to an evident increase in the viscosity, which resulted in inhomogeneous and irregular deposition of the film-forming mixture on the film mold. Therefore, 40 mg/mL was established as the maximum concentration of $AgNO_3$. After casting, the polymer mixtures were UV irradiated for 20 min in the presence of the photoinitiator Irgacure 2959. The photocured mixtures were then heat dried at 40 °C for 15 h, and the obtained films were peeled off from the glass support and visually observed. All the obtained films showed an evident and marked tendency to shrink at the end of the drying process; this phenomenon was less evident in samples with lower AgNPs content. Therefore, to limit this film defect and, at the same time, improve film handling, further films were prepared, varying the concentrations of GG-MA and Gly (samples B_{40}, C_{40}, D_{40}, E_{40} in Table 1). In these cases, it was observed that increasing Gly from 3.0 to 4.0% *w/v* still resulted in evident film shrinkage, whereas the characteristics of the film were considerably improved when the concentration of Gly was reduced from 3.0 to 2.0% *w/v*. The appearance of the films and the tendency to shrink were further improved when the concentration of GG-MA was reduced from 2.0 to 1.5 *w/v*

(samples D_{40} and E_{40} in Table 1). The rheological analyses (flow-sweep measurements and oscillatory temperature-sweeps analyses) were not repeated on these samples, since the polymer concentration was reduced to 1.5% *w/v*, and it was reasonable to assume adequate rheological properties for casting in these cases as well. Both D_{40} and E_{40} films did not shrink markedly and almost preserved the diameter of the glass support. At the same time, these films showed consistency and flexibility suitable for their possible application as wound dressings, particularly those obtained from GG-MA 1.5% and Gly 1.0% *w/v* mixtures. These concentrations were therefore employed for the preparation of films with different AgNPs content. However, when mixed with $AgNO_3$, the film-forming solutions still showed inappropriate rheological properties for even casting on the glass support. To avoid these problems, the weight ratio between GG-MA and $AgNO_3$ was half reduced, and a double volume of the film-forming mixture (passing from 6 mL to 12 mL) was casted on the support. In this way, the formation of homogeneous and uniform films was possible, reaching a concentration of $AgNO_3$ as high as 40 mg/mL. Obviously, by increasing the final volume of the film-forming solution, it was necessary to further optimize the duration of the drying step. In particular, the drying time was prolonged to 18 h in order to obtain finished films with optimal residual moisture content, which is fundamental for proper film handling. Finally, nanocomposite films with different AgNPs content (samples F_5, F_{10}, F_{20}, F_{30}, F_{40} in Table 1) could be obtained using five different $AgNO_3$ concentrations (5, 10, 20, 30 and 40 mg/mL), GG-MA at 1.5% *w/v*, Gly at 1.0% *w/v* and casting a final volume of 12 mL. Under these conditions, it was possible to produce the nanocomposite films reported in Figure 1B. Despite the high concentrations of $AgNO_3$, particularly in the F_{40} formulation, the formation of crosslinked networks was not hampered but maybe assisted by silver.

3.2. Film Characterization

All the optimized films were characterized for the thickness and the tensile properties, and the results are reported in Table 2.

Table 2. Thickness, tensile modulus and tensile strength of films F_5, F_{10}, F_{20}, F_{30} and F_{40}. The measurements were carried out at least in triplicate, and the results are reported as mean values ± standard deviation.

Sample	Thickness (μm)	Tensile Modulus (MPa)	Tensile Strength (MPa)
F_5	72.2 ± 2.6	2.13 ± 0.24	0.41 ± 0.08
F_{10}	97.0 ± 6.4	2.70 ± 0.28	0.45 ± 0.07
F_{20}	116.0 ± 9.0	3.05 ± 0.24	0.47 ± 0.06
F_{30}	130.8 ± 6.4	3.21 ± 0.17	0.59 ± 0.03
F_{40}	152.3 ± 10.6	3.43 ± 0.30	0.61 ± 0.04

The thickness was measured in six different points of each film to assess their homogeneity and uniformity. The obtained results showed the formation of films having almost uniform thickness, thus confirming the suitability of the set-up conditions adopted for the casting and drying processes. Moreover, a progressive increase in the thickness values of the films can be observed as the GG-MA/$AgNO_3$ weight ratio decreases, as expected.

The tensile properties of the films were also evaluated, and the resulting tensile modulus and strength values are reported in Table 2. A stiffening and strengthening effect for increasing AgNPs content can be observed—in particular, an increase of 61% in tensile modulus and of 48% in tensile strength is achieved moving from F_5 to F_{40} formulation. Standard deviation values highlight a variation in the range of 5–15% from the mean value, highlighting the good repeatability in the tensile properties. These results are coherent with the ones reported by Thiagamani et al. [47] for banana peel powder and AgNPs cellulose-based films and by Fan et al. [48] for cellulose nanocrystals and AgNPs PVA films.

The optimized films were also characterized for morphology and color by FE-SEM and colorimetry, respectively. The morphological and elemental analyses of all the F formulations (F_5, F_{10}, F_{20}, F_{30} and F_{40}) are reported in Figure 3. All the films show a smooth surface and three typical peaks, namely, the ones of carbon (C), oxygen (O) and silver (Ag). The first two peaks can be ascribed to the polymeric nature of the film being the main components of the backbone. Concerning the Ag peak deriving from the nanoparticles, it displays an increasing intensity, moving from 5 mg/mL to 40 mg/mL, thus confirming the increasing number of AgNPs dispersed in the film. Small traces of chloride can be also detected in the samples and must be ascribed to the buffer solution used to remove glycerol from the films. This procedure was necessary to achieve sample desiccation fundamental to ensuring specimen analyzability through SEM.

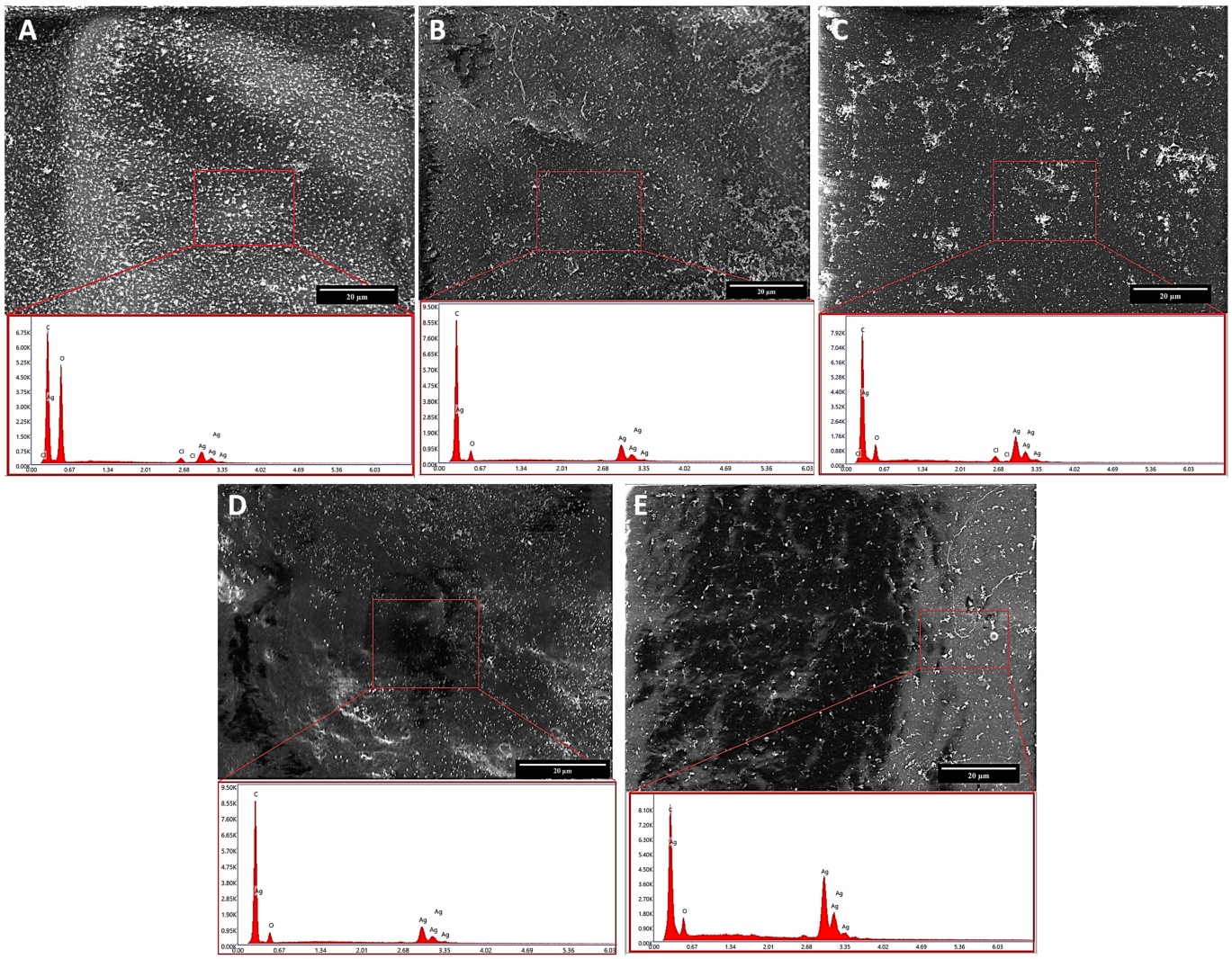

Figure 3. SEM micrographs and corresponding EDS analysis of (**A**) F_5, (**B**) F_{10}, (**C**) F_{20}, (**D**) F_{30} and (**E**) F_{40} film, respectively. The scale bar is 20 µm.

Color analyses were also performed on the finished films. Figure 1B shows a uniform color distribution and a constant browning expressed by the fresh films obtained after the photocuring process, consistent with the increasing AgNPs content. On the contrary, the reflectance curves recorded on the corresponding heat dried systems showed a constant rise correlated with a constant increase in the L* values (from 20 to 35) from F_5 to F_{30} (Figure 4A). This result is apparently at odds with the increase in the a* and b* values and the correlated color saturation, which rises from 9 to 14. In F_{40}, a weak decrease of b*,

reflecting on the related saturation, was observed, but a similar trend, with a further L* increase, was shown, denoting that the rise of this parameter is relatively independent of the other two parameters a* and b* (Table 3).

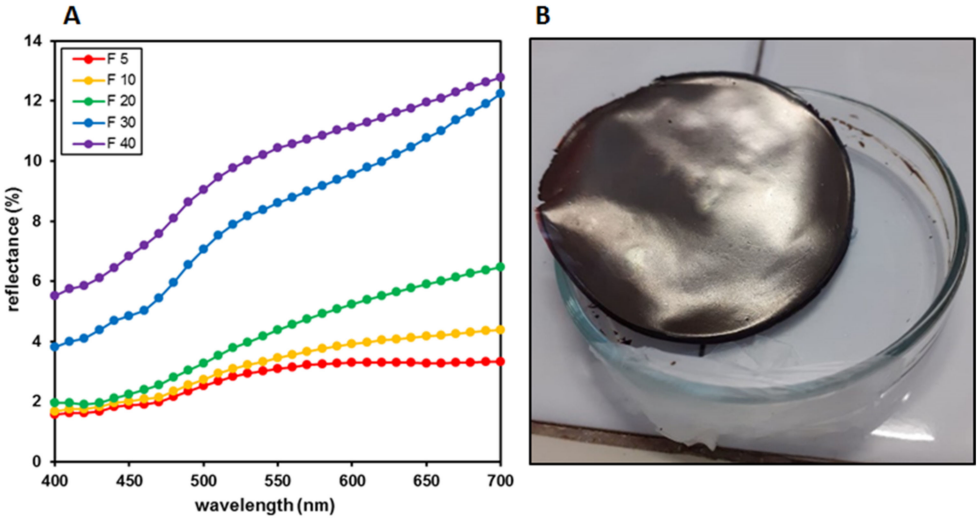

Figure 4. (**A**) Reflectance curves of films F_5, F_{10}, F_{20}, F_{30} and F_{40}. (**B**) Photograph of F_{40} film showing the mirror effect observed after the heat drying step.

Table 3. Colorimetric parameters of heat dried films F_5, F_{10}, F_{20}, F_{30} and F_{40}.

Film Samples	L*	a*	b*	C^*_{ab}	h°
F_5	19.68	−0.02	8.62	8.62	91.34
F_{10}	21.39	0.02	9.88	9.95	83.04
F_{20}	24.34	1.02	12.78	13.03	78.75
F_{30}	34.83	1.21	13.88	13.91	85.72
F_{40}	38.16	2.54	11.10	11.11	89.85

On the whole, this means that, notwithstanding the constant browning, which was also visually perceived on the films' surfaces (Figure 4B), what is really expressed by the reflectance curves is the appearance of the mirror effect, which in turn is correlated with the increased silver content and its clustering in the solid phase, obtained during the heat drying process [49,50].

3.3. Swelling Measurements

The results obtained from the dynamic swelling studies conducted at 37.0 °C in PB (pH = 7.4) on films containing increasing AgNPs concentrations are reported in Figure 5A. A progressive decrease in the *Q* value is evident, passing from F5 to F40 film (blue data in Figure 5B). However, an evident loss of AgNPs and probably of Gly was observed during the swelling experiments. Indeed, as soon as the films came into contact with the swelling medium, an outward diffusion of AgNPs took place. It is likely that Gly was also involved in the diffusion process and lost from the films, as already reported for GG-based OTFs [40]. Therefore, the *Q* value, typically calculated as the ratio between the swollen and dry weight of the film, is not ideal to describe the swelling process of these films. If, on the one hand, the film adsorbs PB going into swelling, on the other hand, some film components diffuse toward the external medium and are lost from the film. Therefore, the obtained *Q* values are not very reliable and, for this reason, they were corrected, taking into account Gly and silver loss. To this end, a series of swelling experiments were carried out, limiting to 15 min the contact time of the films with the swelling medium. After this time, each system was recovered, dried and weighed to estimate the entity of weight loss dependent on the outward diffusion of Gly and AgNPs. The measured weight values (W_e)

confirmed that, during the swelling process, an effective decrease in the weight of the film sample took place. Moreover, using these W_e values, the swelling degree of the films was recalculated and expressed as water uptake (*WU*). The obtained results are reported in Figure 5B (red data). It can be observed that, in any case, even taking into account the loss of AgNPs and Gly that occurred during the swelling process, the *Q* and *WU* values follow the same decreasing trend. Indeed, the water uptake capacity of the films also decreases with increasing AgNPs content, and this behavior may be explained by the hydrophobic nature of the AgNPs or, alternatively, by a silver-mediated crosslinking of GG-MA. It may be likely that silver is also involved in the network formation such that more silver means a denser crosslinked structure and consequently a lower swelling degree. Therefore, even if some components of the films are lost during the swelling process, the AgNPs still present inside the films influence and limit the swelling capacity of the system. While both the *Q* and *WU* parameters can be used to describe the swelling ability of these nanocomposite films, the *WU* values are, in our opinion, more reliable and allow for the better assessment of the behavior of these systems when in contact with a wound, particularly an exudative one.

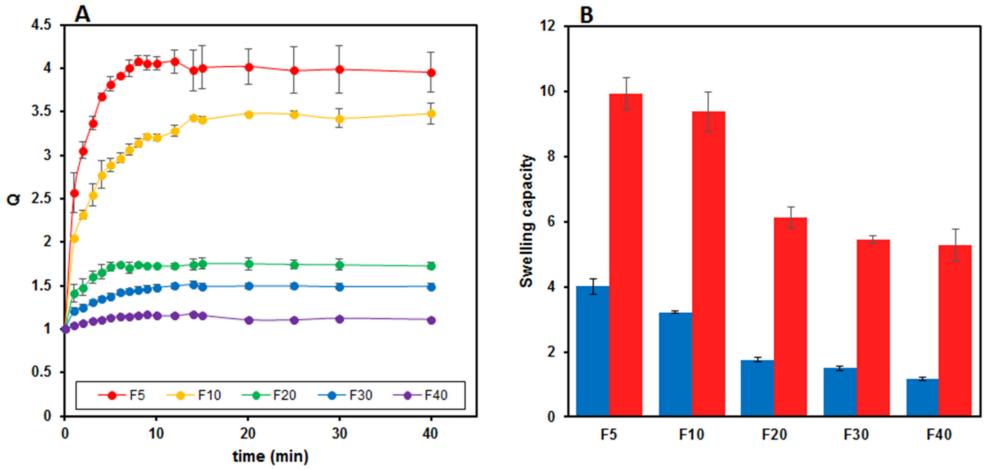

Figure 5. Swelling capacity of nanocomposite films measured in PB (pH = 7.4) at 37.0 ± 0.1 °C. (**A**) Dynamic swelling over time. (**B**) Comparison between the swelling degree (blue bars) and water uptake capacity (red bars) of films with different AgNPs content. Results are reported as the mean ± the standard deviation (n = 3).

3.4. Release Studies

The release of AgNPs was studied in PB (pH = 7.4) at 37.0 ± 0.1 °C and monitored performing color and DLS analyses on samples of the release medium taken at different times. The results reported in Figure 6A show a constant browning correlated with a smooth lowering of the reflectance curves. Differently from the logarithmic trends shown by the lightness and the tonality (Figure 6B,C), the color saturation (C^*_{ab}) reaches a maximum between 15 min and 20 min, followed by a substantial stabilization at slightly lower values (Figure 6D). Considered on the whole, the color data of the release medium seem to indicate that these nanocomposite films could be adaptable to a slow and prolonged release of AgNPs and could potentially represent a good and interesting system to maintain a constant silver content in the wound. DLS measurements evidenced a progressive and almost rapid increase in the hydrodynamic diameter of AgNPs in the release medium (Figure 6E). Therefore, quantitative information could hardly be obtained from colorimetric data, because color parameters are influenced by the number of AgNPs released over time but also by their size [51,52].

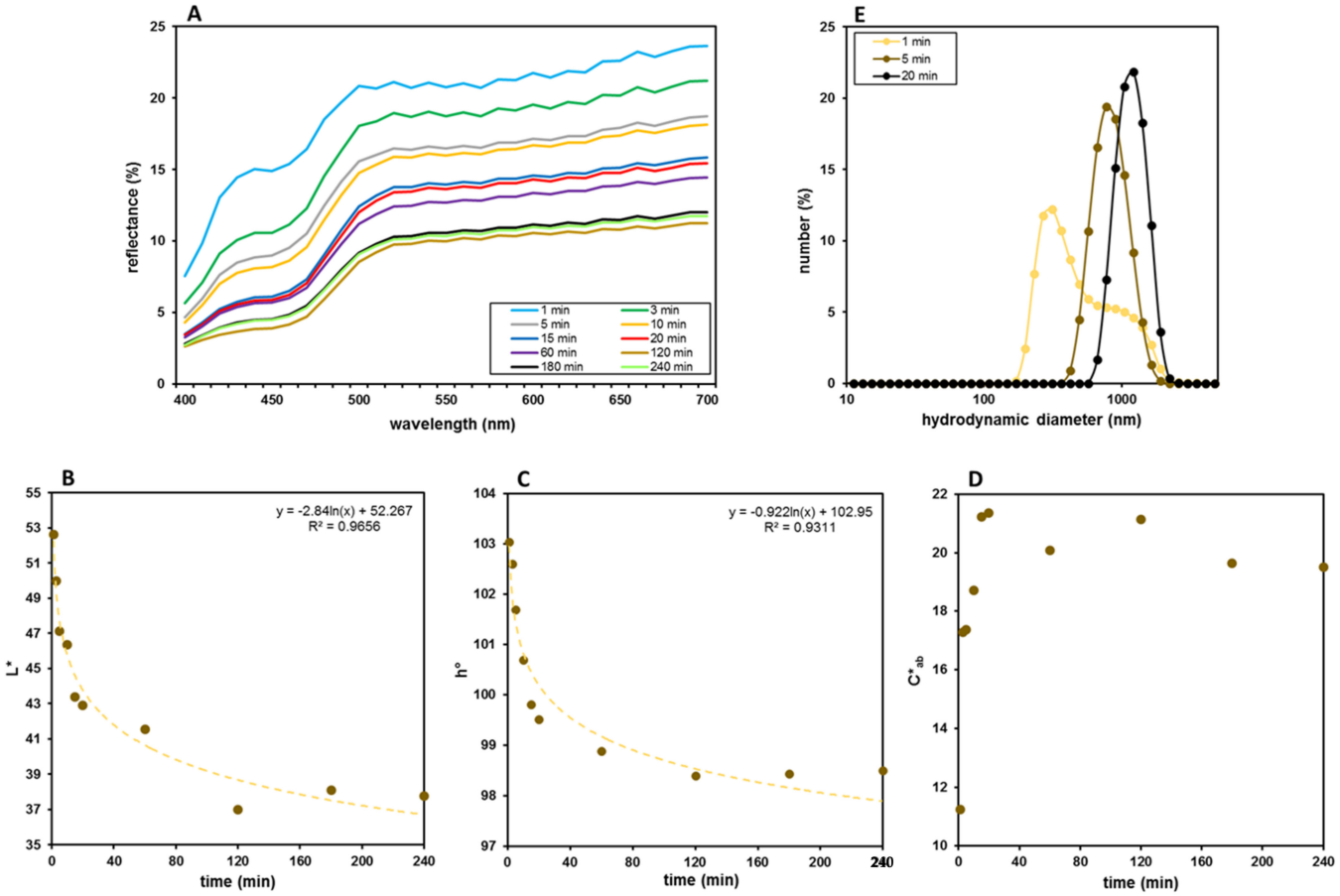

Figure 6. Release of AgNPs in PB (pH = 7.4) from F_{40} films evaluated by colorimetric and DLS analyses of the release medium over time. (**A**) Reflectance curves recorded at different time points. Trends of (**B**) L*, (**C**) h° and (**D**) C^*_{ab} values. (**E**) Hydrodynamic diameter of released AgNPs measured at three different and representative time points.

3.5. Antimicrobial Activity of Films Loaded with AgNPs

To verify the possible application of the GG-MA films loaded with AgNPs as dressings for the treatment of infected wounds, antimicrobial activity assays were carried out in solid and liquid culture media.

3.5.1. Antimicrobial Activity in Solid Culture Media (Diffusion Test)

The halos formed after 24 h of incubation of the double layer plates were all of a few millimeters of diameter (c.a. 5 mm), independently from the Ag concentration in the GG-MA based film. Indeed, the halos were the same for all Ag concentrations assayed, probably because the silver contained in the disks did not diffuse into the soil. It is possible that the agar medium was not sufficiently hydrated to allow for adequate AgNPs diffusion. This type of assay does not allow for the proper assaying of the antimicrobial activity of polymeric films; therefore, further studies were carried out working under experimental conditions capable of better allowing the release of AgNPs.

3.5.2. Antimicrobial Activity in Liquid Culture Media

The evaluation of the antimicrobial activity of films with AgNPs carried out in liquid culture media showed that, for both strains, after 24 h of incubation, the concentration of bacteria significantly decreased with respect to the control ($p < 0.0001$) for each Ag concentration assayed. The bacteria concentration decreased with the increasing of AgNPs concentrations in the film, particularly with *S. aureus* (Figure 7A). On the contrary, similar effects were produced on the *E. coli* strain by formulations from F_5 to F_{30}, whereas the F_{40}

film caused a marked reduction of bacteria concentration. Indeed, the oscillations observed for this strain were repeated in all the experiments performed, and the observed differences among the F_5, F_{10}, F_{20} and F_{30} formulations were not significant, whereas significant differences were observed between the F_{30} and F_{40} films. Furthermore, the highest Ag concentration tested (80 mg/mL, obtained using two samples of F_{40} film) turned out to be bactericidal for both the strains. Further studies were carried out on F_{40} nanocomposites films to test their antibacterial activity over time. To this end, the F_{40} films were challenged daily with 10^8 microorganisms for 4 days [53]. The results reported in Figure 8 show that F_{40} films possess substantial antibacterial potential, particularly against *E. coli*. Maximum activity is observed at day 1 due to the burst release of silver; however, even at days 2 and 3, the nanocomposite film is still able to reduce the initial number of microorganisms by at least four log fold. The level of contamination of infected wounds is not always easily predictable; however, it can be safely considered that the challenge of 10^8 microorganisms per day for 4 days would be almost unrealistic in a real wound, unless it was grossly reinfected. This test allowed for the maximization of the work that the dressing must do in order to gauge its remaining antimicrobial capacity.

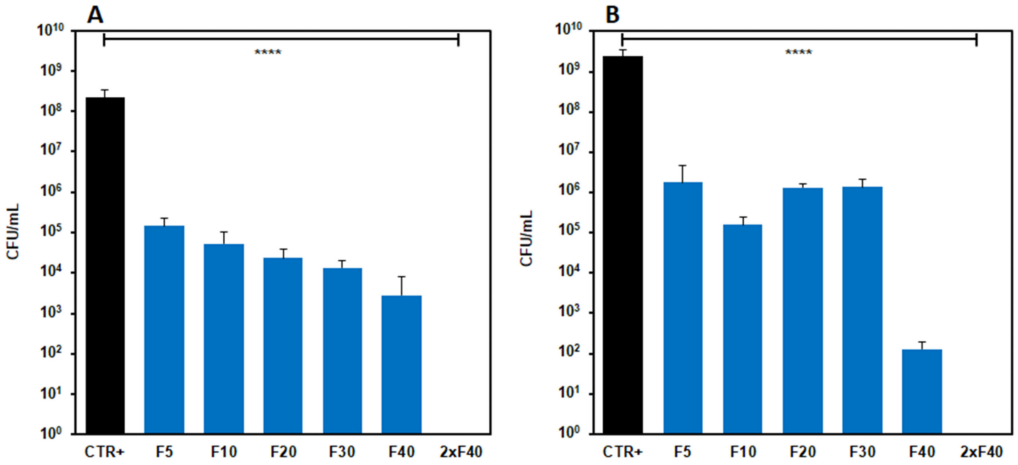

Figure 7. Antimicrobial activity of nanocomposite films tested in liquid culture media on *Staphylococcus aureus* ATCC 6538 and *Escherichia coli* MG1655. Liquid culture media: (**A**) *S. aureus*, (**B**) *E. coli*. Results are reported as the mean ± the standard deviation (n = 3). **** $p < 0.0001$.

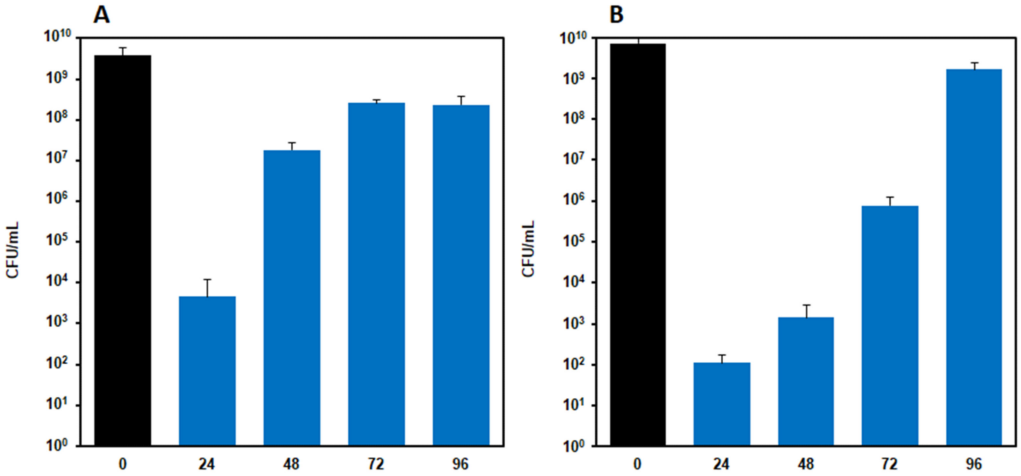

Figure 8. Antimicrobial activity of F40 nanocomposite films tested in liquid culture media on (**A**) *Staphylococcus aureus* ATCC 6538 and (**B**) *Escherichia coli* MG1655. Films were daily moved in fresh culture media containing 10^8 CFU/mL microorganisms for 4 days, and, at each time point (24, 48, 72 and 96 h), the residual bacterial concentration was measured. Results are reported as the mean ± the standard deviation (n = 3).

Results denote that Ag still maintain a good antimicrobial activity versus the two bacterial strains assessed, even when loaded on GG-MA based film, indicating this delivery system to be a good candidate for the treatment of wound infections often difficult to eradicate.

Globally, the obtained results open prospective for the application of photocurable GG derivatives for the fabrication of nanocomposite films with antibacterial properties. GG is only marginally considered in the scenario of the wound dressing materials [39], even if it possesses interesting features to efficiently support wound healing [54–57].

4. Conclusions

Nanocomposite films containing AgNPs were produced through the reduction of Ag^+ to Ag^0 and clustering into nanostructures within polymer networks under UV irradiation. This approach allowed, after casting of the film-forming solution, for the concurrent formation of AgNPs and chemical crosslinking of the photocurable polymer GG-MA. The proposed procedure represents an interesting and safe alternative for silver dressing fabrication.

GG-MA/silver ions and GG-MA/plasticizer weight ratios resulted in the most critical experimental parameters for the formation of homogeneous and uniform nanocomposite films with adequate mechanical properties. In particular, the GG-MA/Ag^+ weight ratio affected the rheological properties of the film-forming mixture, which critically influence the solvent casting process and the even distribution of the mixture on the support. Instead, the GG-MA/Gly weight ratio affected the shrinkage of the film after heat drying. Therefore, both these parameters were finely optimized for the formation of homogeneous, uniform and resistant films containing increasing concentrations of AgNPs, as evaluated by SEM observation and tensile tests. The presence of the nanoparticles modestly influenced the mechanical properties of the final films, whereas it significantly affected their swelling capacity. Specifically, increasing concentrations of AgNPs determined a progressive decrease in the swelling ability of the films, even considering the partial loss of film components (plasticizer and AgNPs) during the swelling studies. The release of AgNPs was qualitatively investigated by colorimetric analysis, which revealed the ability of the films to provide sustained release of AgNPs over time. The outward diffusion of AgNPs was fundamental for the antibacterial activity of the films when tested on *Staphylococcus aureus* and *Escherichia coli.* Indeed, the proposed films showed the capacity to significantly decrease the bacteria concentration with respect to the control. Globally, the proposed approach allows for the development of nanocomposite films with a facile and safe synthesis procedure, which avoids the use of toxic reagents for silver reduction. The obtained films showed interesting features and have potential application as innovative dressing materials for infected wound management.

Author Contributions: Conceptualization, L.D.M., P.P. and M.A.C.; methodology, L.D.M., S.S., S.C., M.A.C., P.P. and J.T. (Jacopo Tirillò); validation, M.A.C., J.T. (Jacopo Tirillò), L.D.M., S.S., S.P., S.C. and P.P.; formal analysis, M.A.C., J.T. (Jordan Trilli), L.D.M., S.S., S.P., S.C., C.S. and P.P.; investigation, P.S., L.D.M., F.C., C.B., G.R., V.C.C., J.T. (Jordan Trilli) and C.S.; resources, M.A.C., J.T. (Jacopo Tirillò), S.S., S.P., S.C. and P.P.; data curation, L.D.M., F.C., S.C., P.P., G.R. and S.S.; writing—original draft preparation, M.A.C., L.D.M., S.S., C.S., J.T. (Jacopo Tirillò), S.C. and P.P.; writing—review and editing, L.D.M., F.C., C.B., G.R., V.C.C., J.T. (Jacopo Tirillò), M.A.C., S.P., P.P., S.S., J.T. (Jordan Trilli) and C.S.; visualization, P.P and L.D.M.; supervision, M.A.C., J.T. (Jacopo Tirillò), S.S., S.P., S.C. and P.P.; project administration, M.A.C., J.T. (Jacopo Tirillò), S.S., S.P., S.C. and P.P. All authors have read and agreed to the published version of the manuscript.

Funding: This research received no external funding.

Institutional Review Board Statement: Not applicable.

Informed Consent Statement: Not applicable.

Data Availability Statement: The data presented in this study are available on request to the corresponding authors.

Conflicts of Interest: The authors declare no conflict of interest.

Sample Availability: Samples of the compounds are available from the corresponding authors.

References

1. Proksch, E.; Brandner, J.M.; Jensen, J.M. The skin: An indispensable barrier. *Exp. Dermatol.* **2008**, *17*, 1063–1072. [CrossRef]
2. Eming, S.A.; Martin, P.; Tomic-Canic, M. Wound repair and regeneration: Mechanisms, signaling, and translation. *Sci. Transl. Med.* **2014**, *6*, 265sr6. [CrossRef]
3. Demidova-Rice, T.N.; Hamblin, M.R.; Herman, I.M. Acute and impaired wound healing: Pathophysiology and current methods for drug delivery, part 1: Normal and chronic wounds: Biology, causes, and approaches to care. *Adv. Skin Wound Care* **2012**, *25*, 304–314. [CrossRef] [PubMed]
4. Gonzalez, A.C.D.O.; Andrade, Z.D.A.; Costa, T.F.; Medrado, A.R.A.P. Wound healing—A literature review. *An. Bras. Dermatol.* **2016**, *91*, 614–620. [CrossRef] [PubMed]
5. Olsson, M.; Järbrink, K.; Divakar, U.; Bajpai, R.; Upton, Z.; Schmidtchen, A.; Car, J. The humanistic and economic burden of chronic wounds: A systematic review. *Wound Repair Regen.* **2019**, *27*, 114–125. [CrossRef] [PubMed]
6. Negut, I.; Grumezescu, V.; Grumezescu, A.M. Treatment strategies for infected wounds. *Molecules* **2018**, *23*, 2392. [CrossRef]
7. Kuwahara, R.; Uchino, M.; Ikeuchi, H.; Bando, T.; Sasaki, H.; Yasuhara, M.; Kimura, K.; Goto, Y.; Horio, Y.; Minagawa, T.; et al. Effect of Changing surgical instruments before wound closure to prevent wound infection in lower GI surgery: A randomized controlled trial. *Dis. Colon Rectum* **2022**, *65*, 100–107. [CrossRef]
8. World Union of Wound Healing Societies (WUWHS), Florence Congress, Position Document. Management of Biofilm. Wounds International. Available online: https://www.woundsinternational.com/resources/details/position-document-management-biofilm (accessed on 23 September 2016).
9. Zhao, R.; Liang, H.; Clarke, E.; Jackson, C.; Xue, M. Inflammation in chronic wounds. *Int. J. Mol. Sci.* **2016**, *17*, 2085. [CrossRef]
10. Okur, M.E.; Karantas, I.D.; Şenyiğit, Z.; Üstündağ Okur, N.; Siafaka, P.I. Recent trends on wound management: New therapeutic choices based on polymeric carriers. *Asian J. Pharm. Sci.* **2020**, *15*, 661–684. [CrossRef]
11. Las Heras, K.; Igartua, M.; Santos-Vizcaino, E.; Hernandez, R.M. Chronic wounds: Current status, available strategies and emerging therapeutic solutions. *J. Control. Release* **2020**, *328*, 532–550. [CrossRef]
12. Martinengo, L.; Olsson, M.; Bajpai, R.; Soljak, M.; Upton, Z.; Schmidtchen, A.; Car, J.; Järbrink, K. Prevalence of chronic wounds in the general population: Systematic review and meta-analysis of observational studies. *Ann. Epidemiol.* **2019**, *29*, 8–15. [CrossRef]
13. Rezvani Ghomi, E.; Khalili, S.; Nouri Khorasani, S.; Esmaeely Neisiany, R.; Ramakrishna, S. Wound dressings: Current advances and future directions. *J. Appl. Polym. Sci.* **2019**, *136*, 47738. [CrossRef]
14. Saghazadeh, S.; Rinoldi, C.; Schot, M.; Kashaf, S.S.; Sharifi, F.; Jalilian, E.; Nuutila, K.; Giatsidis, G.; Mostafalu, P.; Derakhshandeh, H.; et al. Drug delivery systems and materials for wound healing applications. *Adv. Drug Deliv. Rev.* **2018**, *127*, 138–166. [CrossRef]
15. Asadi, N.; Pazoki-Toroudi, H.; Del Bakhshayesh, A.R.; Akbarzadeh, A.; Davaran, S.; Annabi, N. Multifunctional hydrogels for wound healing: Special focus on biomacromolecular based hydrogels. *Int. J. Biol. Macromol.* **2020**, *170*, 728–750. [CrossRef]
16. Shi, C.; Wang, C.; Liu, H.; Li, Q.; Li, R.; Zhang, Y.; Liu, Y.; Shao, Y.; Wang, J. Selection of appropriate wound dressing for various wounds. *Front. Bioeng. Biotechnol.* **2020**, *8*, 182. [CrossRef]
17. Brumberg, V.; Astrelina, T.; Malivanova, T.; Samoilov, A. Modern wound dressings: Hydrogel dressings. *Biomedicines* **2021**, *9*, 1235. [CrossRef]
18. Leyva-Gómez, G.; González-Torres, M.; Alcalá-Alcalá, S.; Bernal-Chávez, S.A.; Morales-Morfin, J.C.; González-Del Carmen, M.; Sharifi-Rad, J.; Figueroa-González, G.; Reyes-Hernández, O.D.; Del Prado-Audelo, M.L.; et al. Development of films from natural sources for infections during wound healing. *Cell. Mol. Biol. (Noisy-le-grand)* **2021**, *67*, 96–100. [CrossRef]
19. Savencu, I.; Iurian, S.; Porfire, A.; Bogdan, C.; Tomuță, I. Review of advances in polymeric wound dressing films. *React. Funct. Polym.* **2021**, *168*, 105059. [CrossRef]
20. Li, R.; Liu, K.; Huang, X.; Li, D.; Ding, J.; Liu, B.; Chen, X. Bioactive Materials Promote Wound Healing through Modulation of Cell Behaviors. *Adv. Sci.* **2022**, *9*, 2105152. [CrossRef]
21. Udayakumar, G.P.; Muthusamy, S.; Selvaganesh, B.; Sivarajasekar, N.; Rambabu, K.; Banat, F.; Sivamani, S.; Sivakumar, N.; Hosseini-Bandegharaei, A.; Show, P.L. Biopolymers and composites: Properties, characterization and their applications in food, medical and pharmaceutical industries. *J. Environ. Chem. Eng.* **2021**, *9*, 105322. [CrossRef]
22. Sánchez-López, E.; Gomes, D.; Esteruelas, G.; Bonilla, L.; Lopez-Machado, A.L.; Galindo, R.; Cano, A.; Espina, M.; Ettcheto, M.; Camins, A.; et al. Metal-Based nanoparticles as antimicrobial agents: An overview. *Nanomater.* **2020**, *10*, 292. [CrossRef] [PubMed]
23. Mihai, M.M.; Dima, M.B.; Dima, B.; Holban, A.M. Nanomaterials for wound healing and infection control. *Mater.* **2019**, *12*, 2176. [CrossRef] [PubMed]
24. Nqakala, Z.B.; Sibuyi, N.R.S.; Fadaka, A.O.; Meyer, M.; Onani, M.O.; Madiehe, A.M. Advances in nanotechnology towards Development of silver nanoparticle-based wound-healing agents. *Int. J. Mol. Sci.* **2021**, *22*, 11272. [CrossRef] [PubMed]

25. Nowak, M.; Barańska-Rybak, W. Nanomaterials as a successor of antibiotics in antibiotic-resistant, biofilm infected wounds? *Antibiotics* **2021**, *10*, 941. [CrossRef]
26. Paladini, F.; Pollini, M. Antimicrobial silver nanoparticles for wound healing application: Progress and future trends. *Materials* **2019**, *12*, 2540. [CrossRef]
27. Badhwar, R.; Mangla, B.; Neupane, Y.R.; Khanna, K.; Popli, H. Quercetin loaded silver nanoparticles in hydrogel matrices for diabetic wound healing. *Nanotechnology* **2021**, *32*, 505102. [CrossRef]
28. Alcântara, M.T.S.; Lincopan, N.; Santos, P.M.; Ramirez, P.A.; Brant, A.J.C.; Riella, H.G.; Lugão, A.B. Simultaneous hydrogel crosslinking and silver nanoparticle formation by using ionizing radiation to obtain antimicrobial hydrogels. *Radiat. Phys. Chem.* **2020**, *169*, 108777. [CrossRef]
29. González-Sánchez, M.I.; Perni, S.; Tommasi, G.; Morris, N.G.; Hawkins, K.; López-Cabarcos, E.; Prokopovich, P. Silver nanoparticle based antibacterial methacrylate hydrogels potential for bone graft applications. *Mater. Sci. Eng. C* **2015**, *50*, 332–340. [CrossRef]
30. Yuan, Y.; Ding, L.; Chen, Y.; Chen, G.; Zhao, T.; Yu, Y. Nano-silver functionalized polysaccharides as a platform for wound dressings: A review. *Int. J. Biol. Macromol.* **2022**, *194*, 644–653. [CrossRef]
31. Spirescu, V.A.; Chircov, C.; Grumezescu, A.M.; Vasile, B. Ștefan; Andronescu, E. Inorganic nanoparticles and composite films for antimicrobial therapies. *Int. J. Mol. Sci.* **2021**, *22*, 4595. [CrossRef]
32. Shi, G.; Chen, W.; Zhang, Y.; Dai, X.; Zhang, X.; Wu, Z. An Antifouling hydrogel contained silver nanoparticles for modulating therapeutic immune response in chronic wound healing. *Langmuir* **2019**, *35*, 1837–1845. [CrossRef]
33. Liu, Z.; Yan, J.; Miao, Y.-E.; Huang, Y.; Liu, T. Catalytic and antibacterial activities of green-synthesized silver nanoparticles on electrospun polystyrene nanofiber membranes using tea polyphenols. *Compos. B Eng.* **2015**, *79*, 217–223. [CrossRef]
34. Panáček, A.; Kvítek, L.; Prucek, R.; Kolář, M.; Večeřová, R.; Pizúrová, N.; Sharma, V.K.; Nevěčná, T.J.; Zbořil, R. Silver Colloid Nanoparticles: Synthesis, Characterization, and Their Antibacterial Activity. *J. Phys. Chem. B* **2006**, *110*, 16248–16253. [CrossRef]
35. Kalantari, K.; Mostafavi, E.; Afifi, A.M.; Izadiyan, Z.; Jahangirian, H.; Rafiee-Moghaddam, R.; Webster, T.J. Wound dressings functionalized with silver nanoparticles: Promises and pitfalls. *Nanoscale* **2020**, *12*, 2268–2291. [CrossRef]
36. Krishnan, P.D.; Banas, D.; Durai, R.D.; Kabanov, D.; Hosnedlova, B.; Kepinska, M.; Fernandez, C.; Ruttkay-Nedecky, B.; Nguyen, H.V.; Farid, A.; et al. Silver Nanomaterials for Wound Dressing Applications. *Pharmaceutics* **2020**, *12*, 821. [CrossRef]
37. Pangli, H.; Vatanpour, S.; Hortamani, S.; Jalili, R.; Ghahary, A. Incorporation of silver nanoparticles in hydrogel matrices for controlling wound infection. *J. Burn Care Res.* **2021**, *42*, 785–793. [CrossRef]
38. Roppolo, I.; Doriguzzi Bozzo, A.; Castellino, M.; Chiappone, A.; Perrone, D.; Bejtka, K.; Bocchini, S.; Sangermano, M.; Chiolerio, A. Dual step irradiation process for in situ generation and patterning of silver nanoparticles in a photocured film. *RSC Advances* **2016**, *6*, 14832–14843. [CrossRef]
39. Rahimi, M.; Noruzi, E.B.; Sheykhsaran, E.; Ebadi, B.; Kariminezhad, Z.; Molaparast, M.; Mehrabani, M.G.; Mehramouz, B.; Yousefi, M.; Ahmadi, R.; et al. Carbohydrate polymer-based silver nanocomposites: Recent progress in the antimicrobial wound dressings. *Carbohydr. Polym.* **2020**, *231*, 115696. [CrossRef]
40. Paolicelli, P.; Petralito, S.; Varani, G.; Nardoni, M.; Pacelli, S.; Di Muzio, L.; Tirillò, J.; Bartuli, C.; Cesa, S.; Casadei, M.A. Effect of glycerol on the physical and mechanical properties of thin gellan gum films for oral drug delivery. *Int. J. Pharm.* **2018**, *547*, 226–234. [CrossRef]
41. Pacelli, S.; Paolicelli, P.; Avitabile, M.; Varani, G.; Di Muzio, L.; Cesa, S.; Tirillò, J.; Bartuli, C.; Nardoni, M.; Petralito, S.; et al. Design of a tunable nanocomposite double network hydrogel based on gellan gum for drug delivery applications. *Eur. Polym. J.* **2018**, *104*, 184–193. [CrossRef]
42. Pacelli, S.; Paolicelli, P.; Dreesen, I.; Kobayashi, S.; Vitalone, A.; Casadei, M.A. Injectable and photocross-linkable gels based on gellan gum methacrylate: A new tool for biomedical application. *Int. J. Biol. Macromol.* **2015**, *72*, 1335–1342. [CrossRef]
43. Adrover, A.; Di Muzio, L.; Trilli, J.; Brandelli, C.; Paolicelli, P.; Petralito, S.; Casadei, M.A. Enhanced Loading Efficiency and Mucoadhesion Properties of Gellan Gum Thin Films by Complexation with Hydroxypropyl-β-Cyclodextrin. *Pharmaceutics* **2020**, *12*, 819. [CrossRef]
44. Aranaz, I.; Harris, R.; Navarro-García, F.; Heras, A.; Acosta, N. Chitosan based films as supports for dual antimicrobial release. *Carbohydr. Polym.* **2016**, *146*, 402–410. [CrossRef]
45. Chen, S.; Qin, J.; Du, J. Cross-linkable yet biodegradable polymer films. *Acta Phys.-Chim. Sin.* **2022**, *38*, 2006029. [CrossRef]
46. Coutinho, D.F.; Sant, S.; Shin, H.; Oliveira, J.T.; Gomes, M.E.; Neves, N.M.; Khademhosseini, A.; Reis, R.L. Modified gellan gum hydrogels with tunable physical and mechanical properties. *Biomaterials* **2010**, *31*, 7494–7502. [CrossRef]
47. Thiagamani, S.M.K.; Rajini, N.; Siengchin, S.; Rajulu, A.V.; Hariram, N.; Ayrilmis, N. Influence of silver nanoparticles on the mechanical, thermal and antimicrobial properties of cellulose-based hybrid nanocomposites. *Compos. B Eng.* **2019**, *165*, 516–525. [CrossRef]
48. Fan, L.; Zhang, H.; Gao, M.; Zhang, M.; Liu, P.; Liu, X. Cellulose nanocrystals/silver nanoparticles: In-situ preparation and application in PVA films. *Holzforschung* **2019**, *74*, 523–528. [CrossRef]
49. Tsuboi, A.; Nakamura, K.; Kobayashi, N. Multicolor electrochromism showing three primary color states (cyan-magenta-yellow) based on size- and shape-controlled silver nanoparticles. *Chem. Mater.* **2014**, *26*, 6477–6485. [CrossRef]
50. Richardson, T.J.; Slack, J.L.; Armitage, R.D.; Kostecki, R.; Farangis, B.; Rubin, M.D. Switchable mirrors based on nickel-magnesium films. *Appl. Phys. Lett.* **2001**, *78*, 3047–3049. [CrossRef]

51. Prosposito, P.; Burratti, L.; Venditti, I. Silver Nanoparticles as Colorimetric Sensors for Water Pollutants. *Chemosensors* **2020**, *8*, 26. [CrossRef]
52. Chartarrayawadee, W.; Charoensin, P.; Saenma, J.; Rin, T.; Khamai, P.; Nasomjai, P.; On Too, C. Green synthesis and stabilization of silver nanoparticles using *Lysimachia foenum-graecum* Hance extract and their antibacterial activity. *Green Process. Synth.* **2020**, *9*, 107–118. [CrossRef]
53. Greenman, J.; Thorn, R.M.; Saad, S.; Austin, A.J. In vitro diffusion bed, 3-day repeat challenge 'capacity' test for antimicrobial wound dressings. *Int. Wound J.* **2006**, *3*, 322–3299. [CrossRef] [PubMed]
54. Ng, J.Y.; Zhu, X.; Mukherjee, D.; Zhang, C.; Hong, S.; Kumar, Y.; Gokhale, R.; Ee, P.L.R. Pristine gellan gum-collagen interpenetrating network hydrogels as mechanically enhanced anti-inflammatory biologic wound dressings for burn wound therapy. *ACS Appl. Bio. Mater.* **2021**, *4*, 70–1482. [CrossRef] [PubMed]
55. Zhang, X.M.; Pan, Y.J.; Li, S.K.; Xing, L.; Niu, X. Doubly crosslinked biodegradable hydrogels based on gellan gum and chitosan for drug delivery and wound dressing. *Int. J. Biol. Macromol.* **2020**, *164*, 2204–2214. [CrossRef]
56. Dohle, E.; Scherrieble, A.; Doser, M.; Al-Maawi, S.; Hoss, M.; Dauner, M.; Sader, R.; Kirkpatrick, C.J.; Ghanaati, S. Co-culture model for cutaneous wound healing to assess a porous fiber-based drug delivery system. *Tissue Eng. Part C Methods* **2020**, *26*, 75–484. [CrossRef]
57. Li, W.; Jian, X.; Zou, Y.; Wu, L.; Huang, H.; Li, H.; Hu, D.; Yu, B. The fabrication of a gellan gum-based hydrogel loaded with magnesium ions for the synergistic promotion of skin wound healing. *Front. Bioeng. Biotechnol.* **2021**, *9*, 709679. [CrossRef]

~ SECTION II~

HYDROGELS AS SCAFFOLDS FOR TISSUE ENGINEERING

Due to their high-water content, biocompatibility, soft texture and porous structure, hydrogels have attracted great attention among scientists, establishing themselves as the biomaterials that most closely resemble natural living tissues. As a result, they are the first biomaterials designed for use in the human body, showing endless properties that make them suitable for a broad spectrum of both biomedical and pharmaceutical applications [208,209].

Hydrogels have undergone numerous definitions over the years [210]. However, the most common one describes them as three-dimensional, hydrophilic, polymeric networks capable of absorbing significant amounts of water or biological fluids, increasing their volume while maintaining their structure due to the presence of chemical and/or physical cross-links between polymer chains [210,211]. Their ability to incorporate great quantities of water is directly related to the presence of hydrophilic groups (e.g., -OH, -COOH, $-SO_3H$, $-NH_2$) on the backbone of network-forming polymers and confers them a high degree of biocompatibility because their hydrophilic surfaces exhibit a low interfacial free energy when in contact with body fluids, which results in a low tendency for protein adsorption and cell adhesion, thereby minimizing the possibility of undesirable reactions after implantation. A high degree of flexibility as well as soft and rubbery consistency are additional effects deriving from the high-water content of hydrogels and greatly contribute to their thorough coexistence and integration with the surrounding living tissues, preventing any inflammatory responses that could follow their implant in the human body [212]. The set of these unique features, combined with the likelihood to easily modulate their physical, chemical, and mechanical properties by acting directly on the nature of network-forming polymers and their cross-linking degree, makes hydrogels an interesting matter of research [213] as well as promising materials for drug delivery [214-217], wound healing [218-221] and tissue engineering [222-225] applications.

Tissue engineering is a multidisciplinary field which applies the principles of engineering and life sciences with the aim of repairing and regenerating human tissues

and/or organs damaged by diseases, accidents or aging by exploiting a combination of biomaterials, cells and growth factors to overcome the complications related to the lack of compatible donors and those deriving from organ transplants that could compromise patients' quality of life [226-229]. The combination of cells, scaffold, and growth factors is referred to as “the triad” since they represent the critical component of tissue engineering. Each component of the triad performs a specific function: cells synthesize extracellular matrix (ECM) to conform the novel tissue; scaffold provides suitable support and environment for cell function, adhesion, and proliferation; growth factors or other bioactive molecules facilitate and stimulate cells to regenerate the damaged tissue [230]. Therefore, to encourage cell ingrowth from native tissues or functionally regenerate them with transplanted cells, tissue engineering approaches require the fabrication of biomaterials into scaffolds that faithfully mimic the structural and biochemical functionalities of the natural ECM [228,230]. Because of the above-mentioned unique properties, hydrogels are biomaterials extremely similar to the natural ECM in terms of both composition and mechanical properties. As a result, they have been extensively studied as vehicles to deliver cells and scaffolds to encapsulate them, as well as fillers to repair defects and promote the healing of damaged tissues while reducing the risk of infection [228], highlighting the potential of these biomaterials in the tissue engineering field.

2.1 Classification of hydrogels

Depending on the specific aspect under consideration, hydrogels can be categorized in a variety of ways, as illustrated in Figure 7 [231]. However, the most common classification method allows hydrogels to be divided into two main groups, physical or reversible hydrogels and chemical or irreversible ones, according to the forces involved in the building up of the polymeric network. In chemical hydrogels, the network is mainly held together by covalent and permanent bonds, which can eventually be broken through hydrolysis or the use of enzymes [232,233]. Depending on the functional groups available on polymer chains, several synthetic approaches can be employed to achieve the covalent cross-linking. One of the most investigated strategies is radical polymerization, which involves the generation of radical species from either vinyl

monomers, which polymerized *in situ* resulting in the formation of stable 3D-structures in the presence of cross-linking agents, or natural occurring polymers whose backbone has previously been modified by the introduction of (meth)acrylic groups, such as gelatin [234-236] or hyaluronic acid [236-238], to name a few. In most cases, radicals are produced by combining radical initiators such as ammonium peroxydisulfate (APS) and N,N,N',N'-tetramethylethylenediamine (TEMED), or by exposing polymeric solutions containing a photo-initiator to UV light for a variable amount of time. Factors that determine the efficiency of such light-initiated reactions are the light wavelength(s) and intensity, exposure time, type and concentration of photo-initiator, as well as concentration of oxygen or other radical scavenging molecules present in the sample [239].

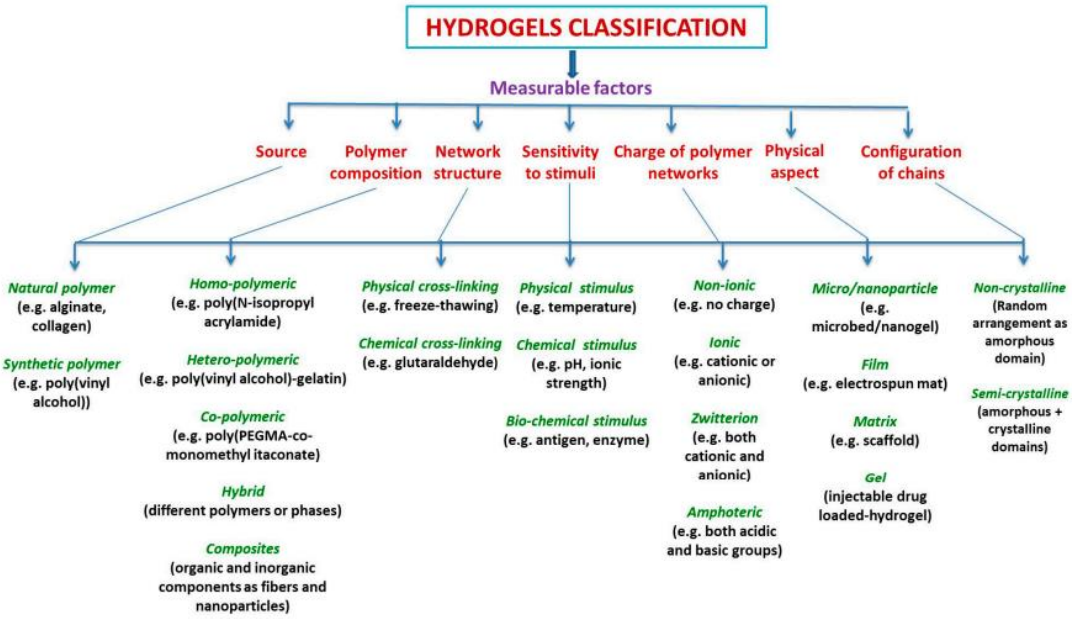

Figure 7. Classification of hydrogels [231].

Other strategies for developing chemical hydrogels involve the reaction of complementary groups present on the backbone of network-forming polymers. Condensation reactions and Schiff-base formation have been widely investigated for the design of mechanically stable gels [240,241]. In this context, click-chemistry has gained an ever-growing popularity due to the ease, versatility, regiospecificity and lack of by-products of the reactions, which are typically performed under mild conditions, beginning with readily accessible, inexpensive raw materials, and ending with stable,

physiologically appropriate, and easily isolatable products. Azide-alkyne cycloadditions and Michael-type additions as well as Diels-Alder, thiol–ene, and oxime reactions are examples of click-chemistry reactions usually employed in the construction of chemical hydrogels [240]. Recently, the use of enzymes in developing covalent networks has attracted great attention mainly due to the mild conditions required for the polymer cross-linking and the substrate specificity of the enzyme, which allows to avoid unwanted side reactions or potential toxicity. However, a fine control of the pH and temperature conditions is necessary to ensure the optimal efficiency of the enzyme catalyst activity [242].

Physical hydrogels, on the other hand, are produced when molecular entanglements and physiochemical interactions, such as hydrogen bonding, hydrophobic interactions, charge condensation, metal coordination, or supramolecular chemistry are established between polymer chains [243]. This type of hydrogels is usually developed through freeze-thawing, stereo complex formation, ionic interaction, and hydrogen bonding. In this case, the construction of the network is completely reversible and highly dependent on specific properties of the surrounding environment [212,243]. Based on this, physical hydrogels have sparked considerable interest due to their versatile responses to external stimuli (e.g., temperature, pH, ionic strength), ease of processing and self-healing properties [244]. One of the main advantages of these systems lies in their ability to undergo gelation without the need for cross-linkers, radiation sources, or additives, reducing the risk of cellular toxicity induced by the possible release of cytotoxic cross-linking chemicals from the polymer network, and preventing damage to the structure of drugs and proteins loaded into the matrices potentially caused by the highly reactive species formed during radical polymerization, which could also affect cellular metabolism [243]. Based on the aforementioned, it is clear that the cross-linking nature plays a significant role in determining the properties of the resulting hydrogels. However, even the density of cross-links should be taken into account because it has a major effect on the porosity of the network and, consequently, on its mechanical and swelling properties [245], both of which are crucial in assessing the potential use of hydrogels for biomedical and pharmaceutical purposes.

2.2 Properties of hydrogels

The first step in developing hydrogels for biomedical applications is to thoroughly understand and analyze their main properties, which must meet different requirements depending on the intended use of the hydrogel and the environment in which it will be placed [246]. Biocompatibility, biodegradability, non-toxicity as well as appropriate water absorption, structural stability, and mechanical properties are just a few of the fundamental features required for the effective use of hydrogels in tissue engineering. In general, an ideal scaffold should be designed to mimic the native ECM as closely as possible, thus offering cells a 3D and highly hydrated environment while providing temporary structural support for their growth and proliferation, promoting cell migration toward specific sites, stimulating cell-polymer and cell-cell interactions, allowing for proper transport of gases, nutrients, and waste, and controlling the structure and function of the engineered tissue [230]. Furthermore, scaffolds should degrade at a rate suitable to support the formation of new functional tissues for as long as necessary to enable native cell proliferation and organization, but ultimately clear once the tissue can be supported by the natively produced ECM [228]. Based on the above, the effectiveness of hydrogels as tissue engineering scaffolds must be assessed in light of a wide range of variables, among which the structuring of matrix pores, specifically their size and degree of interconnection, has proven to be a key factor in determining their potential use in tissue regeneration, due to the impact that it has on the swelling and mechanical properties of hydrogels as well as on their ability to promote cell growth and proliferation.

2.2.1 Swelling capacity and mechanical properties of conventional hydrogels: the effect of porosity

The most important feature of hydrogels, which distinguished them from any other biomaterial, is their ability to swell when in contact with water or another thermodynamically compatible solvent [247]. When a dry hydrogel meets an aqueous solution, a multi-step process of hydration and subsequent swelling of the polymeric structure begins [248]. Water molecules first interact with the most polar, hydrophilic active sites of the hydrogel matrix, then moving to the hydrophobic ones that are

exposed on the network surfaces during the hydration process. This causes the polymeric chains to relax and the entire system to expand without undergoes disintegration due to the presence of chemical and/or physical cross-links between polymer chains, which avoid the network dissolution in aqueous media. Swelling continues until the osmotic forces that drive hydration are offset by elastic retraction forces of the polymer network and, as a result, the system achieves an equilibrium state (equilibrium water content), thus stopping to further swell [247-249]. Understanding hydration phenomena in hydrogels is critical because their structural composition contains approximately 90% of water [248]. Therefore, hydrogels possess a biphasic structure composed of a polymer network, which confers elastic properties, surrounded by an aqueous solution associated with the viscous behavior of these systems [250]. Based on this, hydrogels have two main regimes of mechanical properties, rubber elasticity and viscoelasticity, which are directly related to the amount of water incorporated in the polymer matrix [251]. The viscoelastic behavior of hydrogels is critical for their effective use as tissue engineering scaffolds. Indeed, the stiffness of the 3D-structure has been found to influence the ability of cells to proliferate, differentiate, and migrate. It was observed that cells exposed to more rigid substrates proliferate faster and migrate more slowly, showing a higher elastic modulus, particularly in their plasma membrane, and a better-organized actin cytoskeleton than cells grown on softer substrates [247,252,253]. However, each type of tissue performs a particular function in the human body, and as a result, each one has a unique morphology, stiffness, physiology, and biochemistry. Given this, the mechanical requirements for each scaffold are specific to the type of targeted tissue [248]. In this regard, it should be remembered that hydrogels properties can be adapted by acting directly on the cross-linking density of the network, which is a fundamental parameter in determining the porosity and the inner pore size of the system, thus affecting the swelling capacity and the mechanical properties of the resulting gel.

The ability of hydrogels to stimulate angiogenesis as well as the flow of oxygen and nutrients, while ensuring the complete elimination of cellular waste, is influenced by their porosity, which is a crucial component for the practical application of hydrogels in the field of tissue engineering. Controlling cell aggregation, orientation, and function depends on the microscale properties of the individual pores and the groups formed

between them. For instance, the pores <5 μm are essential for neovascularization, while the ones between 5–15 μm have an impact on the ingrowth of fibroblasts. Moreover, the pores with sizes between 20–125 μm encourage the infiltration of adult mammalian cells. Additionally, the pores between 40–100 μm aid in the ingrowth of osteoid, while pores with sizes >500 μm are required for the development of fibrovascular tissue. Hence, the precise control of the matrix porosity can influence the interaction between biomaterial and tissues, thus affecting the final outcome [248]. Unfortunately, conventional hydrogels frequently have small pores that prevent uniform cell distribution across the 3D-structure, and a low degree of interconnection between them, which leads to insufficient waste removal and inadequate nutrition transport, ultimately reducing cell viability. Over the years, various techniques have been explored with the aim of addressing this significant defect of hydrogels, which strongly limits their use as functional scaffolds. A common strategy to fabricate macro-porous hydrogels provides for the use of porogens such as salts, sugar, silica and gelatin spheres, which act as physical impediments, forcing the polymer chains to reticulate around them. Their subsequent removal after gelation leads to the generation of void structures in the polymer network. However, one of the main issues with this approach is the removal of porogen, which is frequently incomplete, and the inappropriate degree of interconnectivity obtained, which limit the usefulness of the resulting systems in encouraging cell infiltration and blood-vessel in-growth [254]. Cryogelation process has proven to be an attractive alternative to conventional strategies for developing macro-porous gels with densely linked internal structures allowing, at the same time, to avoid the problem of porogen removal.

2.2.1.1 Cryogels and cryogelation process

Nowadays, cryogenic methods are used to develop distinctive polymeric materials with the aim of resolving issues primarily in the biomedical, environmental, and food technology fields [255].

Cryotropic gelation is a process whereby hydrogels are formed under semi-frozen conditions [256]. To accomplish this, the starting solution containing the polymer network precursors is cooled to between -5 and -20°C, causing a significant amount of the solvent to crystallize. Water is the most commonly used solvent since it is believed

to be the most effective for producing biocompatible cryogels for biomedical applications [256]. However, other solvents or solvent mixtures with near-zero freezing points, such as benzene, cyclohexane, and dimethyl sulfoxide, may also be used [257,258]. During the formation of solvent crystals, a portion of the gel solution remains in the liquid state. As a result, hydrogel components such as monomers, oligomers, or polymers are concentrated in liquid micro-phases via a process known as cryo-concentration [254], which is crucial for the development of the polymer network because it can not only completely counterbalance the negative impacts caused by low temperature, but also considerably reduce the critical concentration of gelation (CCG) of the precursors, becoming the main driving force for the formation of these systems [259]. After a suitable gelation period, the cryogel is brought back to room temperature, where the melting of solvent crystals results in the formation of a highly interconnected macro-porous structure. Although solvent crystals create sharp-edged pores, the surface tension at the liquid/pore wall interface causes the pores to become rounded when the material is fully hydrated [254]. Figure 8 depicts a schematic representation of cryogelation process [260].

Due to the presence of interconnected macro-pores, full hydration is achieved considerably quicker in sponge-like cryogels when compared to conventional hydrogels. For tissue engineering applications it is desirable that the pores within polymer matrices are highly interconnected to promote cell migration and proliferation, while reducing inaccessible areas. The need for pore interconnectivity highlights a significant advantage of cryogelation over other pore-forming techniques, as cryogels are inherently highly interconnected. In fact, during solvent crystallization, solvent crystals expand until the leading-edge contacts another crystal front, resulting in highly interconnected porous structures [254].

Gelation, like conventional hydrogels, can occur through a variety of mechanisms, which include the formation of covalent bonds or physical interactions (ionic bonding, hydrogen bonding, and others) between polymer chains. Also in this case, the most frequently employed method for polymer crosslinking is radical polymerization, which requires the use of radical initiators, such as APS and TEMED, to generate highly reactive species from (meth)acrylate derivatives [256].

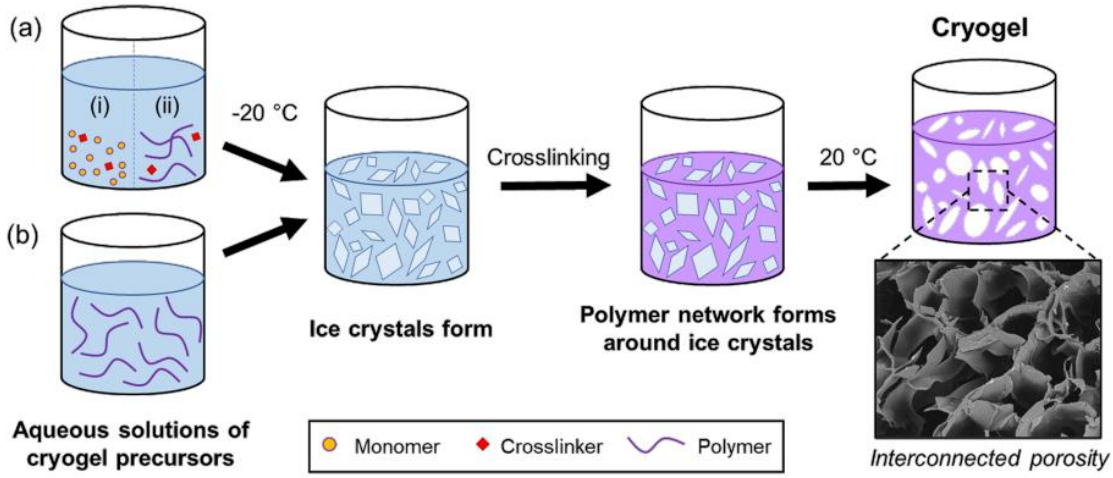

Figure 8. Schematic representation of cryogelation, using (a) monomers/small molecules (i) or polymeric precursors (ii) to form chemically cross-linked cryogels, or (b) polymeric precursors to form physically cross-linked cryogels. Temperatures are indicative [260].

Despite the apparent ease of cryogelation process, several parameters need to be carefully studied and evaluated to produce systems that match cryogel criteria. First, freezing conditions, both in terms of temperature and cooling rate, have a significant impact on the pore size, wall thickness and density, thereby affecting the mechanical and swelling properties of the final product. Depending on the different rates of solvent crystals growth, largest pores are produced at the highest freezing temperatures and slowest cooling rates, whereas smallest pores are created at lower temperatures and faster freezing rates [256]. However, in order to achieve a homogeneous macro-porous structure, it is fundamental that solvent crystals form before the gelation of polymer precursors is complete [261]. In fact, if gelation occurs more rapidly than ice crystal formation, large, interconnected pores do not form, and the resulting cryogel has a morphology similar to a conventional hydrogel, thus showing a brittle structure characterized by less porosity and mechanical strength [256,262].

Another factor to consider is that a temperature gradient will exist during cryogelation. The exterior of the sample will be exposed to cold temperatures first, resulting in faster freezing rates and smaller pore sizes than the inner cryogel material, thus leading to a heterogeneous and graduated pore size distribution, which is advantageous for their use in tissue engineering because many human tissues also exhibit this heterogeneous morphology [260,263,264]. Based on the foregoing, gelation kinetics and solvent crystal nucleation are key factors in determining cryogel microstructure, which can be

controlled by varying parameters such as temperature, concentration and molecular weight of polymer precursors, as well as concentration of radical initiators or cross-linker agents.

The physical characteristics of cryogels, such as their elastic, swelling, and interconnecting pore features, can significantly affect their stability and, ultimately, the type of applications they can be used for. In comparison to conventional hydrogels, cryogels offer superior porosity and, as a result, improved mechanical properties and swelling capacity, which have propelled their use in biomedicine. Because of these distinguishing characteristics, cryogels can easily revert to their original shape and size following mechanical compression such as syringe injection, making them an important consideration when designing materials for specific biomedical applications [265].

2.2.2 Biological properties of hydrogels: the role of network-forming polymers on cell adhesion

ECM, composed of a dynamic and complex array of glycoproteins, collagens, glycosaminoglycans and proteoglycans, not only forms the cell microenvironment providing bulk, shape, and strength to many tissues *in vivo*, but also offers a spatial context for cell signaling events, regulating cell behavior, polarity, migration, differentiation, proliferation, and survival. The biological effects of ECM, critical for tissue development, are mostly attributable to its close connection with the intracellular cytoskeleton of cells, which is achieved by the binding of ECM elements to certain receptors expressed on cell membranes [266]. Among cell surface receptors, integrins are the most studied due to their critical role in cell signaling and ECM remodeling [267-270]. They are composed of α- and β-subunits, each of which, when combined to form a dimer, has a distinct function and affinity for specific ECM elements. It is generally recognized that integrin composition significantly influences the subsequent signaling processes, which in turn affect cell behavior and fate. These receptors have a unique ability to respond to the molecular composition and physiochemical properties of ECM and to integrate mechanical and chemical input by interacting with a variety of distinct structural and signaling molecules, including the membrane-associated cytoskeleton proteins (focal adhesion proteins), such as talin, α-actinin, filamin, paxillin, or vinculin [266,271]. These proteins serve as linkers between integrins and the actin cytoskeleton,

which is directly connected to the nuclear membrane, cellular organelles, and various enzymes, and allows to control several intracellular processes crucial to cell behavior, such as transport and secretion of different molecules, endocytosis, and the choice between cell proliferation, differentiation or apoptosis [271].

Naturally, besides integrins, other receptors are involved in mediating the interaction between cells and ECM components, such as syndecans, a group of membrane-intercalated proteoglycans that collaborate with integrins to provide cellular attachment to their surrounding matrix, and cadherins, which control cell-cell and cell-ECM adhesion and regulate cell behavior and ECM production [272].

Based on the foregoing, the success of hydrogels as tissue engineering scaffolds is dependent not only on the matrix structure and its swelling and mechanical properties, which can be easily improved using cryotropic gelation, but also on their ability to participate in critical cellular processes by promoting cell recognition and adhesion. In this context, the composition of polymer networks is of critical relevance because it influences the biological properties of the resulting system and, therefore, cell response. Despite synthetic biopolymers show good biocompatibility, biodegradability and non-toxicity, they typically have poor cell adhesive properties. For instance, PEG, poly(2-hydroxyethyl methacrylate) (PHEMA), and poly(vinyl alcohol) (PVA), three of the most commonly used synthetic polymers in tissue engineering, exhibit negligible cell and protein binding [273]. These polymers are often involved in non-receptor-mediated cell adhesion, which is accomplished through the generation of weak chemical bonds, such as hydrogen bonding, electrostatic, polar, or ionic interactions between different molecules on cell membranes and functional chemical groups available on polymer backbones. However, this type of interactions cannot guarantee adequate signal transduction from extracellular environments into cells or the survival of anchorage-dependent cells, which will undergo apoptosis if they are unable to synthesize and deposit their own ECM molecules in a relatively short period of time (usually in 24 to 48 h after seeding) [271]. In this regard, another crucial aspect to consider is the hydrophilic nature of polymer networks, which prevents ECM components from adhering to scaffold surfaces [246], thus interfering with their mediating role in cell-hydrogel interactions. As a result, to ensure cell adhesion, synthetic polymers must be derivatized either through the formation of composite scaffolds or through functionalization with

bioactive motifs. Most commonly, this is accomplished by attaching synthetic peptide sequences known to mediate cell binding on polymer backbones, although their incorporation would affect the physical properties of resulting hydrogels [273]. Among cell adhesive peptides, the tri-amino acid sequence arginine-glycine-aspartate, commonly referred to as RGD peptide, is the most extensively studied as it has been shown to be highly effective at promoting the attachment of various cell types to a wide range of materials [274]. It is the principal integrin-binding domain present within ECM proteins, and it has been demonstrated that a sufficiently high density of RGD motif, that allows for a precise spatial distribution pattern of integrins, appears to be required to initiate an optimal cellular response [266,274]. In this scenario, polymers such as collagen and gelatin offer great advantages over synthetic ones because they are naturally endowed with this peptide along with other sequences that can promote cell binding and control the degradation of the structure.

Collagen is the major component of ECM and the most prevalent protein in mammalian tissues. It is a fibrous structural protein consisting of three parallel left-handed polypeptide strands arranged in a right-handed triple helix, which offers mechanical support and resistance to natural tissues while also defining the diverse cell disposition within them [213,256]. Based on this, collagen should be an ideal candidate for the development of scaffolds that imitate the ECM environment and promote cell proliferation and differentiation [256]. However, its high cost and immunogenicity, as well as its low mechanical strength and generation of degradation products with potential thrombogenic effects, severely limit the practical use of collagen in biomedical applications [213].

Gelatin (Gel), produced by partially hydrolyzing collagen, is regarded to be a better alternative to its precursor due to its low cost, improved stability, water solubility and purity [256]. These advantages, along with its biocompatible nature and the presence of specific cell adhesion and degradation patterns in its amino acid sequence, place gelatin among the top materials for tissue engineering applications.

2.2.2.1 Gelatin

Gelatin is a heterogeneous mixture of polypeptides derived from the partial hydrolysis of type I collagen [275]. Both collagen and gelatin share a primary structure with up to 20 different amino acids in varying proportions, whose composition and sequence differs from one source to another. For example, pigskin gelatin and bone gelatin do not contain cysteine, which is present in fish scale and bone, while having lower content of glycine (Gly) in comparison with mammalian sources.

Collagen and gelatin molecules are structurally made up of repeating sequences of Gly-X-Y, where X and Y are mostly proline (Pro) and hydroxyproline (Hypro). Depending on the raw material and conditions of collagen conversion, each gelatin molecule may have a molecular weight ranging from 10,000 to several hundred thousands of Daltons. During the extraction process, tropocollagen molecules, made of three polypeptide chains arranged in triple helices, are broken down into single α-chains, covalently linked double α-chain species (β chains), and triple α-chain species (γ chains) or lower polypeptides. The amount of each chain is affected by the pre-extraction and extractions conditions, such as pH, temperature, and extraction time, which in turn determines the molecular weight of gelatin and, therefore, its final properties. Generally, there are two forms of gelatin available, depending on the pre-extraction method employed: acidic pre-treatment (type A) barely affects the amide groups while the alkaline pre-treatment (type B) targets the amide groups of asparagine and glutamine, hydrolyzing them into carboxyl groups, thus converting many of these residues to aspartate and glutamate. Due to the presence of both acidic and basic functional groups, gelatin exhibits an amphoteric behavior [276].

Because of its high biocompatibility, biodegradability, low cost, easy availability, and non-toxicity after degradation, gelatin is widely used in medicine and food sectors, for example, as a plasma substitute in clinics and a stabilizer for protein preparations such as vaccines. It is also much less antigenic than collagen as a denatured product, while retaining its cell adhesion properties and matrix metalloproteinase (MMP) attachment sites [275]. It also has a huge amount of lateral functional groups that allow it to form covalent bonds with growth factors and cytokines [277]. As a result, gelatin matrices are considered promising materials to promote cell growth, migration, proliferation, and

differentiation, as well as cell-mediated enzymatic degradation, which is required for novel ECM deposition [275]. The main drawback of Gel-based hydrogels is the lack of mechanical and thermal stability caused by the physical gelation of gelatin chains as a function of temperature [278-280]. However, the various functional groups available, such as carboxyl groups of aspartic and glutamic acid residues, hydroxyl groups of serine and threonine, and amino groups of lysine, can be used to produce derivatives that can be covalently cross-linked with the goal of designing acceptable and physiologically stable ECM biomimetic scaffolds [275]. Among all the derivatizations investigated, the modification of gelatin with methacrylic groups to produce gelatin methacryloyl (GelMA) has proven to be the most convenient and straightforward material processing for tissue engineering applications. This modification generally involves less than 5% of the amino acid residues and most of the functional amino acid sequences, such as the RGD and MMP-degradable motifs, are unaffected [277]. As a result, GelMA is an excellent candidate and a versatile platform for tissue engineering (Figure 9) [277,281].

Although different protocols for the synthesis of GelMA have been reported in the literature, they all essentially refer, with minor variations, to the general method described for the first time by Van Den Bulcke in 2000 [282]. Therefore, GelMA is usually synthesized by a direct reaction of Gel with methacrylic anhydride (MAA) in phosphate buffer (PBS, pH=7.4) at 50°C. However, this synthesis protocol has several issues, all of which are primarily related to the biphasic nature of the reaction environment: an excessive amount of MAA, long purification times, and significant variability in the derivatization degree (DD) of the obtained products [277]. To get around these restrictions, a new method for producing GelMA under homogeneous single-phase reaction conditions has recently been proposed [277]. The innovative method calls for the use of an organic dipolar aprotic solvent, such as DMSO, to dissolve both Gel and MAA. Gel should exhibit greater chain flexibility under these conditions, increasing its functional groups' accessibility and causing them to be more reactive. In fact, it has been observed that replacing water with DMSO prevents the formation of the triple-helix collagen-like structures typical of Gel in water [283,284], resulting in the production of GelMA derivatives with different properties from those obtained through the traditional biphasic synthesis procedure.

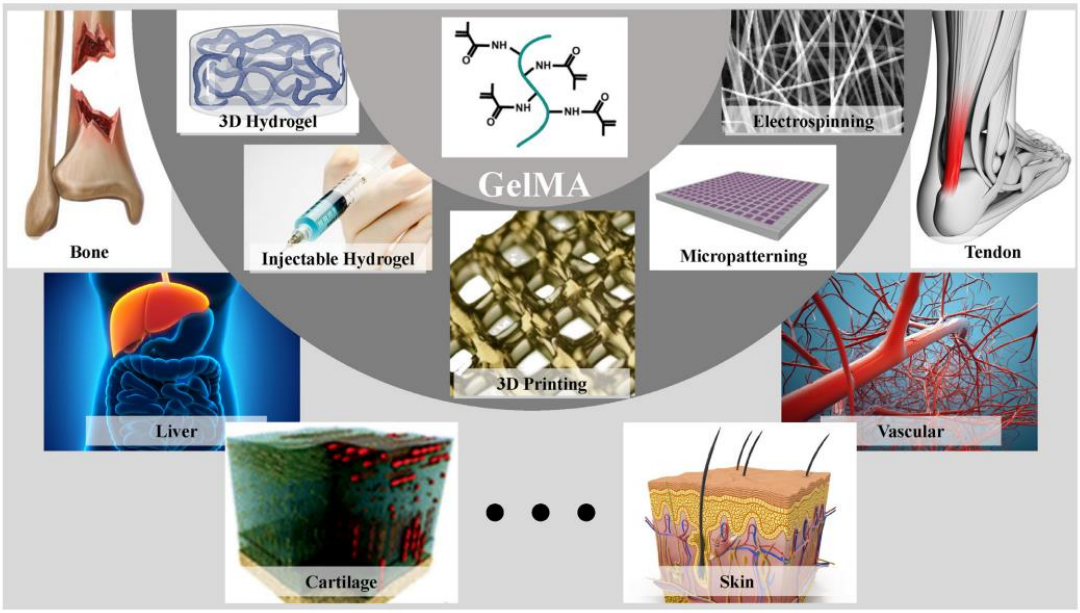

Figure 9. Biomedical applications of GelMA hydrogel. GelMA designed as injectable hydrogels, 3D printed scaffold, electrospun fibrous membrane, and micropatterns for various tissues regeneration, such as bone, cartilage, tendon, vasculature, skin, and liver [281].

The use of DMSO was observed to be critical in determining the DD reproducibility and unique rheological behavior of single-phase GelMA, which has proven to be a suitable material for the design of cryogels via APS/TEMED-mediated radical polymerization. The chemical cross-linking of methacrylic groups enables the production of cryogels with higher mechanical strength than native Gel, where temperature-dependent gelation of the polymeric solution may also affect the proper course of cryogel formation. GelMA-based cryogels can withstand autoclave sterilization temperatures and pressures while retaining their main properties and functionality [285,286]; however, they are still unsuitable for long-term experiments/applications due to their weakness and rapid degradation rate even in the absence of cells [278]. The combination of GelMA with other methacrylate biopolymers proved to be a successful tactic for dealing with this issue.

It should be remarked that GelMA can be further modified by utilizing other functional groups present in its structure, resulting in the development of derivatives with highly adaptable properties for various biomedical applications.

2.2.2.2 *Dextran*

Dextran (Dex) is considered the most important exopolysaccharide for medical and industrial applications. It is produced through fermentation of lactic acid bacteria (LAB) or by employing their enzymes in the presence of sucrose as a carbon source. Dextran consists of a linear chain of D-glucoses linked together by α-(1→6) bonds, with possible branches of D-glucoses connected by α-(1→4), α-(1→3), or α-(1→2) bonds (Figure 10). In industry, it is obtained through the culture of *Leuconostoc mesenteroides* NRRL B512, a bacterium generally recognized as safe (GRAS) which produce dextran molecules with high stability due to their particular composition which consists of 95% α-(1→6) bonds and 5% branches with α-(1→3) bonds. Each dextran is unique and complex, differing from others in term of molecular weight as well as in type and degree of branching. These parameters, critical for determining the properties of the resulting polymer and their applications in the biomedical and pharmaceutical fields, are strongly dependent on the fermentation conditions (e.g., temperature and sucrose availability) and producing strain (or enzyme) [287].

Because of its biocompatibility, low toxicity, low cost, and ease of modification, dextran is widely employed in several biomedical applications [288]. For example, dextrans are widely used to reduce vascular thrombosis and inflammatory response, as well as to prevent ischemia and reperfusion injury after organ transplantation, acting as scavengers against reactive oxygen species and reducing excess platelet activation. Its volume expanding properties can improve blood flow, and its soluble complexes can be used to replace lost blood in emergency situations. Dextran is also commonly used as coating material to protect and improve biocompatibility, as well as in a variety of other applications [289].

The large number of hydroxylic groups available on the polymeric backbone makes dextran suitable for various types of chemical modification, resulting in the development of derivatives with specific properties that could be used for the preparation of various scaffolds, such as spheres [290-292], tubules [293], and hydrogels [294-296] which have already demonstrated to be highly effective as drug delivery systems, tissue regeneration devices, and cell therapy vectors [297].

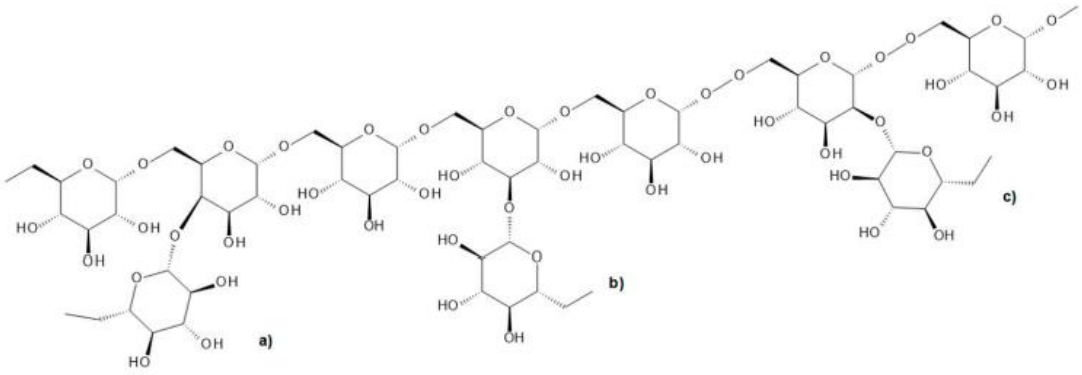

Figure 10. Dex backbone formed by D-glucose units with α-(1→6) bonds and different branching bonds: (a) α-(1→4), (b) α-(1→3), and (c) α-(1→2) [287].

The most frequent chemical modification of dextran involves grafting methacrylic groups onto the polymer backbone by using glycidil methacrylate. The methacrylate derivative of dextran (DexMA) offers a significant advantage over other polymers in the fabrication of hydrogels, allowing the creation of systems with exceptional mechanical properties that can be further tailored by varying the methacrylation degree of the resulting derivative [298]. However, the lack of particular cell adhesion and signaling sites severely restricts the use of DexMA for the development of tissue engineering scaffolds [299]. Hence, DexMA is frequently combined with other biopolymers to enhance its biological response, resulting in the generation of materials that exhibit both great biocompatibility and superior mechanical properties. Notably, chemically coupled copolymer hydrogels keep each polymer's advantageous features while also gaining the mechanically improved performance offered by the densely entangled networks. Regarding this, the combination of DexMA and GelMA has shown promise for the creation of single-network hydrogels, demonstrating favorable outcomes for the purpose of tissue regeneration [298].

Using the information provided above as a foundation, we looked into the possibility of designing macro-porous scaffolds based on GelMA and DexMA using the cryotropic gelation method, paying close attention to how the polymer composition affected the amount of radical initiator needed to create cryogels as well as the key characteristics of the final systems.

Both polymer derivatives exhibit considerable biodegradability. Gel is subject to the action of gelatinases, matrix metalloproteases whose zinc-dependent catalytic activity is

of fundamental importance for many biological processes such as tissue repair and remodulation, wound healing, embryogenesis, morphogenesis, angiogenesis, as well as cell proliferation, differentiation migration and apoptosis [300]. The binding sites of these enzymes are unaffected by the derivatization of Gel with methacrylic groups, making GelMA vulnerable to degradation mediated by enzymes [277]. Dextran molecules, on the other hand, are hydrolyzed by dextranases, which are bacterial enzymes found in the human colon [301]. Biodegradation is a fundamental property that tissue engineering scaffolds must have, and the degradation rate of the structures should be precisely controlled because it should coincide with the production of new ECM in order to support proper tissue regeneration.

Gelatin-based spongy and compressive resistant cryogels with shape recovery ability as ideal scaffolds to support cell adhesion for tissue regeneration

*Laura Di Muzio[1], Chiara Brandelli[1], Vito Cosimo Carriero[1], Claudia Sergi[2], Jacopo Tirillò[2], Alessandra Adrover[2], Elisa Messina[3], Roberto Gaetani[4], Stefania Petralito[1], Maria Antonietta Casadei[1], Patrizia Paolicelli[1]**

[1] *Department of Drug Chemistry and Technologies, Sapienza University of Rome, 00185 Rome, Italy*

[2] *Department of Chemical Engineering Materials Environment, Sapienza University of Rome, 00184 Rome, Italy*

[3] *Department of Maternal, Infantile, and Urological Sciences, "Umberto I" Hospital, 00185 Rome, Italy*

[4] *Department of Molecular Medicine, Sapienza University of Rome, 00185 Rome, Italy*

UNDER REVISION (Biomacromolecules)

*Corresponding author: Prof. Patrizia Paolicelli
Department of Drug Chemistry and Technologies
Sapienza University of Rome
Piazzale Aldo Moro 5
00185 – Rome
Italy
Ph: 0039 06 4991 3173
E-mail: patrizia.paolicelli@uniroma1.it

Abstract

Methacryloyl gelatin (GelMA) was blended with dextran methacrylate (DexMA) to produce interpenetrated and macroporous networks via cryostructuring and radical crosslinking of the polymers at subzero temperatures. The experimental set-up was optimized to allow the formation of monolithic networks characterized by highly uniform and interconnected porous structure. The total polymers mass, the amount of the gel-forming reagents and particularly the rheological properties of GelMA resulted the most critical factors for the fabrication of homogeneous and not collapsed scaffolds. Indeed, only the use of GelMA with very low gelation temperature resulted in the formation of uniform monolithic cryogels. However, blending with DexMA produced general worsening of the mechanical properties of the scaffolds, due to DexMA interference with secondary structuring of GelMA during the cryogelation process. DexMA also had negative effect on the ability of the cryogel to support growth and proliferation of HaCat cells, bringing to slower cell adhesion to the scaffold.

Keywords: cryogels; dextran methacrylate; methacryloyl gelatin; scaffolds; 3D cell culturing; tissue engineering

1. Introduction

The field of tissue engineering focuses on the use of scaffolds to encourage cell growth and tissue regeneration at the wound site or *in vitro*.[1,2] A scaffold provides a network imitating the native tissue, serving as an extracellular matrix (ECM) analogue. Hydrogels have been extensively investigated for application in this field.[3,4] They are formed through the physical or chemical crosslinking of polymer aqueous solutions, resulting in tridimensional networks with high water retention. These scaffolds are commonly utilized for applications such as drug delivery, cell-encapsulation and tissue engineering.[5] Despite their popularity, the pore size of hydrogels do not allow cell penetration to efficiently occur throughout the scaffold and often lead to irregular cell dispersion, as well as decreased cell viability from lack of nutrient transport and waste removal.[6] For this reason, different strategies have been investigated over the last years to increase the pore size of hydrogels and improve their interconnectivity.[7] One of the most interesting approach is based on the ice templating and cryogelation process, which has been established for the development of macroporous hydrophilic gels, known as cryogels. Although cryogel-type materials have been under study since 1982,[8] they become popular as scaffold for tissue regeneration only in recent years.[9]

The cryotropic gelation process works under frozen conditions, whereby most of the solvent is frozen, and the dissolved gel precursors get concentrated in the nonfrozen liquid microphase (cryoconcentration process), in which gelation proceeds. After complete crosslinking, the melting or removal of solvent crystals that function as porogens leaves behind a system of large and continuously interconnected pores. Therefore, in contrast to traditional hydrogels, cryogels have a system of interconnected macropores with dense pore walls, resulting from the cryoconcentration process, which provide relatively high mechanical strength and elasticity.[10]

Similarly to hydrogels, cryogels can be constructed out of both natural and synthetic polymers. In a recent work, we developed novel spongy cryogel systems based on the natural polysaccharide dextran (Dex) and the synthetic polymer polyethylene glycol (PEG), both functionalized with methacrylic groups (i.e. DexMA and PEGDMA) to produce a chemical network through free radical crosslinking reaction.[11] The natural polysaccharide Dex was selected for its biocompatibility, high water solubility, and ease of modification with different types of chemical functionalities, including methacrylic groups (DexMA). While the combination of DexMA and PEGDMA provided a system suitable as drug delivery platform for biomedical applications that require an interconnected scaffold for localized delivery of therapeutic molecules, these networks still possess unsatisfactory features when used as scaffold for tissue regeneration. In particular, the main drawback of all the systems so far investigated depends on the absence of specific cell signaling motifs able to adequately support cell adhesion and proliferation. Therefore, even if these DexMA/PEGDMA cryogels possess good biocompatibility and do not elicit any cytotoxic effect *in vitro*, they need further superficial treatments, such as dopamine coating, to allow their proper application in tissue engineering.[12,13] This approach may effectively improve the ability of the scaffold to support cell adhesion, proliferation and matrix deposition, but it may impair the porous structure of the polymer network. Therefore, in this work we modified the composition of the scaffolds substituting PEGDMA with a polymer that possesses biological cues and is able to enhance the bioactivity of the final construct. To reach this goal we used gelatin (Gel) functionalized with methacryloyl groups (GelMA) because in comparison with cryogels obtained from synthetic polymers, gelatin-based cryogels showed evident and undisputed superiority.[14] Gel is a polymer obtained from the partial hydrolytic degradation of collagen, the most abundant protein of some connective tissues. It is less immunogenic, higher soluble in aqueous media and more cost-effective

than collagen and additionally shares with its precursor some typical bioactive amino acid sequences, such as the arginine–glycine–aspartic acid (RGD) motif and the matrix metalloproteinases (MMP)-sensitive degradation sites. The tripeptide RGD was originally identified as the sequence within fibronectin that mediates cell attachment. Later on the RGD motif was found in numerous other proteins, including collagen, and it was recognized its role in supporting cell adhesion in many of these proteins. The integrins, a family of cell-surface proteins, act as receptors for cell adhesion molecules. A subset of the integrins recognize the RGD motif within their ligands, the binding of which mediates both cell-substratum and cell-cell interactions.[15,16] Instead, the MMP-sensitive peptide sequences are proteolytically cleavable sequences able to promote cell-mediated degradation. All these features make Gel desiderable candidate for synthesis of polymeric networks for biomedical applications.[17] Therefore, in this work GelMA was combined with DexMA to produce interpenetrated and macroporous polymer networks by free radical crosslinking carried out at subzero temperatures. The experimental set up was suitably investigated and optimized to allow the formation of polymeric networks with a high GelMA content. The effect of the network composition on the porosity, swelling, elasticity and mechanical properties of the cryogels was evaluated and compared to the corresponding hydrogel formulations, prepared at room temperature. Finally, the ability of the prepared cryogels to adequately support cell adhesion and proliferation was studied in order to assess their suitability to serve as scaffold for tissue regeneration purposes.

2. Materials and methods

2.1. Materials

Type A gelatin from pig skin (~300 g Bloom), dextran (Dex) from *Leuconostoc* ssp. (Mn 40,000), anhydrous dimethyl sulfoxide (DMSO), deuterated water (D_2O), methacrylic

anhydride (MAA), triethylamine (TEA), nicotinamide (Nic), ammonium persulfate (APS), *N,N,N′,N′*-tetramethylenediamine (TEMED), glycidyl methacrylate (GMA), 4-dimethyl aminopyridine (DMAP), vitamin B12, methanol Chromasolv™ (MeOH), acetic acid (CH_3COOH), dialysis membranes (cut-off 12-14 kDa) and L-glutamine were purchased from Sigma Aldrich. Absolute ethanol (EtOH), 37% *w/w* hydrochloric acid (HCl), monobasic potassium phosphate (KH_2PO_4) and sodium hydroxide in pellets (NaOH) were purchased from Carlo Erba. Vybrant® CDFA SE cell tracer kit, alamarBlue™ cell viability reagent and Primocin™ were purchased from Invitrogen, Fetal Bovine Serum (FBS) from Gibco, Dulbecco's Phosphate Buffered Saline (PBS, 1X) from Aurogene, DMEM culture medium from Lonza and penicillin-streptomycin solution (10,000 U/mL) was obtained from BioWhittaker.

2.2 Synthesis and characterization of GelMA

GelMA was synthesized following two different procedures.[18]

2.2.1 Two-phase synthesis of GelMA

Gel was solubilised for 1 h at 50 °C in phosphate buffer (PBS, pH = 7.4) at a concentration of 10% *w/v* under vigorous magnetic stirring. Following complete solubilisation, 1.5 mL of MAA/g Gel were added drop by drop. The resulting biphasic system was left to react at 50 °C for 3 h, and the reaction was interrupted by dilution (x5) with PBS previously heated at 50 °C. The mixture was dialyzed at a temperature above 37 °C to avoid gelation of the polymer inside the dialysis tubes. After 5 days of dialysis, the polymer solution was freeze-dried with a LIO 5P freeze-dryer (5 Pascal, Italy) equipped with a vacuum pump Adixen (Alcatel, France). The obtained polymer was labelled as $GelMA_{dp}$.

2.2.2 Single-phase synthesis of GelMA

The single-phase procedure involves the solubilisation of Gel in anhydrous DMSO at a concentration of 5% *w/v* for 1 h at 50 °C, under magnetic stirring. After complete solubilisation, 0.3 mL/g of MAA was added and the solution was kept under magnetic stirring at 50 °C for 3 h. Then, it was dialyzed exhaustively against deionized water at 37 °C for 3 days and freeze-dried. The obtained polymer was labelled as $GelMA_{sp}$.

2.2.3 Characterization of GelMA

Aliquots (10 mg) of $GelMA_{dp}$ and $GelMA_{sp}$ were dissolved in 0.7 mL of D_2O for ^1H NMR analysis. All spectra were recorded using a Bruker AC-400 spectrometer (Germany).

^1H NMR analysis was employed to evaluate the successful methacryalation of Gel and to determine the degree of derivatization (DD) of the polymer, using and internal standard for the scope. To this end, 10 mg of $GelMA_{dp}$ and $GelMA_{sp}$ were first dissolved in 0.5 mL of D_2O, and then 0.2 mL of a 1 mg/mL solution of the internal standard nicotinamide in D_2O were added. The DD of both $GelMA_{dp}$ and $GelMA_{sp}$ was 0.53 ± 0.02 mmol/g. The ^1H NMR characterization for GelMA is reported in the supplementary material (Figure S1).

2.3 Synthesis and characterization of dextran methacrylate (DexMA)

DexMA was synthesized as reported in a previous study with slight modification.[19] Briefly, dextran (2.5 g) was solubilised in anhydrous DMSO (20 mL). Subsequently, DMAP (0.71 g) and GMA (0.26 mL) were added to the polymeric solution, and the reaction was maintained under stirring for 24 h at room temperature. At the end of the reaction time, the polymer was precipitated by dropwise addition of the reaction mixture to absolute EtOH (100 mL). The precipitate was filtered, and the recovered solid was

dissolved in distilled water (30 mL). The pH of the polymer solution was neutralized with 0.1 M HCl. The polymer was purified by dialysis against distilled water and then freeze-dried. The polymer was characterized by ^{1}H NMR, recording the spectrum in D_2O. ^{1}H NMR analysis was employed to evaluate the successful methacryalation of Dex and to determine the DD of DexMA, which was calculated using the internal standard nicotinamide. The degree of methacrylation was found to be 5 ± 1%. The ^{1}H NMR spectrum of DexMA is reported in the supplementary material (Figure S2).

2.4 Cryogels and hydrogels preparation

Cryogels and hydrogels containing different DexMA and GelMA weight ratios were synthesized by free radical crosslinking method, with ammonium persulfate (APS) as the initiator agent and *N,N,N′,N′*-tetramethylethylenediamine (TEMED) as the catalyst.

GelMA and DexMA were solubilised in distilled water at 50 °C under mild magnetic stirring for 15 min and, after complete solubilisation, the solution was cooled to room temperature before the addition of the crosslinking reagents (APS and TEMED). The amount of APS ($mmol_{APS}$) was varied considering the total mmoles of methacrylic groups ($mmol_{MG}$) of the polymer solution, as reported in Table 1. Specifically, different $mmol_{APS}/mmol_{MG}$ ratios were tested, whereas a costant ratio $mmol_{APS}/mmol_{TEMED}$ of 0.9 was used for all the samples. The total volume of the polymer solution, after APS and TEMED addition, was set to 2 mL. The polymer solutions containing the crosslinking reagents were placed into a cryostat M408-BVC (MPM Instruments, Italy) at −12.0 ± 1.0 °C for 4 h for cryogels fabrication. After this time, they were freeze-dried to remove the ice crystals and obtain the final macroporous scaffolds.

The optimal cryogel samples were also produced as hydrogels configuration of same composition (i.e. $GelMA_3/DexMA_3$; $GelMA_4/DexMA_2$ and $GelMA_6$), which were obtained using the amounts of crosslinking reagents reported in entries 8, 12 and 17 of

Table 1. The hydrogels were formed at room temperature (25.0 ± 1.0 °C) and were stored at 4°C overnight to allow complete polymer crosslinking, then they were frozen at −40 °C and freeze-dried.

Both cryogels and hydrogels samples were prepared in cylindrical glass molds (diameter 20 mm, height 40 mm).

Table 1. *Composition of cryogel samples and amount of APS used for their preparation in relation to the total amount of methacrylic groups. The volume of the solution was kept constant (2 mL), as well as the* $mmol_{APS}/mmol_{TEMED}$ *ratio used, which was equal to 0.9.*

Entry	**Sample**	**GelMA (%, *w/v*)**	**DexMA (%, *w/v*)**	**$mmol_{APS}/mmol_{MG}$**	**Notes**
1	$GelMA_5/DexMA_5$	5	5	0.20	Gel formation, but too compact structure
2		5	5	0.15	No gel formation
3	$GelMA_4/DexMA_4$	4	4	0.25	Gel formation, but too compact structure
4		4	4	0.20	No gel formation
5	$GelMA_3/DexMA_3$	3	3	0.90	Hydrogel-like structure
6		3	3	0.60	Hydrogel-like structure
7		3	3	0.50	Cryogel formation with suboptimal swelling and mechanical properties
8		3	3	0.45	Cryogel formation with optimal swelling and mechanical properties
9		3	3	0.40	Cryogel formation with suboptimal swelling and mechanical properties
10		3	3	0.30	No gel formation
11	$GelMA_4/DexMA_2$	4	2	0.60	Hydrogel-like structure
12		4	2	0.50	Cryogel formation with optimal swelling and mechanical properties
13		4	2	0.45	Cryogel formation with suboptimal swelling and mechanical properties
14		4	2	0.40	Cryogel formation with suboptimal swelling and mechanical properties
15		4	2	0.30	No gel formation
16	$GelMA_6$	6	----	0.60	Hydrogel-like structure

17		6	----	0.55	Cryogel formation with optimal swelling and mechanical properties
18		6	----	0.50	Cryogel formation with suboptimal swelling and mechanical properties
19		6	----	0.45	Gel formation with partially collapsed structure
20		6	----	0.30	No gel formation
21	$GelMA_2/DexMA_4$	2	4	0.55	No gel formation
22		2	4	0.50	No gel formation
23		2	4	0.40	No gel formation
24		2	4	0.30	No gel formation
25	$DexMA_6$	----	6	0.50	No gel formation
26		----	6	0.45	No gel formation
27		----	6	0.30	No gel formation
28		----	6	0.20	No gel formation

2.5. Rheological analysis

Time-sweep analyses were carried out using a Discovery TA HR-1 stress-control rheometer. Polymer solutions containing APS and TEMED were characterized for their rheological properties using a cone-plate geometry with a diameter of 40 mm (α 1.005°, gap 27 μm). Opportune amounts of GelMA and DexMA were dissolved in distilled water at 50 °C under mild magnetic stirring for 15 min. After complete solubilisation, the solutions were allowed to cool down, then APS and TEMED were added and aliquots of the samples (0.3 mL) were quickly loaded onto the Peltier plate of the rheometer. Oscillatory time-sweeps were carried out at the constant frequency of 1 Hz monitoring the evolution of the storage (G′) and loss (G″) moduli as a function of time, at the constant temperature of 10.00 °C. The gel-sol transition was determined by the G'/G'' crossover. All the experiments were carried out at least in triplicate. For each sample, the linear viscoelastic range was previously evaluated using oscillatory strain-sweep tests: a 1% maximum deformation was used.

2.6 Physical characterization of cryogels and hydrogels

2.6.1 Compression tests

The compressive properties of freeze-dried cryogels and hydrogels were evaluated through a universal testing machine Zwick/Roell Z010 equipped with a 10 kN load cell employing a test speed of 1 mm/min. Cryogel and hydrogel systems were tested in dry conditions and after hydration.

The best cryogel configuration from the mechanical response perspective, i.e. $GelMA_6$ cryogels, was further investigated by performing repeated compressive cycles in wet conditions to assess material toughness. In particular, cryogels were subjected to 5 compressive cycles up to a 55 % deformation and allowing for one minute of rest between subsequent compressive tests.

2.6.2 Scanning electron microscopy

The morphology of freeze-dried cryogels and hydrogels was evaluated through a field-emission scanning electron microscope (FE-SEM) MIRA 3 by Tescan. Due to their low electrical conductivity, all specimens were sputter coated with a thin layer of gold to prevent charging. The coating process was carried out in vacuum conditions (0.4 mbar) for 2 min by a sputter coater Edwards S150B applying a voltage of 1 kV and an electrical current of 40 mA to the gold electrode. The morphology of as-received and dried-compressed cryogels and hydrogels was investigated to underline the different compressive response of the two systems. Moreover, cryogels morphology was also investigated after dry compression and subsequent hydration, but also after hydration and subsequent compression.

2.6.3 Tomography

High resolution micro-CT observations were performed for both cryogel and hydrogel configurations through an UltraTom CT scanner by RX Solutions. A resolution of 1.5 μm was used, with a beam current of 157 μA and an accelerating voltage of 50 kV. A 3D volumetric reconstruction (volumetric rendering) of the specimens and a segmentation analysis were performed by analyzing the acquired images through the Avizo 8.1 software.

2.6.4 Absorption and swelling studies

The maximum fluid uptake of cryogels and hydrogels was tested by measuring the volume of PBS (pH=7.4) absorbed. PBS was pre-heated at the temperature of 37.0 ± 0.5 °C and then added dropwise to the surface of freeze-dried cryogels and hydrogels. The addition of PBS was interrupted when the maximum uptake capacity of the gels was reached, and a drop of buffer was visible at the bottom of the sample. The analyses were carried out in triplicate, and the results are reported as the mean values ± the standard deviation.

The swelling degree of the gels was also determined in PBS. To this end, freeze-dried cryogel and hydrogel samples were weighed and then placed in an excess volume of PBS at 37.0 ± 0.5 °C. At established time points, the samples were taken and the excess of PBS gently wiped off before weighing. The swelling degree (Q) was expressed as:

$Q = W_s/W_d$

where W_s and W_d were the weights of the swollen and dry sample, respectively. Each experiment was performed in triplicate, and the results were reported as the mean values ± the standard deviation.

2.7 Release studies

The release rate of vitamin B12 from cryogels and hydrogels was investigated in order to have insights into the internal structure of the different configurations of the polymer networks. Vitamin B12-loaded cryogels and hydrogels were prepared dissolving vitamin B12 in the polymer solution prior to the crosslinking step, carried out as as described in *Section 2.4*. However, cryogels were obtained loading 2.5 mg of vitamin B12 in 2 mL of polymer solution, whereas hydrogels were prepared dissolving 1.25 mg of vitamin B12 in 1 mL of polymer solution. The vitamin B12-loaded cryogels and hydrogels were freeze-dried before performing the release study. Each sample was introduced into an Erlenmeyer flask containing 20 mL of PBS (pH 7.4) and maintained at 37.0 ± 0.5 °C under magnetic stirring (200 rpm) for the duration of the analysis. At established time points, aliquots of the release medium (250 μL) were taken and immediately replaced with an identical volume of fresh PBS, in order to maintain constant the total volume of the release medium. Withdrawals were made every minute during the first 5 min, every 5 min untile 20 min, every 10 min until the first hour, every 30 min up to 2 h, every hour until 10 h, and finally after 24 h. The concentration of vitamin B12 released was evaluated by HPLC analysis. The HPLC system consisted of a Perkin Elmer Series 200 LC pump, equipped with a 235C Diode Array Detector. The analyses were carried out using a Merck Hibar LiChrocart (250–4.5 μm) RP-18 column, setting the flow rate to 0.7 mL/min and using a 70:30 *v/v* mixture of 0.1 M CH_3COOH/MeOH as eluent. A calibration curve in the range from 0.5 to 250 μg/mL was used to quantify the concentration of vitamin B12, which wa monitored at λ = 360 nm. Each experiment was performed in triplicate, and the results were reported as the mean values ± the standard deviation.

2.8 Cell culture

Aneuploid human immortal keratinocytes (HaCats) were used to evaluate scaffolds biocompatibility and cell behavior. Cells were expanded in T-75 flasks and cultured at 37 °C and 5% CO_2 in DMEM supplemented with 10% *v/v* of FBS, 1% *v/v* of L-glutamine and 1% *v/v* of an antibiotic solution consisting of penicillin and streptomycin.

2.8.1 Cytocompatibility studies

Cylindrical samples of cryogels (diameter 5 mm, height 2 mm) were steam sterilized at 121°C for 10 min and then incubated in complete DMEM (500 µL) at 37 °C for 15 days without agitation. At the end of the incubation time, the media were collected and used to evaluate potential cytotoxic extractables and leachables from cryogels. To this end, HaCats were seeded in a 96-well plate at a density of $3x10^3$cells/well and cultured with 100 µL culture medium at 37 °C and 5% CO_2. After 48 h, the culture medium was removed and the metabolic activity was measured by the alamarBlue metabolic activity assay according to the manufacturer's protocol (10% *v/v* in media) and the absorbance at 570 and 630 nm was measured with a microplate reader (Robonik®, readwell TOUCH Elisa Plate Analyser). The results were used as baseline. The cells were then cultured in the media previously incubated with the different cryogels or fresh culture medium as a control for additional 24 and 48 h. At the end of each incubation time the alamarBlue metabolic activity assay was repeated and the cell viability was obtained by normalizing the results to the control group. Each experiment was performed in triplicate, and the results were reported as the mean values ± the standard deviation.

2.8.2 Adhesion and proliferation studies

Before cell seeding, cylindrical samples of cryogels (diameter 5 mm, height 2 mm) were steam sterilized at 121°C for 10 min and then placed individually into a 96-well plate.

Cells were collected, suspended in 30 µL culture media and then seeded on top of the different cryogels at a density of 2.5×10^6/cryogel and incubated at 37 °C and 5% CO_2 for 1 h to allow cell adhesion to the scaffolds. After this incubation time, 200 µL of culture media was added into each well. To evaluate cell viability and proliferation, cells were stained with a 10 µM solution of Vybrant® CFDA SE dye in PBS and imaged at different time points (2, 7, 10, 15, 21, and 30 days). To this end, culture medium was removed and replaced with 250 µL of staining solution. Plates were incubated at 37 °C and 5% CO_2 for 15 min and then washed with DMEM, before imaging with a fluorescent microscope (Leica DMI4000B). At least ten images were taken at each time point in the middle and at the edges of both sides of the cryogels.

At the same time points, cell proliferation was also evaluated by the alamarBlue assay, carried out as previously described. Specifically, culture medium was removed, the constructs were rinsed with PBS and incubated for 2h with 250 µL of a 10% *v/v* alamarBlue solution in DMEM. The absorbance was measured as previously described and the obtained values were used to quantify cell viability and proliferation over time. Each measurement was performed in triplicate, and the results were reported as the mean values ± the standard deviation.

2.9 Statistical analysis

The statistical analysis was performed using two-way analysis of variance (ANOVA) to determine any significant differences among different groups tested. All analyses were carried out with GraphPad Prism 9. p-value of less than 0.05 indicates statistical significance.

3. Results and Discussion

3.1 Cryogels preparation and optimization

Interpenetrated polymer networks were formed combining two different methacryloyl polymers, namely DexMA and GelMA. A free radical crosslinking process, carried out at -12 °C for 4 h in the presence of the crosslinkers APS and TEMED, was used to allow the formation of interconnected macroporous networks, according to the procedure schematized in Figure 1. First attempts were made using $GelMA_{dp}$ synthesized following the conventional double-phase procedure.[20] Interpenetrated polymer networks were produced starting from 1:1 *w/w* DexMA and $GelMA_{dp}$ mixtures. Different parameters were modified, including DexMA and $GelMA_{dp}$ concentrations and the amount of the crosslinking reagents, in order to control the crosslinking kinetics and allow ice nucleation and crystals growth before network formation. Anyway, in all the cases, polymer networks with evident collapsed structure, like that reported in Figure 1A, were obtained.

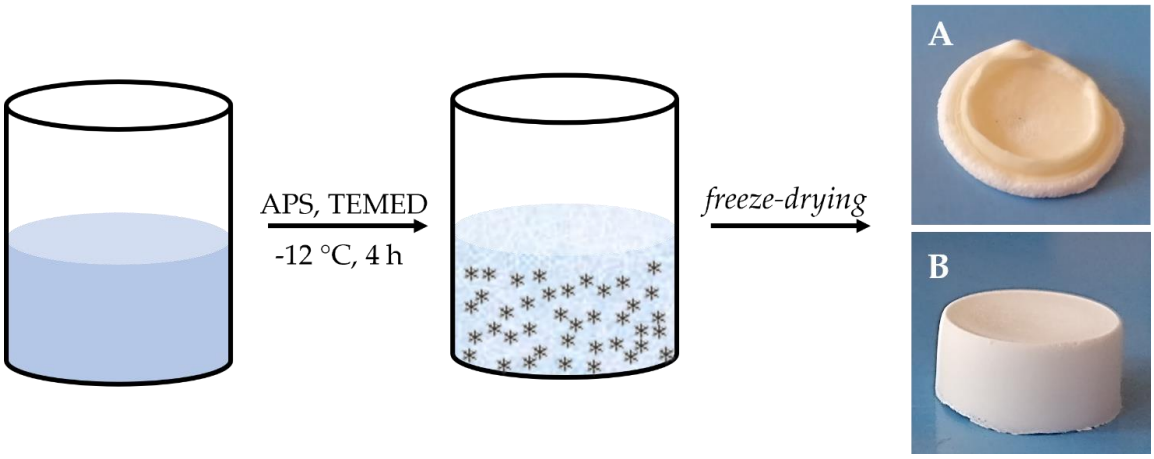

Figure 1. Schematic of the procedure used to produce cryogels. A) Image of a typical cryogel obtained using $GelMA_{dp}$ (GelMA synthesized according to the two-phase procedure described in *Section 2.2.1*) showing collapsed structure. B) Image of a typical cryogel prepared using $GelMA_{sp}$ (GelMA synthesized according to the single-phase procedure described in *Section 2.2.2*) showing not collapsed structure.

Completely different results were achieved using $GelMA_{sp}$ synthesized according to a recently proposed single-phase procedure in DMSO.[18] Indeed, this polymer allowed the formation of homogeneous structures without evident signs of melt-back or network collapse, as reported in Figure 1B. It has been assumed that the observed differences were due to the different rheological behavior of $GelMA_{dp}$ and $GelMA_{sp}$ with temperature. Much lower gelation temperatures were reported for $GelMA_{sp}$ compared to $GelMA_{dp}$. Therefore, it is possible that the low temperatures required for cryogel formation may cause early physical gelation of the $GelMA_{dp}$, which may apply a series of resistance forces that can restrict the diffusion of water molecules to the ice lattice, thus hindering ice growth and affecting the shape of the final ice crystals, as well as the subsequent chemical crosslinking.[21] For this reason, further investigations were carried out using $GelMA_{sp}$ exclusively. This polymer was used to prepare several different chemical networks exploring the role of different parameters on the formation of macroporous interpenetrated gel systems. In specific, the total polymer concentration, the weight polymer ratio and the amount of the crosslinkers APS and TEMED were changed as reported in Table 1. All the samples were freeze-dried, and after freeze-drying the obtained constructs were visually observed in the dry state and after rehydration to evaluate the formation of macroporous networks, considering that ideal cryogels should possess homogeneous structure, should immediately and hugely swell when in contact with water or aqueous solutions and should possess elastic structure (see video 1 and 2). Unfortunately, the optimization of the experimental conditions for cryogel formation needs to follow a trial and error approach. Indeed, there are not adequate analytical methods to evaluate the appropriate amounts of polymers and crosslinking reagents at a given temperature, when network formation is operated at subzero temperatures. It is known that cryoconcentration of gel precursors is essential for developing proper cryostructures, leading to the successful formation of cryogels.

Cryoconcentration is a phenomenon that involves the formation of an unfrozen liquid microphase with consequent temperature-induced increased concentration of solutes. It has been observed that this cryoconcentration phenomenon accelerates the reaction of precursor molecules leading to polymerization, crosslinking and formation of strong polymeric networks. For this reason, the ice crystal formation needs to start slightly earlier than the polymerization and crosslinking to make sure that cryoconcentration is well accomplished and ice crystals can effectively act as porogens. In case the polymerisation and crosslinking of gel precursors starts before nucleation and growth of ice crystals, cryoconcentration will not be achieved, leading to the formation of hydrogels rather than cryogels.[10] Based on these considerations, it is essential to finely adjust the amounts of the gel precursors in order to allow slow polymerization and crosslinking kinetics before initiation of ice crystallization. In this sense, helpful information can be obtained with oscillation time-sweep tests, which allow to monitor the evolution of storage (G') and loss (G'') moduli of a polymer system as a function of time operating at constant temperature (Figure 2A). This analysis can be used for optimization of the experimental conditions needed for cryogel preparation, even if it shows some important limitations that have to be taken into account. The main drawback is represented by temperature. Indeed, the analysis cannot be easily carried out at the subzero temperatures used for cryogel preparation, therefore only qualitative and non-generalizable information can be gathered from the test, because the analytical conditions do not faithfully reflect those existing during the network formation. At subzero temperatures, additional phenomena may occur and affect the final outcome of the cryogelation process, as in the case of $GelMA_{dp}$. Therefore, the experimental conditions required for the formation of macroporous gel systems should be finely optimized with a trial and error approach. In this sense, it can be observed in Figure 2B that different amounts of APS were needed to allow the formation of cryogels with

different GelMA content. Specifically, while 0.45 $mmol_{APS}/mmol_{GM}$ resulted optimal for $GelMA_3/DexMA_3$ cryogel system (containing 3% *w/v* of both polymers), it was necessary to increase the ratio to 0.50 and 0.55 for $GelMA_4/DexMA_2$ (containing 4% *w/v* of GelMA and 2% *w/v* of DexMA) and $GelMA_6$ (containing 6% *w/v* of GelMA) samples, respectively. Indeed, when 0.45 $mmol_{APS}/mmol_{GM}$ was used to prepare $GelMA_6$ cryogels, the time-sweep analysis evidenced that the gelification occurred almost at the same time of the $GelMA_3/DexMA_3$ cryogels (Figure 2C), but the sample showed clear collapsed structure (Figure 2D), compared to that obtained using 0.55 $mmol_{APS}/mmol_{GM}$ (Figure 2E). It is evident that, in these cases, the crosslinking kinetics did not only depend on the total concentration of methacryloyl groups ($6.4 \times 10^{-2}\ mmol$ for $GelMA_6$ and $5.0 \times 10^{-2}\ mmol$ for $GelMA_3/DexMA_3$), but also other factors were influencing the final outcome. In particular, it is possible that higher amounts of GelMA caused an increase in the viscosity of the unfrozen liquid microphase formed during the freezing process, which may had hampered the chemical crosslinking of the polymers. For this reason, faster crosslinking kinetics were required for optimal cryogel formation when the polymer network composition was changed and the amount of GelMA increased.

Under the experimental conditions found, it was possible to prepare three different polymer networks – namely $GelMA_3/DexMA_3$, $GelMA_4/DexMA_2$ and $GelMA_6$ – with homogeneous macroscopic structure and huge PBS uptake capacity (Figure 2F). On the contrary, it was not possible to obtain adequate cryostructuring of polymer mixtures with DexMA content higher than GelMA ($GelMA_2/DexMA_4$ and $DexMA_6$ samples), even changing opportunely the amounts of APS and TEMED used (Table 1). Similar results were obtained when the cryogels were prepared keeping the gel precursors at -12 °C for 2 h, instead of 4 h (data not shown). Therefore, further investigations were carried out on cryogels samples prepared with this experimental set-up (-12 °C and 2 h).

The same compositions ($GelMA_3/DexMA_3$, $GelMA_4/DexMA_2$ and $GelMA_6$) were produced also at room temperature to obtain the corresponding hydrogel systems. It can be observed from Figure S3 the evident difference in the dimensions of a typical hydrogel construct compared to the corresponding cryogel system of same composition, in both dry and wet conditions, which suggests an actual difference in the internal microstructure.

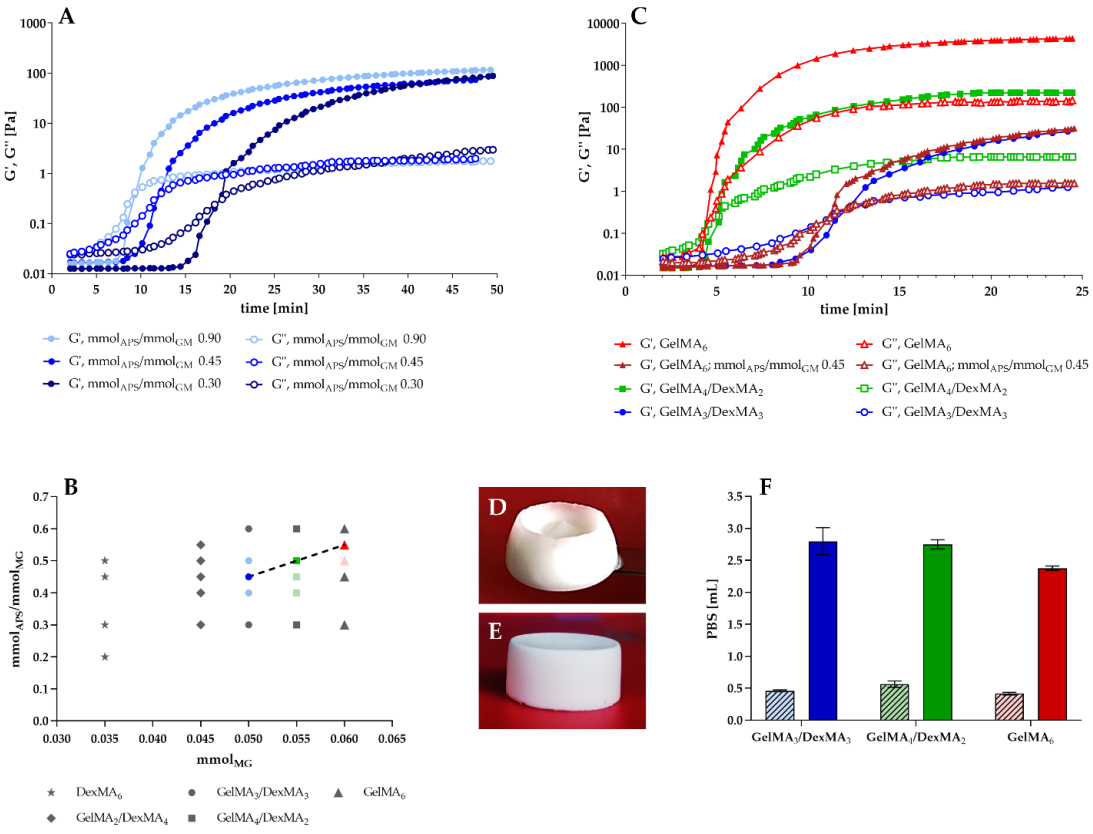

Figure 2. (A) Time sweep analysis of $GelMA_3/DexMA_3$ solutions containing different amounts of APS (0.30, 0.45 and 0.9 $mmol_{APS}/mmol_{MG}$), showing the effect of the radical initiator on the crosslinking kinetics of the polymers. (B) Diagram showing the mmoles of the radical initiator APS required for the proper formation of cryogel constructs, starting from polymer solutions with different content of methacrylic groups ($mmol_{MG}$). Grey symbols represent no cryogel formation; light coloured symbols represent suboptimal cryogel formation and dark coloured symbols represent optimal cryogel formation. (C) Time sweep analysis of polymer solutions with different GelMA content, showing that factors other than the total concentration of methacrylic groups affect the proper formation of cryogel constructs. (D,E) Images of $GelMA_6$ cryogels obtained using 0.45 and 0.55 $mmol_{APS}/mmol_{GM}$, respectively. (F) Volume of PBS (pH 7.4) absorbed by cryogel and hydrogel constructs.

3.2 Physical characterization of cryogels and hydrogels

3.2.1 Swelling characterization

The actual formation of cryogel networks was indirectly demonstrated by swelling measurements in PBS (pH 7.4). Figure 3A shows the behavior of the swelling degree $Q(t)$ as a function of time for cryogels and hydrogels. It can be readly observed that (i) the swelling dynamics of cryogels is significantly faster than that for the hydrogels and (ii) the asymptotic values Q_∞ are markedly larger for cryogels than for hydrogels. The swelling model developed in[22] was adopted to estimate the effective PBS diffusivity in the three hydrogel constucts. Figure 3B shows the behavior of $\frac{M_t^{PBS}}{M_\infty^{PBS}}$ *vs* time for the three hydrogels under investigation and the comparison with model predictions with the following effective PBS diffusivities $D = (3 \pm 0.2) \times 10^{-9} m^2/s$ for GelMA$_3$/DexMA$_3$, $D = (2 \pm 0.3) \times 10^{-8} m^2/s$ for GelMA$_4$/DexMA$_2$, and $D = (1.5 \pm 0.3) \times 10^{-9} m^2/s$ for GelMA$_6$. The PBS diffusivities in the cryogels can be estimated as at least one order of magnitude larger than that for the corresponding hydrogels and accout for a different porosity of cryogels compared to hydrogels constructs, as also suggested by their different dimensions (Figure 3C, 3D).

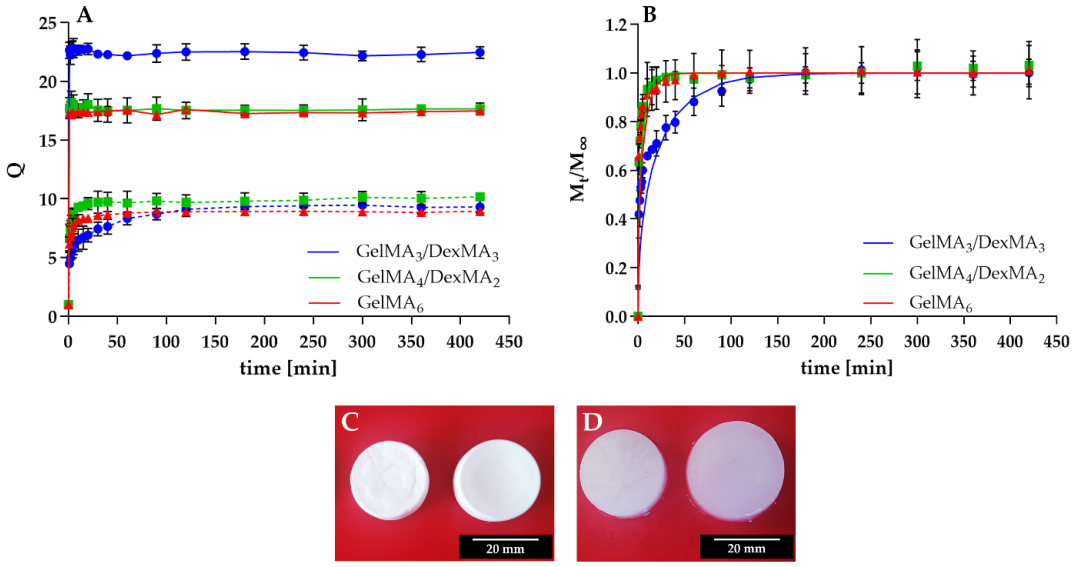

Figure 3. (A) Swelling degree $Q(t)$ *vs* time for hydrogels (dashed lines) and cryogels (solid lines). (B) Comparison between experimental data for $\frac{M_t^{PBS}}{M_\infty^{PBS}}$ *vs* time and the swelling-model predictions (continuous lines). (C) Exemplifcative image of dry hydrogel (on the left) and cryogel (on the right) samples. (D) Exemplifcative image of swelled hydrogel (on the left) and cryogel (on the right) samples.

3.2.2 Morphological characterization

One of the most important features of polymer scaffolds is the microstructure, which can affect many of their properties. In particular, scaffold porosity, pore size, and the overall pore structure all have important effects upon cell infiltration into biomaterial constructs and consequent tissue formation. Indeed, as extensively reported in literature,[23–26] the main drawback of hydrogels, which prevents their spread use in tissue engineering, is the lack of interconnected macropores which can cause insufficient vascularization or may lead to decreased cell viability due to lack of nutrient transport and waste removal. On the contrary, cryogels are characterized by a wide network of interconnected macropores as a consequence of cryotropic gelation.

This pronounced difference in cryogels and hydrogels morphology was acknowledged even in the present work as confirmed by the micrographs shown in Figure 4 and the microCTs reported in Figure 5A and 5B for cryogel and hydrogel monoliths,

respectively. Cryogels are characterized by a high interconnected porosity characterized by a uniform shape, dimension and dispersion in the specimen. Therefore, the adopted experimental conditions enabled the formation of monolithic polymer networks with no dominant pore orientation, which suggests homogenous cooling across the entirety of the scaffold during the freezing process.[27–29] Quite the opposite, hydrogels display a more massive nature with a worse connection between pores which develop mainly in parallel to cylinder sample rotation axis, as can be noticed from the segmentation in Figure 5. Moreover, a strong disomogeneity in hydrogels pore dispersion, shape and dimensions can be observed in the original microCTs, where some more dense zones and some large hole areas can be detected.

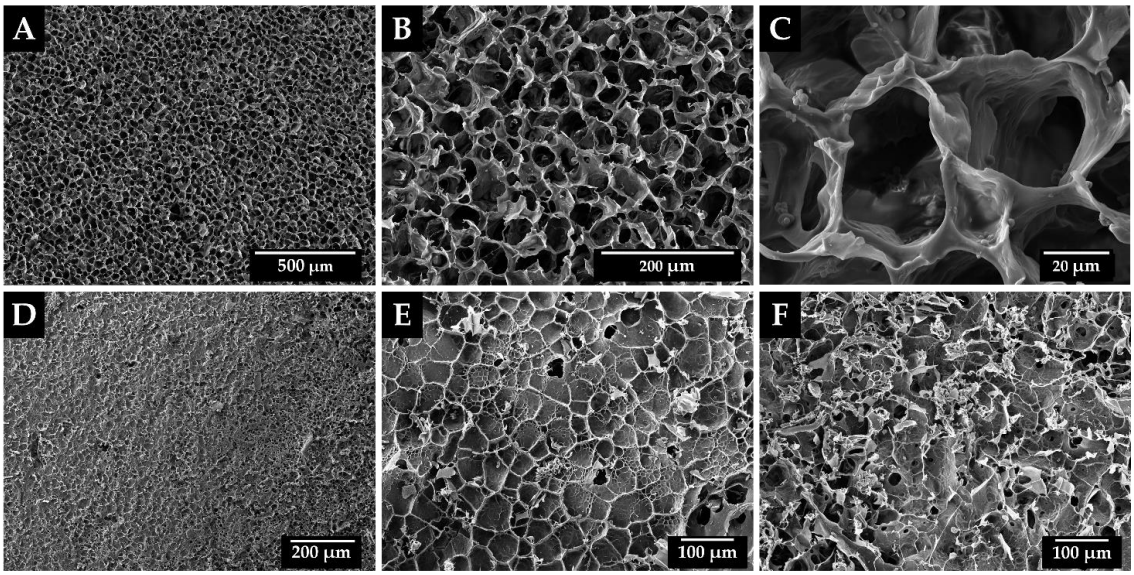

Figure 4. Micrographs of $GelMA_3/DexMA_3$ cryogels at (A) 500 µm, (B) 200 µm and (C) 20 µm and $GelMA_3/DexMA_3$ hydrogels at (D) 200 µm and (E,F) 100 µm. Similar results were obtained for all the different cryogels and hydrogels produced.

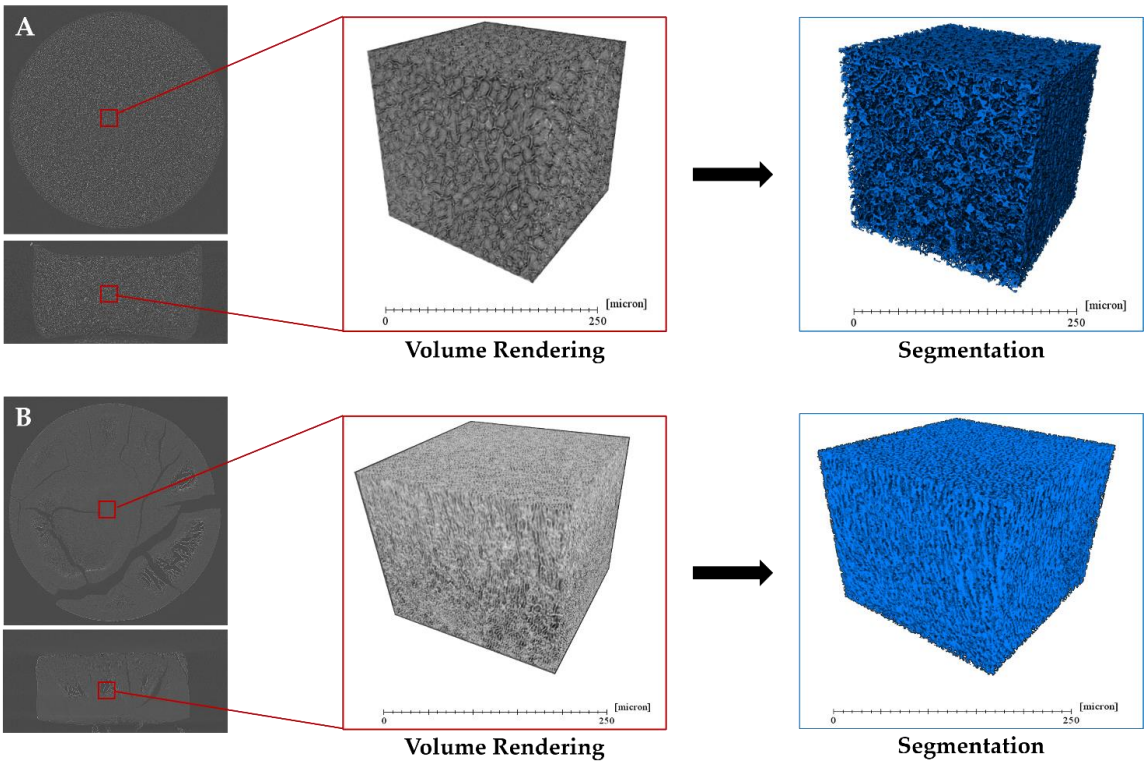

Figure 5. MicroCTs to obtain volume rendering and perform segmentation of $GelMA_3/DexMA_3$ (A) cryogel and (B) hydrogel. Similar results were obtained for all the different cryogels and hydrogels produced.

3.2.3 Mechanical characterization

The compressive properties of cryogels and hydrogels were evaluated in both wet and dry conditions. Due to the porous structure of both cryogels and hydrogels, their compressive curves in dry conditions display a trend comparable with the ones of polymeric foams employed as core materials in sandwich structures for engineering structural purposes. In particular, three different regions can be detected as proved by the compressive curves reported in Figure 6A. The first region is the elastic region, which is characterized by a linear trend and describes the elastic response of the cell walls. This region extends up to the yielding point where cells collapse begins and the second region, i.e. the plateau region, begins. This part of the curve is characterized by an almost constant stress where cells undergo a progressive buckling and collapse. This region extends up to the densification point where opposite cell walls start to touch each

other determining a steep increase of the stress required to go on deforming the material. To properly describe these three distinct zones, three parameters were extrapolated: the compressive modulus, the plateau stress and the densification stress. The compressive modulus was calculated as the slope of the straight line which characterizes the first region of the curve. The plateau stress was evaluated by isolating the elastic region and the plateau region, evaluating their interpolation lines and identifying their intersection point. Finally, the densification stress was calculated according to the procedure proposed by Avalle et al.[30] where the efficiency of the material, i.e. the ratio between the energy absorbed by the material up to a certain strain ε and the stress σ itself, is plotted as a function of the compressive stress. In particular, the stress value at which the efficiency reaches its maximum is exactly the densification stress.

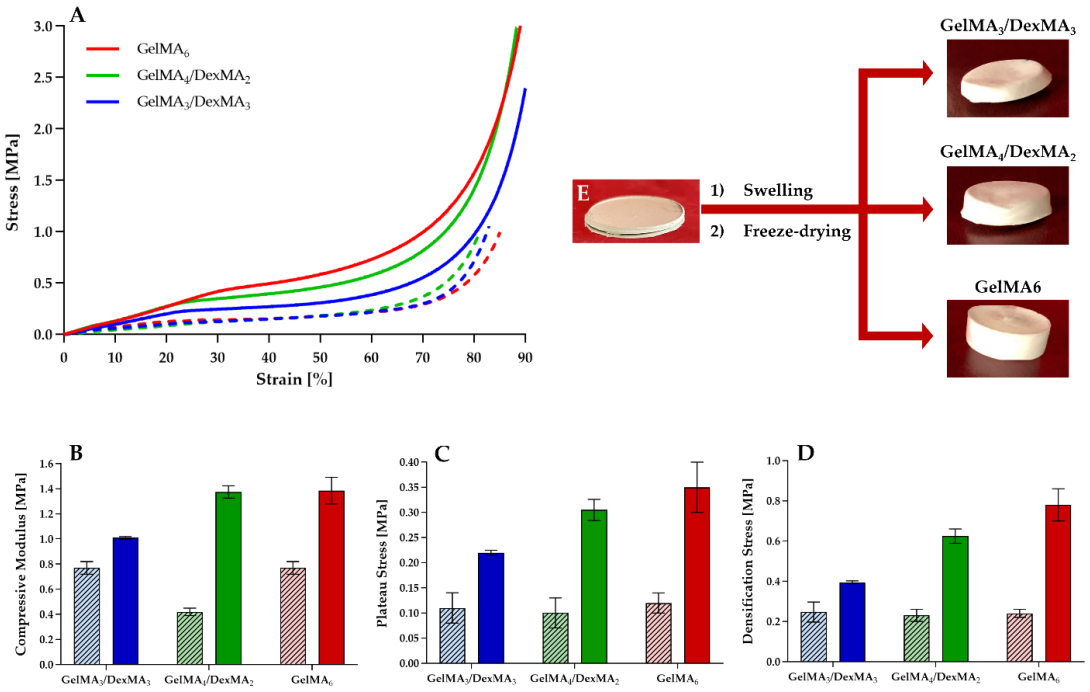

Figure 6. (A) Compressive curves of cryogels (solid lines) and hydrogels (dashed lines). (B) Compressive modulus, (C) plateau stress and (D) densification stress of the different cryogel (solid bars) and hydrogel (dashed bars) configurations in dry conditions. (E) Exemplificative image of a cryogel at the end of the compression test carried out in dry conditions and images of the different cryogels after compression, hydration and freeze-drying, showing their different ability to recover the original shape and dimensions.

The compressive properties of the different cryogel and hydrogel configurations are summarized in Figures 6B, 6C and 6D. The most important outcome is that cryogels mechanical properties outperform significantly hydrogels ones with an increase between 31.17 % and 227 % in the compressive modulus, between 100 % and 205 % in the plateau stress and between 59.9 % and 225 % in the densification stress. These results are perfectly comparable with the ones reported by Ak et al.,[31] who compared silk fibroin hydrogels and cryogels. Furthermore, Ström et al.[32] already pointed out the intrinsic low mechanical strength of hydrogels while investigating high mechanically stable hyaluronan cryogels.

The improved toughness of cryogels over hydrogels is also confirmed by the micrographs of partially compressed cryogels and hydrogels reported in Figure 7. Cryogels cell walls are able to bend and buckle (Figure 7A) reaching an almost complete folding (Figure 7B) without undergoing fracture. On the contrary, the brittle nature of hydrogels leads to fracture of the massive zones (Figure 7C) and to the collapse of the cells (Figure 7D). A further proof of the outstanding toughness of cryogles is given by the micrographs in Figure 7E, 7F and 7G, which show the morphology of cryogels after a compression at 90 % strain and subsequent hydration and freeze-dying. Cells shape and dimension do not display any sign of the high compressive deformation imposed, thus proving the high reversible deformability of this class of gels. In particular, $GelMA_6$ cryogels can be collapsed by a mechanical force and completetly resume their original shape and dimensions after hydration and freeze-drying (Figure 6E). Similar results were already reported for gelatin cryogels crosslinked via carbodiimide chemistry.[33]

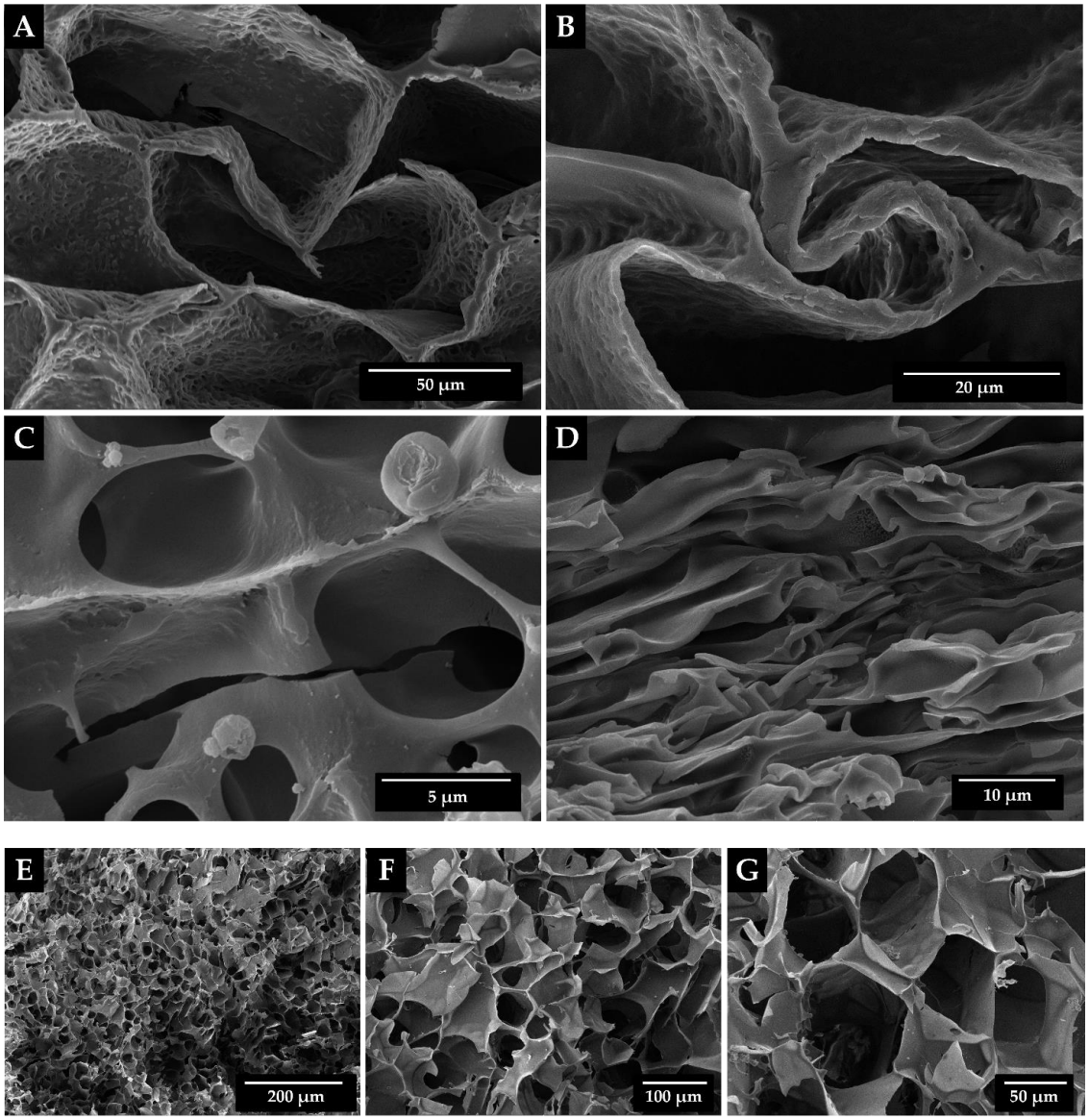

Figure 7. Partially compressed $GelMA_6$ (A,B) cryogel and (C,D) hydrogel. (E,F,G) Micrographs of $GelMA_6$ cryogels after compression at 90 % strain and subsequent hydration.

On the contrary, the addition of DexMA negatively affects the mechanical response of the dry cryogels. In particular, a decrease of 27 % in compressive modulus, of 37 % in plateau stress and of 49 % in densification stress was observed for increasing content of DexMA. In their work, Zhu et al.[34] reported that gelatin displays a partial triple helix structure at low temperatures and that GelMA samples are able to preserve a certain degree of gelatin secondary structure even though the functionalization with methacryloyl groups can interfere with helix formation. Moreover, they report that a

higher methacryloyl functionalization of gelatin could further hinder triple helix formation and promote random coil formation. In light of these results, it is clear that the introduction of DexMA in gelatin systems tends to break macromolecules symmetry thus probably interefering with secondary structuring of GelMA and hindering the formation of triple helix regions, which may determine a reduction of the mechanical response of the cryogel. These results are particularly interesting considering that GelMA networks are usually reinforced blending the polymer with different foreign materials, which include polymers and nanomaterials, for achieving desirable mechanical features to allow their application for tissue engineering purposes.[17]

The compressive properties of both hydrogels and cryogels were also evaluated in wet conditions and the relative results are reported in Figures 8A, 8B and 8C. Both types of construts reveal a strong decrease in their compressive properties as a consequence of hydration. The plasticizing effect of water determines a reduction of at least two order of magnitude in the compressive properties of both gel systems. Even after hydration cryogels outperform significantly hydrogels with an increase between 50 % and 400 % in the compressive modulus and between 10 % and 615 % in the densification stress. Moreover, as already observed in dry conditions, the cryogels synthesized only with GelMA are the ones characterized by the best compressive properties. The only difference with the compressive results in dry conditions can be observed for the $GelMA_3/DexMA_3$ and the $GelMA_4/DexMA_2$ cryogels, in fact $GelMA_3/DexMA_3$ displays slightly higher compressive properties with respect to $GelMA_4/DexMA_2$. According to the swelling data, $GelMA_3/DexMA_3$ absorbs little higher quantity of water that will exert, when compressed, a higher counterpressure inside cryogel cells thus determining this slight increase in its compressive response.

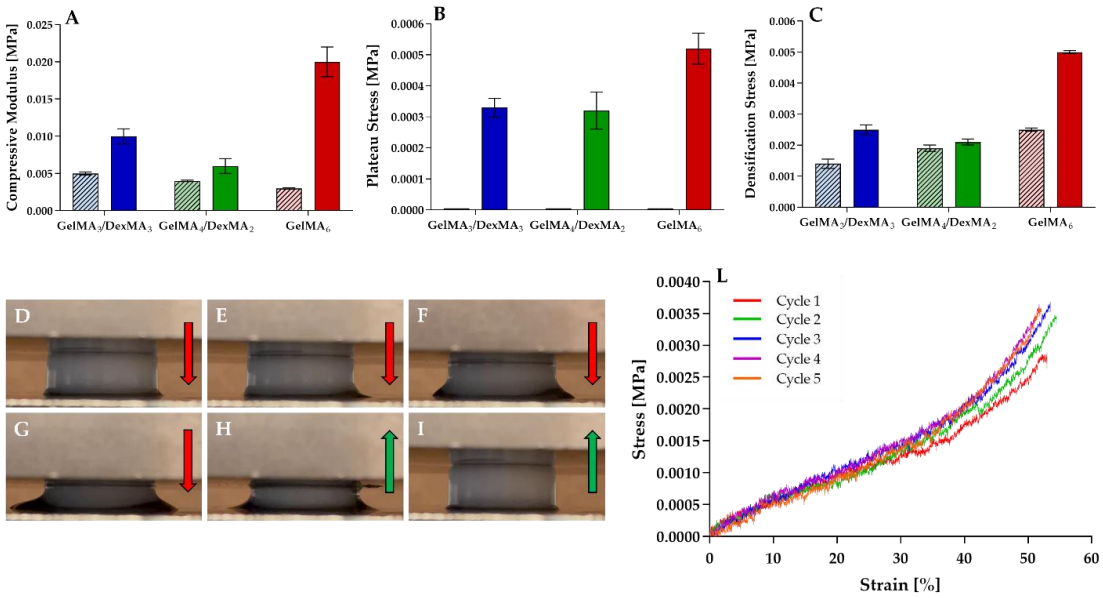

Figure 8. (A) Compressive modulus, (A) plateau stress and (C) densification stress of the different cryogel (solid bars) and hydrogel (dashed bars) configurations after hydration. (D,E,F,G) Photographs of a cryogel during the compression test in wet conditions at 0, 30, 50 and 70% compressive deformation, respectively and (H,I) the following decompression. (L) Cyclical compressive curves of a swelled $GelMA_6$ cryogel performed up to 55 % deformation.

The high reversible deformability and toughness of cryogels was also confirmed for the hydrated and then compressed samples, as proved by the pictures taken during compression tests shown in Figures 8 from D to I and by the micrographs in Figure 9, which show the microstructure of all cryogel constructs, i.e. $GelMA_6$ (A, B), $GelMA_4/DexMA_2$ (C, D) and $GelMA_3/DexMA_3$ (E, F). It is possible to notice how pore shape and dimension appear almost unaffected by the 90 % compressive deformation applied to the specimens.

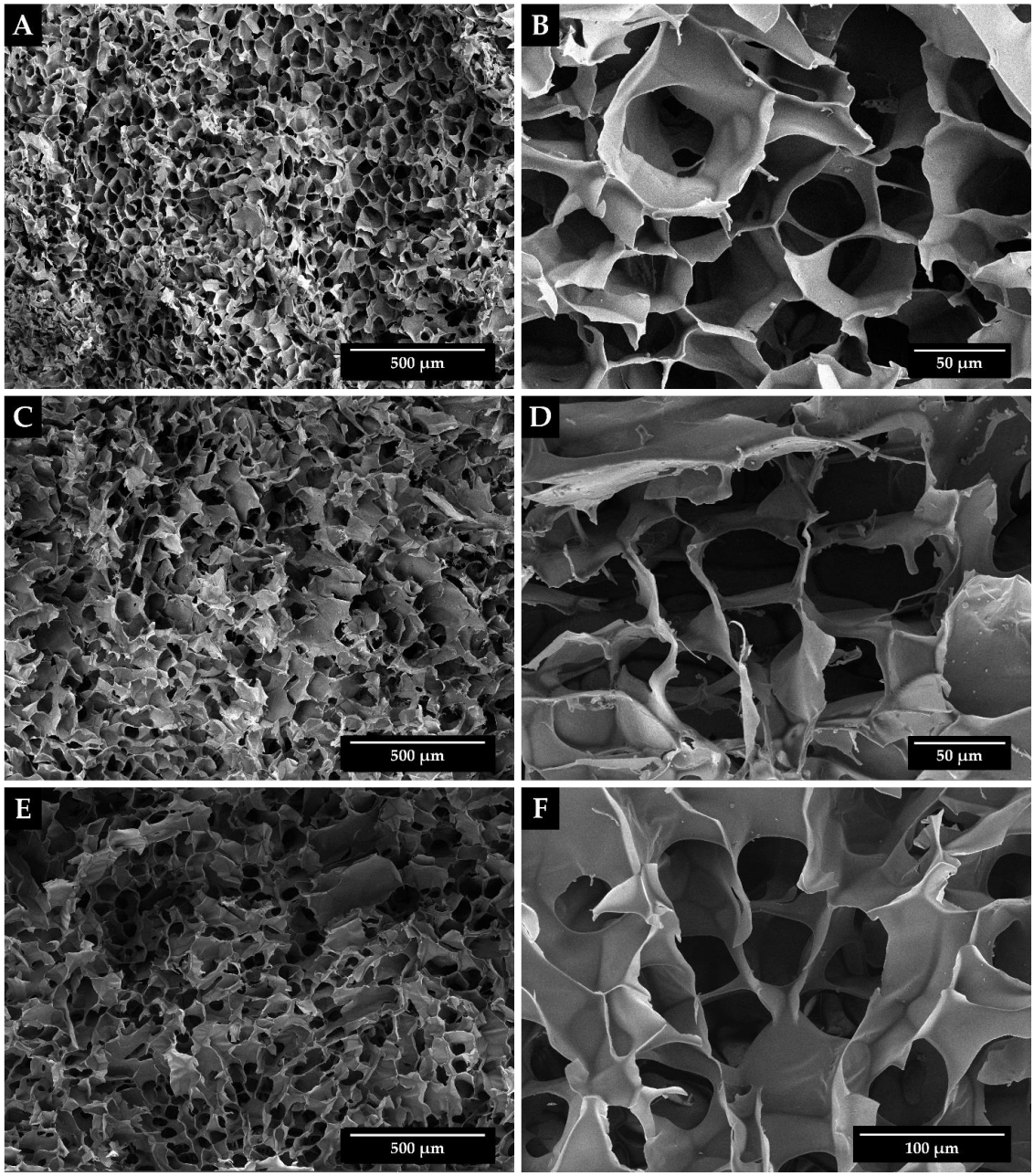

Figure 9. Micrographs of (A,B) $GelMA_6$, (C,D) $GelMA_4/DexMA_2$ and (E,F) $GelMA_3/DexMA_3$ cryogels compressed at 90 % strain after being rehydrated and freeze-dried.

A further confirmation of the tough nature of cryogels was given by the cyclical quasi-static compressive tests performed on the $GelMA_6$ construct, i.e., the best one from the compressive resistance perspective. In specific, results reported in Figure 8L show the five-cycle compressive curves of the $GelMA_6$ cryogels. No significant changes in both compressive modulus and plateau stress can be observed between subsequent cycles,

while a progressive shifting towards upper stress and lower strain values can be detected for the densification region. This can be ascribed to a partial residual folding of the cell walls after the previous compressive cycle, resulting from a partial water loss, which speeds up the densification stage in the next compression. The results obtained are comparable with the ones reported by Zhang et al.[35] for gelatin-hydroxyapatite composite cryogels, who already acknowledged the great differences in terms of toughness between cryogels and hydrogels through 10 cycles compressive tests.

Therefore, ice templating and criogelation resulted a more effective approach to improve the mechanical properties of GelMA-based constructs, compared to other methods developed to control mechanics and microarchitecture of bioactive polymer platforms.[36,37]

3.2.3 Release studies

To have further insights into the microstructure of the fabricated cryogels and evaluate the effect of DexMA on GelMA cryostructuring, some release studies were carried out, using vitamin B12 for the scope. Indeed, wheter DexMA affects the criogelation process, then a difference in the release behavior of an entrapped molecule may be expected.[38] It was found that the addition of DexMA to GelMA actually influences the release properties of the cryogels. Figure 10 shows the release curves of vitamin B12 from $GelMA_6$, $GelMA_4$/$DexMA_2$ and $GelMA_3$/$DexMA_3$ cryogels. From the log-log plot of $\frac{M_t}{M_\infty}$ *vs* time (fraction of solute released up to time t) it can be observed that all the three release kinetics exhibit a non-fickian behavior

$$\frac{M_t}{M_\infty} = Kt^n \quad for \quad \frac{M_t}{M_\infty} \leq 0.5 \div 0.6$$

characterized by a diffusional exponent n>0.5, 0.5 being the limiting value characterizing fickian release from non-swellable or completely swollen cylindrical

devices.[39] Indeed, it is reasonable to assume that the release process of vitamin B12 from cryogels occurs after complete swelling is achieved since the swelling phenomenon is extremely fast and the cylindrical device is completely swollen after the first minute of contact with the PBS solution.

The diffusional exponent is n=0.62 ± 0.02 for both cryogels $GelMA_4/DexMA_2$ and $GelMA_3/DexMA_3$ and n=0.8 ± 0.01 for $GelMA_6$. The significantly larger value of the diffusional exponent observed for $GelMA_6$ indicates a stronger effect of cryconcentration for pure GelMA cryogels, responsible for a more markedly non-fickian release kinetics. Actually, in the absence of the cryoconcentration process, like in the case of pure GelMA hydrogels, the release kinetics is fickian, as shown in Figure 11A and 11B, and characterized by a diffusional exponent n=0.47 ± 0.01 perfectly in accordance with the expected value for a purely diffusive/fickian release (with perfect sink conditions) from a completely swollen cylindrical device characterized by an aspect ratio (swollen radius)/(swollen half thickness)=R_{sw}/H_{sw}=(9.22 ± 0.02 mm)/(1.47 ± 0.01mm)=6.27. These results account for a difference in the microstructures of the different cryogels samples, according to their composition. More specifically, they support the experimental observation of the need of using different amounts of the crosslinking reagents (APS and TEMED) for the proper crosslinking of the polymer solutions with different GelMA content. They also support the findings of the mechanical characterization of these cryogels, which already evidenced the interference of DexMA with the secondary structuring of GelMA, with consequent formation of scaffolds with different internal microstructure.

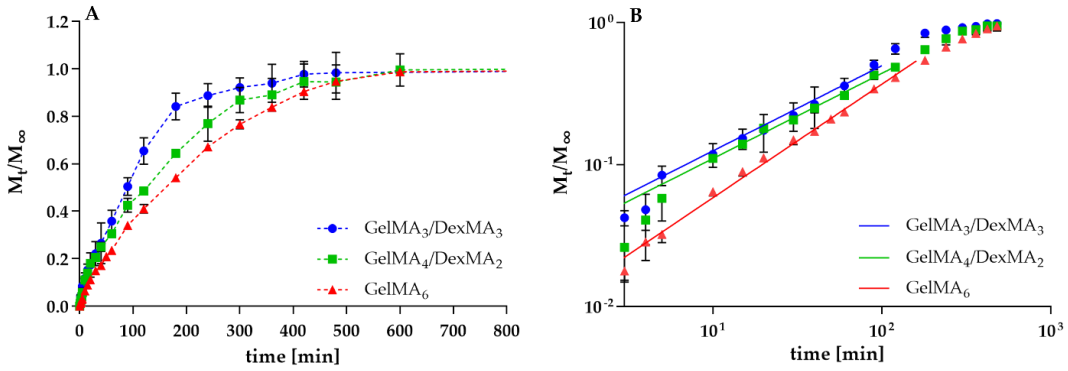

Figure 10. (A) Release curves of vitamin B12 from $GelMA_6$, $GelMA_4/DexMA_2$ and $GelMA_3/DexMA_3$ cryogels. (B) Same data plotted in log-log scale to highlight the scaling exponent, namely n=0.62 for $GelMA_4/DexMA_2$ and $GelMA_3/DexMA_3$ and n=0.81 for $GelMA_6$**.**

Figure 11A shows the behavior of release curves for $GelMA_6$ cryogel and hydrogel. For a fair comparison of the release kinetics, one should account for the fact that the cylindrical cryogel has a swollen half thickness H_{sw}=4.5 ± 0.03 mm about three times larger than that of the $GelMA_6$ hydrogel. For this reason, in order to rescale the effect of device thickness, Figure 11B shows the fractional drug release $\frac{M_t}{M_\infty}$ as function of the rescaled time t $D_{PBS}/(H_{sw})^2$, where D_{PBS}=4.43x10^{-10} m^2/s is the bare diffusion coefficient of vitamin B12 in PBS.[40] Figure 11B clearly shows that the release kinetics from the cryogel is initially slower than that from hydrogel, while it becomes significantly faster for $\frac{M_t}{M_\infty} > 0.6$ and this is unexpected if one considers the larger porosity of the cryogel and the celerity of the swelling process.

The release curve from $GelMA_6$ hydrogel is accurately described by a simple diffusion equation with perfect sink boundary condition in a swollen cylindrical device with half thickness $H_{sw} \approx 1.47$ mm and radius $R_{sw} \approx 18.9$ mm

$$\frac{\partial c(r,z,t)}{\partial t} = D_{hyd}\left(\frac{\partial^2 c}{\partial z^2} + \frac{1}{r}\frac{\partial}{\partial r}\left(r\frac{\partial c}{\partial r}\right)\right), \quad 0 < r < R_{sw}, \quad -H_{sw} < z < H_{sw} \tag{1}$$

$$c(R_{sw}, z, t) = 0, \quad c(r, H_{sw}, t) = 0, \quad \left.\frac{\partial c}{\partial z}\right|_{z=0} = 0 \tag{2}$$

$$c(r,z,0) = c_0 \tag{3}$$

$$\frac{M_t}{M_\infty} = \frac{c_0(\pi R_{sw}^2 H_{sw}) - \int_0^{H_{sw}} dz \int_0^{R_{sw}} c(r,z,t)\, 2\pi r dr}{c_0(\pi R_{sw}^2 H_{sw})} \tag{4}$$

The best fit value for the effective diffusion coefficient of vitamin B12 in the hydrogel D_{hyd} is 3.32x10^{-10} m^2/s, about 75% of the bare diffusivity D_{sw} in PBS. The numerical result of the fickian transport model eqs. (1-4) are shown in Figure 11B (black curve) in excellent agreement with experimental release data for GelMA$_6$ hydrogel.

A more complex transport model should be introduced in order to describe the non-fickian behavior of the release curve of vitamin B12 from GelMA$_6$ cryogel. It can be explained by assuming that a large part of the loaded drug is entrapped, by cryoconcentration effect, in the microporous dense stationary phase (polymer network) and irreversibly released in the macroporous mobile phase where diffusion takes place with a diffusivity close to the bare diffusivity D_{sw} of vitamin B12 in PBS.[41]

Let $c_s(r,z,t)\ and\ c_m(r,z,t)$ be the drug concentrations in the stationary and mobile phases, respectively. The transport equation for c_s and c_m read as

$$\frac{\partial c_s(r,z,t)}{\partial t} = -k c_s, \quad c_s(r,z,0) = \alpha\, c_0 \tag{5}$$

$$\frac{\partial c_m(r,z,t)}{\partial t} = D_{cry}\left(\frac{\partial^2 c_m}{\partial z^2} + \frac{1}{r}\frac{\partial}{\partial r}\left(r\frac{\partial c_m}{\partial r}\right)\right) + k c_s, \quad 0 < r < R_{sw}, \quad -H_{sw} < z < H_{sw} \tag{6}$$

$$c_m(R_{sw},z,t) = 0, \quad c_m(r,H_{sw},t) = 0, \quad \left.\frac{\partial c_m}{\partial z}\right|_{z=0} = 0 \tag{7}$$

$$c_m(r,z,0) = (1-\alpha)\, c_0 \tag{8}$$

$$\frac{M_t}{M_\infty} = \frac{c_0(\pi R_{sw}^2 H_{sw}) - \int_0^{H_{sw}} dz \int_0^{R_{sw}} (c_s + c_m)\, 2\pi r dr}{c_0(\pi R_{sw}^2 H_{sw})} \tag{9}$$

where k [1/s] is the mass transfer coefficient between the two phases, D_{cry} the effective drug diffusion coefficient in the macroporous mobile phase and α the initial partition coefficient of the drug between the two phases. By assuming $D_{cry} = D_{sw}$, the two controlling/fitting parameters are k and α. Figure 11B shows the excellent agreement

between experimental release data and model predictions with k =1.8x10^{-4} [1/s] and $\alpha = 0.8$. The best-fit value of α implies that 80% of the total drug loaded is initially trapped in the stationary phase. The best-fit value of k implies a Damkoler number $kH_{sw}^2/D_{cry} \simeq 8.2$ representing the ratio between the characteristic time for diffusion in the mobile phase and the characteristic time for mass transfer between phases. Therefore, the initial behavior of the release curve is slower, being controlled by the linear mass transfer between phases. Subsequently, the release curve accelerates, being controlled by the diffusion process in the mobile phase. The model accurately predicts the non-fickian initial scaling characterized by a diffusion exponent n=0.81 as well as the long-term behavior of the experimental release curve from cryogel.

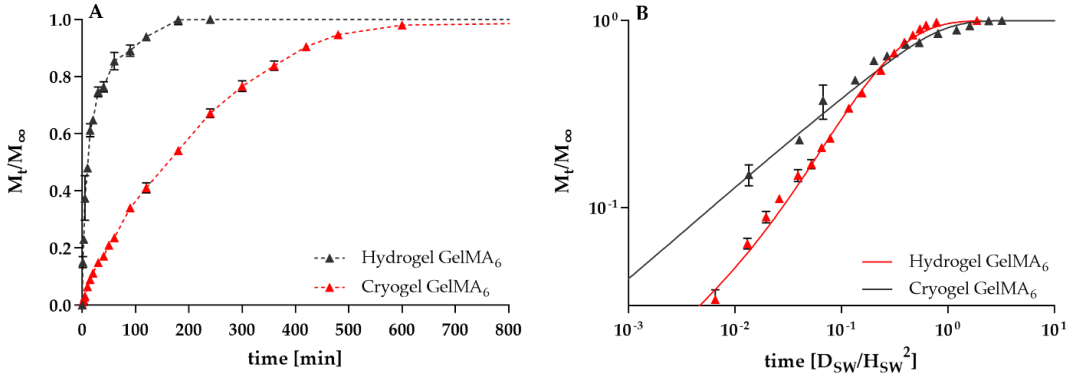

Figure 11. (A) Comparison between release curves of vitamin B12 from GelMA$_6$ cryogel and hydrogel. (B) Same data plotted in log-log scale with the rescaled time t D_{sw}/H_{sw}^2. Continuous lines show model predictions, eqs. (1-4) for the hydrogel and eqs. (5-8) for the cryogel.

3.3 Cell studies

The biocompatibility and ability of cryogels to support cell adhesion and proliferation was investigated using HaCats for the scope. In specific, biocompatibility was indirectly evaluated on steam sterilized and freeze-dried cryogel samples, which were rehydrated and kept in complete DMEM at 37 °C for 15 days without agitation. At the end of the

incubation time, the media were collected and tested for potential cytotoxic extractables and leachables released from the cryogels. Results reported in Figure 12A show no reduction in cell viability compared to the control for all the samples tested indicating that potential cryogels degradation products that may occur during extended cell culture time are not citotoxic Once verified the biocompatibility of the cryogels, they were further investigated for cell their properties in supporting cell survival, adhesion, and proliferation. To this end, sterilized dry cryogel samples were rehydrated and cells laden using different seeding protocols, as reported in the supporting material. The best results were obtained when the dry scaffolds were rehydrated with a cell suspension, using a volume almost corresponding to the equilibrium swelling degree of the cryogel. This procedure allowed to limit huge loss of cells resulting from the high porosity and pore interconnectivity of the cryogels. After seeding, the different scaffolds were imaged at different time points with a fluorescence microscope to observe cell behavior and adhesion. The results are reported in Figure 12B.

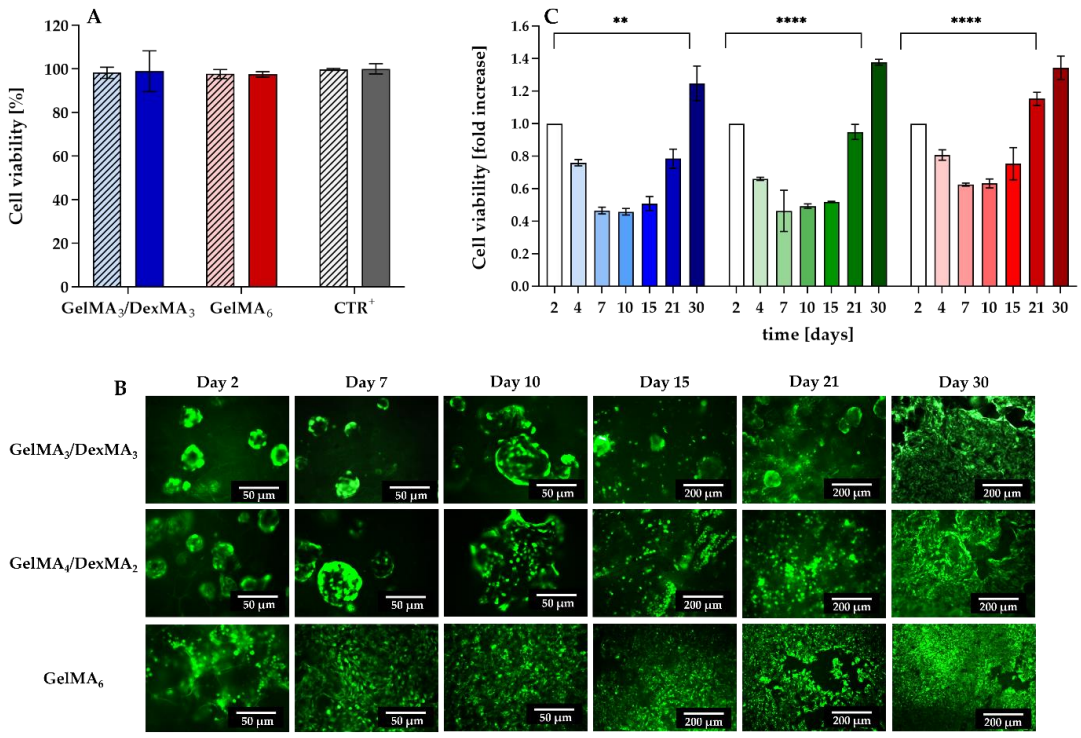

Figure 12. (A) Extractable and leachable testing to evaluate cytocompatibility of compounds that may leach from cryogels, assayed on HaCat cells at 24 h (dashed bars) and 48 h (solid bars). (B) Fluorescence microscopy images of HaCat cells seeded on the different cryogels, taken at different time points. (C) Cell proliferation on the different cryogels ($GelMA_3/DexMA_3$ - blue bars; $GelMA_4/DexMA_2$ - green bars and $GelMA_6$ - red bars) evaluated by the alamarBlue assay. Data were normalized to day 2 value. **p<0.002 ; ****p<0.0001

In all the cases, it can be observed that single cells present within the scaffolds first agglomerate to form loosely adhesive cell spheroids, then they start to distribute evenly along the pores of the scaffolds (Figure S4) and finally attach to the them (Figure 12B). It can also be observed that the cryogel composition affects the process of cell adhesion. Indeed, $GelMA_3/DexMA_3$ and $GelMA_4/DexMA_2$ showed that the majority of seeded cells formed spheroids, which were still visible up to 15 and 10 days from seeding respectively. On the other end, lesser spheroids were present in the $GelMA_6$ cryogels after 2 days, with many single cells adhering to the cryogel directly. After 7 days, cells further spread into the scaffold showing a higher cell density which further increased until the end of the culture period. Therefore, the higher the GelMA content of the cryogel the quicker resulted the attachment and spreading of the cells within the

scaffold. This finding was also confirmed by the alamarBlue assay, which was used to assess cell viability and proliferation. The results reported in Figure 12C show, for all the samples tested, an initial decrease in the measured values which indicates a decrease in cell number. This is likely due to a combination of cell leaking from the scaffold, due to its large pores, and cell death. After 10 days from seeding, no further decrease was measured and a trend inversion was observed starting from this point. The results reflect what has also been observed by fluorescence images, where the decrease in cell number coincide with the spheroid formation observed after 10 days in culture followed by cell spreading and growth up to 1 month. The observed behavior seems to be proportional to the GelMA content of the scaffold.

Overall, these results indicate that GelMA-based cryogels are suitable systems to support cell adhesion and proliferation.

4. Conclusions

Monolithic GelMA-based cryogels were produced via cryostructuring and radical crosslinking of the polymers at subzero temperatures. The rheological properties of the starting GelMA resulted particularly critical to allow the fabrication of homogeneous and not collapsed scaffolds. Indeed, only the use of GelMA characterized by very low gelation temperature resulted in the formation of large and uniform cryogels. Moreover, the use of GelMA alone led to the formation of highly compressive resistant scaffolds, which exhibited complete shape-recover ability after compression and rehydration. Instead, contrary to what usually reported about the need of blending GelMA to other materials to improve its mechanical properties, when the polymer was combined with DexMA a general worsening of the compressive properties of the scaffolds was observed, which was explained considering the interference of DexMA with the secondary structuring of GelMA during the cryogelation process.

All the developed cryogels were able to adequately support growth and proliferation of HaCat cells, even if the presence of DexMA had a negative effect on the adhesion process of the cells to the scaffold. Further investigation is needed for actual translation of the developed GelMA-based cryogels in tissue engineering. Anyway, they show interesting features and great potential for application in this field.

Supporting Information: ^{1}H NMR spectra for GelMA and DexMA (DOC) and additional experimental details, including photographs of cryogels as cell scaffolds (DOC). Videos of swelling cryogels (MP4).

Acknowledgment

The authors would like to acknowledge the MIUR for the financial support. The authors wish also to acknowledge Prof. Claudio Talora (Department of Molecular Medicine – Sapienza University of Rome) for providing HaCat cells.

References

(1) Kumar, A.; Jacob, A. Techniques in Scaffold Fabrication Process for Tissue Engineering Applications: A Review. *J. Appl. Biol. Biotechnol.* **2022**, *10* (3), 163–176.

(2) Adel, I. M.; Elmeligy, M. F.; Elkasabgy, N. A. Conventional and Recent Trends of Scaffolds Fabrication: A Superior Mode for Tissue Engineering. *Pharmaceutics* **2022**, *14* (2), 306.

(3) Yang, Q.; Peng, J.; Xiao, H.; Xu, X.; Qian, Z. Polysaccharide Hydrogels: Functionalization, Construction and Served as Scaffold for Tissue Engineering. *Carbohydr. Polym.* **2022**, *278*, 118952.

(4) Radulescu, D. M.; Neacsu, I. A.; Grumezescu, A. M.; Andronescu, E. New Insights of Scaffolds Based on Hydrogels in Tissue Engineering. *Polymers (Basel).* **2022**, *14* (4), 799.

(5) Chopra, H.; Singh, I.; Kumar, S.; Bhattacharya, T.; Rahman, M. H.; Akter, R.;

Kabir, M. T. A Comprehensive Review on Hydrogels. *Curr. Drug Deliv.* **2022**, *19* (6), 658–675.

(6) Xu, F.; Dawson, C.; Lamb, M.; Mueller, E.; Stefanek, E.; Akbari, M.; Hoare, T. Hydrogels for Tissue Engineering: Addressing Key Design Needs Toward Clinical Translation. *Front. Bioeng. Biotechnol.* **2022**, *10*, 849831.

(7) De France, K. J.; Xu, F.; Hoare, T. Structured Macroporous Hydrogels: Progress, Challenges, and Opportunities. *Adv. Healthc. Mater.* **2018**, *7* (1).

(8) Lozinsky, V. I.; Vainerman, E. S.; Rogozhin, S. V. Study of Cryostructurization of Polymer Systems - II. The Influence of Freezing of a Reacting Mass on the Properties of Products in the Preparation of Covalently Cross-Linked Gels. *Colloid Polym. Sci.* **1982**, *260* (8), 776–780.

(9) Savina, I. N.; Zoughaib, M.; Yergeshov, A. A. Design and Assessment of Biodegradable Macroporous Cryogels as Advanced Tissue Engineering and Drug Carrying Materials. *Gels* **2021**, *7* (3), 79.

(10) Shiekh, P. A.; Andrabi, S. M.; Singh, A.; Majumder, S.; Kumar, A. Designing Cryogels through Cryostructuring of Polymeric Matrices for Biomedical Applications. *Eur. Polym. J.* **2021**, *144*, 110234.

(11) Pacelli, S.; Di Muzio, L.; Paolicelli, P.; Fortunati, V.; Petralito, S.; Trilli, J.; Casadei, M. A. Dextran-Polyethylene Glycol Cryogels as Spongy Scaffolds for Drug Delivery. *Int. J. Biol. Macromol.* **2021**, *166*, 1292–1300.

(12) Barros, N. R.; Chen, Y.; Hosseini, V.; Wang, W.; Nasiri, R.; Mahmoodi, M.; Yalcintas, E. P.; Haghniaz, R.; Mecwan, M. M.; Karamikamkar, S.; Dai, W.; Sarabi, S. A.; Falcone, N.; Young, P.; Zhu, Y.; Sun, W.; Zhang, S.; Lee, J.; Lee, K.; Ahadian, S.; Dokmeci, M. R.; Khademhosseini, A.; Kim, H. J. Recent Developments in Mussel-Inspired Materials for Biomedical Applications. *Biomater. Sci.* **2021**, *9* (20), 6653–6672.

(13) Pacelli, S.; Paolicelli, P.; Petralito, S.; Subham, S.; Gilmore, D.; Varani, G.; Yang, G.; Lin, D.; Casadei, M. A.; Paul, A. Investigating the Role of Polydopamine to Modulate Stem Cell Adhesion and Proliferation on Gellan Gum-Based Hydrogels. *ACS Appl. Bio Mater.* **2020**, *3* (2), 945-951.

(14) He, Y.; Wang, C.; Wang, C.; Xiao, Y.; Lin, W. An Overview on Collagen and Gelatin-Based Cryogels: Fabrication, Classification, Properties and Biomedical Applications. *Polymers (Basel).* **2021**, *13* (14), 2299.

(15) Berrier, A. L.; Yamada, K. M. Cell-Matrix Adhesion. *J. Cell. Physiol.* **2007**, *213*

(3), 565–573.

(16) Bellis, S. L. Advantages of RGD Peptides for Directing Cell Association with Biomaterials. *Biomaterials* **2011**, *32* (18), 4205–4210.

(17) Sakr, M. A.; Sakthivel, K.; Hossain, T.; Shin, S. R.; Siddiqua, S.; Kim, J.; Kim, K. Recent Trends in Gelatin Methacryloyl Nanocomposite Hydrogels for Tissue Engineering. *J. Biomed. Mater. Res. A* **2021**, *110* (3), 708–724.

(18) Di Muzio, L.; Cienzo, F.; Paolicelli, P.; Petralito, S.; Garzoli, S.; Brandelli, C.; Trilli, J.; Casadei, M. A. A Convenient Strategy to Synthesize Highly Tunable Gelatin Methacryloyl with Very Low Gelation Temperature. *Eur. Polym. J.* **2021**, *154*, 110538.

(19) Giannuzzo, M.; Corrente, F.; Feeney, M.; Paoletti, L.; Paolicelli, P.; Tita, B.; Vitali, F.; Casadei, M. A. pH-Sensitive Hydrogels of Dextran: Synthesis, Characterization and in Vivo Studies. *J. Drug Target.* **2008**, *16* (9), 649–659.

(20) Van Den Bulcke, A. I.; Bogdanov, B.; De Rooze, N.; Schacht, E. H.; Cornelissen, M.; Berghmans, H. Structural and Rheological Properties of Methacrylamide Modified Gelatin Hydrogels. *Biomacromolecules* **2000**, *1* (1), 31–38.

(21) Joukhdar, H.; Seifert, A.; Jüngst, T.; Groll, J.; Lord, M. S.; Rnjak-Kovacina, J. Ice Templating Soft Matter: Fundamental Principles and Fabrication Approaches to Tailor Pore Structure and Morphology and Their Biomedical Applications. *Adv. Mater.* **2021**, *33* (34).

(22) Adrover, A.; Paolicelli, P.; Petralito, S.; Muzio, L. Di; Trilli, J.; Cesa, S.; Tho, I.; Casadei, M. A. Gellan Gum/Laponite Beads for the Modified Release of Drugs: Experimental and Modeling Study of Gastrointestinal Release. *Pharmaceutics.* **2019**, *11* (4), 187.

(23) Okay, O.; Lozinsky, V. I. Synthesis and Structure–Property Relationships of Cryogels. *Adv. Polym. Sci.* **2014**, *263*, 103–157.

(24) Hixon, K. R.; Lu, T.; Sell, S. A. A Comprehensive Review of Cryogels and Their Roles in Tissue Engineering Applications. *Acta Biomater.* **2017**, *62*, 29–41.

(25) Henderson, T. M. A.; Ladewig, K.; Haylock, D. N.; McLean, K. M.; O'Connor, A. J. Cryogels for Biomedical Applications. *J. Mater. Chem. B* **2013**, *1* (21), 2682–2695.

(26) Memic, A.; Colombani, T.; Eggermont, L. J.; Rezaeeyazdi, M.; Steingold, J.; Rogers, Z. J.; Joshi Navare, K.; Mohammed, H. S.; Bencherif, S. A.; Memic, A.; Colombani, T.; Eggermont, L. J.; Rezaeeyazdi, M.; Rogers, Z. J.; Navare, K. J.;

Mohammed, H. S.; Bencherif, S. A. Latest Advances in Cryogel Technology for Biomedical Applications. *Adv. Ther.* **2019**, *2* (4), 1800114.

(27) Van Vlierberghe, S.; Dubruel, P.; Lippens, E.; Cornelissen, M.; Schacht, E. Correlation between Cryogenic Parameters and Physico-Chemical Properties of Porous Gelatin Cryogels. *J. Biomater. Sci. Polym. Ed.* **2009**, *20* (10), 1417–1438.

(28) Savina, I. N.; Ingavle, G. C.; Cundy, A. B.; Mikhalovsky, S. V. A Simple Method for the Production of Large Volume 3D Macroporous Hydrogels for Advanced Biotechnological, Medical and Environmental Applications. *Sci. Rep.* **2016**, *6*, 21154.

(29) Koshy, S. T.; Ferrante, T. C.; Lewin, S. A.; Mooney, D. J. Injectable, Porous, and Cell-Responsive Gelatin Cryogels. *Biomaterials* **2014**, *35* (8), 2477–2487.

(30) Avalle, M.; Belingardi, G.; Montanini, R. Characterization of Polymeric Structural Foams under Compressive Impact Loading by Means of Energy-Absorption Diagram. *Int. J. Impact Eng.* **2001**, *25* (5), 455–472.

(31) Ak, F.; Oztoprak, Z.; Karakutuk, I.; Okay, O. Macroporous Silk Fibroin Cryogels. *Biomacromolecules* **2013**, *14*, 719–727.

(32) Ström, A.; Larsson, A.; Okay, O. Preparation and Physical Properties of Hyaluronic Acid-Based Cryogels. *J. Appl. Polym. Sci.* **2015**, *132* (29), 42194.

(33) Tao, J.; Hu, Y.; Wang, S.; Zhang, J.; Liu, X.; Gou, Z.; Cheng, H.; Liu, Q.; Zhang, Q.; You, S.; Gou, M. A 3D-Engineered Porous Conduit for Peripheral Nerve Repair. *Sci. Rep.* **2017**, *7*, 46038.

(34) Zhu, M.; Wang, Y.; Ferracci, G.; Zheng, J.; Cho, N. J.; Lee, B. H. Gelatin Methacryloyl and Its Hydrogels with an Exceptional Degree of Controllability and Batch-to-Batch Consistency. *Sci. Rep.* **2019**, *9* (1), 6863.

(35) Zhang, Y.; Leng, H.; Du, Z.; Huang, Y.; Liu, X.; Zhao, Z.; Zhang, X.; Cai, Q.; Yang, X. Efficient Regeneration of Rat Calvarial Defect with Gelatin-Hydroxyapatite Composite Cryogel. *Biomed. Mater.* **2020**, *15* (6), 065005.

(36) Kim, S.; Park, M. R.; Choi, C.; Kim, J. B.; Cha, C. Synergistic Control of Mechanics and Microarchitecture of 3D Bioactive Hydrogel Platform to Promote the Regenerative Potential of Engineered Hepatic Tissue. *Biomaterials* **2021**, *270*, 120688.

(37) Baruffaldi, D.; Palmara, G.; Pirri, C.; Frascella, F. 3D Cell Culture: Recent Development in Materials with Tunable Stiffness. *ACS Appl. bio Mater.* **2021**, *4* (3), 2233–2250.

(38) Li, J.; Mooney, D. J. Designing Hydrogels for Controlled Drug Delivery. *Nat. Rev. Mater.* **2016**, *1* (12), 16071.

(39) Ritger, P. L.; Peppas, N. A. A Simple Equation for Description of Solute Release I. Fickian and Non-Fickian Release from Non-Swellable Devices in the Form of Slabs, Spheres, Cylinders or Discs. *J. Control. Release* **1987**, *5* (1), 23–36.

(40) Brazel, C. S.; Peppas, N. A. Mechanisms of Solute and Drug Transport in Relaxing, Swellable, Hydrophilic Glassy Polymers. *Polymer (Guildf).* **1999**, *40* (12), 3383–3398.

(41) Gun'ko, V. M.; Savina, I. N.; Mikhalovsky, S. V. Cryogels: Morphological, Structural and Adsorption Characterisation. *Adv. Colloid Interface Sci.* **2013**, *187–188*, 1–46.

TABLE OF CONTENTS GRAPHIC

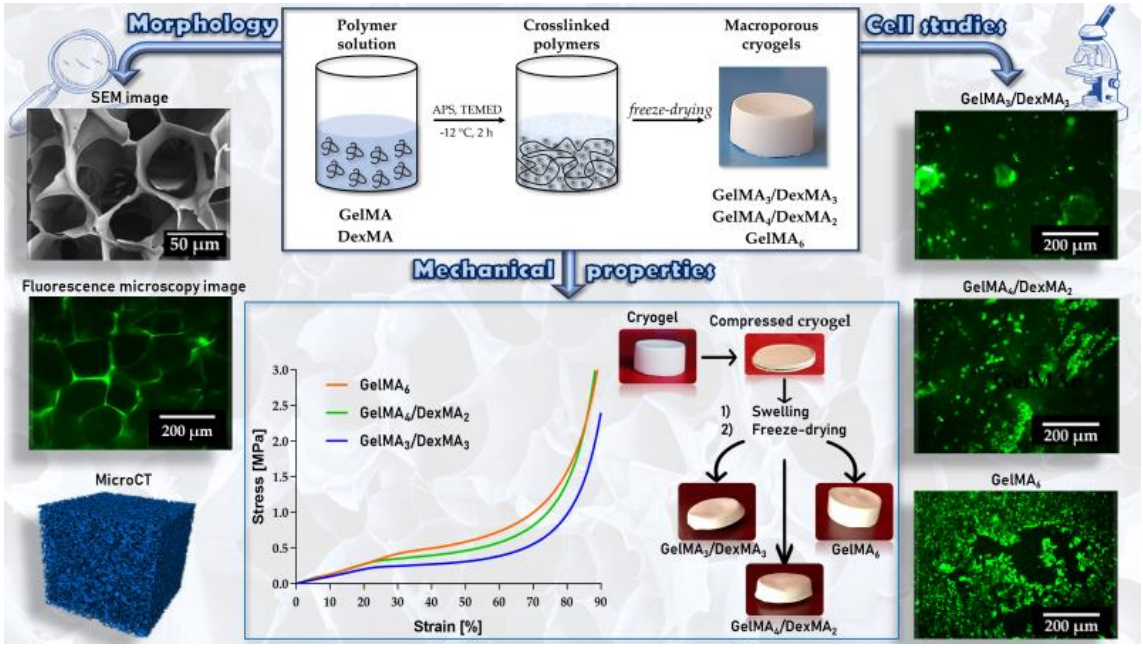

SUPPORTING INFORMATION

Gelatin-based spongy and compressive resistant cryogels with shape recovery ability as ideal scaffolds to support cell adhesion for tissue regeneration

Laura Di Muzio[1], Chiara Brandelli[1], Vito Cosimo Carriero[1], Claudia Sergi[2], Jacopo Tirillò[2], Alessandra Adrover[2], Elisa Messina[3], Roberto Gaetani[4], Stefania Petralito[1], Maria Antonietta Casadei[1], Patrizia Paolicelli[1]*

[1] Department of Drug Chemistry and Technologies, Sapienza University of Rome, 00185 Rome, Italy

[2] Department of Chemical Engineering Materials Environment, Sapienza University of Rome, 00184 Rome, Italy

[3] Department of Maternal, Infantile, and Urological Sciences, "Umberto I" Hospital, 00185 Rome, Italy

[4] Department of Molecular Medicine, Sapienza University of Rome, 00185 Rome, Italy

*Corresponding author: Prof. Patrizia Paolicelli
Department of Drug Chemistry and Technologies
Sapienza University of Rome
Piazzale Aldo Moro 5
00185 – Rome
Italy
Ph: 0039 06 4991 3173
E-mail: patrizia.paolicelli@uniroma1.it

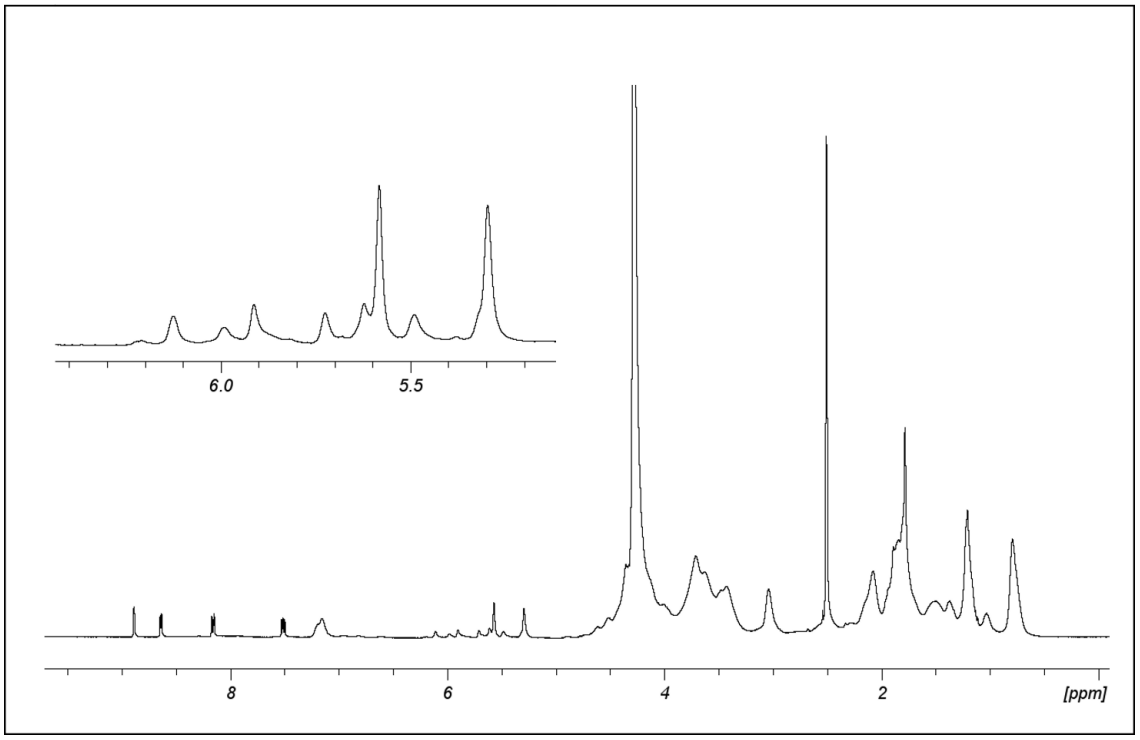

Figure S1. ^{1}H NMR spectrum of GelMA in DMSO-d_6 showing the signals of the vinyl protons of the methacrylic groups. The ^{1}H NMR spectrum was used to calculate the derivatization degree of the polymer using an internal standard (nicotinamide) for the scope (DD = 0.53 ± 0.02 mmol/g).

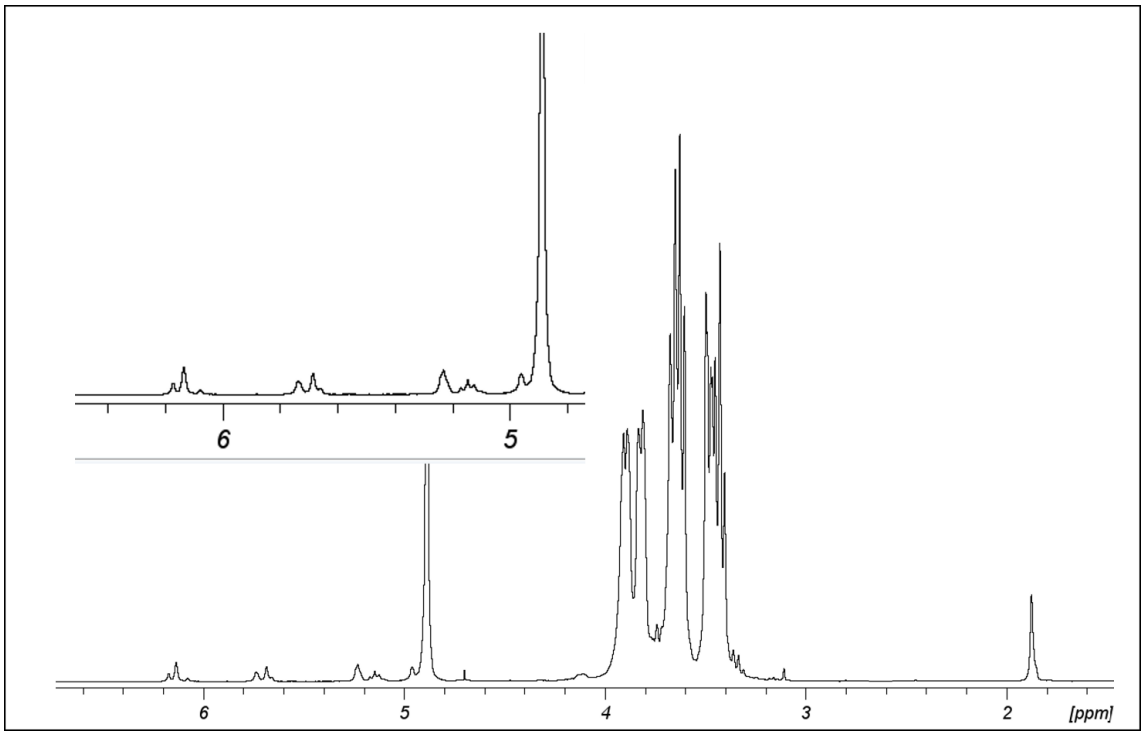

Figure S2. ^{1}H NMR spectrum of DexMA in D_2O showing the signals of the vinyl (δ 6.09 and 5.67 ppm) and methyl (δ 1.90 ppm) protons of the methacrylic groups. The ^{1}H NMR spectrum was used to calculate the derivatization degree of the polymer using an internal standard (nicotinamide) for the scope (DD = 5 ± 1 %).

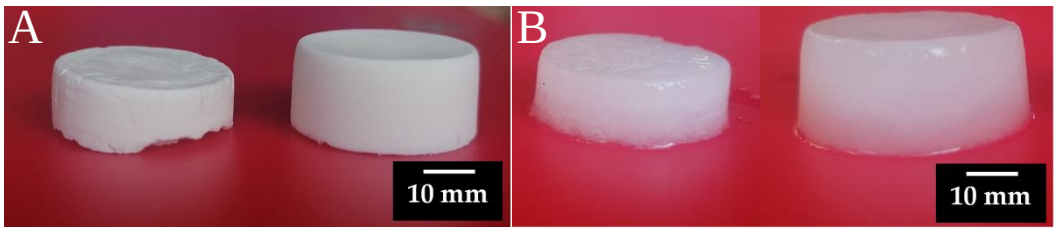

Figure S3. Exemplificative images of (A) dry and (B) swelled $GelMA_6$ hydrogel (on the left) and cryogel (on the right) showing their different dimensions before and after hydration. Similar results were obtained for all the developed samples.

Seeding protocols

Before seeding the cells, cylindrical samples of cryogels (diameter 5 mm, height 3 mm) were steam sterilized at 121°C for 10 min and then placed individually into a 96-well plate. Cells were then seeded on top of the cryogels using three different seeding protocols.

Following the first protocol, a pellet of 5×10^6 or 2.5×10^6 cells was laden on top of each dry cryogel. After 1 h from seeding, 200 µL of complete DMEM medium was added. However, this procedure caused collapse of the scaffold, particularly with the pellet formed by 5×10^6 cells, and a very dishomogeneous cells distribution within the scaffols. Other attempts were made seeding a cell pellet on top of each cryogel pre-swelled in complete DMEM. However, this method did not allowed achieving even cells distribution within the scaffolds. Instead, better results were obtained following the seeding protocol described in *section 2.7.2*.

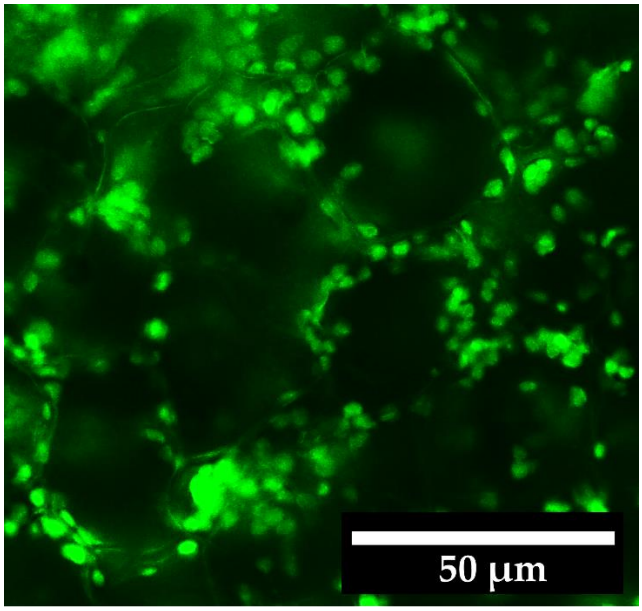

Figure S4. Exemplificative image of the $GelMA_6$ cryogel seeded with HaCat cells showing the distribution of the cells along the edges of the scaffold pores.

CONCLUSIONS

The purpose of the present research work has been to investigate innovative approaches to expand the application of biopolymer matrices in biomedical and pharmaceutical fields. In particular, the focus has been on polymer thin films and hydrogels and their current use as drug delivery systems, wound dressings, and tissue engineering scaffolds. Based on its film-forming properties, gellan gum was chosen to produce polymer thin films, both in its unmodified form and after a suitable chemical modification, in an effort to address some of the major issues that could arise during the development of these formulations, which mainly concern the drug-loading capacity, bioadhesion, and incorporation of silver nanoparticles (AgNPs). In the specific, the strategies proposed involved the addition of hydroxypropyl-β-cyclodextrin in films based on non-derivatized GG to prevent the crystallization of a model BCS I drug (fluconazole). Instead, the derivatization of GG carboxyl groups with dopamine (GGDA) was explored as a semi-synthetic approach for mimicking marine-inspired bioadhesion processes. Finally, a methacrylate derivative of GG (GG-MA) was used to produce through UV irradiation and in a single manufacturing step, thin nanocomposite films containing AgNPs. All the films were produced using the solvent casting technique, which entails first depositing a film-forming polymeric solution on the surface of a solid support, then evaporating the solvent and converting the polymeric solution into a solid film. The resulting products were characterized in terms of thickness, swelling capacity and tensile strength. Furthermore, the release profile of the active substance included in the formulation was investigated. Specifically, studies were carried out to evaluate the release of both fluconazole from GG-based thin films and AgNPs from GG-MA nanocomposite films, confirming their potential use as buccal drug delivery systems and wound dressings, respectively. Additionally, the antibacterial effect of AgNPs, which is fundamental for the application of these polymer matrices in the treatment of poorly healing skin lesions, was also demonstrated.

Although hydrogels are considered the biomaterials that most closely resemble natural living tissues, the small pore size and low interconnectivity, has been found to be inadequate for cell growth and proliferation. An improvement can be achieved by using the technique known as "cryogelation", which involves cross-linking of polymer chains

at temperatures lower than the freezing point of the solvent, in most cases represented by water. The removal of water crystals, which act as porogens, results in the development of polymeric matrices (cryogels) with highly interconnected macro-porous structures capable of promoting a homogenous distribution of cells, while ensuring the diffusion of oxygen and nutrients as well as proper removal of cellular waste. To promote cell recognition and adhesion, which are essential for mimicking the biological functions of the natural ECM, dextran methacrylate (DexMA) was combined with the methacryloyl derivative of gelatin (GelMA) produced following an innovative single-phase synthetic protocol and characterized by a very low gelation temperature. Therefore, cryogels were developed through radical polymerization of the methacrylate derivatives performed using APS/TEMED as radical crosslinking agents. The weight ratio of DexMA and GelMA was varied with the aim of increasing the amount of GelMA in the polymer matrix, and the effect of the polymer composition on the internal structure of the resulting systems was evaluated by FE-SEM microscopy, swelling studies and mechanical tests. Finally, the results of cell tests demonstrated the effectiveness of such cryogels as three-dimensional scaffolds for supporting cellular growth and proliferation.

BIBLIOGRAPHY

1. Todros, S., Todesco, M. and Bagno, A. Biomaterials and their biomedical applications: from replacement to regeneration. *Processes*, 2021, 9, 1949. https://doi.org/10.3390/pr9111949.
2. Ratner, B.D., Zhang, G. A History of Biomaterials. *Biomaterials Science. An Introduction to Materials in Medicine*, 4th ed.; Ratner, B.D., Hoffman, A.S., Schoen, F.J., Lemons, J.E., Eds.; Elsevier Academic Press: London, UK, 2020.
3. Biomaterials: Basic principles. *An Introduction to Biomaterials Science and Engineering*. Chapter 4, 2021, 82-93. https://doi.org/10.1142/9789811228186_0004.
4. Ratner, B.D. and Bryant, S.J. Biomaterials: where we have been and where we are going. *Annu. Rev. Biomed. Eng.*, 2004, 6:41–75. Doi: 10.1146/annurev.bioeng.6.040803.140027.
5. Maniruzzaman, M., Boateng, S.J., Snowden, M.J. and Douroumis, D. A review of Hot-Melt extrusion: process technology to pharmaceutical products. *International Scholarly Research Notices*, 2012, 2012:1-9. https://doi.org/10.5402/2012/436763.
6. Sevinç Özakar, R., Özakar, E. Current overview of oral thin films. *Turk J Pharm Sci*, 2021, 18(1):111-121. DOI: 10.4274/tjps.galenos.2020.76390.
7. Borges, A.F., Silva, C., Coelho, J.F., Simones, S. Oral films: current status and future perspectives: I — Galenical development and quality attributes. *Journal of Controlled release*, 2015, 206:1-19. https://doi.org/10.1016/j.jconrel.2015.03.006.
8. Sharma, D., Kaur, D., Verma, S., Singh, D. Fast Dissolving Oral Films Technology: A Recent Trend for An Innovative Oral Drug Delivery System. *International Journal of Drug Delivery*. 2015, 7:60-75.
9. Karki, S., Kim, H., Na, S.J., Shin, D., Jo, K., Lee, J. Thin films as an emerging platform for drug delivery. *Asian Journal of Pharmaceutical Sciences.* 2016, 11:559-574. https://doi.org/10.1016/j.ajps.2016.05.004.
10. Ng, Y.C., McAuley, W.J., Qi, S. Stabilisation of amorphous drugs under high humidity using pharmaceutical thin films. *European Journal of Pharmaceutics and Biopharmaceutics*. 2013, 84:555-565. https://doi.org/10.1016/j.ejpb.2013.01.008.
11. Kumari, A., Sharma, P.K., Garg, V.K., Garg, G. Ocular inserts - Advancement in therapy of eye diseases. *Journal of Advanced Pharmaceutical Technology and Research*. 2010, 1:291-296.
12. Irfan, M., Rabel, S., Bukhtar, Q., Qadir, M.I., Jabeen, F., Khan, A. Orally disintegrating films: A modern expansion in drug delivery system. *Saudi Pharm J*. 2016, 24(5):537-546. Doi: 10.1016/j.jsps.2015.02.024.
13. Adrover, A., Di Muzio, L., Trilli, J., Brandelli, C., Paolicelli, P., Petralito, S., Casadei, M.A. Enhanced Loading Efficiency and Mucoadhesion Properties of Gellan Gum Thin Films by Complexation with Hydroxypropyl-β-Cyclodextrin. *Pharmaceutics.* 2020, 12(9):819. Doi: 10.3390/pharmaceutics12090819.
14. Savencu, I., Iurian, S., Porfire, A., Bogdan, C., Tomuța, I. Review of advances in polymeric wound dressing films. *Reactive and Functional Polymers.* 2021, 168(6):105059. Doi:10.1016/j.reactfunctpolym.2021.105059.
15. Reza, K.H., Chakraborty, P. Recent industrial development in Oral Thin Film Technology: An Overview. *PharmaTour*. 2016, 4(8):17-22.
16. Preis, M., Woertz, C., Kleinebudde, P., Breitkreutz, J. Oromucosal film preparations: classification and characterization methods. *Expert Opin Drug Deliv*. 2013, 10(9):1303-17. Doi: 10.1517/17425247.2013.804058.
17. Kunte, S., Tandale, P. Fast dissolving strips: A novel approach for the delivery of verapamil. J *Pharm Bioallied Sci*. 2010, 2(4):325-8. Doi: 10.4103/0975-7406.72133.
18. El-Setouhy, D.A., Shawky, N., El-Malak ABD. Formulation of a novel tianeptine sodium orodispersible film. *AAPS PharmSciTech*. 2010, 11(3):1018-25. Doi: 10.1208/s12249-010-9464-2.
19. Mukhopadhyay, R., Gain, S., Verma, S., Singh, B., Vyas, M., Mehta, M., Haque, A. Polymers in designing the mucoadhesive films: A comprehensive review. International Journal of Green Pharmacy, 2018 (Suppl), 12(2):S330.
20. Dixit, R.P., Puthli, S.P. Oral strip technology: Overview and future potential. *Journal of Controlled Release*. 2009, 139(2):94–107. Doi: 10.1016/j.jconrel.2009.06.014.
21. Siemann, U. (2005). Solvent cast technology – a versatile tool for thin film production. In: Stribeck, N., Smarsly, B. (eds) *Scattering Methods and the Properties of Polymer Materials. Progress in Colloid and Polymer Science*, vol 130. Springer, Berlin, Heidelberg. https://doi.org/10.1007/b107336.
22. Russo, E., Selmin, F., Baldassari, S., Gennari, C.G.M, Caviglioli, G., Cilurzo, F., Minghetti, P., Parodi, B. A focus on mucoadhesive polymers and their application in buccal dosage forms. Journal of Drug Delivery Science and Technology. 2016, 32:113-125. https://doi.org/10.1016/j.jddst.2015.06.016

23. Kathpalia, H., Gupte, A. An introduction to fast dissolving oral thin film drug delivery systems: a review. *Curr Drug Deliv*. 2013, 10(6):667-84. Doi: 10.2174/15672018100613112515024 9.
24. Verma, S., Kumar, N., Sharma, P.K., Buccal film: an advance technology for oral drug delivery. *Adv Biol Res*. 2014, 8:260-267.
25. Repka, M.A., Gutta, K., Prodduturi, S., Munjal, M., Stodghill, S.P. Characterization of cellulosic hot-melt extruded films containing lidocaine. *Eur J Pharm Biopharm*. 2005, 59(1):189-96. Doi: 10.1016/j.ejpb.2004.06.008.
26. Shimoda, H., Taniguchi K. Preparation of fast dissolving oral thin film containing dexamethasone: A possible application to antiemesis during cancer chemotherapy. *European Journal of Pharmaceutics and Biopharmaceutics*. 2009; 73: 361-365. Doi: 10.1016/j.ejpb.2009.08.010.
27. Nishimura, M., Matsuura, K., Tsukioka, T., Yamashita, H., Inagaki, N., Sugiyama, T., Itoh Y. In vitro and in vivo characteristics of prochlorperazine oral disintegrating film. *International Journal of Pharmaceutical Sciences.* 2009, 368(1-2):98–102. Doi: 10.1016/j.ijpharm.2008.10.002.
28. Ghodake, P.P, Karande, K.M., Osmani, R.A., Bhosale, R.R., Harkare, B.R., Kale, B.B. Mouth Dissolving Films: Innovative Vehicle for Oral Drug Delivery. *International Journal of Pharma Research & Review*. 2013, 2(10):41-47.
29. Crowley, M.M., Zhang, F. Pharmaceutical applications of hot-melt extrusion: Part I. *Drug Dev Ind Pharm*. 2007, 33:909-926.
30. Repka, M.A., Majumdar, S., Battu, S.K., Srirangam, R., Upadhye, S.B. Applications of hot-melt extrusion for drug delivery. *Expert Opin Drug Deliv*. 2008, 5(12):1357-76. Doi: 10.1517/17425240802583421.
31. Repka, M.A., Prodduturi, S., Stodghill, S.P. Production and characterization of hot-melt extruded films containing clotrimazole. *Drug Dev Ind Pharm*. 2003, 29(7):757-65. Doi: 10.1081/ddc-120021775.
32. Repka, M.A., McGinity, J.W. Bioadhesive properties of hydroxypropylcellulose topical films produced by hot-melt extrusion. *J Control Release*. 2001, 70(3):341-51. DOI: 10.1016/s0168-3659(00)00365-5.
33. Breitenbach, J. Melt extrusion: from process to drug delivery technology. *European Journal of Pharmaceutics and Biopharmaceutics*, 2002, 54(2):107–117. https://doi.org/10.1016/S0939-6411(02)00061-9.
34. Chokshi, R., Zia, H. Hot-Melt Extrusion Technique: A Review. *Iranian Journal of Pharmaceutical Research*. 2004, 3: 3-16.
35. Radhakisan, U.R., Chavan, V., Tribhuvan, N. Mouth Dissolving Film and Their Patent: An Overview. *International Research Journal of Pharmacy*. 2012, 3(9); 39-42.
36. Reza, K.H., Chakraborty, P. Recent industrial development in Oral Thin Film Technology: An Overview. *PharmaTutor*. 2016, 4(8); 17-22.
37. Frey. Film Strips and Pharmaceuticals. *Pharma Mfg & Packag Sourcer*. 2006; 92– 93.
38. Preis, M., Breitkreutz, J., Sandler, N. Perspective: Concepts of printing technologies for oral film formulations. *Int J Pharmaceut*. 2015. https://doi.org/10.1016/j.ijpharm.2015.02.032.
39. Genina, N., Fors, D., Petri, Vakili, H., Ihalainen, P., Pohjala, L., Ehlers, H., Kassamakov, I., Haeggström, E., Vuorela, P., Peltonen, J., Sandler, N. Tailoring controlled-release oral dosage forms by combining inkjet and flexographic printing techniques. *Eur J Pharm Sci*. 2012, 47(3):615-23. Doi: 10.1016/j.ejps.2012.07.020.
40. Corniello, C. Quick dissolving strips: from concept to commercialization. *Drug Del. Technol*. 2006. 6(2):68–71.
41. Frankhauser, C., Slominski, G., Meyer, S. Disintegrable oral films. U.S. Patent 2007/0202057, Aug. 30, 2007.
42. Saini, P., Kumar, A., Sharma, P., Visht, S. Fast Disintegrating Oral Films: A Recent Trend of Drug Delivery. *Int. J. Drug Dev*. & Res. 2012, 4(4): 80-94.
43. Rowe, R.C., Sheskey, P.J., Owen, S.C. (Eds.). Handbook of Pharmaceutical Excipients. Pharmaceutical press, London. 2006.
44. Rowe, R.C., Forse, S.F. The effect of polymer molecular weight on the incidence of film cracking and splitting on film coated tablets. *J. Pharm. Pharmacol*. 1980, 32(8):583–584.
45. Rowe, R.C., Forse, S.F. The effect of film thickness on the incidence of the defect bridging of intagliations on film coated tablets. *J. Pharm. Pharmacol*. 1980, 32(9):647–648.
46. Rowe, R.C, Forse, S.F. The effect of plasticizer type and concentration on the incidence of bridging of intagliations onfilm-coated tablets. *J. Pharm. Pharmacol*. 1981, 33(3):174–175.
47. Pramod Kumar, T.M., Desai, K.G., Shivkumar, H.G. Mechanism of buccal permeation enhancers. *Indian J. Pharm. Educ*. 2002, 36(3):147– 151.

48. McElnay, A.C., Swarbrick, J., Boyloan, J.C. Encyclopedia of Pharmaceutical Technology; Marcel Dekker: New York; 1988, Vol. 2; p 189.
49. Udayakumar, G.P., Muthusamy, S., Selvaganesh, B., Sivarajasekar, N., Rambabu, K., Banat, F., Sivamani, S., Sivakumar, N., Hosseini-Bandegharaei, A., Show, P.L. Biopolymers and composites: Properties, characterization and their applications in food, medical and pharmaceutical industries. *J. Environ. Chem. Eng.* 2021, 9, 105322. https://doi.org/10.1016/j.jece.2021.105322
50. Sánchez-López, E., Gomes, D., Esteruelas, G., Bonilla, L., Lopez-Machado, A.L., Galindo, R., Cano, A., Espina, M., Ettcheto, M., Camins, A., et al. Metal-Based nanoparticles as antimicrobial agents: An overview. *Nanomaterials*. 2020, 10, 292. Doi: 10.3390/nano10020292
51. Mihai, M.M., Dima, M.B., Dima, B., Holban, A.M. Nanomaterials for wound healing and infection control. *Materials*. 2019, 12, 2176. Doi: 10.3390/ma12132176.
52. Nqakala, Z.B.; Sibuyi, N.R.S.; Fadaka, A.O.; Meyer, M.; Onani, M.O.; Madiehe, A.M. Advances in nanotechnology towards Development of silver nanoparticle-based wound-healing agents. *Int. J. Mol. Sci*. 2021, 22, 11272. Doi: 10.3390/ijms222011272.
53. Ali, S., Quadir, A. High molecular weight povidone polymer-based films for fast dissolving drug delivery applications. *Drug Del. Technol*. 2007, 7(6):36–43.
54. Cilurzo, F., Cupone, I.E., Minghetti, P., Selmin, F., Montanari, L. Fast dissolving films made of maltodextrins. *Eur. J. Pharm. Biopharm*. 2008, 70(3):895–900.
55. Nishimura, M., Matsuura, K., Tsukioka, T., Yamashita, H., Inagaki, N., Sugiyama, T., Itoh, Y. In vitro and in vivo characteristics of prochlorperazine oral disintegrating film. *Int J Pharm*. 2009, 368(1–2):98–102.
56. Alopaeus, J.F., Hellfritzsch, M., Gutowski, T., Scherlie, R., Almeida, A., Sarmento, B., Skalko-Basnet, N., Tho, I. Mucoadhesive buccal films based on a graft co-polymer – A mucin-retentive hydrogel scaffold. *European Journal of Pharmaceutical Sciences*. 2019. Doi: https://doi.org/10.1016/j.ejps.2019.105142.
57. Birudaraj, R., Mahalingam, R., Li, X., Jasti, B.R. Advances in buccal drug delivery. *Crit. Rev. Ther. Drug Carrier Syst*. 2005, 22(3):295 – 330. Doi: 10.1615/critrevtherdrugcarriersyst.v22.i3.20.
58. Ludwig, A. The use of mucoadhesive polymers in ocular drug delivery. *Adv Drug Deliv Rev*. 2005, 57(11):1595-639. Doi: 10.1016/j.addr.2005.07.005.
59. Peppas, N.A., Sahlin, J.J. Hydrogels as mucoadhesive and bioadhesive materials: a review. *Biomaterials*. 1996, 17(16):1553-61. Doi: 10.1016/0142-9612(95)00307-x.
60. Grabovac, V., Guggi, D., Bernkop-Schnürch, A. Comparison of the mucoadhesive properties of various polymers. Adv Drug Deliv Rev. 2005, 57(11):1713-23. Doi: 10.1016/j.addr.2005.07.006.
61. Kharenko, E.A., Larionova, N.I., Demina, N.B. Mucoadhesive drug delivery systems (review). *Pharm Chem J*. 2009, 43:200–208. https://doi.org/10.1007/s11094-009-0271-6.
62. Ponchel, G., Irache, J. Specific and non-specific bioadhesive particulate systems for oral delivery to the gastrointestinal tract. *Adv Drug Deliv Rev*. 1998, 34(2-3):191-219. Doi: 10.1016/s0169-409x(98)00040-4.
63. Smart, J.D. The basics and underlying mechanisms of mucoadhesion. *Adv Drug Deliv Rev*. 2005, 57(11):1556-68. Doi: 10.1016/j.addr.2005.07.001.
64. Pacheco, M.S., Barbieri, D., Da Silva, C.F., De Moraes, M.A. A review on orally disintegrating films (ODFs) made from natural polymers such as pullulan, maltodextrin, starch, and others. International Journal of Biological Macromolecules. 2021, 178:504-513
65. Rezaee, F., Ganji, F. Formulation, characterization, and optimization of captopril fast-dissolving oral films, AAPS PharmSciTech. 2018, 19:2203–2212, https://doi. org/10.1208/s12249-018-1027-y.
66. Sharma, R., Kamboj, S., Singh, G., Rana, V. Development of aprepitant loaded orally disintegrating films for enhanced pharmacokinetic performance, Eur. J. Pharm. Sci. 2016, 84:55–69, https://doi.org/10.1016/j.ejps.2016.01.006.
67. Esim, O., Ozkan, C.K., Kurbanoglu, S., Arslan, A., Tas, C., Savaser, A., Ozkan, S.A., Ozkan, Y. Development and in vitro/in vivo evaluation of dihydroergotamine mesylate loaded maltodextrin-pullulan sublingual films, Drug Dev. Ind. Pharm. 2019, 45:914–921, https://doi.org/10.1080/03639045.2019.1578788.
68. El-Malah, Y., Nazzal, S. "Real-time" disintegration analysis and D-optimal experimental design for the optimization of diclofenac sodium fast-dissolving films, Pharm. Dev. Technol. 2013, 18:1355–1360, https://doi.org/10.3109/10837450. 2012.700936

69. Sayed, S., Ibrahim, H.K., Mohamed, M.I., El-Milligi, M.F. Fast-dissolving sublingual films of terbutaline sulfate: formulation and in vitro/in vivo evaluation, Mol. Pharm. 2013, 10:2942–2947, https://doi.org/10.1021/mp4000713
70. Raza, S.N., Kar, A.H., Wani, T.U., Khan, N.A. Formulation and evaluation of mouth dissolving films of losartan potassium using 32 factorial design, Int. J. Pharm. Sci. Res. 2019, 10:1402–1411, https://doi.org/10.13040/IJPSR.0975-8232.10(3).1402-11.
71. Shi, L.L, Xu, W.J., Cao, Q.R., Yang, M., Cui, J.H. Preparation, characterization and in vitro evaluation of a polyvinyl alcohol/sodium alginate based orodispersible film containing sildenafil citrate, Pharmazie. 2014, 69:327–334, https://doi.org/ 10.1691/ph.2014.317.
72. Cardelle-Cobas, A., Madureira, A.R., Costa, E., Barros, R., Tavaria, F.K., Pintado, M.E. Development of oral strips containing chitosan as active ingredient: a product for buccal health, Int. J. Polym. Mater. Polym. Biomater. 2015, 64:906–918, https:// doi.org/10.1080/00914037.2015.1030661.
73. Patil, S.B.S, Daswadkar, S. A Comprehensive Review: Natural Polymers Used for Fast Dissolving Mouth Film. Int. J. Pharm. Sci. Rev. Res. 2002, 65(2):14-21
74. Chandramouli, M., Shivalingappa, R.P., Basavanna, V., Doddamani, S., Shanthakumar, D.C., Nagarajaiah, S.R., Ningaiah, S. Oral Thin-films from Design to Delivery: A Pharmaceutical Viewpoint. Biointerface Research in Applied Chemistry. 2022, 13(2):2023.
75. Bodini, R.B., Guimarães, J. das G.L., Monaco-Lourenço, C.A., Aparecida de Carvalho, R. Effect of starch and hydroxypropyl methylcellulose polymers on the properties of orally disintegrating films, J. Drug Deliv. Sci. Technol. 51 (2019) 403–410, https:// doi.org/10.1016/j.jddst.2019.03.028
76. Serrano, D.R., Fernandez-Garcia, R., Mele, M., Healy, A.M., Lalatsa, A. Designing fastdissolving orodispersible films of amphotericin B for oropharyngeal candidiasis, Pharmaceutics. 2019, 11. https://doi.org/10.3390/pharmaceutics11080369.
77. Vidyadhara, S., Sasidhar, R.L., Balakrishna, T., Vardhan, M.S. Formulation of rizatriptan benzoate fast dissolving buccal films by emulsion evaporation technique, Int. J. Pharm. Investig. 2015, 5:101. https://doi.org/10.4103/2230-973x.153387
78. Paolicelli, P., Petralito, S., Varani, G., Nardonia, M., Pacelli, S., Di Muzio, L., Tirillò, J., Bartuli, C., Cesa, S., Casadei, M.A., Adrover, A. Effect of glycerol on the physical and mechanical properties of thin gellan gum films for oral drug delivery. *International Journal of Pharmaceutics.* 2018, 547:226-234. Doi: 10.1016/j.ijpharm.2018.05.046
79. Zia, K.M., Tabasum, S., Khan, M.F., Akram, N., Akhter, N., Noreen, A., Zuber, M. Recent trends on gellan gum blends with natural and synthetic polymers: A review. *Int J Biol Macromol*. 2018, 109:1068-1087. doi: 10.1016/j.ijbiomac.2017.11.099.
80. Prezotti, F.G., Siedle, I., Boni, F.I., Chorilli, M., Müller, I., Cury, B.S.F. Mucoadhesive films based on gellan gum/pectin blends as potential platform for buccal drug delivery. *Pharm Dev Technol*. 2020, 25(2):159-167. doi: 10.1080/10837450.2019.1682608.
81. Fernandes, F.P., Fortes, A.C., da Cruz Fonseca, S.G., Breitkreutz, J., Ferraz, H.G. Manufacture and Characterization of Mucoadhesive Buccal Films Based on Pectin and Gellan Gum Containing Triamcinolone Acetonide. *International Journal of Polymer Science*. 2018, 1-10. https://doi.org/10.1155/2018/2403802.
82. Li, A., Khan, I.N., Khan, I.U., Yousaf, A.M., Shahzad, Y. Gellan Gum-Based Bilayer Mucoadhesive Films Loaded with Moxifloxacin Hydrochloride and Clove Oil for Possible Treatment of Periodontitis. *Drug Des Devel Ther*. 2021, 15:3937-3952. doi: 10.2147/DDDT.S328722.
83. Heinemann, R.J.B., Vanin, F.M., De Carvalho, R.A., Trindade, M.A., FávaroTrindade, C.S. Characterization of low cost orally disintegrating film (ODF), Polimeros. 2017, 27:48–54. https://doi.org/10.1590/0104-1428.2409.
84. Tedesco, M.P., Monaco-Lourenço, C.A., Carvalho, R.A. Gelatin/hydroxypropyl methylcellulose matrices — polymer interactions approach for oral disintegrating films, Mater. Sci. Eng. 2016, 69:668–674. https://doi.org/10.1016/j.msec.2016. 07.023
85. Irfan, M., Rabel, S., Bukhtar, Q., Qadir, M.I., Jabeen, F., Khan, A. Orally disintegrating films: A modern expansion in drug delivery system, Saudi Pharmaceutical Journal (2015), doi: http://dx.doi.org/ 10.1016/j.jsps.2015.02.024

86. Parejiya, P.B., Patel, R.C., Mehta, D.M., Shelat, P.K., Barot, B.S. Quick dissolving films of nebivolol hydrochloride: formulation and optimization by a simplex lattice design. Journal of Pharmaceutical Investigation. 2012, 43:343-351.
87. Bansal, S., Bansal, M., Garg, G. Formulation and evaluation of fast dissolving film of an antihypertensive drug. Int. J. Pharm. Chem. Bio. Sci. 2013, 3:1097-1108.
88. Nappinnai, M., Chandanbala, R., Balaijirajan, R. Formulation and evaluation of nitrendipine buccal films. Indian journal of pharmaceutical sciences. 2008, 70:631-635.
89. Peh, K.K, Wong, C.F. Polymeric films as vehicle for buccal delivery: swelling, mechanical, and bioadhesive properties, J Pharm Pharm Sci. 1999, 2:53-61.
90. Alanazi, F.K., Rahman, A.A.A, Mahrous, G.M., Alsarra, I.A. Formulation and physicochemical characterisation of buccoadhesive films containing ketorolac, J. Drug Deliv. Sci. Technol. 2007, 17:183-192.
91. Naseri-Nosar, M., Ziora, Z.M. Wound Dressings from Naturally-occurring Polymers: A Review on Homopolysaccharide-based Composites. *Carbohydrate Polymers*. 2018, 189:379-398. https://doi.org/10.1016/j.carbpol.2018.02.003.
92. Rezvani Ghomi, E., Khalili, S., Nouri Khorasani, S., Esmaeely Neisiany, R., and Ramakrishna, S. Wound dressings: Current advances and future directions. *J. Appl. Polym. Sci*. 2019, 136:47738. https://doi.org/10.1002/app.47738.
93. Koehler, J., Brandl, F.P., and Goepferich, A.M. Hydrogel wound dressings for bioactive treatment of acute and chronic wounds. *Eur. Polym. J.* 2018, 100:1–11. https://doi.org/10.1016/j.eurpolymj.2017.12.046.
94. Xiang, J., Shen, L., and Y. Hong. Status and future scope of hydrogels in wound healing: Synthesis, materials and evaluation. *Eur. Polym. J.* 2020, 130:109609. https://doi.org/10.1016/j.eurpolymj.2020.109609.
95. Zhang, C., Wu, B., Zhou, Y., Zhou, F., Liu, W., and Wang, Z. Mussel-inspired hydrogels: From design principles to promising applications. *Chem. Soc*. Rev. 2020, 49:3605–3637.
96. Spotnitz. W.D., and Burks, S. Hemostats, sealants, and adhesives III: A new update as well as cost and regulatory considerations for components of the surgical toolbox. *Transfusion*. 2012, 52:2243–2255. DOI:10.1111/j.1537-2995.2012.03707.x.
97. Pan, Z., Ye, H. and Wu, D. Recent advances on polymeric hydrogels as wound dressings. APL Bioeng. 2021, 5(1):011504. Doi: 10.1063/5.0038364.
98. Sahana, T.G., Rekha, P.D. Biopolymers: Applications in wound healing and skin tissue engineering. Mol Biol Rep. 2018, 45(6):2857-2867. Doi: 10.1007/s11033-018-4296-3.
99. Karadeniz, F., Sung, H.K., and Kim, H.S. Natural Origin Polymers: Applications as Wound Care Materials. *Journal of Life Science*. 2019, 29(3):382-393. DOI: https://doi.org/10.5352/JLS.2019.29.3.382.
100. Boateng, J. and Catanzano, O. Advanced therapeutic dressings for effective wound healing—a review. *J. Pharm. Sci*. 2015, 104(11):3653-3680. Doi: 10.1002/jps.24610.
101. Chaudhari, A., Vig, K., Baganizi, D., Sahu, R., Dixit, S., Dennis, V., Singh, S., Pillai, S., Chaudhari, A. A., Vig, K., Baganizi, D. R., Sahu, R., Dixit, S., Dennis, V., Singh, S. R. and Pillai, S. R. Future prospects for scaffolding methods and biomaterials in skin tissue engineering: a review. *Int. J. Mol. Sci*. 2016, 17(12):1974. Doi: 10.3390/ijms17121974.
102. Simões, D., Miguel, S.P., Ribeiro, M.P., Coutinho, P., Mendonça, A.G. and Correia, I.J. Recent advances on antimicrobial wound dressing: a review. *Eur. J. Pharm. Biopharm*. 2018, 127:130-141. Doi: 10.1016/j.ejpb.2018.02.022.
103. Houghton, P.J., Hylands, P.J., Mensah, A.Y., Hensel, A. and Deters, A.M. In vitro tests and ethnopharmacological investigations: wound healing as an example. *J. Ethnopharmacol.* 2005, 100(1-2):100-107. Doi: 10.1016/j.jep.2005.07.001.
104. Morgan, C. and Nigam, Y. Naturally derived factors and their role in the promotion of angiogenesis for the healing of chronic wounds. *Angiogenesis*. 2013, 16(3):493-502. Doi: 10.1007/s10456-013-9341-1.
105. Pereira, R.F. and Bártolo, P.J. Traditional therapies for skin wound healing. *Adv. Wound Care*. 2016, 5(5):208-229. Doi: 10.1089/wound.2013.0506.
106. Tsala, D.E., Amadou, D. and Habtemariam, S. Natural wound healing and bioactive natural products. *Phytopharmacology*. 2013, 4:532-560.

107. Savencu, I., Iurian, S., Porfire, A., Bogdan, C., Tomuța, I. Review of advances in polymeric wound dressing films. *Reactive and Functional Polymers*. 2021, 168:105059. https://doi.org/10.1016/j.reactfunctpolym.2021.105059.
108. Arif, M.M., Khan, S.M., Gull, N., A Tabish, T., Zia, S., Khan, R.U., Awais, S.M., Butt, M.A. Polymer-based biomaterials for chronic wound management: Promises and challenges. *Int J Pharm*. 2021, 598:120270. Doi: 10.1016/j.ijpharm.2021.120270.
109. Chircov, C., Grumezescu, A.M., Bejenaru, L.E. Hyaluronic acid-based scaffolds for tissue engineering. *Rom. J. Morphol. Embryol*. 2018, 59(1):71–76.
110. Graçaa, M.F.P., Miguela, S.P., Cabrala, C.S.D., Correia, I.J. Hyaluronic acid—Based wound dressings: A review. Carbohydrate Polymers. 2020, 241:116364. https://doi.org/10.1016/j.carbpol.2020.116364.
111. Reddy, M.S.B, Ponnamma, D., Choudhary. R., Sadasivuni, K.K. A Comparative Review of Natural and Synthetic Biopolymer Composite Scaffolds. Polymers. 2021, 13:1105. Doi: 10.3390/polym13071105.
112. Biagini, G., Bertani, A., Muzzarelli, R., Damadei, A., DiBenedetto, G., Belligolli, A., Riccotti, G., Zucchini, C. and Rizzoli, C. Wound management with N-carboxybutyl chitosan. *Biomaterials*. 1991, 12:281-286.
113. Aderibigbe, B.A. and Buyana, B. Alginate in wound dressings. *Pharmaceutics.* 2018, 10:42.
114. Yang, D., Jones, K.S. Effect of alginate on innate immune activation of macrophages. *J. Biomed. Mater. Res. Part A.* 2009, 90A:411-418.
115. Hoenich, N.A. Cellulose for medical applications: past, present, and future. *BioResources*. 2007, 1:270-280.
116. Wagenhäuser, M.U., Mulorz, J., Ibing, W., Simon, F., Spin, J. M., Schelzig, H. and Oberhuber, A. Oxidized (non)-regenerated cellulose affects fundamental cellular processes of wound healing. *Sci. Rep*. 2016, 6:32238.
117. Feketshane, Z., Alven, S., Aderibigbe, B.A. Gellan Gum in Wound Dressing Scaffolds. *Polymers.* 2022, *14*(19):4098. https://doi.org/10.3390/polym14194098.
118. Mahmood, H., Khan, I.U., Asif, M., Khan, R.U., Asghar, S., Khalid, I., Khalid, S.H., Irfan, M., Rehman, F., Shahzad, Y., Yousaf, A.M., Younus, A., Niazi, Z.R., Asim, M. In vitro and in vivo evaluation of gellan gum hydrogel films: Assessing the co impact of therapeutic oils and ofloxacin on wound healing. *Int J Biol Macromol*. 2021, 166:483-495. doi: 10.1016/j.ijbiomac.2020.10.206.
119. Osmałek, T., Froelich, A., Tasarek, S. Application of gellan gum in pharmacy and medicine. *International Journal of Pharmaceutics*. 2014, 466(1-2):328-340. Doi: 10.1016/j.ijpharm.2014.03.038.
120. Hishamuddin, N.I., Razali, M.H., Amin, K.A.M. Application of Gellan Gum Biopolymer in Biomedical Applications: A Review. *Makara Journal of Science*. 2022, 26(1):11−24. Doi: 10.7454/mss.v26i1.1271.
121. Pamfil, D., Schick, C., Vasile, C. New Hydrogels Based on Substituted Anhydride Modified Collagen and 2-Hydroxyethyl Methacrylate. Synthesis and Characterization. *Ind. Eng. Chem. Res*. 2014, 53:11239–11248.
122. Yu, L., Wei, M. Biomineralization of Collagen-Based Materials for Hard Tissue Repair. *IJMS* 2021, 22:944.
123. Bellis, S.L. Advantages of RGD peptides for directing cell association with biomaterials. *Biomaterials*. 2011, 32:4205-4210.
124. Rouse, J.G., Van Dyke, M.E. A Review of Keratin-Based Biomaterials for Biomedical Applications. *Materials*. 2010, 3:999–1014.
125. Hill, P., Brantley, H.; Van Dyke, M. Some Properties of Keratin Biomaterials: Kerateines. *Biomaterials*. 2010, 31:585–59.
126. Arthe, R., Arivuoli, D., Ravi, V. Preparation and characterization of bioactive silk fibroin/paramylon blend films for chronic wound healing. *Int. J. Biol. Macromol*. 2020, 154:1324–1331. https://doi.org/10.1016/j.ijbiomac.2019.11.010.
127. Zhang, X., Chen, Z., Bao, H., Liang, J., Xu, S., Cheng, G., Zhu, Y. Fabrication and characterization of silk fibroin/Curcumin sustained-release film. *Materials*. 2019, 12(20) https://doi.org/10.3390/ma12203340.
128. Bacelar, A.H., Silva-Correia, J., Oliveira, J.M. and Reis, R.L. Recent progress on gellan gum hydrogels provided by functionalization strategies. *Journal of Material Chemistry B*. 2016, 4(37):6164-6174. Doi: 10.1039/c6tb01488g.
129. Morris, E.R., Gothard, M.G.E., Hember, M.W.N., Manning, C.E., Robinson, G. Conformational and rheological transitions of welan, rhamsan and acylated gellan. *Carbohydrate Polymers*. 1996, 30:165–175.

130. Mazen, F., Milas, M., Rinaudo, M. Conformational transition of native and modified gellan. *International Journal of Biological Macromolecules*. 1999, 26:808 109–118.
131. Grasdalen, H. and Smidsrod, O. Gelation of Gellan Gum. *Carbohydrate Polymers*. 1987, 7:371-393.
132. Shinkar, D.M., Dhake, A.S., Setty, C.M. Drug delivery from the oral cavity: a focus on mucoadhesive buccal drug delivery systems. *PDA J Pharm Sci Technol*. 2012, 66(5):466-500. Doi: 10.5731/pdajpst.2012.00877.
133. Razali, M.H., Ismail, N.A., Amin, K.A.M. Fabrication and characterization of antibacterial titanium dioxide nanorods incorporating gellan gum films. *J. Pure Appl. Microbiol*. 2019, 13: 1909–1916. https://doi.org/10.22207/JPAM.13.4.03.
134. Ismail, N.A., Mat Amin, K.A., Razali, M.H. Novel gellan gum incorporated TiO2 nanotubes film for skin tissue engineering. *Mater. Lett*. 2018, 228: 116– 120. https://doi.org/10.1016/j.matlet.2018. 05.140.
135. Razali, M.H., Ismail, N.A., Mohd Zulkafli, M.F.A., Amin, K.A.M. 3D Nanostructured materials: TiO2 nanoparticles incorporated gellan gum scaffold for photocatalyst and biomedical applications. *Mater. Res. Express*. 2018, 5:035039, https://doi.org/10.1088/2053-1591/AAB5F5.
136. Razali, M.H., Ismail, N.A., Mat Amin, K.A. Titanium dioxide nanotubes incorporated gellan gum bio-nanocomposite film for wound healing: Effect of TiO2 nanotubes concentration. Int. J. Biol. Macromolecules. 2020, 153: 1117–1135, https://doi.org/1 0.1016/j.ijbiomac.2019.10.242.
137. Ferris, C., Stevens, L., Gilmore, K., Mume, E., Greguric, I., Kirchmajer, D.M., Wallace G., Panhuis, M. Peptide modification of purified gellan gum. *J. Mater. Chem. B*. 2015, 3(6):1106-1115. DOI:10.1039/C4TB01727G.
138. Lee, W., Choi, J.H., Lee, J., Youn, J., Kim, W., Jeon, G., Lee, S.W., Song, J.E., Khang, G. Dopamine-Functionalized Gellan Gum Hydrogel as a Candidate Biomaterial for a Retinal Pigment Epithelium Cell Delivery System. *ACS Appl Bio Mater*. 2021, 4(2):1771-1782. doi: 10.1021/acsabm.0c01516.
139. Hearnden, V., Sankar, V., Hull, K., Juras, D.V., Greenberg, M., Kerr, A.R., Lockhart, P.B., Patton, L.L., Porter, S., Thornhill, M.H. New developments and opportunities in oral mucosal drug delivery for local and systemic disease. *Adv Drug Deliv Rev*. 2012, 64(1):16-28. Doi: 10.1016/j.addr.2011.02.008.
140. Patel, V.F., Liu, F., Brow, M.B. Advances in oral transmucosal drug delivery. *J. Control. Release.* 2011, 153:106–116.
141. Madhav, N.V.S., Shakya, A.K., Singh, K. Oro-transmucosal drug delivery system: A review. *J. Control. Release*. 2009, 140:2–11.
142. Lam, J.K., Xu, Y., Worsley, A., Wong, I.C. Oral transmucosal drug delivery for pediatric use. *Adv Drug Deliv Rev*. 2014, 73:50-62. Doi: 10.1016/j.addr.2013.08.011.
143. Perumal, V.A., Govender, T., Lutchman, D., Mackraj, I. Investigating a new approach to film casting for enhanced drug content uniformity in polymeric films. *Drug Dev Ind Pharm*. 2008, 34(10):1036-47. doi: 10.1080/03639040801928952.
144. Jadhav, Y.G., Galgatte, U.C., Chaudhari, P.D. Challenges in formulation development of fast dissolving oral films. Indo Am J Pharma Res. 2013, 3:1746-1751.
145. Qi, S., Moffat, J.G., Yang, Z. Early-stage phase separation in pharmaceutical solid dispersion thin films under high humidity: improved spatial understanding using probe-based thermal and spectroscopic nanocharacterization methods. *Mol Pharm*. 2013, 10(3):918-30. doi: 10.1021/mp300557q.
146. Lee, S.S., Muralidharan, S., Woll, A., Loth, M.A., Li, Z., Anthony, J.E., Haataja, M., Loo, Y.L. Understanding heterogeneous nucleation in binary, solution-processed, organic semiconductor thin films. *Chem. Mater*. 2012, 24:2920−2928. https://doi.org/10.1021/cm3010858.
147. Sun, Y., Zhu, L., Wu, T., Cai, T., Gunn, E.M., Yu, L. Stability of amorphous pharmaceutical solids: crystal growth mechanisms and effect of polymer additives. *AAPS J*. 2012, 14:380–388. doi: 10.1208/s12248-012-9345-6.
148. Qi, S., Marchaud, D., Craig, D.Q.M. An Investigation into the Mechanism of Dissolution Rate Enhancement of Poorly Water-Soluble Drugs from Spray Chilled Gelucire 50/13 Microspheres. *J. Pharm. Sci*. 2010, 99(1):262−274. DOI: 10.1002/jps.21832.
149. Gupta, P., Thilagavathi, R., Chakraborti, A.K., Bansal, A.K. Role of molecular interaction in stability of celecoxib-PVP amorphous systems. *Mol. Pharm*. 2005, 5:384–391. https://doi.org/10.1021/mp050004g.
150. Zhu, L., Wong, L., Yu, L. Surface-enhanced crystallization of amorphous nifedipine. *Mol. Pharm*. 2008, 5:921–926. https://doi.org/10.1021/mp8000638.

151. Wu, T., Sun, Y., Yu, L. Inhibiting surface crystallization of amorphous indomethacin by nanocoating. *Langmuir*. 2007, 23:5148–5153. https://doi.org/10.1021/la070050i.
152. Dohnalek, Z., Kimmel, G., Ciolli, R., Stevenson, K., Smith, R., Kay, B. The effect of the underlying substrate on the crystallization kinetics of dense amorphous solid water films. *J. Chem. Phys.* 2000, 112:13. https://doi.org/10.1063/1.481166.
153. Mortazavi, S.A., Smart, J.D. An investigation into the role of water movement and mucus gel dehydration in mucoadhesion. *Journal of Controlled Release*. 1993, 25(3):197-203. https://doi.org/10.1016/0168-3659(93)90078-J.
154. Salamat-Miller, N., Chittchang, M., Johnston, T.P. The use of mucoadhesive polymers in buccal drug delivery. *Advanced Drug Delivery Reviews*. 2005, 57(11):1666-1691. https://doi.org/10.1016/j.addr.2005.07.003.
155. Lee, J.W., Park, J.H., Robinson, J.R. Bioadhesive-based dosage forms: the next generation. *J Pharm Sci*. 2000, 89(7):850-66. Doi: 10.1002/1520-6017(200007)89:7<850::AID-JPS2>3.0.CO;2-G.
156. Ch'ng, H.S., Park, K., Kelly, P., Robinson, J.R. Bioadhesive polymers as platform for oral controlled drug delivery. II. Synthesis and evaluation of some swelling, water-insoluble bioadhesive polymers. *J. Pharm Sci*. 1985, 74(4):399 – 404.
157. Park, H., Amiji, M., Park, K. Mucoadhesive hydrogels effective at neutral pH. Proc. *Int. Symp. Control. Release Bioact. Mater*. 1989, 16:217–218.
158. Hagerstrom, H., Paulsson, M., Edsman, K. Evaluation of mucoadhesion for two polyelectrolyte gels in simulated physiological conditions using a rheological method. *Eur. J. Pharm. Sci*. 2000, 9 (3):301–309.
159. Sigurdsson, H., Loftsson, T., Lehr, C. Assessment of mucoadhesion by a resonant mirror biosensor. *Int. J. Pharm*. 2006, 325 (1–2), 75– 8.
160. Kamath, K.R., Park, K. Mucosal Adhesive Preparations. In Encyclopedia of Pharmaceutical Technology; Swarbrick, J., Boylan, J. C., Eds.; Marcel Dekker: New York, 1994; pp 133–138.
161. Ugwoke, M.I., Agu, R.U., Verbeke, N., Kinget, R. Nasal mucoadhesive drug delivery: background, applications, trends and future perspectives. *Adv Drug Deliv Rev*. 2005, 57(11):1640-65. doi: 10.1016/j.addr.2005.07.009.
162. Lehr, C.M., Poelma, F.C.G., Junginger, H.E.; Tukker, J.J. An estimate of turnover time of intestinal mucus gel layer in the rats, in situ loop. *Int. J. Pharm*. 1991, 70(1):235–240.
163. Zhang, W., Wang, R., Sun, Z., Zhu, X., Zhao, Q., Zhang, T., Cholewinski, A., Yang, F.K., Zhao, B., Pinnaratip, R., Forooshani, P.K., Lee, B.P. Catechol-functionalized hydrogels: biomimetic design, adhesion mechanism, and biomedical applications. *Chem Soc Rev*. 2020, 49(2):433-464. doi: 10.1039/c9cs00285e.
164. Bovone, G., Dudaryeva, O.Y., Marco-Dufort, B., Tibbitt, M.W. Engineering Hydrogel Adhesion for Biomedical Applications via Chemical Design of the Junction. *ACS Biomater. Sci. Eng*. 2021, 7(9):4048–4076. https://doi.org/10.1021/acsbiomaterials.0c01677.
165. Sudre, G., Olanier, L., Tran, Y., Hourdet, D., Creton, C. Reversible Adhesion between a Hydrogel and a Polymer Brush. *Soft Matter*. 2012, 8:8184–8193. https://doi.org/10.1039/C2SM25868D.
166. Kord Forooshani,P., Lee, B.P. Recent approaches in designing bioadhesive materials inspired by mussel adhesive protein. *J Polym Sci A Polym Chem*. 2017, 55(1):9-33. doi: 10.1002/pola.28368.
167. Waite, J.H., Andersen, S.O. 3,4-dihydroxyphenylalanine in an insoluble shell protein of Mytilus edulis. *Biochim. Biophys. Acta*. 1978, 541:107–114. https://doi.org/10.1016/0304-4165(78)90271-4.
168. Ninan, L., Monahan, J., Stroshine, R.L., Wilker, J.J., Shi, R. Adhesive strength of marine mussel extracts on porcine skin. *Biomaterials*. 2003, 24(22):4091-9. doi: 10.1016/s0142-9612(03)00257-6.
169. Burzio, L.O., Burzio, V.A., Silva, T., Burzio, L.A., Pardo, J. Environmental bioadhesion: themes and applications. *Curr. Opin. Biotechnol*. 1997, 8:309–312. https://doi.org/10.1016/S0958-1669(97)80008-0.
170. Li, C.H, Zuo, J.L. Self-Healing Polymers Based on Coordination Bonds. Advanced Materials. 2019, 1903762. DOI: 10.1002/adma.201903762.
171. Holten-Andersen, N., Harrington M.J., Birkedal, H., Lee, B.P, Messersmith, P.B., Lee, K.Y.C., Waite, J.H. pH-induced metal-ligand cross-links inspired by mussel yield self-healing polymer networks with near-covalent elastic moduli. *Proc. Natl. Acad. Sci. USA*. 2011, 108(7):2651–2655. https://doi.org/10.1073/pnas.1015862108.
172. Holten-Andersen, N., Jaishankar, A., Harrington, M.J., Fullenkamp, D.E., DiMarco, G., He, L., McKinley, G.H., Messersmith, P.B., Lee, K.Y.C. Metal-coordination: using one of nature's tricks to

control soft material mechanics. *J. Mater. Chem*. B. 2014, 2:2467– 2472. https://doi.org/10.1039/C3TB21374A.
173. Krogsgaard, M., Behrens, M.A., Pedersen, J.S., Birkedal, H. Self-healing mussel-inspired multi-pH-responsive hydrogels. *Biomacromolecules.* 2013, 14(2):297-301. doi: 10.1021/bm301844u.
174. Kim, B.J., Cheong, H., Hwang, B.H., Cha, H.J. Mussel-Inspired Protein Nanoparticles Containing Iron(III)–DOPA Complexes for pH-Responsive. *Drug Delivery Chem*. 2015, 127:7426–7430. https://doi.org/10.1002/ange.201501748.
175. Lee, B.P., Narkar, A., Wilharm, R. Effect of metal ion type on the movement of hydrogel actuator based on catechol-metal ion coordination chemistry. *Sens. Actuator. B: Chem*. 2016, 227:248–254. http://doi.org/10.1016/j.snb.2015.12.038.
176. Lee, B.P., Konst, S. Novel Hydrogel Actuator Inspired by Reversible Mussel Adhesive Protein Chemistry. *Adv. Mater*. 2014, 26:3415–3419. https://doi.org/10.1002/adma.201306137.
177. Kim, B.J., Kim, S., Oh, D.X., Masic, A., Cha, H.J., Hwang, D.S. Mussel-inspired adhesive protein-based electrospun nanofibers reinforced by Fe(iii)–DOPA complexation. *J. Mater. Chem. B*. 2015, 3:112–118. https://doi.org/10.1039/C4TB01496K.
178. Krogsgaard, M., Andersen, A., Birkedal, H. Gels and threads: mussel-inspired one-pot route to advanced responsive materials *Chem. Commun*. 2014, 50, 13278–13281. https://doi.org/10.1039/C4CC05293E.
179. Pillai, K.V., Renneckar, S. Cation-pi interactions as a mechanism in technical lignin adsorption to cationic surfaces. *Biomacromolecules*. 2009, 10(4):798-804. doi: 10.1021/bm801284y.
180. Das, S., Rodriguez, N.R.M., Wei, W., Waite, J.H., Israelachvili, J.N. Peptide Length and Dopa Determine Iron-Mediated Cohesion of Mussel Foot Proteins. *Adv. Funct. Mater*. 2015, 25:5840–5847. https://doi.org/10.1002/adfm.201502256.
181. Kim, S., Faghihnejad, A., Lee, Y., Jho, Y., Zeng, H., Hwang, D.S. Cation–π interaction in DOPA-deficient mussel adhesive protein mfp-1. *J. Mater. Chem. B*. 2015, 3:738–743. https://doi.org/10.1039/C4TB01646G.
182. Sato, T., Aoyagi, T., Ebara, M., Auze´ly-Velty, R. Catechol-modified hyaluronic acid: in situ-forming hydrogels by auto-oxidation of catechol or photo-oxidation using visible light. *Polymer Bulletin*. 2017, 74:4069–4085.
183. Moulay, S. Recent Trends in Mussel-Inspired Catechol-Containing Polymers. Part 1 (A Review). Oriental Journal of Chemistry. 2018, 34(3):1153-1197. http://dx.doi.org/10.13005/ojc/340301.
184. Lakshminarayanan, R., Madhavi S., Poh Choo Sim, C. Oxidative Polymerization of Dopamine: A High-Definition Multifunctional Coatings for Electrospun Nanofibers - An Overview. *Dopamine - Health and Disease*. 2018. DOI: 10.5772/intechopen.81036.
185. Lee, H., Dellatore, S.M., Miller, W.M., Messersmith, P.B. Mussel-Inspired Surface Chemistry for Multifunctional Coatings. *Science*. 2007, 318(5849):426-30. doi: 10.1126/science.1147241.
186. Batul, R., Tamanna, T., Khaliqb, A., Yu. A. Recent progress in the biomedical applications of polydopamine nanostructures. *Biomaterials Science*. 2017, 5:1204-1229. https://doi.org/10.1039/C7BM00187H.
187. Gowda, A.H.J., Bu, Y., Kudina, O., Krishna, K.V., Bohara, R.A., Eglin, D., Pandit, A. Design of tunable gelatin-dopamine based bioadhesives. International Journal of Biological Macromolecules. 2020, 164:1384-1391. https://doi.org/10.1016/j.ijbiomac.2020.07.195.
188. Agrawal, P., Soni, S., Mittal, G., Bhatnagar, A. Role of polymeric biomaterials as wound healing agents. *Int J Low Extrem Wounds*. 2014, 13(3):180-90. doi: 10.1177/1534734614544523.
189. Liang, Y., Liang, Y., Zhang, H., Guo, B. Antibacterial biomaterials for skin wound dressing. *Asian J Pharm Sci*. 2022, 17(3):353-384. doi: 10.1016/j.ajps.2022.01.001.
190. Cutting, K., White, R.J. Maceration of the skin and wound bed 1: its nature and causes. *J Wound Care*. 2002, 11:275-278.
191. Maaz Arif, M., Khan, S.M., Gull, N., Tabish, T.A., Zia, S., Ullah Khan, R., Awais, S.M., Arif Butt, M. Polymer-based biomaterials for chronic wound management: Promises and challenges. *Int J Pharm.* 2021, 598:120270. doi: 10.1016/j.ijpharm.2021.120270.
192. Caló, E., Khutoryanskiy, V.V. Biomedical applications of hydrogels: A review of patents and commercial products. *European Polymer Journal*. 2015, 65:252-267. https://doi.org/10.1016/j.eurpolymj.2014.11.024.

193. Hafezi, F., Scoutaris, N., Douroumis, D., Boateng, J. 3D printed chitosan dressing crosslinked with genipin for potential healing of chronic wounds. *Int. J. Pharm*. 2019, 560:406–415. https://doi.org/10.1016/j.ijpharm.2019.02.020.
194. Weller, C.D., Team, V., Sussman, G. First-line interactive wound dressing update: a comprehensive review of the evidence. *Front. Pharmacol*. 2020, 11:155. https:// doi.org/10.1007/s40257-013-0046-410.3389/fphar.2020.00155.
195. Naskar, A., Kim, K.S. Recent Advances in Nanomaterial-Based Wound-Healing Therapeutics. *Pharmaceutics*. 2020, 12(6):499. doi: 10.3390/pharmaceutics12060499.
196. Mihai, M.M., Dima, M.B., Dima, B., Holban, A. Nanomaterials for Wound Healing and Infection Control. *Materials*. 2019, 12:2176. doi: 10.3390/ma12132176.
197. Di Muzio, L., Simonetti, P., Carriero, V.C., Brandelli, C., Trilli, J., Sergi, C., Tirillò, J., Cairone, F., Cesa, S., Radocchia, G., Schippa, S., Petralito, S., Paolicelli, P., Casadei, M.A. Solvent Casting and UV Photocuring for Easy and Safe Fabrication of Nanocomposite Film Dressings. *Molecules,* 2022, 27, 2959. https:// doi.org/10.3390/molecules27092959.
198. Xu, L., Wang, Y.Y., Huang, J., Chen, C.Y., Wang, Z.X., Xie, H. Silver nanoparticles: Synthesis, medical applications and biosafety. *Theranostics*. 2020, 10(20):8996-9031. doi: 10.7150/thno.45413.
199. Li, W.R., Sun, T.L., Zhou, S.L., Ma, Y.M., Shi, Q.S., Xie, X.B., Huang, X.M. A comparative analysis of antibacterial activity, dynamics, and effects of silver ions and silver nanoparticles against four bacterial strains. International Biodeterioration & Biodegradation. 2017, 123:304-310. https://doi.org/10.1016/j.ibiod.2017.07.015.
200. Wang, Z.X., Chen, C.Y., Wang, Y., Li, F.X.Z., Huang, J., Luo, Z.W. et al. Ångstrom scale silver particles as a promising agent for low toxicity broad spectrum potent anticancer therapy. *Adv Funct Mater.* 2019; 29:1808556. DOI:10.1002/adfm.201808556.
201. Lin, J., Huang, Z., Wu, H., Zhou, W., Jin, P., Wei, P., et al. Inhibition of autophagy enhances the anticancer activity of silver nanoparticles. *Autophagy*. 2014; 10:2006-2020. DOI: 10.4161/auto.36293.
202. Mikhailova, E.O. Silver Nanoparticles: Mechanism of Action and Probable Bio-Application. *J Funct Biomater*. 2020, 11(4):84. doi: 10.3390/jfb11040084.
203. Pangli, H., Vatanpour, S., Hortamani, S., Jalili, R., Ghahary, A. Incorporation of Silver Nanoparticles in Hydrogel Matrices for Controlling Wound Infection. *J Burn Care Res*. 2021, 42(4):785-793. doi: 10.1093/jbcr/iraa205.
204. Shi, G., Chen, W., Zhang, Y., Dai, X., Zhang, X., Wu, Z. An Antifouling hydrogel contained silver nanoparticles for modulating therapeutic immune response in chronic wound healing. *Langmuir.* 2019, 35:1837–1845. https://doi.org/10.1021/acs.langmuir.8b01834.
205. Roppolo, I., Doriguzzi Bozzo, A., Castellino, M., Chiappone, A., Perrone, D., Bejtka, K., Bocchini, S., Sangermano, M., Chiolerio, A. Dual step irradiation process for in situ generation and patterning of silver nanoparticles in a photocured film. *RSC Advances*. 2016, 6:14832–14843. https://doi.org/10.1039/C5RA24234G.
206. Yagci, Y., Sangermano, M., G. Rizza. Synthesis and Characterization of Gold−Epoxy Nanocomposites by Visible Light Photoinduced Electron Transfer and Cationic Polymerization Processes. *Polymer*. 2008, 49:5195-5198. https://doi.org/10.1021/ma801776y.
207. Sangermano, M., Roppolo, I., Camara, V.H.A, Dizman, C., Ates, S., Torun, L., Yagci, Y. Polysulfone/Metal Nanocomposites by Simultaneous Photoinduced Crosslinking and Redox Reaction. *Macromolecular Materials and Engineering*. 2011, 296:820-825. https://doi.org/10.1002/mame.201000440.
208. Kopecek, J. Hydrogel biomaterials: a smart future? *Biomaterials*. 2007, 28(34):5185-92. doi: 10.1016/j.biomaterials.2007.07.044.
209. Caló, E., Khutoryanskiy, V.V. Biomedical applications of hydrogels: A review of patents and commercial products. *European Polymer Journal*. 2015, 65:252–267. https://doi.org/10.1016/j.eurpolymj.2014.11.024.
210. Ahmed, E.M. Hydrogel: Preparation, characterization, and applications: A review. *J Adv Res*. 2015, 6(2):105-21. doi: 10.1016/j.jare.2013.07.006.
211. Peppas, N.A, Bures, P., Leobandung, W., Ichikawa, H. Hydrogels in pharmaceutical formulations. *Eur J Pharm Biopharm*. 2000, 50(1):27-46. doi: 10.1016/s0939-6411(00)00090-4.
212. Parhi, R. Cross-Linked Hydrogel for Pharmaceutical Applications: A Review. *Adv Pharm Bull*. 2017, 7(4):515-530. doi: 10.15171/apb.2017.064.

213. Calvo Catoira, M., Fusaro, L., Di Francesco, D., Ramella, M., Boccafoschi, F. Overview of natural hydrogels for regenerative medicine applications. *Journal of Materials Science: Materials in Medicine*. 2019, 30:115. https://doi.org/10.1007/s10856-019-6318-7.
214. Takei, T., Yoshihara, R., Danjo, S., Fukuhara, Y., Evans, C., Tomimatsu, R., Ohzuno, Y., Yoshida, M. Hydrophobically-modified gelatin hydrogel as a carrier for charged hydrophilic drugs and hydrophobic drugs. *Int. J. Biol. Macromol*. 2020, 149:140–147. https://doi.org/10.1016/j.ijbiomac.2020.01.227.
215. Zhao, X., Wang, Z. A pH-sensitive microemulsion-filled gellan gum hydrogel encapsulated apigenin: Characterization and in vitro release kinetics. *Colloids Surf. B Biointerfaces.* 2019, 178:245–252. https://doi.org/10.1016/j.colsurfb.2019.03.015.
216. Nazlı, A.B., Açıkel, Y.S. Loading of cancer drug resveratrol to pH-Sensitive, smart, alginate-chitosan hydrogels and investigation of controlled release kinetics. *J. Drug Deliv. Sci. Technol*. 2019, 53:101199. https://doi.org/10.1016/j.jddst.2019.101199.
217. Fonseca, L.P., Trinca, R.B., Felisberti, M.I. Amphiphilic polyurethane hydrogels as smart carriers for acidic hydrophobic drugs. *Int. J. Pharm*. 2018, 546:106–114. DOI: 10.1016/j.ijpharm.2018.05.034.
218. Wang, P., Huang, S., Hu, Z., Yang, W., Lan, Y., Zhu, J., Hancharou, A., Guo, R., Tang, B. In situ formed anti-inflammatory hydrogel loading plasmid DNA encoding VEGF for burn wound healing. *Acta Biomater*. 2019, 100:191–201. https://doi.org/10.1016/j.actbio.2019.10.004.
219. Tamahkar, E., Özkahraman, B., Sülo ˘glu, A.K.; Idil, N., Perçin, I. A novel multilayer hydrogel wound dressing for antibiotic release. *J. Drug Deliv. Sci. Technol*. 2020, 58:101536. https://doi.org/10.1016/j.jddst.2020.101536.
220. Wang, Z., Hu, W., Du, Y., Xiao Y., Wang X., Zhang S., Wang J., and Mao C. Green gas-mediated cross-linking generates biomolecular hydrogels with enhanced strength and excellent hemostasis for wound healing. *ACS Appl. Mater. Interfaces.* 2020, 12:13622–13633. https://doi.org/10.1021/acsami.9b21325.
221. Abbasi, A.R., Sohail, M., Minhas, M.U., Khaliq, T., Kousar, M., Khan, S., Hussain, Z., and Munir, A. Bioinspired sodium alginate based thermosensitive hydrogel membranes for accelerated wound healing. *Int. J. Biol. Macromol.* 2020, 155:751–765. https://doi.org/10.1016/j.ijbiomac.2020.03.248.
222. Carthew, J., Donderwinkel, I., Shrestha, S., Truong, V.X., Forsythe, J.S., Frith, J.E. In situ miRNA delivery from a hydrogel promotes osteogenesis of encapsulated mesenchymal stromal cells. *Acta Biomater*. 2020, 101:249–261.
223. Bombaldi de Souza, R.F., Bombaldi de Souza, F.C., Thorpe, A., Mantovani, D., Popat, K.C., Moraes, Â.M. Phosphorylation of chitosan to improve osteoinduction of chitosan/xanthan-based scaffolds for periosteal tissue engineering. *Int J Biol Macromol*. 2020, 143:619-632. doi: 10.1016/j.ijbiomac.2019.12.004.
224. Hsu, F.Y., Chen, J.J., Sung, W.C., Hwang, P.A. Preparation of a Fucoidan-Grafted Hyaluronan Composite Hydrogel for the Induction of Osteoblast Differentiation in Osteoblast-Like Cells. *Materials.* 2021, 14:1168. doi: 10.3390/ma14051168.
225. Fan, C., Shi, J., Zhuang, Y., Zhang, L., Huang, L., Yang, W., Chen, B., Chen, Y., Xiao, Z., Shen, H., Zhao, Y., Da, J. Myocardial-infarction-responsive smart hydrogels targeting matrix metalloproteinase for on-demand growth factor delivery. *Adv. Mater.* 2019, 31:1902900. https://doi.org/10.1002/adma.201902900.
226. Vacanti, J.P., Langer, R. Tissue engineering: the design and fabrication of living replacement devices for surgical reconstruction and transplantation. *Lancet*. 1999, 354, 1:SI32-4. doi: 10.1016/s0140-6736(99)90247-7.
227. Langer, R. Tissue engineering. *Molecular Therapy*. 2000, 1(1):12-15. Doi:10.1006/mthe.1999.0003.
228. Xu, F., Dawson, C., Lamb, M., Mueller, E., Stefanek, E., Akbari, M., Hoare, T. Hydrogels for Tissue Engineering: Addressing Key Design Needs Toward Clinical Translation. *Front Bioeng Biotechnol*. 2022, 10:849831. doi: 10.3389/fbioe.2022.849831.
229. Radulescu, D.M., Neacsu, I.A., Grumezescu, A.M., Andronescu, E. New Insights of Scaffolds Based on Hydrogels in Tissue Engineering. *Polymers (Basel).* 2022, 14(4):799. doi: 10.3390/polym14040799.
230. Pita-Lopez, M.L., Fletes-Vargas, G., Espinosa-Andrews, H., Rodríguez-Rodríguez, R. Physically cross-linked chitosan-based hydrogels for tissue engineering applications: A state-of-the-art review. *European Polymer Journal*. 2021, 145:110176. https://doi.org/10.1016/j.eurpolymj.2020.110176.
231. Vasile, C., Pamfil, D., Stoleru, E., Baican, M. New Developments in Medical Applications of Hybrid Hydrogels Containing Natural Polymers. *Molecules*. 2020, 25(7):1539. doi: 10.3390/molecules25071539.

232. Yang, J., Jacobsen, M.T., Pan, H., Kopecek, J. Synthesis and characterization of enzymatically degradable PEG-based peptide-containing hydrogels. *Macromol Biosci*. 2010, 10(4):445-54. doi: 10.1002/mabi.200900295.
233. Bajpai, S.K., Saxena, S. Enzymatically degradable and pH-sensitive hydrogels for colon-targeted oral drug delivery. I. Synthesis and characterization. *Journal of Applied Polymer Science*. 2004, 92:3630-3643. https://doi.org/10.1002/app.20283.
234. Vigata, M., O'Connell, C.D., Cometta, S., Hutmacher, D.W., Meinert, C., Bock, N. Gelatin Methacryloyl Hydrogels for the Localized Delivery of Cefazolin. *Polymers (Basel)*. 2021, 13(22):3960. doi: 10.3390/polym13223960.
235. Goto R, Nishida E, Kobayashi S, Aino M, Ohno T, Iwamura Y, Kikuchi T, Hayashi JI, Yamamoto G, Asakura M, Mitani A. Gelatin Methacryloyl-Riboflavin (GelMA-RF) Hydrogels for Bone Regeneration. *Int J Mol Sci*. 2021, 22(4):1635. doi: 10.3390/ijms22041635.
236. Velasco-Rodriguez, B., Diaz-Vidal, T., Rosales-Rivera, L.C., García-González, C.A., Alvarez-Lorenzo, Al-Modlej, A., Domínguez-Arca, V., Prieto, G., Barbosa, S., Soltero Martínez, J.F.A., Taboad, P. Hybrid Methacrylated Gelatin and Hyaluronic Acid Hydrogel Scaffolds. Preparation and Systematic Characterization for Prospective Tissue Engineering Applications. *Int. J. Mol. Sci*. 2021, 22(13):6758. https://doi.org/10.3390/ijms22136758.
237. Oudshoorn, M.H.M., Rissmann, R., Bouwstra, J.A., Hennink, W.E. Synthesis of methacrylated hyaluronic acid with tailored degree of substitution. *Polymer*. 2007, 48(7):1915-1920. https://doi.org/10.1016/j.polymer.2007.01.068.
238. Ondeck, M.G., Engler, A.J. Mechanical Characterization of a Dynamic and Tunable Methacrylated Hyaluronic Acid Hydrogel. *J Biomech Eng*. 2016, 138(2):021003. doi: 10.1115/1.4032429.
239. Schuurmans, C.C.L., Mihajlovic, M., Hiemstra, C., Ito, K., Hennink, W.E., Vermonden, T. Hyaluronic acid and chondroitin sulfate (meth)acrylate-based hydrogels for tissue engineering: Synthesis, characteristics and pre-clinical evaluation. *Biomaterials*. 2021, 268:120602. doi: 10.1016/j.biomaterials.2020.120602.
240. Madduma-Bandarage, U.S.K., Madihally, S.V. Synthetic hydrogels: Synthesis, novel trends, and applications. *Journal of Applied Polymer Science.* 2020, 138(19):50376. DOI: 10.1002/app.50376.
241. Akhtar, M.F., Hanif, M., Ranjha, N.M. Methods of synthesis of hydrogels … A review. *Saudi Pharm J*. 2016, 24(5):554-559. doi: 10.1016/j.jsps.2015.03.022.
242. Teixeira, L.S., Feijen, J., van Blitterswijk, C.A., Dijkstra, P.J., Karperien, M. Enzyme-catalyzed crosslinkable hydrogels: emerging strategies for tissue engineering. *Biomaterials*. 2012, 33(5):1281-90. doi: 10.1016/j.biomaterials.2011.10.067.
243. Bustamante-Torres, M., Romero-Fierro, D., Arcentales-Vera, B., Palomino, K., Magaña, H., Bucio, E. Hydrogels Classification According to the Physical or Chemical Interactions and as Stimuli-Sensitive Materials. *Gels*. 2021, 7(4):182. doi: 10.3390/gels7040182.
244. Cao, H., Chang, X., Mao, H., Zhou, J., Wu, Z.L., Shan, G., Bao, Y., Pan, P. Stereocomplexed physical hydrogels with high strength and tunable crystallizability. *Soft Matter*. 2017, 13(45):8502-8510. https://doi.org/10.1039/C7SM01491K.
245. Holback, H., Yeo, Y., Park, K. Hydrogel swelling behavior and its biomedical applications. *Biomedical Hydrogels*. 2011, 3-24. https://doi.org/10.1533/9780857091383.1.3.
246. Drury, J.L., Mooney, D.J. Hydrogels for tissue engineering: scaffold design variables and applications. *Biomaterials*. 2003, 24(24):4337-51. doi: 10.1016/s0142-9612(03)00340-5.
247. Radulescu, D.M., Neacsu, I.A., Grumezescu, A.M., Andronescu, E. New Insights of Scaffolds Based on Hydrogels in Tissue Engineering. *Polymers (Basel)*. 2022, 14(4):799. doi: 10.3390/polym14040799.
248. Karoyo, A.H., Wilson, L.D. A Review on the Design and Hydration Properties of Natural Polymer-Based Hydrogels. *Materials (Basel)*. 2021, 14(5):1095. doi: 10.3390/ma14051095.
249. Chirani, N., Yahia, Lh., Gritsch, L., Motta, F.L., Chirani, S., Faré, S. History and Applications of Hydrogels. *Journal of Biomedical Sciences.* 2015, 4(2). DOI: 10.4172/2254-609X.100013.
250. Cacopardo, L., Guazzelli, N., Nossa, R., Mattei, G., Ahluwalia, A. Engineering hydrogel viscoelasticity. *J Mech Behav Biomed Mater*. 2019, 89:162-167. doi: 10.1016/j.jmbbm.2018.09.031.
251. Boardman, P. Modelling the Mechanical Properties of Hydrogel. iGEM, 2020.
252. Li, X., Sun, Q., Li, Q., Kawazoe, N., Chen, G. Functional Hydrogels with Tunable Structures and Properties for Tissue Engineering Applications. *Front Chem*. 2018, 6:499. doi: 10.3389/fchem.2018.00499.

253. Vedadghavami, A., Minooei, F., Mohammadi, M.H., Khetani, S., Rezaei Kolahchi, A., Mashayekhan, S., Sanati-Nezhad A. Manufacturing of hydrogel biomaterials with controlled mechanical properties for tissue engineering applications. *Acta Biomater*. 2017, 62:42-63. doi: 10.1016/j.actbio.2017.07.028.
254. Henderson, T.M.A., Ladewig, K., Haylock, D.N., McLeanb, K.M., O'Connor, A.J. Cryogels for biomedical applications. *J. Mater. Chem*. B. 2013, 1:2682. DOI: 10.1039/c3tb20280a.
255. Rogers, Z.J., Bencherif, S.A. Cryogelation and Cryogels. *Gels*. 2019, 5(4):46. doi: 10.3390/gels5040046.
256. Savina, I.N., Zoughaib, M., Yergeshov, A.A. Design and Assessment of Biodegradable Macroporous Cryogels as Advanced Tissue Engineering and Drug Carrying Materials. *Gels*. 2021, 7(3):79. doi: 10.3390/gels7030079.
257. Dogu, S., Okay, O. Tough organogels based on polyisobutylene with aligned porous structures. *Polymer*. 2008, 49:4626–4634.
258. Tureyen, O.E., Yilmaz, A., Yakan, S.D., Yetiskin, B., Okay, O., Okay, O.S. Performance of butyl rubber-based macroporous sorbents as passive samplers. *Environ. Sci. Pollut. Res*. 2021, 28:3766–3773.
259. He, Y., Wang, C., Wang, C., Xiao, Y., Lin, W. An Overview on Collagen and Gelatin-Based Cryogels: Fabrication, Classification, Properties and Biomedical Applications. *Polymers (Basel)*. 2021, 13(14):2299. doi: 10.3390/polym13142299.
260. Jones, L.O., Williams, L., Boam, T., Kalmet, M., Oguike, C., Hatton, F.L. Cryogels: recent applications in 3D-bioprinting, injectable cryogels, drug delivery, and wound healing. *Beilstein J Org Chem*. 2021, 17:2553-2569. doi: 10.3762/bjoc.17.171.
261. Hwang, Y.S., Zhang, C., Varghese, S. Poly(ethylene glycol) cryogels as potential cell scaffolds: effect of polymerization conditions on cryogel microstructure and properties. *J. Mater. Chem*. 2010, 20:345–351.
262. Chang, K.H., Liao, H.T., Chen, J.P. Preparation and characterization of gelatin/hyaluronic acid cryogels for adipose tissue engineering: In vitro and In Vivo studies. *Acta Biomater*. 2013, 9:9012–9026.
263. Macková, H., Plichta, Z., Hlídková, H., Sedláček, O., Konefal, R., Sadakbayeva, Z., Dušková-Smrčková, M., Horák, D., Kubinová, Š. Reductively Degradable Poly(2-hydroxyethyl methacrylate) Hydrogels with Oriented Porosity for Tissue Engineering Applications. *ACS Appl. Mater. Interfaces*. 2017, 9:10544–10553. doi:10.1021/acsami.7b01513
264. Sen, T., Ozcelik, B., Ozmen, M.M. Tough and hierarchical porous cryogel scaffolds preparation using n-butanol as a non-solvent. *Int. J. Polym. Mater. Polym. Biomater*. 2019, 68:411–416. doi:10.1080/00914037.2018.1452225.
265. Memic, A., Colombani, T., Eggermont, L.J., Rezaeeyazdi, M., Steingold, J., Rogers, Z.J., Joshi Navare, K., Mohammed, H.S., Bencherif, S.A. Latest Advances in Cryogel Technology for Biomedical Applications. Advanced Therapeutics. 2019, 2(4):1800114. https://doi.org/10.1002/adtp.201800114.
266. Kim, S.H., Turnbull, J., Guimond, S. Extracellular matrix and cell signalling: the dynamic cooperation of integrin, proteoglycan and growth factor receptor. *J Endocrinol*. 2011, 209(2):139-51. doi: 10.1530/JOE-10-0377.
267. Hynes, R.O. Integrins: versatility, modulation, and signaling in cell adhesion. *Cell*. 1992, 69(1):11-25. doi: 10.1016/0092-8674(92)90115-s.
268. Hynes, R.O. Integrins: a family of cell surface receptors. *Cell*. 1987, 48(4):549-54. doi: 10.1016/0092-8674(87)90233-9.
269. Ruoslahti, E., Pierschbacher, M.D. New perspectives in cell adhesion: RGD and integrins. *Science.* 1987, 238(4826):491-7. doi: 10.1126/science.2821619.
270. Cukierman, E., Pankov, R., Stevens, D.R., Yamada, K.M. Taking cell-matrix adhesions to the third dimension. *Science*. 2001, 294(5547):1708-12. doi: 10.1126/science.1064829.
271. Bacáková, L., Filová, E., Rypácek, F., Svorcík, V., Starý, V. Cell adhesion on artificial materials for tissue engineering. *Physiol Res*. 2004, 53 Suppl 1:S35-45.
272. Ahearne, M. Introduction to cell-hydrogel mechanosensing. *Interface Focus*. 2014, 4(2):20130038. doi: 10.1098/rsfs.2013.0038.
273. Spicer, C.D. Hydrogel scaffolds for tissue engineering: the importance of polymer choice. *Polymer Chemistry*. 2020, 11:184. https://doi.org/10.1039/C9PY01021A.
274. Bellis, S.L. Advantages of RGD peptides for directing cell association with biomaterials. *Biomaterials.* 2011, 32(18):4205-10. doi: 10.1016/j.biomaterials.2011.02.029.

275. Tan, G., Xu, J., Yu, Q., Zhang, J., Hu, X., Sun, C., Zhang, H. Photo-Crosslinkable Hydrogels for 3D Bioprinting in the Repair of Osteochondral Defects: A Review of Present Applications and Future Perspectives. *Micromachines (Basel).* 2022, 13(7):1038. doi: 10.3390/mi13071038.
276. Su, K., Wang, C. Recent advances in the use of gelatin in biomedical research. *Biotechnol Lett*. 2015, 37(11):2139-45. doi: 10.1007/s10529-015-1907-0.
277. Di Muzio, L., Cienzo, F., Paolicelli, P., Petralito, S., Garzoli, S., Brandelli, C., Trilli, J., Casadei, M.A. A convenient strategy to synthesize highly tunable gelatin methacryloyl with very low gelation temperature. European Polymer Journal. 2021, 154:110538. https://doi.org/10.1016/j.eurpolymj.2021.110538.
278. Velasco-Rodriguez, B., Diaz-Vidal, T., Rosales-Rivera, L.C., García-González, C.A., Alvarez-Lorenzo, C., Al-Modlej, A., Domínguez-Arca, V., Prieto, G., Barbosa, S., Soltero Martínez, J.F.A, Taboada, P. Hybrid Methacrylated Gelatin and Hyaluronic Acid Hydrogel Scaffolds. Preparation and Systematic Characterization for Prospective Tissue Engineering Applications. *Int. J. Mol. Sci*. 2021, 22:6758. https:// doi.org/10.3390/ijms22136758.
279. Eke, G., Mangir, N., Hasirci, N., MacNeil, S., Hasirci, V. Development of a UV crosslinked biodegradable hydrogel containing adipose derived stem cells to promote vascularization for skin wounds and tissue engineering. *Biomaterials*. 2017, 129:188–198. doi: 10.1016/j.biomaterials.2017.03.021.
280. Rebers, L., Granse, T., Tovar, G.E.M., Southan, A., Borchers, K. Physical Interactions Strengthen Chemical Gelatin Methacryloyl Gels. *Gels*. 2019, 5(1):4. doi: 10.3390/gels5010004.
281. Piao, Y., You, H., Xu, T., Bei, H.P., Zvi Piwko, I., Kwan, Y.Y., Zhao, X. Biomedical applications of gelatin methacryloyl hydrogels. Engineered Regeneration. 2021, 2:47-56. https://doi.org/10.1016/j.engreg.2021.03.002.
282. Van Den Bulcke, A.I., Bogdanov, B., De Rooze, N., Schacht, E.H., Cornelissen, M., Berghmans, H. Structural and rheological properties of methacrylamide modified gelatin hydrogels. *Biomacromolecules*. 2000, 1(1):31-8. doi: 10.1021/bm990017d.
283. Van Hoorick, J., Gruber, P., Markovic, M., Tromayer, M., Van Erps, J., Thienpont, H., Liska, R., Ovsianikov, A., Dubruel, P., Van Vlierberghe, S. Cross-Linkable Gelatins with Superior Mechanical Properties Through Carboxylic Acid Modification: Increasing the Two-Photon Polymerization Potential. *Biomacromolecules*. 2017, 18(10):3260-3272. doi: 10.1021/acs.biomac.7b00905.
284. Sajkiewicz, P., Kołbuk, D. Electrospinning of gelatin for tissue engineering – molecular conformation as one of the overlooked problems. 2014, 25:2009-2022. https://doi.org/10.1080/09205063.2014.975392.
285. Villard, P., Rezaeeyazdi, M., Colombani, T., Joshi-Navare, K., Rana, D., Memic, A., Bencherif, S.A. Autoclavable and Injectable Cryogels for Biomedical Applications. *Adv Healthc Mater*. 2019, 8(17):e1900679. doi: 10.1002/adhm.201900679.
286. Han, M-E., Kang, B.J., Kim, S.H., Kim, H.D., Hwang, N.S. Gelatin-based extracellular matrix cryogels for cartilage tissue engineering. Journal of Industrial and Engineering Chemistry. 2017, 45:421-429. https://doi.org/10.1016/j.jiec.2016.10.011.
287. Díaz-Montes, E. Dextran: Sources, Structures, and Properties. *Polysaccharides*. 2021, 2(3):554-565; https://doi.org/10.3390/polysaccharides2030033.
288. Maia, J., Evangelista, M.B., Gil, H., Ferreira, L. Dextran-based materials for biomedical applications. *Carbohydrates Applications in Medicine*. 2014, 31-53.
289. Sun, G., Mao, J.J. Engineering dextran-based scaffolds for drug delivery and tissue repair. *Nanomedicine (Lond).* 2012, 7(11):1771-84. doi: 10.2217/nnm.12.149. PMID: 23210716; PMCID: PMC4620435.
290. Franssen, O., Vandervennet, L., Roders, P., Hennink, W.E. Degradable dextran hydrogels: controlled release of a model protein from cylinders and microspheres. *J Control Release*. 1999, 60(2–3):211–221. doi: 10.1016/s0168-3659(99)00074-7.
291. Liebert, T., Hornig, S., Hesse, S., Heinze, T. Nanoparticles on the basis of highly functionalized dextrans. *J Am Chem Soc*. 2005, 127(30):10484–10485. doi: 10.1021/ja052594h.
292. Long, L.X., Yuan, X.B., Chang, J. Self-assembly of polylactic acid and cholesterol-modified dextran into hollow nanocapsules. *Carbohydr Polym*. 2012, 87(4):2630–2637.
293. Sun, G., Chu, C.C. Self-assembly of chemically engineered hydrophilic dextran into microscopic tubules. *ACS Nano*. 2009, 3(5):1176–1182. doi: 10.1021/nn800704q.

294. Sun, G., Chu, C.C. Synthesis, characterization of biodegradable dextran-allyl isocyanate-ethylamine/ polyethylene glycol-diacrylate hydrogels and their in vitro release of albumin. *Carbohydr Polym*. 2006, 65(3):273–287. DOI: 10.1016/j.carbpol.2006.01.015.
295. Sun, G., Shen, Y.I., Ho, C.C., Kusuma, S., Gerecht, S. Functional groups affect physical and biological properties of dextran-based hydrogels. *J Biomed Mater Res Part A*. 2010, 93A(3):1080–1090. doi: 10.1002/jbm.a.32604.
296. Sun, G.M., Chen, F.A., Chu, C.C. Effects of precursor and cross-linking parameters on the properties of dextran-allyl isocyanate-ethylamine/poly(ethylene glycol diacrylate) biodegradable hydrogels and their release of ovalbumin. *J Biomater Sci Polym Ed*. 2009, 20(14):2003–2022. doi: 10.1163/156856208X396353.
297. Van Tomme, S.R., Hennink, W.E. Biodegradable dextran hydrogels for protein delivery applications. *Expert Rev Med Devices*. 2007, 4(2):147–164. doi: 10.1586/17434440.4.2.147.
298. Wang, H., Zhou, L., Liao, J., Tan, Y., Ouyang, K., Ning, C., Ni, G., Tan, G. Cell-laden photocrosslinked GelMA-DexMA copolymer hydrogels with tunable mechanical properties for tissue engineering. *J Mater Sci Mater Med.* 2014, 25(9):2173-83. doi: 10.1007/s10856-014-5261-x.
299. Liu, Y., Chan-Park, M.B. Hydrogel based on interpenetrating polymer networks of dextran and gelatin for vascular tissue engineering. *Biomaterials*. 2009, 30(2):196–207. doi: 10.1016/j.biomaterials.2008.09.041.
300. Laronha, H., Caldeira, J. Structure and Function of Human Matrix Metalloproteinases. *Cells.* 2020, 9(5):1076. doi: 10.3390/cells9051076.
301. Miao, T., Wang, J., Zeng, Y., Liu, G., Chen, X. Polysaccharide-Based Controlled Release Systems for Therapeutics Delivery and Tissue Engineering: From Bench to Bedside. *Adv Sci (Weinh).* 2018, 5(4):1700513. doi: 10.1002/advs.201700513.
302. Di Muzio, L., Paolicelli, P., Brandelli, C., Cesa, S., Trilli, J., Petralito, S., Casadei, M.A. Injectable and in-situ gelling dextran derivatives containing hydrolysable groups for the delivery of large molecules. *Gels.* 2021, 7(4):150. https://doi.org/10.3390/gels7040150.
303. van Dijk-Wolthuis, W.N., van Steenbergen, M.J., Underberg, W.J., Hennink, W.E. Degradation kinetics of methacrylated dextrans in aqueous solution. *J Pharm Sci*. 1997 Apr;86(4):413-7. doi: 10.1021/js9604220. PMID: 9109041.

APPENDIX

OTHER PUBLICATIONS

European Polymer Journal 154 (2021) 110538

Contents lists available at ScienceDirect

European Polymer Journal

journal homepage: www.elsevier.com/locate/europolj

A convenient strategy to synthesize highly tunable gelatin methacryloyl with very low gelation temperature

Laura Di Muzio, Federica Cienzo, Patrizia Paolicelli, Stefania Petralito, Stefania Garzoli, Chiara Brandelli, Jordan Trilli, Maria Antonietta Casadei *

Dipartimento di Chimica e Tecnologie del Farmaco, "Sapienza" Università di Roma, P.le Aldo Moro 5, 00185 Rome, Italy

ARTICLE INFO

Keywords:
Gelatin methacryloyl synthesis
^{1}H NMR
Internal standard method
Rheology
Gelation temperature
Derivatization degree

ABSTRACT

Gelatin methacryloyl (GelMA) is a polymeric derivative of gelatin (Gel) widely used in tissue engineering, as well as in wound dressing and drug delivery field. This work offers an alternative and convenient method for the synthesis and characterization of GelMA. In particular, the methacrylation was carried out under homogeneous single-phase reaction conditions, which allows of obtaining a good reproducibility of the derivatization degree of the polymer in a simple and fast way. The experimental conditions were adequately optimized to have the methacrylation of only ε-amino groups of lysine and hydroxylysine, as confirmed by FT-IR and ^{1}H NMR analysis. The degree of derivatization of GelMA was determined using an internal standard applied to ^{1}H NMR analysis. Based on these measurements, it was found that the optimized reaction proceeds to complete functionalization of ε-amino groups of lysine and hydroxylysine. The effect of the reaction conditions on the rheological properties of GelMA was investigated through temperature sweep experiments and compared with those of the polymer obtained under traditional heterogeneous reaction conditions. A significant difference was found in the gelation temperature of GelMA synthesized following the two different procedures. In particular, the proposed single-phase synthetic protocol gave a polymer which behaves like a solution when used at 10% w/v concentration and even at temperatures as low as 5 °C, whereas the polymer obtained with the classic biphasic procedure behaves like a gel within the same range of temperatures and when used at the same concentration. These results are particularly interesting as they could open GelMA to new applications particularly in the biomedical field.

1. Introduction

The use of polymers in tissue engineering field is getting more and more widespread, as it provides support for cell growth before surgical implantation, but also replacement of different damaged tissues, performing their characteristics and functions [1]. The material used must have adequate chemical, physical and mechanical properties, similar to the biological tissue to replace, which may range from a rigid and resistant tissue such as bone, to a fibrous tissue like the heart valves, until to a soft tissue like the skin [2–4]. Among all investigated polymers, gelatin (Gel) is considered a very promising and attractive biomaterial and is widely investigated for biomedical applications [5,6]. Gel is a well-known biodegradable and biocompatible polymer obtained from the hydrolytic degradation of collagen, the most abundant protein present in the connective tissue of skin, cartilage and bones. The growing interest in Gel use stems from its numerous advantages and desirable features: it is a highly available and economic polymer and, compared to its precursor, less immunogenic and more soluble. At the same time, it preserves the typical bioactive groups of collagen, such as the amino acid sequence RGD (Arg-Gly-Asp) and the MMP-sensitive degradation sites (Matrix MetalloProteinases), which promote cell adhesion, migration, differentiation and proliferation. Furthermore, Gel has many lateral functional groups (carboxylic, amino and hydroxyl groups), that allow the formation of covalent bonds with growth factors and cytokines, to promote further the mentioned cellular processes. For all these outstanding properties, Gel has proven to be easier to use for biomedical purposes and very suitable as an extracellular matrix mimic for regenerative medicine. Indeed, it has been broadly used both to fabricate scaffolds for tissue engineering application and to produce bioinks for 3D bioprinting. However, due to Gel solubility at body temperature, high susceptibility to proteolysis and poor mechanical properties of its physical hydrogels, several strategies were developed to

* Corresponding author: Department of Drug Chemistry and Technologies. "Sapienza" University of Rome, Piazzale Aldo Moro 5, 00185 Rome, Italy.
E-mail address: mariaantonietta.casadei@uniroma1.it (M. Antonietta Casadei).

https://doi.org/10.1016/j.eurpolymj.2021.110538
Received 22 April 2021; Received in revised form 14 May 2021; Accepted 24 May 2021
Available online 27 May 2021

increase the thermal, mechanical and enzymatic stability of Gel networks at physiological conditions, via the formation of chemical crosslinks [7–11]. Gel can be crosslinked either without prior modification or after functionalization of its side groups. Among all the investigated crosslinking alternatives, the modification of Gel with methacrylic groups to give gelatin methacryloyl (GelMA) emerged as the most convenient and straightforward material processing for tissue engineering purposes [12–17]. GelMA is a derivative of Gel containing methacrylamide groups and a usually lower number of methacrylic esters. The introduction of methacrylic substituents gives the polymer the property of crosslinking to form chemical hydrogels with the desired properties. The chemical modification of Gel with methacrylic groups generally involves less than 5% of the amino acid residues and most functional amino acid motifs, such as the RGD and MMP-degradable motifs, are not affected by the derivatization. Therefore, GelMA is certainly an ideal candidate and a versatile platform for tissue engineering. Although different protocols have been reported in the literature for the synthesis of GelMA [12], essentially, they all refer, with minor modifications, to the general method described for the first time by Van Den Bulcke in 2000 [13]. According to this procedure, GelMA is synthesized by direct reaction of Gel with methacrylic anhydride (MAA) in phosphate buffer (PBS, pH=7.4) at 50 °C. The synthesis protocol presents several problems, all essentially related to the biphasic nature of the reaction environment: an excessive quantity of added MAA, long purification times and extensive variability of the derivatization degree (DD) of the obtained product. Various attempts have been made in order to improve the synthesis procedure for Gel methacrylation [18–22] and although some progress has been made, GelMA synthesis still remains suboptimal. This drawback has stimulated our interest in the research for an alternative method of GelMA synthesis, which envisaged a reaction in a single phase, in order to reduce both the amount of added anhydride and the consequent purification time, and make reproducible the polymer DD. Therefore, the present work focuses on the optimization of the synthesis of GelMA in homogeneous single-phase reaction conditions and on the characterization of the obtained derivatives. To this end, an organic dipolar aprotic solvent, such as DMSO, was used to dissolve both Gel and MAA. Under these conditions Gel should show a superior chain flexibility, and, as a result, the accessibility of its functional groups should be increased, making them more prone to react. Indeed, replacement of water by DMSO is reported to prevent the formation of collagen-like triple-helix structures typical of Gel in water [23,24]. Therefore, the single-phase reaction conditions could give GelMA derivatives showing different properties compared to those obtained by the classic biphasic synthesis procedure. Indeed, the properties of GelMA solutions depend on the chemical structure of the deployed macromonomers, and in particular on the derivatization degree [18]. For this reason, particular attention was paid to the quantification of the methacrylation degree, that is fundamental to optimize the crosslinking kinetics of GelMA and to tailor the biophysiochemical properties of the polymer and its derived hydrogels. However, the DD cannot be easily determined in a unique and reproducible manner due to the variability in the composition of the polymer [25]. Indeed, considering the complex composition of Gel and the presence of different functional groups on the amino acid residues, both lateral hydroxyl groups and amine groups can possibly react with MAA during functionalization of the protein, giving both methacrylamide and methacrylate derivatives. Therefore, in this work, an internal standard method associated to ^{1}H NMR analysis was adopted for the accurate quantification of the DD and to evaluate its effect on the rheological properties of the polymer. Other spectroscopic analyses were also used to determine the amount of MAA necessary to produce the selective derivatization of lysine and hydroxylysine residues.

2. Materials and methods

2.1. Materials

Type A gelatin from pig skin (~300 g Bloom), anhydrous dimethylsulfoxide (DMSO), deuterated water (D_2O), deuterated dimethylsulfoxide (DMSO-d_6), methacrylic anhydride (MAA), triethylamine (TEA), nicotinamide (Nic), 2-hydroxyethyl methacrylate (HEMA), N-*tert*-butyldimethylsilyl-N-methyltrifluoroacetamide (MTBSTFA), N-methyl-N-(trimethylsilyl) trifluoroacetamide (MSTFA), bis(trimethylsilyl) acetamide (BSA), N,N-dimethylformamide, pyridine and dialysis tubes (cut-off 12–14 kDa) were purchased from Sigma Aldrich. Ethanol (EtOH), 37% w/w hydrochloric acid (HCl), glacial acetic acid (CH_3COOH), monobasic potassium phosphate (KH_2PO_4), sodium hydroxide in pellets (NaOH) and distilled water were purchased from Carlo Erba. Potassium bromide (KBr) for FT-IR analysis was obtained from Fluka. All the reagents were of analytical purity.

2.2. Synthesis of GelMA

2.2.1. Two-phase synthesis of GelMA

GelMA was synthesized following the method reported in the literature [13]. Briefly, Gel was solubilised for 1 h at 50 °C in phosphate buffer (PBS, pH=7.4) at a concentration of 10% w/v under vigorous magnetic stirring. Following complete solubilisation, 2.5 or 1.5 mL of MAA/g Gel were added drop by drop. The resulting biphasic system was left to react at 50 °C for 3 h, and the reaction was interrupted by dilution (x5) with PBS previously heated at 50 °C. The mixture was dialyzed at a temperature above 37 °C to avoid gelation of the polymer inside the dialysis tubes. After 5 days of dialysis, the polymer solution was freeze-dried with a LIO5P freeze-dryer. The obtained polymers were labelled as $GelMA_{2.5\text{-dp}}$ and $GelMA_{1.5\text{-dp}}$, according to the amount of MAA used.

2.2.2. Single-phase synthesis of GelMA

The new synthetic strategy involves the solubilisation of Gel in anhydrous DMSO at a concentration of 5% w/v for 1 h at 50 °C, under magnetic stirring. After complete solubilisation, MAA was added in different proportions in order to evaluate the influence of the reagent quantity on the methacrylation degree of the final product. The solution was kept under magnetic stirring at 50 °C; then it was dialyzed exhaustively against deionized water at 37 °C for 3 days and freeze-dried. Beside the amount of MAA, also the addition of triethylamine (TEA) and the reaction time were investigated as parameters potentially affecting the functionalization of GelMA. All the experimental applied conditions are summarized in Table 1.

2.3. FT-IR characterization

All the synthesized polymers were analysed by FT-IR spectroscopy in the solid state, as such or dispersed in dry KBr. The spectra were recorded with a Spectrum-One Perkin Elmer spectrophotometer equipped with an ATR detector, in the range of 4000–600 cm^{-1} and processed with Spekwin32 software.

Table1
Experimental conditions of the single-phase synthesis of GelMA.

	MAA (mL/g Gel)	[Gel] (% w/v)	TEA:MAA (mol ratio)	Reaction time (h)
$GelMA_{2.5}$	2.5	5	1:1	24
	2.5	5	1:1	3
	2.5	5	–	3
$GelMA_{1.0}$	1.0	5	–	3
$GelMA_{0.5}$	0.5	5	–	3
$GelMA_{0.3}$	0.3	5	–	3
$GelMA_{0.1}$	0.1	5	–	3

2.4. NMR characterization and determination of the derivatization degree

Aliquots (10 mg) of the polymer samples were dissolved in 0.7 mL of D_2O for ^1H NMR analysis. All spectra were recorded using a Bruker AC-400 spectrometer.

^1H NMR analysis was also employed to determine the degree of derivatization (DD) of GelMA, using an internal standard. For this purpose, 10 mg of GelMA were first dissolved in 0.5 mL of D_2O, and then 0.2 mL of a 1 mg/mL solution of nicotinamide in D_2O were added.

2.5. Quantification of lysine content of gelatin

The lysine content of Gel was determined on hydrolyzed samples of the polymer. To this end, hydrolysis was carried out following a standard procedure [26]. Raw Gel was dissolved in 6 N HCl at concentration 10 mg/mL and hydrolyzed at 110 °C for 24 h, under argon atmosphere.

2.5.1. GC–MS determination of lysine content

The lysine content of Gel was determined by GC–MS analysis on hydrolyzed Gel samples.

For the generation of reliable quantitative data, 180 μL of 3,4-dihydroxybenzoic acid as internal standard was added to 40 μL of the hydrolyzate. The obtained solution was dried in an oven at 40° C for 15 h.

For the derivatization of the sample, three different silylation reagents were used: N-*tert*-butyldimethylsilyl-N-methyltrifluoroacetamide (MTBSTFA), N-methyl-N-(trimethylsilyl) trifluoroacetamide (MSTFA) and bis(trimethylsilyl) acetamide (BSA). In all cases 250 μL of each single reagent were added to the dried solution at 80 °C for a reaction time of 4 h. Only with MTBSTFA, 100 μL of N,N-dimetilformammide (DMF) and 5 μL of triethylamine (TEA) were also added, and the reaction was catalyzed by 5 μL of pyridine. Better yields were obtained by using BSA reagent.

The derivatized samples were analyzed with a Perkin-Elmer GC–MS system, consisting of a gas chromatograph Perkin Elmer Clarus 500 model (Waltham, MA, USA), equipped with flame ionization detector (FID) directly coupled to a mass spectrometer with an electron ionization (EI) source. A Varian FactorFour VF-1 fused-silica capillary column (length 60 m × 0.32 mm ID × 1.0 μm film thickness) was used with helium as carrier gas (1.0 mL/min). One μL of derivatized sample was injected onto the column. The injector temperature was 250 °C. The oven GC temperature profile was: isothermal hold at 100 °C for 1 min followed by a ramp of 8 °C/min to 200 °C, a second ramp to 350 °C at rate of 8 °C/min hold for 10 min; the injector temperature was 280 °C.

The mass spectrometer operative conditions were the following: ionization voltage, 70 eV; ion source temperature, 200 °C; scan mode, 40.0–500.0 mass range.

2.5.2. NMR determination of lysine content

The lysine content of Gel was determined by ^1H NMR analysis on hydrolyzed Gel samples. The samples for the ^1H NMR analysis were prepared by vacuum-drying aliquots (0.5 mL) of the hydrolysate and solubilising them in 0.6 mL of D_2O. 15 μL of a 50 mg/mL solution of 2-hydroxyethyl methacrylate (HEMA) in D_2O was added to each sample as internal standard.

2.6. Rheological measurements

Gel and GelMA solutions were characterized for their rheological properties using a Discovery TA HR-2 stress-control rheometer. A parallel-plate geometry with a diameter of 40 mm (α 1.005°, gap 27 μm) was used for all the experiments. Solutions of Gel, $GelMA_{0.1}$ and $GelMA_{1.5\text{-}dp}$ (10% and 15% w/v) were prepared by solubilising the polymers in demineralized water at 50.00 °C under magnetic stirring for 1 h. Aliquots of 0.3 mL of the obtained solutions were loaded onto the Peltier plate of the rheometer at 50.00 °C and the temperature was decreased till 15.00 °C. The samples were held between the plates at 15.00 °C for 10 min before starting the analysis. All measurements were carried out using a solvent trap to prevent water evaporation. Oscillatory temperature-sweeps were performed by increasing the temperature from 15.00 to 45.00 °C, at constant frequency of 1 rad/s and heating rate of 3.00 °C/min. The gel-sol transition temperature ($T_{gel\text{-}sol}$) was determined by the G'/G'' crossover temperature. All the experiments were carried out at least in triplicate. For each sample, the linear viscoelastic range was previously evaluated using oscillatory strain-sweep tests: a 10% maximum deformation was used.

3. Results and discussion

3.1. Synthesis and characterization of GelMA

The two-phase protocol for GelMA synthesis was proposed for the first time by Van Den Bulcke [13] and extensively applied by several different research groups with just minor modifications. Despite the wide diffusion of this synthesis protocol, it suffers from various problems and drawbacks. In particular, the use of an excessive quantity of MAA, long purification times and poor batch-to-batch reproducibility are the main issues, which are related to the specific conditions adopted for the reaction. Indeed, Gel methacrylation proceeds under two-phase reaction conditions, so that the rate of MAA addition and the conditions of mixing might have deep effects on the quality of the dispersion, and consequently, on the DD of the final product. Therefore, in this work, an effort was made to develop a strategy to synthesize GelMA under homogeneous single-phase reaction conditions, in order to eliminate the drawbacks of the currently used method. To this end, an organic dipolar aprotic solvent, such as DMSO, able to dissolve both Gel and MAA, was chosen for the reaction. The polymer concentration was fixed at 5% w/v and after 1 h of solubilisation, triethylamine (TEA) and MAA (1:1 mol ratio) were added. TEA was used to neutralize the methacrylic acid produced, as its formation could slow down the methacrylation reaction of Gel and reduce the DD of the obtained derivatives [22]. Therefore, equimolar amounts of TEA and MAA were used in the synthesis protocol. In a first attempt, 2.5 mL MAA/g Gel were used, which correspond to the same amount of anhydride usually employed in the two-phase reaction procedure. The reaction was continued for 24 and 3 h, and after these two reaction times the solution was submitted to exhaustive dialysis and then lyophilized.

FT-IR spectra were recorded on both derivatives and compared with raw Gel. The FT-IR spectrum of $GelMA_{2.5}$ obtained after 24 h of reaction shows a characteristic signal at 1723 cm^{-1}, that can be attributed to the stretching vibration of the carbonyl ($\nu_{C=O}$) of an ester group (red curve in Fig. 1). It is likely that, using a high amount of MAA, the derivatization of Gel involves not only the ε-amino group of the lysine and hydroxylysine residues, but also the side-chain OH groups of other amino acids. Same results were also achieved reducing significantly the reaction time, showing that the reaction is fast and quantitative already after 3 h. Moreover, the reaction was also conducted without the use of TEA and, also in this case, no relevant differences were observed in the resulting product, evidencing the capacity of Gel to self-buffer the pH of the medium during the reaction.

Based on these results the subsequent reactions were carried out fixing at 3 h the reaction time and removing the base, whereas the amount of MAA was varied. By reducing the amount of the anhydride from 2.5 to 1.0 g/mL, no significant variations were observed in the FT-IR spectra of the derivatized polymers, as shown in Fig. 1 (red and green curves).

On the contrary, lowering further the MAA volume to 0.5, 0.33 and 0.1 mL, the band at 1723 cm^{-1} was no more visible. Therefore, changing the amount of MAA, methacrylate and/or methacrylamide derivatives of Gel can be obtained. For a useful comparison, FT-IR spectra of the products obtained after 3 h of reaction time and using 2.5, 1.0, 0.5, 0.3 and 0.1 mL of MAA per g of gelatin ($GelMA_{2.5}$, $GelMA_{1.0}$, $GelMA_{0.5}$, $GelMA_{0.3}$ and $GelMA_{0.1}$), are reported in Fig. 1. According to these

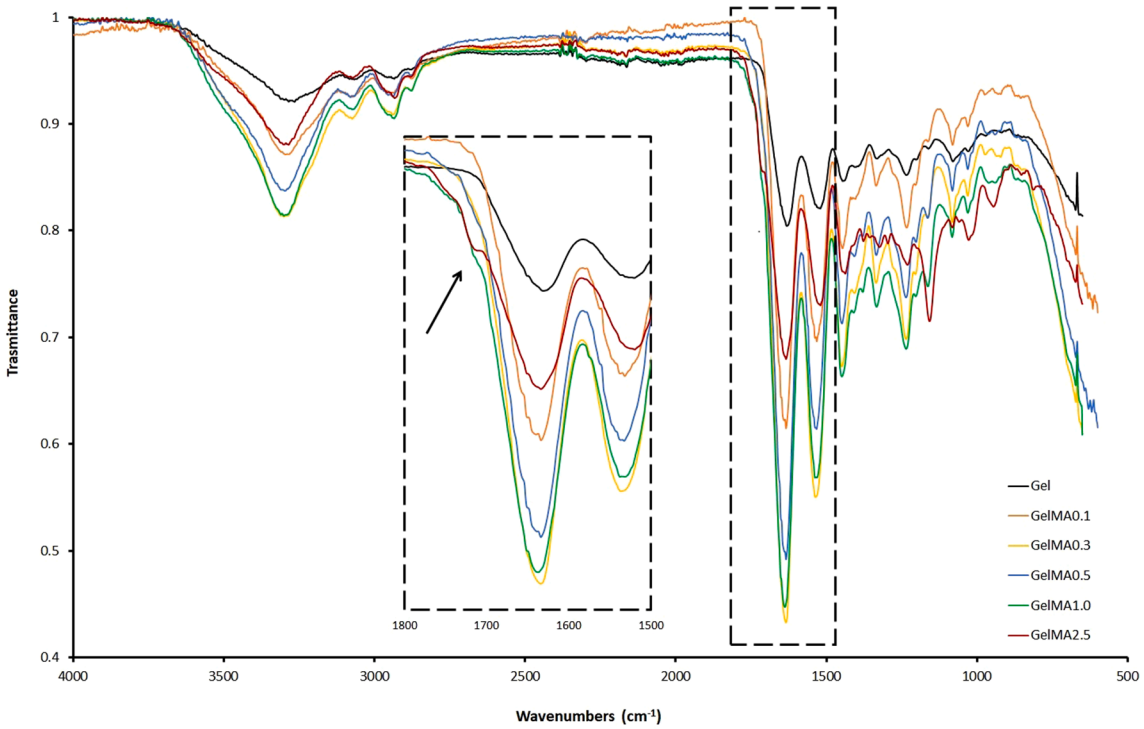

Fig. 1. FT-IR spectra of Gel and GelMA obtained with different amount of methacrylic anhydride. In the dashed box it is reported an expansion of the spectra from 1500 to 1800 cm^{-1}. The arrow points at the band at 1723 cm^{-1} attributed to the $\nu_{C=O}$ of an ester group.

results, the molar ratio between Gel and MAA has a deep effect on the methacrylation of the polymer and in particular, it seems to be possible to finely regulate the feed ratio of Gel to MAA to produce the preferential derivatization of the ε-amino group of lysine and hydroxylysine residues, instead of a mixture of gelatin methacrylamide and gelatin methacrylate.

To further characterize the products obtained, all these derivatives were subjected to ^{1}H NMR analysis (Fig. 2). $GelMA_{2.5}$, $GelMA_{1.0}$, $GelMA_{0.5}$ and $GelMA_{0.3}$ spectra show multiple peaks in the region of methacrylic protons, that indicates the formation, in all these cases, of both methacrylamide and methacrylate derivatives. However, while FT-IR spectroscopy evidenced this behaviour only for $GelMA_{2.5}$ and $GelMA_{1.0}$, ^{1}H NMR analysis proved that multi-derivatization of Gel occurs also when 0.5 and 0.3 mL of MAA were used to produce $GelMA_{0.5}$ and $GelMA_{0.3}$, respectively.

Only the ^{1}H NMR spectrum of the product obtained with 0.1 mL MAA/g Gel ($GelMA_{0.1}$) shows two distinct signals relating to the vinyl protons of methacrylamide group, suggesting a selective derivatization of lysine and hydroxylysine amino acids (Fig. 2). These results confirm that when the reaction is carried out in DMSO, the accessibility of the functional groups of Gel is increased and they are more prone to react. Additionally, the ^{1}H NMR spectra of all the GelMA products did not show the presence of the byproduct methacrylic acid, whose specific peaks normally appear at 5.7, 5.3 and 1.8 ppm. Therefore, unlike other synthesis procedures [27], in this case it was possible to obtain the complete purification of GelMA.

The main challenge of GelMA synthesis is to precisely control the DD and consequently the properties of GelMA, because less controllable reaction systems can lead to less reproducible outcomes. All the diverse biomedical applications of this polymer critically depend on the possibility to finely tune its physicochemical properties by adjusting the DD. In this way, GelMA derived biomaterials result in tailored solution viscosity, gelling behaviour, equilibrium degree of swelling as well as mechanical strength. While the precise evaluation of the GelMA DD

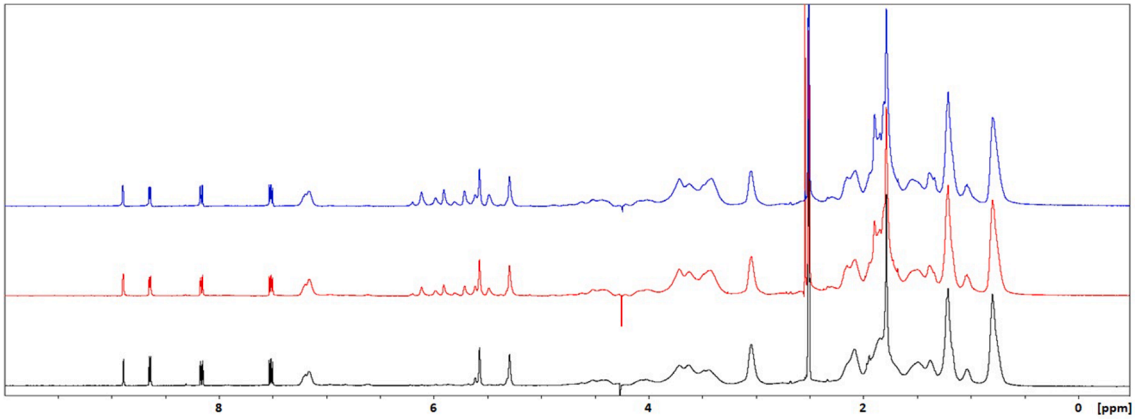

Fig. 2. ^{1}H NMR spectra of $GelMA_{2.5}$ (blue), $GelMA_{0.5}$ (red) and $GelMA_{0.1}$ (black). The grey area evidenced the peaks between 5.0 and 6.4 ppm corresponding to vinyl protons of methacrylate and methacrylamide groups.

represents a fundamental characterization to fully exploit the advantageous properties of this polymer in the biomedical field, current applied analytical techniques are inappropriate for correct characterization of GelMA and accurate quantification of its DD. Indeed, common techniques for quantifying the DD of GelMA include monitoring the decrease of free lysine amino groups upon modification. This can be achieved either by spectrophotometric assays, such as the Habeeb's method based on the use of 2,4,6-trinitrobenzensulfonic acid (TNBSA) to give the trinitrophenyl derivative of the protein [28], or by ^{1}H NMR spectroscopy, integrating the ε-CH_2 signal of lysine at 2.9 ppm [29]. While both these methods are rather simple, it is evident, that they can be properly applied only with methacrylamide derivatives of Gel, as methacryl groups bound to hydroxyl residues are fully neglected. Another method using ^{1}H NMR spectroscopy relies on the signal of the aromatic protons of Gel, which can be used to calculate the total content of methacryloyl groups of GelMA, provided that the aromatic amino acid content of the Gel raw material is known [18]. Therefore, accurate application of this method requires prior determination of the precise amino acid composition of the starting Gel. All that considered, for the purpose of DD quantification of GelMA, we adopted an alternative procedure, similar to the method recently proposed by Claaßen and coworkers [25]. This method is based on ^{1}H NMR spectroscopy with the use of an internal standard. Nicotinamide was chosen as internal standard to evaluate the DD of GelMA.

The quantification of the DD of the Gel derivatives was achieved through comparison of the integrals of the standard signals with those of the methacrylic protons. In specific, the mmoles of methacrylic groups present in 10 mg of sample were determined from the ratio between the average area of the methacrylic protons and the area of the aromatic proton of nicotinamide at 8.84 ppm, and taking into account the mmoles of the standard used. The DD was expressed as mmoles of methacrylic groups per gram of polymer ($mmol_{MA}$/g Gel). This method allowed to calculate the total degree of methacrylation of GelMA, but also to differentiate between methacrylamide and methacrylate derivatives, as reported in Fig. 3. To separate the contribution of methacrylate and methacrylamide groups the peaks were attributed according to literature data [25,27]. In specific, the signal at 5.30 ppm (highlighted by the dark blue box in the ^{1}H NMR reported in Fig. 3A) was used to quantify the methacrylamide groups, whereas the signals at 5.49, 5.81, 6.12 and 6.21 ppm (highlighted by the light blue box in the ^{1}H NMR reported in Fig. 3A) were used to calculate the methacrylate groups. The results of the calculations of the DD are shown in Fig. 3B. The methacrylamide groups remained almost constant for all GelMA derivatives, while the number of methacrylate groups increased with increasing amounts of MAA. Furthermore, the derivatization of lysine and hydroxylysine for $GelMA_{0.1}$ samples was highly reproducible, and equal to 0.39 ± 0.01 $mmol_{MA}$/g Gel.

The products obtained through the single-phase reaction method were compared with those produced by the classic two-phase protocol. The two-phase reactions were carried out using 2.5 and 1.5 mL MAA/g Gel, as commonly reported in literature, and also these derivatives were characterized by ^{1}H NMR. The ^{1}H NMR spectrum of $GelMA_{2.5\text{-dp}}$ exhibited several peaks in the region of the methacrylic protons, therefore indicating that the methacrylation reaction proceeds in a not preferential way for the ε-amino groups of lysine and hydroxylysine. In contrast, $GelMA_{1.5\text{-dp}}$ show two stark peaks of the vinyl protons, as observed for $GelMA_{0.1}$, with a DD of 0.35 ± 0.07 $mmol_{MA}$/g. Therefore, a similar DD can be obtained with the classic synthesis procedure, but using an amount of MAA 15 times higher than that employed for $GelMA_{0.1}$ and with a significantly lower reproducibility.

Once determined the DD of GelMA, further analyses were carried out with the aim of confirming that the use of 0.1 mL MA/g Gel was sufficient to produce the selective derivatization of the ε-amino groups of lysine and hydroxylysine residues. To this end, the mmoles of these amino acids in raw Gel were carefully quantified. A first instrumental analytical approach involved the use of the Gas Chromatography technique and, in order to obtain volatile analytes suitable for GC analysis, the silylation of the amino acids of Gel was performed. Unfortunately, this technique has not proved robust enough in our hands, because the quantitation of lysine was not a reproducible data over time. In addition, some amino acids such as arginine, histidine and hydroxylysine, could not be measured because they were not detected, while their presence in raw Gel is well known. This result led us to use an alternative analytical method, based on ^{1}H NMR spectroscopy with an internal standard. In this case, HEMA was selected as internal standard and the mmoles of lysine were determined considering the ratio between the average area of the vinyl protons of HEMA (6.0–5.6 ppm) and the area of the $–CH_2NH_2$ methylene protons of lysine (2.9 ppm). Knowing the mmoles of HEMA corresponding to the area of methacrylic proton peaks, it was possible to determine those corresponding to the area of lysine. The mmoles of lysine per gram of Gel were equal to 0.30 ± 0.01 mmol/g. This value was comparable and slightly lower than the mmoles of methacrylic groups, confirming an almost selective derivatization of lysine and hydroxylysine residues in $GelMA_{0.1}$ samples. This result also allows confirming the information already obtained by ^{1}H NMR that the synthesis carried out using 0.1 mL MAA/g Gel gave a quantitative reaction involving all lysine residues. A similar result can be obtained following the double-phase synthesis procedure with 1.5 mL MAA/g Gel. In fact, also in this case, the reaction can be considered quantitative and selective for lysine and hydroxylysine, however the amount of MAA needed was 15 times higher than that used in the single-phase reaction protocol.

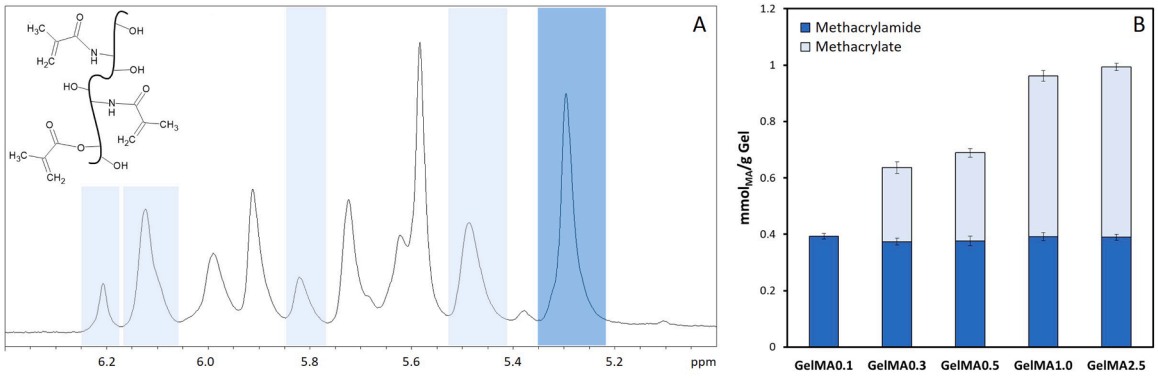

Fig. 3. (A) Expansion of the ^{1}H NMR of $GelMA_{2.5}$ in D_2O. The dark blue and light blue boxes evidenced the signals used to calculate respectively the methacrylamide and methacrylate groups. (B) Effect of the amount of MAA on the DD of GelMA, evaluated by ^{1}H NMR spectroscopy with the use of the internal standard nicotinamide. The DD was expressed as $mmol_{MA}$/g Gel and differentiated between methacrylamide and methacrylate derivatives and for the calculation were considered the peaks evidenced by the dark (methacrylamide) and light blue (methacrylate) areas.

It is therefore evident how to carry out the synthesis in DMSO allows using a much lower amount of anhydride to obtain quantitative and selective derivatization of Gel. Moreover, with this new method of synthesis it is possible to avoid the use of a base to buffer the solution, because the buffer capacity of the gelatin amino acids is enough to maintain constant the pH of the medium during the reaction, without affecting the final DD. Dialysis times are significantly shorter, because it is not necessary to remove the large quantity of salts needed to buffer the methacrylic acid produced, due to the MAA excess. Additionally, the purification process was very effective and allowed obtaining pure polymers with no traces of methacrylic acid. Finally, the possibility of carrying out the synthesis in single-phase conditions eliminates all the experimental variables that dramatically influence the DD of the final product with the classic procedure, and allows attaining high reproducibility of the substitution and batch-to-batch consistency.

3.2. Rheological characterization of GelMA

Temperature sweeps were performed on raw Gel at concentrations major than its critical concentration and on its derivatives $GelMA_{0.1}$ and $GelMA_{1.5\text{-}dp}$. Gel solutions at 10 and 15% w/v were prepared at 50.00 °C, as reported in the experimental Section 2.6, and poured on the rheometer plate. The dependence of the elastic (G') and viscous (G'') moduli from temperature was determined by oscillatory shear deformation, measured during a temperature scan from 15.00 to 45.00 °C (heating rate = 3.00 °C/min). The corresponding mechanical spectra are reported in Fig. 4A.

At 15.00 °C both raw Gel samples are transparent gels due to disseminated physical crosslinks or "junction zones" formed by ordered triple helical collagen-like sequences, separated along the chain contour by peptide residues in the disorder conformation [30]. On heating, both G' and G" moduli of the Gel samples decrease and the crossover and inversion of the two moduli occurs at a temperature value corresponding to the gel-sol transition temperature ($T_{gel\text{-}sol}$), which denotes the transition from an elastic network to a polymeric solution. As expected, increasing the polymer concentration from 10 to 15% w/v, the value of G' modulus increases as well as the $T_{gel\text{-}sol}$ (from 31.56 to 34.85 °C). The mechanical spectra of $GelMA_{0.1}$ and $GelMA_{1.5\text{-}dp}$ are reported in Fig. 4C and D, respectively. Both synthetic procedures of GelMA produced derivatives with G' and $T_{gel\text{-}sol}$ values lower than those of raw Gel at the same concentration. These results indicate that physical structuring is less pronounced when Gel is modified with methacrylic groups that may interfere with helix formation [12]. G' and crossover temperature values increase with the concentration, but they are different for $GelMA_{0.1}$ and $GelMA_{1.5\text{-}dp}$. In particular, the concentration being the same, the G' and the $T_{gel\text{-}sol}$ values are lower for GelMA synthesized in DMSO. In detail, $GelMA_{0.1}$ at 15% w/v shows moduli crossover at 21.05 °C, while $GelMA_{1.5\text{-}dp}$ at 30.44 °C. At a concentration of 10% w/v the crossover temperature of $GelMA_{1.5\text{-}dp}$ is 27.16 °C, whereas $GelMA_{0.1}$ does not present crossover of the G' and G'' moduli over all the temperature range investigated. In order to understand this behaviour, raw Gel was dissolved in DMSO and submitted to the same experimental conditions adopted in the single-phase synthetic procedure, without the addition of MAA. The polymer recovered after dialysis and freeze-drying was submitted to temperature sweep analysis and compared to raw untreated Gel. The mechanical spectra of both treated and untreated polymer at a concentration of 15% w/v are reported in Fig. 4B. It is evident that the $T_{gel\text{-}sol}$ value of the treated Gel (31.33 °C) is lower respect to starting Gel one (34.67 °C). G' of treated and raw Gel were also gone through similar variations. Moreover, the same behaviour was also observed at a

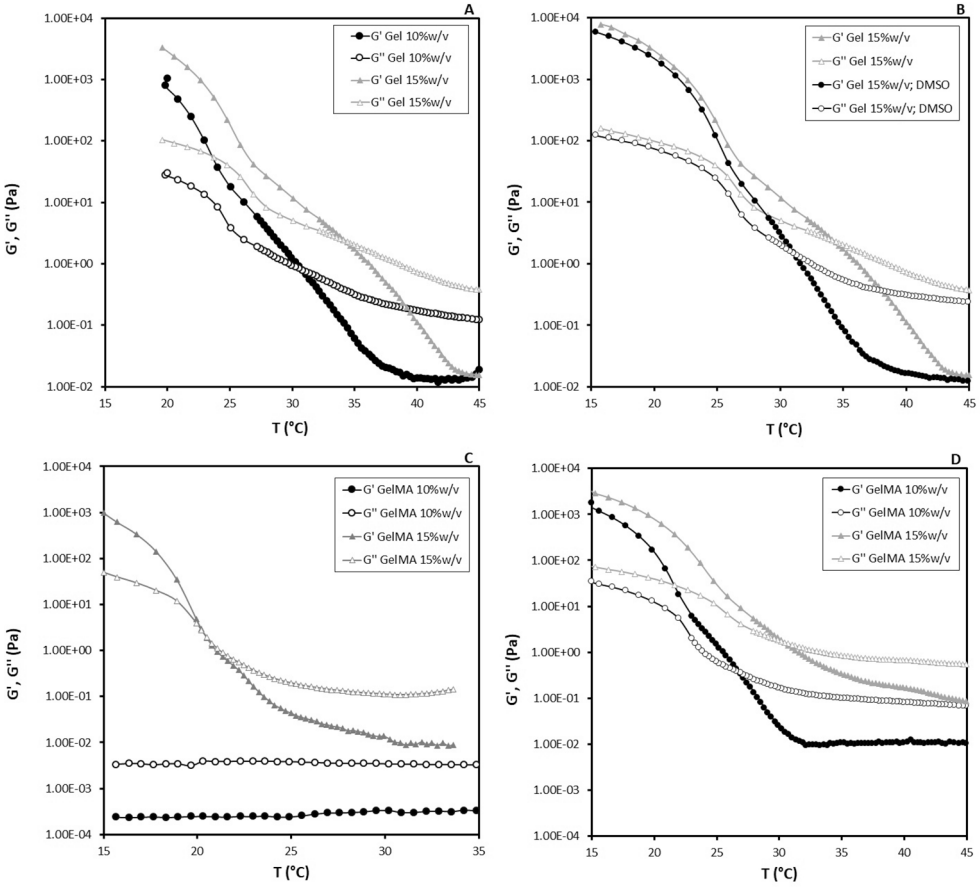

Fig. 4. Temperature sweeps of (A) raw Gel at 10 and 15% w/v. (B) Gel dissolved at 15% w/v in demineralized water in its raw form or after treatment in DMSO, as established in the single-phase synthetic procedure, without the addition of MAA. (C) $GelMA_{0.1}$ at 10 and 15% w/v. (D) $GelMA_{1.5\text{-}dp}$ at 10 and 15% w/v.

concentration of 10% w/v (data not shown). It is probably that DMSO is able to destroy the physical interactions among the polymer chains, which were not completely reformed during the purification step by dialysis. Weakening of the intermolecular and intramolecular interactions of GelMA macromolecules can also be obtained with polymers synthesized according to the classic procedure, but only with samples characterized by very high degree of methacrylation [18].

Therefore, the characteristic rheological behaviour makes GelMA synthesized following the two synthetic procedures adequate and interesting for distinct applications. In some cases, in fact, the solid-like behaviour of GelMA at room temperature may represent a severe limit to its use [18]. The control of the rheological behaviour of the precursor solutions of GelMA has become increasingly interesting. Indeed, future medical technology based on regenerative medicine needs flexible and effective platforms, e.g. liquid handling techniques, which can lead, for example, to easily controllable and automatable processes. As observed, GelMA synthesized according to the novel proposed procedure does not undergo the sol–gel transition up to temperatures around 5 °C, when used at a concentration of 10% w/v, while it is able to form highly reproducible chemical gels due to the great batch-to-batch consistency. Similar results were also obtained with GelMA derivatives with very high methacrylation degree synthesized following the classic biphasic procedure [18]. Anyway, it has been reported that hydrogels produced using methacrylamide GelMA have better properties than those obtained from derivatives characterized by the presence of both methacrylamide and methacrylate groups [31]. Therefore, the results obtained in this work may open GelMA to novel applications in biomedical and pharmaceutical fields.

4. Conclusions

Gelatin methacryloyl-based hydrogels are widely used as polymeric matrix in tissue engineering, wound dressing and drug delivery. Its favourable properties of biocompatibility, biodegradability, non-cytotoxicity, non-immunogenicity and extensive versatility of the mechanical properties, make GelMA hydrogels the biomaterial of choice for these applications.

However, its use frequently suffers from inadequate control of the methacrylation degree and scarce batch-to-batch consistency. The novel method of synthesis of GelMA, and its optimization, has made possible to obtain an excellent reproducibility of the substitution degree of the polymer, maintaining the simplicity of the process and accelerating the purification time.

The application of the internal standard method to the ^{1}H NMR analysis allowed the accurate quantification of the degree of methacrylation of GelMA, which is fundamental to control the mechanical and physical properties of its networks and to formulate polymeric matrices finely tuned for the specific application considered. Therefore, the adoption of this method for the routine characterization of GelMA is suggested and recommended.

Finally, the reaction conditions affect the rheological behaviour of GelMA. The proposed procedure produced derivatives with very low gelation temperatures which could open the polymer to novel applications in the biomedical and pharmaceutical fields.

CRediT authorship contribution statement

Laura Di Muzio: Conceptualization, Data curation, Formal analysis, Investigation, Project administration, Writing - original draft. **Federica Cienzo:** Investigation. **Patrizia Paolicelli:** Conceptualization, Formal analysis, Methodology, Project administration, Writing - original draft. **Stefania Petralito:** Formal analysis, Methodology, Supervision, Writing - original draft. **Stefania Garzoli:** Data curation, Investigation, Methodology, Writing - original draft. **Chiara Brandelli:** Investigation. **Jordan Trilli:** Investigation. **Maria Antonietta Casadei:** Conceptualization, Funding acquisition, Methodology, Supervision, Writing - original draft.

Declaration of Competing Interest

The authors declare that they have no known competing financial interests or personal relationships that could have appeared to influence the work reported in this paper.

Acknowledgements

The authors wish to thank Sapienza University of Rome for the financial support.

Data availability

The raw/processed data required to reproduce these findings cannot be shared at this time due to technical or time limitations.

References

[1] P. Nezhad-Mokhtari, M. Ghorbani, L. Roshangar, J. Soleimani Rad, A review on the construction of hydrogel scaffolds by various chemically techniques for tissue engineering, Eur. Polym. J. 117 (2019) 64–76.
[2] K.S. Ogueri, T. Jafari, J.L. Escobar Ivirico, C.T. Laurencin, Polymeric biomaterials for scaffold-based bone regenerative engineering, Regen, Eng. Transl. Med. 5 (2019) 128–154.
[3] K.H. Nakayama, M. Shayan, N.F. Huang, Engineering biomimetic materials for skeletal muscle repair and regeneration, Adv. Healthc. Mater. 8 (2019) 1801168.
[4] Y. Han, W. Yang, W. Cui, K. Yang, X. Wang, Y. Chen, L. Deng, Y. Zhao, W. Jin, Development of functional hydrogels for heart failure, J. Mater. Chem. B 7 (2019) 1563–1580.
[5] M.C. Echave, R. Hernáez-Moya, L. Iturriaga, J.L. Pedraz, R. Lakshminarayanan, A. Dolatshahi-Pirouz, N. Taebnia, G. Orive, Recent advances in gelatin-based therapeutics, Expert Opin. Biol. Ther. 19 (2019) 773–779.
[6] D.A. Gyles, L.D. Castro, J.O. Carréra Silva, R.M. Ribeiro-Costa, A review of the designs and prominent biomedical advances of natural and synthetic hydrogel formulations, Eur. Polym. J. 88 (2017) 373–392.
[7] J. Van Hoorick, L. Tytgat, A. Dobos, H. Ottevaere, J. Van Erps, H. Thienpont, A. Ovsianikov, P. Dubruel, S. Van Vlierberghe, (Photo-)crosslinkable gelatin derivatives for biofabrication applications, Acta Biomater. 97 (2019) 46–73.
[8] M.C. Echave, L.S. del Burgo, J.L. Pedraz, G. Orive, Gelatin as biomaterial for tissue engineering, Curr. Pharm. Des. 23 (2017) 3567–3584.
[9] V.B. Djagny, Z. Wang, S. Xu, Gelatin: a valuable protein for food and pharmaceutical industries: a review, Crit. Rev. Food Sci. Nutr. 41 (2001) 481–492.
[10] S. Young, M. Wong, Y. Tabata, A.G. Mikos, Gelatin as a delivery vehicle for the controlled release of bioactive molecules, J. Control. Release 109 (2005) 256–274.
[11] S. Gorgieva, V. Kokol, Collagen- vs. Gelatine-Based Biomaterials and Their Biocompatibility: Review and Perspectives, Biomater. Appl. Nanomed. (InTech) (2011), https://doi.org/10.5772/24118.
[12] K. Yue, G. Trujillo-de Santiago, M.M. Alvarez, A. Tamayol, N. Annabi, A. Khademhosseini, Synthesis, properties, and biomedical applications of gelatin methacryloyl (GelMA) hydrogels, Biomaterials 73 (2015) 254–271.
[13] A.I. Van Den Bulcke, B. Bogdanov, N. De Rooze, E.H. Schacht, M. Cornelissen, H. Berghmans, Structural and rheological properties of methacrylamide modified gelatin hydrogels, Biomacromolecules 1 (2000) 31–38.
[14] J.W. Nichol, S.T. Koshy, H. Bae, C.M. Hwang, S. Yamanlar, A. Khademhosseini, Cell-laden microengineered gelatin methacrylate hydrogels, Biomaterials 31 (2010) 5536–5544.
[15] B.J. Klotz, D. Gawlitta, A.J.W.P. Rosenberg, J. Malda, F.P.W. Melchels, Gelatin-methacryloyl hydrogels: towards biofabrication-based tissue repair, Trends Biotechnol. 34 (2016) 394–407.
[16] S. Xiao, T. Zhao, J. Wang, C. Wang, J. Du, L. Ying, J. Lin, C. Zhang, W. Hu, L. Wang, K. Xu, Gelatin methacrylate (GelMA)-based hydrogels for cell transplantation: an effective strategy for tissue engineering, Stem Cell Rev. 15 (2019) 664–667.
[17] D. Loessner, C. Meinert, E. Kaemmerer, L.C. Martine, K. Yue, P.A. Levett, T.J. Klein, F.P. Melchels, A. Khademhosseini, D.W. Hutmacher, Functionalization, preparation and use of cell-laden gelatin methacryloyl–based hydrogels as modular tissue culture platforms, Nat. Protoc. 11 (2016) 727–746.
[18] E. Hoch, C. Schuh, T. Hirth, G.E. Tovar, K. Borchers, Stiff gelatin hydrogels can be photo-chemically synthesized from low viscous gelatin solutions using molecularly functionalized gelatin with a high degree of methacrylation, J. Mater. Sci. Mater. Med. 23 (2012) 2607–2617.
[19] M. Sutter, J. Siepmann, W.E. Hennink, W. Jiskoot, Recombinant gelatin hydrogels for the sustained release of proteins, J. Control. Release 119 (2007) 301–312.
[20] S. Engelhardt, E. Hoch, K. Borchers, W. Meyer, H. Krüger, G.E. Tovar, A. Gillner, Fabrication of 2D protein microstructures and 3D polymer-protein hybrid microstructures by two-photon polymerization, Biofabrication 3 (2011), 025003.
[21] B.H. Lee, H. Shirahama, N.J. Cho, L.P. Tan, Efficient and controllable synthesis of highly substituted gelatin methacrylamide for mechanically stiff hydrogels, RSC Adv. 5 (2015) 106094–106097.

[22] H. Shirahama, B.H. Lee, L.P. Tan, N.J. Cho, Precise Tuning of Facile One-Pot Gelatin Methacryloyl (GelMA) Synthesis, Sci. Rep. 6 (2016) 31036.
[23] J. Van Hoorick, P. Gruber, M. Markovic, M. Tromayer, J. Van Erps, H. Thienpont, R. Liska, A. Ovsianikov, P. Dubruel, S. Van Vlierberghe, Cross-linkable gelatins with superior mechanical properties through carboxylic acid modification: increasing the two-photon polymerization potential, Biomacromolecules 18 (2017) 3260–3272.
[24] P. Sajkiewicz, D. Kołbuk, Electrospinning of gelatin for tissue engineering–molecular conformation as one of the overlooked problems, J. Biomater. Sci. Polym. Ed. 25 (2014) 2009–2022.
[25] C. Claaßen, M.H. Claaßen, V. Truffault, L. Sewald, G.E.M. Tovar, K. Borchers, A. Southan, Quantification of substitution of gelatin methacryloyl: best practice and current pitfalls, Biomacromolecules 19 (2018) 42–52.
[26] D. Roach, C.W. Gehrke, The hydrolysis of proteins, J. Chromatogr. A 52 (1970) 393–404.
[27] M. Zhu, Y. Wang, G. Ferracci, J. Zheng, N.J. Cho, B.H. Lee, Gelatin methacryloyl and its hydrogels with an exceptional degree of controllability and batch-to-batch consistency, Sci. Rep. 9 (2019) 6863.
[28] A.F. Habeeb, Determination of free amino groups in proteins by trinitrobenzenesulfonic acid, Anal. Biochem. 14 (1966) 328–336.
[29] P. Cayot, G. Tainturier, The quantification of protein amino groups by the trinitrobenzenesulfonic acid method: a reexamination, Anal. Biochem. 249 (1997) 184–200.
[30] S.B. Ross-Murphy, Structure and rheology of gelatin gels: recent progress, Polymer 33 (1992) 2622–2627.
[31] J. Zheng, M. Zhu, G. Ferracci, N.J. Cho, B.H. Lee, Hydrolytic stability of methacrylamide and methacrylate in gelatin Methacryloyl and decoupling of gelatin methacrylamide from gelatin methacryloyl through hydrolysis, Macromol. Chem. Phys. 219 (2018) 1800266.

gels

MDPI

Article

Injectable and In Situ Gelling Dextran Derivatives Containing Hydrolyzable Groups for the Delivery of Large Molecules

Laura Di Muzio, Patrizia Paolicelli *, Chiara Brandelli, Stefania Cesa, Jordan Trilli, Stefania Petralito and Maria Antonietta Casadei

Department of Drug Chemistry and Technologies, Sapienza University of Rome, 00185 Rome, Italy; laura.dimuzio@uniroma1.it (L.D.M.); chiara.brandelli@uniroma1.it (C.B.); stefania.cesa@uniroma1.it (S.C.); jordan.trilli@uniroma1.it (J.T.); stefania.petralito@uniroma1.it (S.P.); mariaantonietta.casadei@uniroma1.it (M.A.C.)

* Correspondence: patrizia.paolicelli@uniroma1.it; Tel.: +39-06-4991-3173

Abstract: Recently, we reported the synthesis and characterization of a new dextran derivative obtained by grafting polyethylene glycol methacrylate to a polysaccharide backbone through a carbonate bond. This moiety was introduced because it allows for the fabrication, through a photo-induced crosslinking reaction, of biodegradable hydrogels particularly suitable for the release of high molecular weight molecules. Here, we investigate the influence of the oxyethylene chain length and the molecular weight of the starting dextran on the main properties of the polymeric solutions as well as those of the corresponding hydrogels. All synthesized polymeric derivatives were characterized by FTIR, NMR, and rheological analyses. The photo-crosslinking reaction of the polymers allowed us to obtain biodegradable networks tested for their mechanical properties, swelling, and degradation behavior. The results showed that both the oxyethylene chain length as well as the molecular weight of the starting dextran influenced swelling and degradation of the hydrogel network. As a consequence, the different behaviors in terms of swelling and degradability were able to affect the release of a large model molecule over time, making these matrices suitable candidates for the delivery of high molecular weight drug substances.

Keywords: dextran derivatives; PEG methacrylate; photo-crosslinking reaction; biodegradable hydrogels; injectable hydrogels; in situ gelling polymers; macromolecules delivery

Citation: Di Muzio, L.; Paolicelli, P.; Brandelli, C.; Cesa, S.; Trilli, J.; Petralito, S.; Casadei, M.A. Injectable and In Situ Gelling Dextran Derivatives Containing Hydrolyzable Groups for the Delivery of Large Molecules. *Gels* **2021**, *7*, 150. https://doi.org/10.3390/gels7040150

Academic Editor: Mohsen Akbari

Received: 27 August 2021
Accepted: 22 September 2021
Published: 24 September 2021

1. Introduction

Hydrogels are, in general, considered biocompatible materials due to their high water content and their consistency, which make them similar to the extracellular matrix, minimizing tissue irritation and inflammatory response when used for biomedical or pharmaceutical purposes [1–5]. The porous structure of these networks can house large quantities of water-soluble molecules, so the interest in the use of hydrogels as drug delivery systems is constantly growing [6,7]. The release of active molecules physically incorporated into the hydrogel matrix can be governed by multiple mechanisms such as swelling, diffusion, erosion/degradation, or by the combination of two or more of these mechanisms [8,9]. In particular, if the hydrogel mesh size is larger than the drug hydrodynamic radius, then the diffusion is the driving force for the release process. If, instead, the pores are smaller than the radius of the loaded molecule, swelling and/or degradation processes are required to allow for drug release [10–12]. Considering the internal structure of hydrogels, the release profile can be modulated by varying the lattice density, and, therefore, the polymer architecture, the molecular weight, the concentration, or the chemistry of the system [3].

For the purpose of drug delivery, biodegradable hydrogels are the platform of choice, particularly for the delivery of high molecular weight drugs [13]. Indeed, a successful strategy that allows the controlled release of large molecules is to design a system so that

biodegradability and bioerodability can be modulated and opportunely tailored. Hydrogel degradation not only allows for temporal control of the release of the entrapped bioactive molecule, but it also makes possible the elimination of the carrier once the payload is completely depleted. Hydrogel degradation can occur in the polymer backbone or at the crosslinking points, mediated either by enzymatic or chemical processes, and can be controlled by studying the progressive erosion and rupture of the polymeric network. As a consequence, biodegradable materials can break down inside the body, producing water-soluble intermediates or end-products that can be easily eliminated from the body without harmful or toxic effects.

Based on their degradable features, hydrogels can deliver the drugs following predictable release profiles, at the desired site of action, with no burst effect. All these features make biodegradable hydrogels a really good platform for drug delivery. When used as preformed systems, they must be surgically implanted in the site of interest, but this operation is usually expensive and disadvantageous for the patient. For this reason, nowadays, the interest has shifted to the design of hydrogels that can be administered in less invasive ways such as injectable hydrogels [14,15]. Indeed, injectable hydrogels can be administered as polymeric solutions that convert to viscoelastic systems at the injection site [16,17]. Gelation can occur as a result of external stimuli (such as temperature, pH, and ionic strength) or through the use of physical or chemical tools. In particular, the use of methacrylated polymers allows hydrogels to be produced by UV irradiation. In this scenario, dextran (DEX) functionalized with methacrylic moieties has proven to be an interesting platform for drug delivery [18]. This meanly occurs when methacrylic groups are coupled to a DEX backbone with hydrolyzable carbonate ester bonds, giving the so-called dextran hydroxyethyl methacrylate (DEX-HEMA). While DEX-HEMA forms hydrogels with improved degradability compared to classic dextran methacrylate (DEX-MA—methacrylic groups directly linked to the polysaccharide through ester bonds), the release and rheological properties are still suboptimal for effective application as an injectable and in situ crosslinkable drug delivery system. Therefore, we recently proposed a new derivative coupling DEX with polyethylene glycol methacrylate (PEG-MA) through a carbonate ester bond [19]. The presence of PEG was able to positively affect the mechanical properties of the hydrogels, while the carbonate group allowed for the biodegradation of the network as well as temporal control of the release of an incorporated drug, particularly a high molecular weight drug. Here, we investigate the influence of the length of the oxyethylene lateral chain as well as the molecular weight of DEX on the swelling, mechanical, and release properties of the obtained hydrogels to further control and modulate their biodegradation. To this end, five DEX derivatives were synthesized, fully characterized, and employed for the preparation of hydrogels by photo-induced free radical crosslinking. A large model molecule was loaded into the hydrogels and its release was followed over time.

2. Results and Discussion

2.1. Synthesis of DEX Derivatives

A series of DEX derivatives was synthesized with the aim to introduce methacrylic moieties on the polysaccharide backbone through labile carbonate ester groups, in order to modulate biodegradability of the corresponding photo-crosslinked hydrogels, and in this way obtain suitable and tailorable carriers for the delivery of high molecular weight drugs.

Spacers of different lengths, containing a different number of oxyethylene units, namely one, six, or nine, were employed to link methacrylic groups to the polymer backbone. To this end, the following methacrylate reagents were used: HEMA, $PEG_{360}MA$, and $PEG_{500}MA$. Moreover, as the final goal of the work was the development of an injectable and in situ gelling delivery system, the effect of the molecular weight of the starting DEX was also evaluated. Therefore, both DEX_{40} (M_r 40,000) and DEX_{500} (M_r 500,000)-based methacrylate derivatives were synthesized. The chemical modification of DEX was obtained following a two-step synthesis procedure, as shown in the scheme reported in Figure 1. In the first reaction the hydroxyl group of the methacrylic reagent was acti-

vated by the classic reaction with *N*,*N*′-carbonyldiimidazole (CDI) to produce a reactive methacrylic reagent. After evaporation of the solvent, the intermediate was directly put to react, without prior purification, with DEX in anhydrous DMSO, using 4-DMAP as a nucleophilic catalyst.

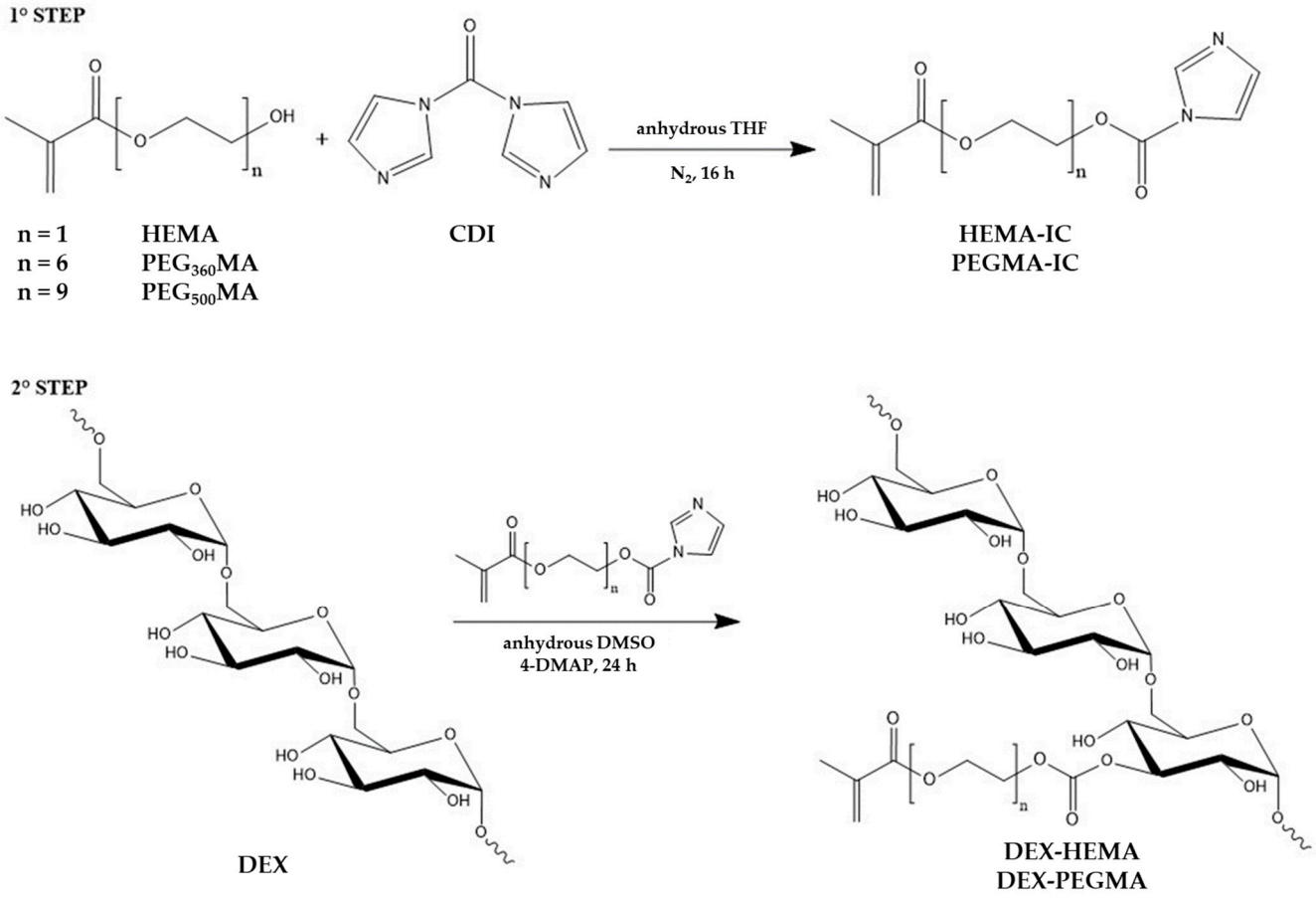

Figure 1. Scheme of the synthesis of methacrylated DEX derivatives.

The same procedure was followed to synthesize all the derivatives, but the polymers obtained from DEX_{500} were precipitated from the reaction mixture using 2-methoxyethanol instead of ethanol, because it allowed for the formation of a fine precipitate, which dissolved rapidly in distilled water, whereas ethanol produced a dense precipitate, which dissolved slowly in water, thereby promoting partial degradation of the polymer. Anyway, the derivative with the highest molecular weight (DEX_{500}-$PEG_{500}MA$) showed poor water solubility even using 2-methoxyethanol for purification, and for this reason, it was discarded and not further considered in this work.

After exhaustive dialysis and freeze-drying, every derivative was submitted to FTIR analysis. As an example, in Figure 2, the spectrum of DEX_{40}-$PEG_{360}MA$ is reported, however, similar results were obtained for all other polymers.

As a consequence of the derivatization, the FTIR spectrum showed the presence of a peak at 1745 cm^{-1} due to the stretching of the carbonate ester bond and another one at 1713 cm^{-1}, characteristic of the carbonyl group of the methacrylic ester.

The polymers were also characterized by ^{1}H- and ^{13}C-NMR. The ^{1}H-NMR spectra reported in Figure 3 confirmed the functionalization. In fact, it was possible to identify the characteristic signals of the vinyl protons at 6.09 and 5.67 ppm and the methyl protons at 1.87 ppm of the methacrylic group [20].

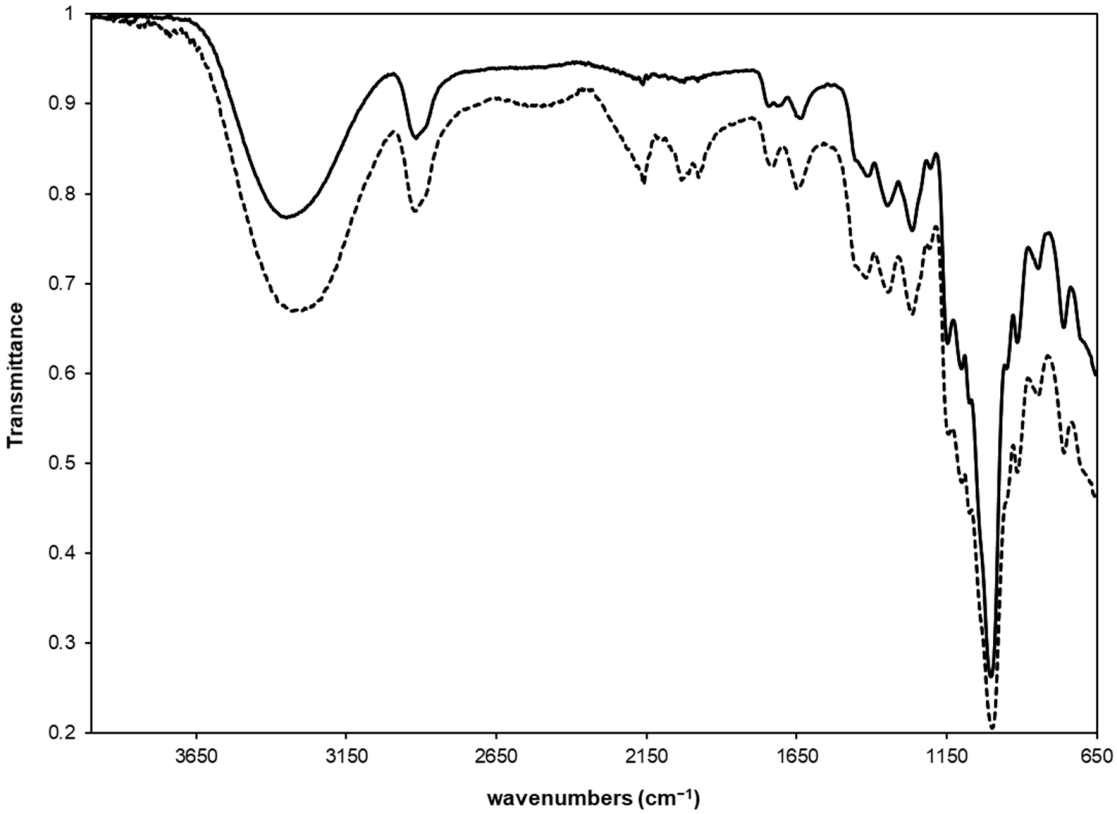

Figure 2. FTIR spectra of DEX_{40}-$PEG_{360}MA$ (solid line) and the corresponding hydrogel (dashed line). The insert represents an expanded region of the spectra from 1900 to 1500 cm^{-1}.

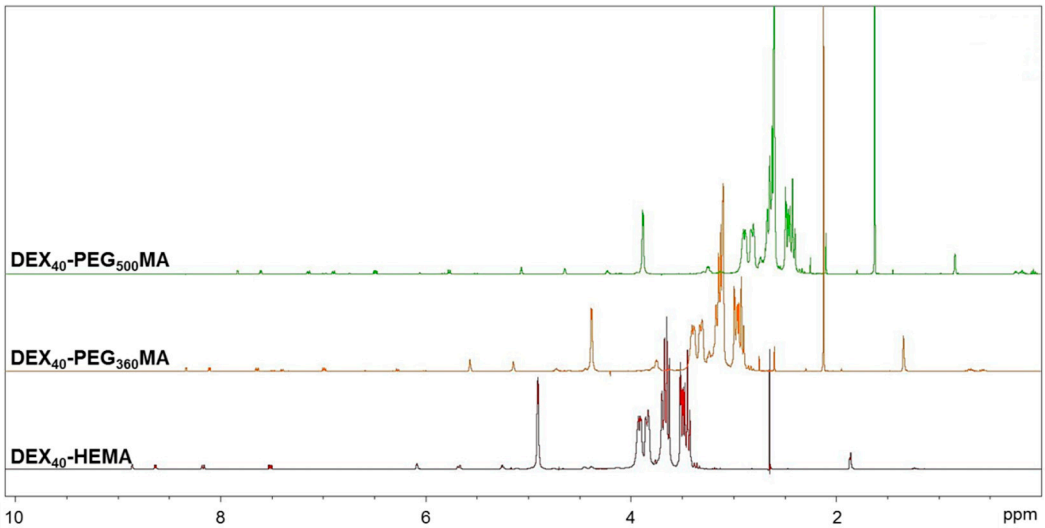

Figure 3. ^{1}H-NMR spectra of DEX_{40} derivatives in D_2O/DMSO-d6.

^{1}H-NMR spectra were also used to calculate the methacrylation degree (DD%) of the polymers. For this achievement, the ^{1}H-NMR spectra were recorded in the presence of an internal standard. Nicotinamide was chosen as the internal standard, as the peaks related to the aromatic protons were in areas of the spectrum where no proton signals of the polymers under examination were present. The internal standard method was used since the methods usually used to calculate the methacrylation degree of DEX derivatives has been proven not to be accurate [21]. One of the most widely applied method calculates the DD% as the ratio between the average of the proton areas of the methacrylic groups

(6.09 and 5.67 ppm) and the anomeric proton area (4.69 ppm). However, the resulting DD% values were poorly reproducible and scarcely accurate due to the presence of the water signal, which falls very close to the anomeric proton, preventing its accurate integration. Moreover, the suppression of the water signal partially alters the peak intensity of the anomeric proton, causing an overestimation of the DD% value. The other method usually used to calculate the methacrylation degree considers the signals of the DEX chain in the range 3.2–4 ppm. However, it was not possible to use this method because the signals of the methylene protons of the oxyethylene chain also fall within this range. For all these reasons, the internal standard method was selected and applied. By comparing the area of a specific standard signal with that relating to the protons of the methacrylic groups and precisely knowing the amount of standard in the sample, it was possible to accurately calculate the mmoles of the methacrylic groups of all the polymeric derivatives. The experimental conditions of the synthesis were opportunely optimized to obtain all the derivatives with DD% = 5 ± 1. This specific value was considered an ideal balance between the hydrophilic and lipophilic portion of the polymer, according to previous results [19].

^{13}C-NMR spectra of the derivatives show peaks that can be referred to the methacrylic group and the oxyethylene chain. As an example, Figure 4 reports the ^{13}C-NMR spectrum of DEX$_{40}$-PEG$_{360}$MA. The signal at 167.0 ppm belongs to the carbonyl ester, whereas those at 136.3 and 126.3 ppm were the resonance peaks of the carbons of the methacrylic double bond; instead, the peak of the methyl group could be observed at 18 ppm. In addition, at 70.3, 66.6, and 64.2 ppm, it was possible to identify the chemical shifts of the carbons of the oxyethylene chain. Finally, the peak at 155.2 ppm can be referred to the carbonate ester group. Similar results were obtained for the other derivatives.

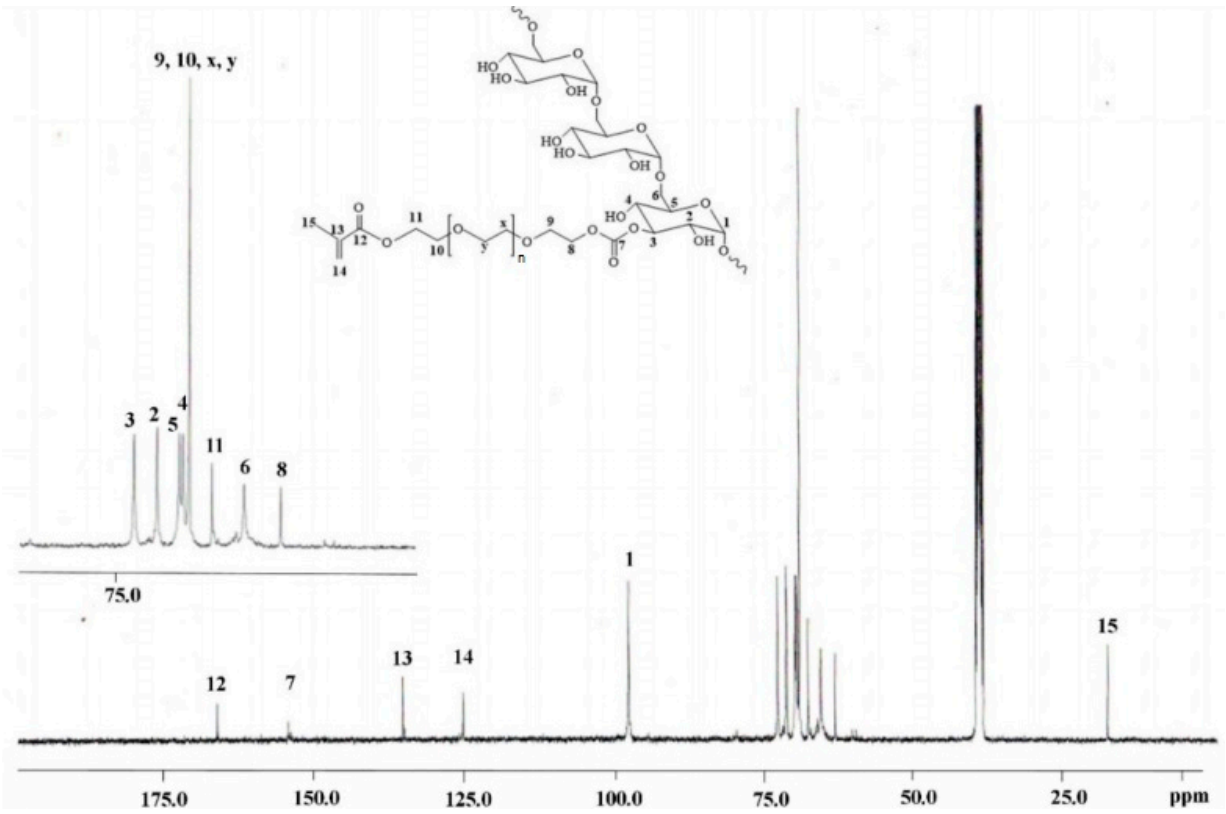

Figure 4. ^{13}C-NMR spectrum of DEX$_{40}$-PEG$_{360}$MA in DMSO-d6.

2.2. Rheological Characterization of Polymeric Solutions

In order to evaluate the possible use of these DEX derivatives as injectable drug delivery systems, their 10% *w*/*v* aqueous solutions were subjected to rheological analysis of the flow properties. The solutions displayed the behavior shown in Figure 5A. All systems showed the same decreasing trend of viscosity as a function of the flow rate, confirming the pseudo-plastic behavior typical of polymeric solutions. The slight increase in viscosity observed for the solutions of DEX-PEGMA polymers with respect to DEX-HEMA could be due to the formation of clusters among PEG chains [22,23] where DEX-HEMA is unable to form. Such interactions increase with the length of the PEG chain. As expected, when the molecular weight of DEX increases, the viscosity increases significantly. In fact, the viscosity of DEX_{500} and its PEGMA derivatives was significantly higher than DEX_{40} and its PEGMA derivatives, at the same concentration. Even in this case, the small difference in viscosity between the two derivatives can be related to cluster formation among the oxyethylene chains. However, the zero-shear viscosity of DEX_{500}-$PEG_{360}MA$ is adequate for its use as an injectable system, and is also high enough to avoid the rapid spread of the polymeric solution in the injection site (see Figure 5B,C).

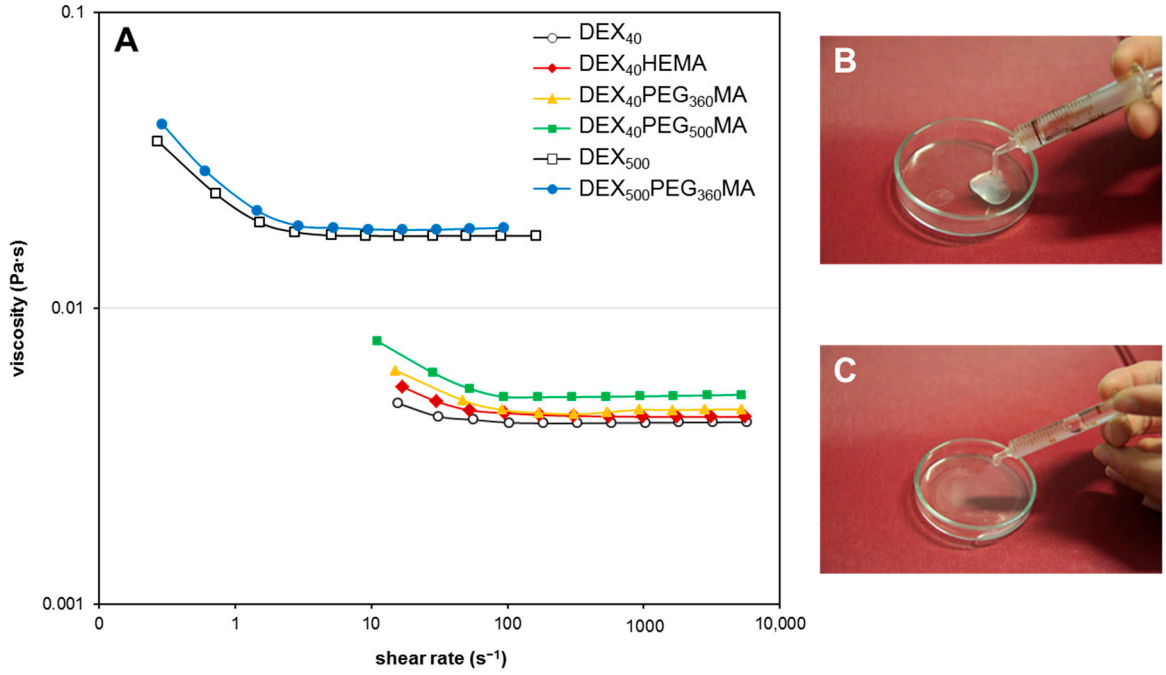

Figure 5. Flow properties of the different DEX derivatives. (**A**) Flow curves of aqueous solutions (10% *w*/*v*) of the derivatives at 37.0 ± 0.1 °C, showing the effect of the oxyethylene chain length and the molecular weight of DEX on the flowing properties of the polymers. (**B**,**C**) Show injectability of DEX_{500}-$PEG_{360}MA$ and DEX_{40}-$PEG_{360}MA$, respectively.

2.3. Hydrogels Preparation and Mechanical Characterization

Hydrogels were prepared by photo-induced free radical crosslinking of 10% *w*/*v* solutions of the different DEX derivatives. An irradiation time of 10 min was found optimal for the conversion of all the solutions into the corresponding hydrogel systems. Once obtained, gels were freeze-dried and analyzed through FTIR to confirm the achievement of the polymer crosslinking in all the matrices. In fact, in the FTIR spectra of the gels, the peak relative to the stretching of the methacrylic ester at 1713 cm^{-1} disappeared, while that of the saturated ester that formed after the photochemical reaction shifted toward the stretching vibrational band of the carbonate ester bond (see the dashed line in Figure 2).

Once prepared, the hydrogels were characterized for their mechanical properties. The study of the mechanical properties is crucial to evaluate the handling and elasticity of the hydrogels. The samples were subjected to rheological analysis under small amplitude os-

cillatory shear conditions, and the relative mechanical spectra within the linear viscoelastic regime of the materials were recorded (Figure 6).

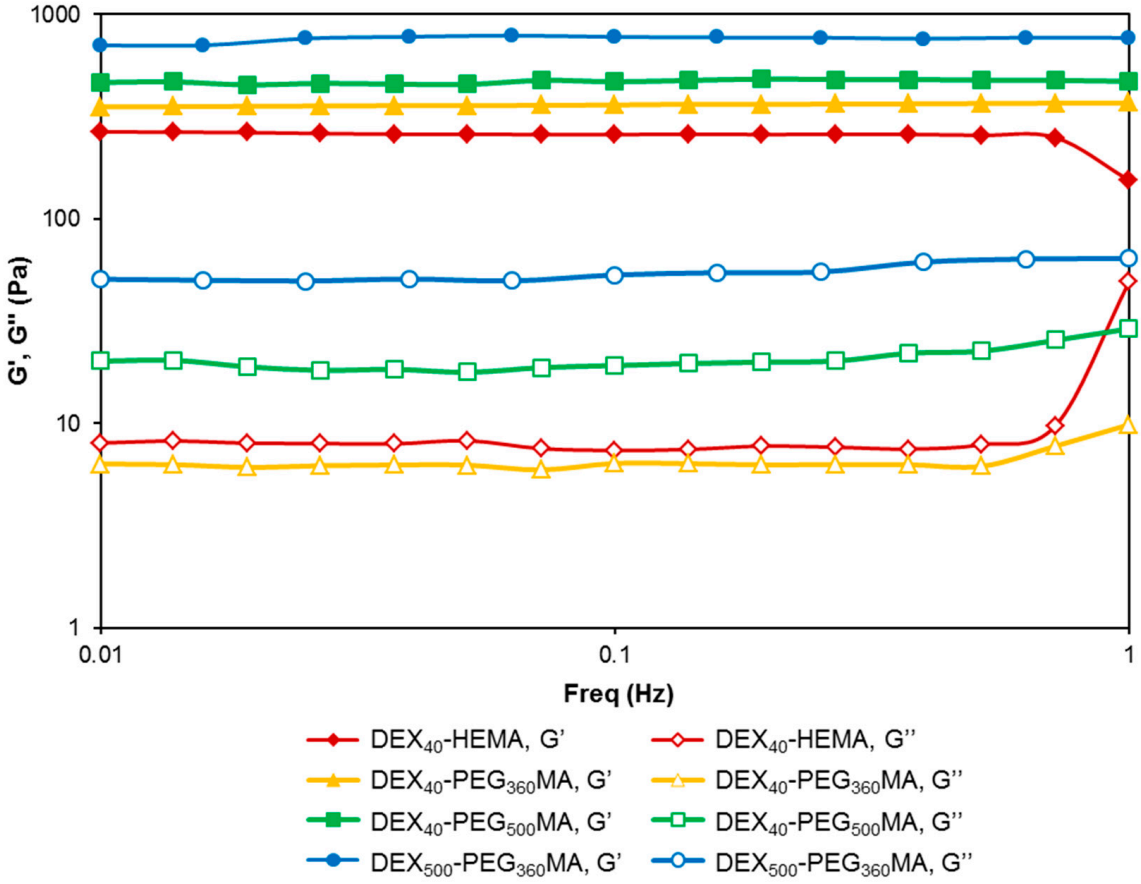

Figure 6. Frequency sweep analysis of all the methacrylated DEX derivatives showing the effect of the oxyethylene chain length and the molecular weight of the polymer backbone on the mechanical properties of the hydrogels (G′ closed symbols, G″ open symbols). The spectra were recorded at 37.0 ± 0.1 °C in the linear viscoelastic region.

All samples showed the typical behavior of gels, with the elastic modulus G′ greater than the viscous modulus G″. It can be seen that all the derivatives obtained from DEX_{40} showed an almost similar behavior with regard to the trend of the G′ and G″ moduli. Furthermore, the absolute values of the two moduli depend on the oxyethylene chain length and increase with it. Considering that the mmoles of crosslinkable methacrylic groups slightly decrease in the order DEX_{40}-$PEG_{500}MA$ < DEX_{40}-$PEG_{360}MA$ < DEX_{40}-HEMA, these results suggest that longer oxyethylene chains promote interactions between polymer chains. Therefore, moving the methacrylic groups away from the polymer backbone facilitates the successive crosslinking and formation of the network. The hydrogel obtained from DEX_{500}-$PEG_{360}MA$ showed the highest values of the two moduli. Therefore, comparing DEX_{40}-$PEG_{360}MA$ and DEX_{500}-$PEG_{360}MA$, the strength of the gel increased with the molecular weight of the starting DEX. This result is in accordance with the viscosity values obtained for the corresponding polymeric solutions and could reflect the greater extent of polymer chain entanglements characteristic of the derivative with higher molecular weight.

Stress–strain profiles were obtained by subjecting the samples to uniaxial compression and the results are reported in Figure 7.

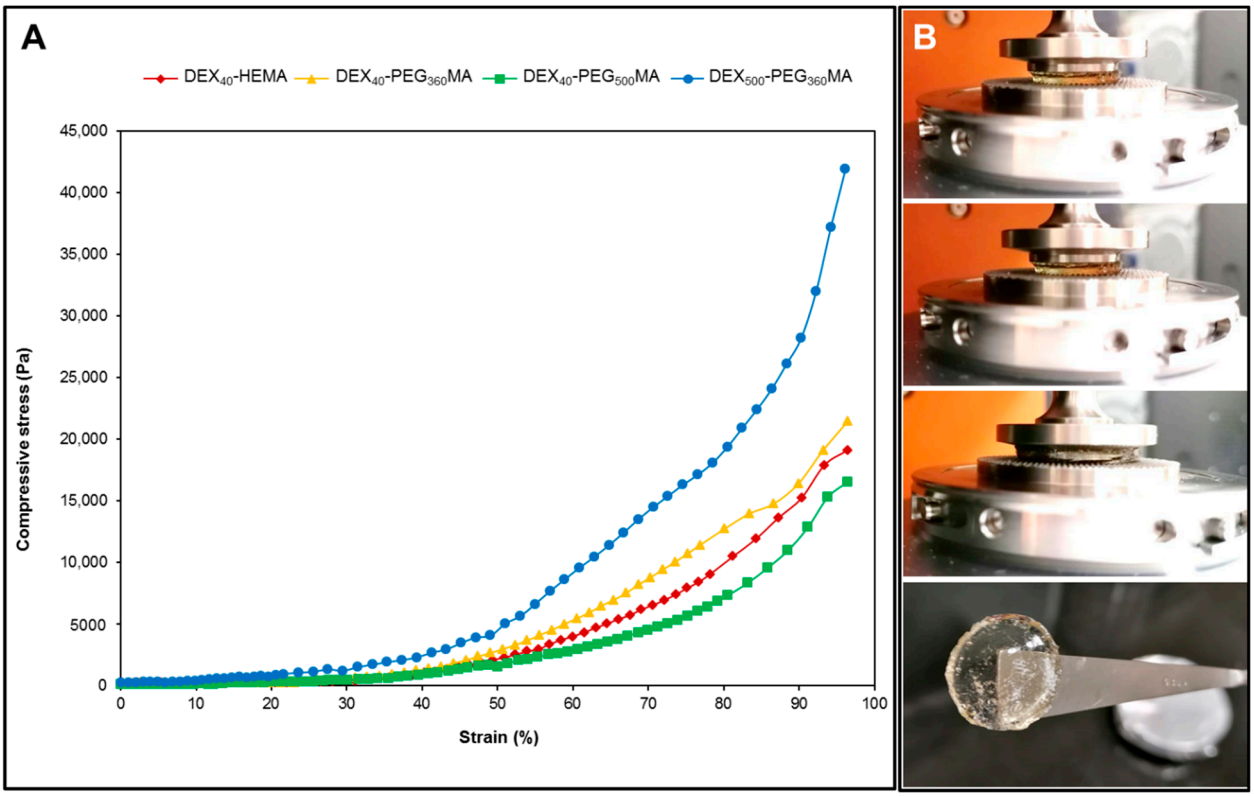

Figure 7. Dynamic mechanical analysis of the hydrogels in compression mode. (**A**) Stress–strain curves of all the methacrylated DEX derivatives submitted to uniaxial compression. (**B**) Sequence of images of DEX_{40}-$PEG_{500}MA$ hydrogel submitted to uniaxial compression and the same hydrogel recovered at the end of the compression test.

The slope of the curve in the range from 0 to 10% of strain was used to calculate the values of the compressive modulus. The length of the oxyethylene chain did not significantly influence the modulus value of the gels when submitted to uniaxial compression. Additionally, it can be observed that the DEX_{40}-$PEG_{500}MA$ derivative showed a different behavior compared to DEX_{40}-HEMA and DEX_{40}-$PEG_{360}MA$ as it can be deformed easier than the other hydrogels, which were obtained from polymers with shorter lateral chains. Indeed, it required the application of lower stress for its compression. In contrast, the increment of the molecular weight of DEX contributed to producing a stiffer structure that requires much higher stress for deformation, probably due to the higher degree of polymer chain entanglement. All the hydrogels were crushed to the maximum allowed by the instrument; moreover, no samples broke during the test, as can be observed in Figure 7B, which shows a sequence of images of the DEX_{40}-$PEG_{500}MA$ hydrogel submitted to uniaxial compression and the same hydrogel recovered at the end of the compression test. Similar results were obtained for all the hydrogels analyzed.

Overall, it is possible to attest that the mechanical properties of the hydrogels were mostly influenced by the molecular weight of the starting DEX, and to a smaller extent by the length of the oxyethylene chain used to link the methacrylate group to the polymeric backbone.

2.4. Swelling and Degradability Properties

Apart from the mechanical properties, it is important to investigate the swelling and degradability properties of the different matrices, as they can deeply influence their performance as drug delivery systems, and, specifically, the amount of drug released over time. Swelling experiments were carried out on freeze-dried gels in PBS (pH 7.4) at 37.0 ± 0.5 °C. The results are reported in Figure 8 as value of $q = W_s/W_d$, where W_s and W_d are the weight of the swollen and dry sample, respectively. Figure 8 shows that the time needed to reach the maximum swelling degree is very different for the various networks, demonstrating

how much the length of the spacer as well as the molecular weight of the backbone can affect the physical–chemical properties of these systems. Specifically, it should be noted that DEX_{40}-HEMA-based hydrogel reached the maximum q value after 120 h, while those based on DEX_{40}-PEG_{360}MA, DEX_{40}-PEG_{500}MA, and DEX_{500}-PEG_{360}MA after 144, 216, and 648 h, respectively. As the molecular weight of DEX and the spacer length increase, the swelling rate slows down. Another peculiarity of these systems is that the maximum swelling degree is not very different, albeit reached in different times. However, DEX_{40}-HEMA-based hydrogels are an exception to this behavior, probably due to its faster degradation. It was interesting to compare the swelling of hydrogels obtained from DEX with the same average molecular weight, but different oxyethylene chain length to highlight its effect on the swelling capacity. The increase in the molecular weight of PEG involves a change in the swelling properties. It is reasonable to assume that the derivative with PEG_{500}MA as the lateral chain has greater ability to form clusters of oxyethylene chains with respect to thePEG_{360}MA derivatives [24,25]. A greater number of oxyethylene units corresponds to a decreased rate of water entry into the polymeric lattice due to the increase in the hydrogel hydrophobicity. Indeed, the hydrophilic–hydrophobic balance in the polymer structure influences cluster formation [26], but also water entrance into the network.

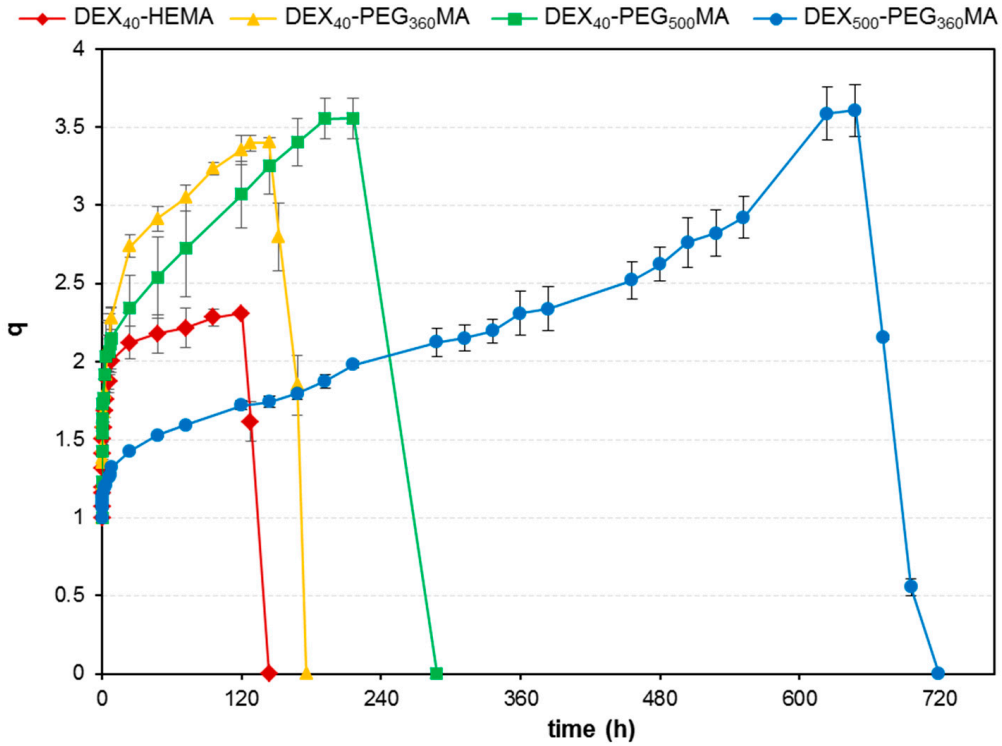

Figure 8. Dynamic swelling profile of all the methacrylated DEX derivatives measured in PBS (pH 7.4) at 37.0 ± 0.5 °C.

The different swelling ability shown by the hydrogels obtained from DEX_{500}-PEG_{360}MA with respect to DEX_{40}-PEG_{360}MA probably depends on the different degree of polymer chain entanglement, in agreement with the viscosity data of the corresponding starting solutions. By following the variation of the q value over time, it is possible to define the degradation profile of these hydrogel systems, which showed a progressive weight loss as a result of the consequent hydrolysis of the carbonate ester bonds and decay of the structure. All the samples decomposed completely within a few days, reaching the maximum value of q followed by a sharp decrease due to the complete degradation of the network [27]. This behavior depends on the gradual bulk erosion of the hydrogel matrix that is strictly related to the rate of water entrance. In particular, progressive bulk erosion was also confirmed by the images taken at different times during the swelling process in PBS. As an example, images of a DEX_{40}-

$PEG_{500}MA$ hydrogel at time zero and after two, four, six, and eight days in PBS are reported in Figure 9. It can be observed a continuous and progressive widening of the hydrogel, which matches and can justify the increase in the q value already discussed.

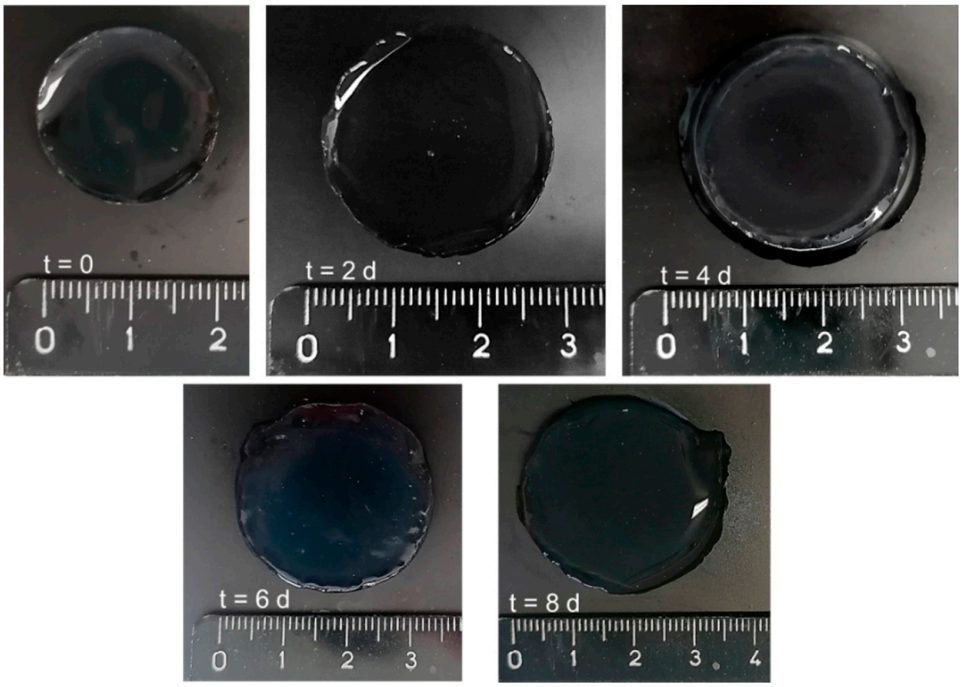

Figure 9. Pictures representing the swelling process of a DEX_{40}-$PEG_{500}MA$ hydrogel in PBS (pH 7.4). The modification in the q value matches the variation in the dimensions of the hydrogel. Pictures were taken at time zero and after 2, 4, 6 and 8 days.

2.5. Release Studies

Release studies were carried out in PBS (pH 7.4) at 37.0 ± 0.5 °C on hydrogels loaded with a fluorescent dextran, employed as a large model molecule. The release profiles obtained from hydrogels prepared using different DEX derivatives are shown in Figure 10. A trend strictly linked to the swelling degree of the polymeric lattice and related to the rate of water entry into the hydrogel, is evident. The speed of water entrance is correlated to the hydrophobicity of the system and therefore it is possible to modulate the drug release simply by increasing the length of the oxyethylene chain.

The release profile from the hydrogels obtained from DEX at higher molecular weight is also reported in Figure 10. The effect of the molecular weight of DEX on the release profiles is much more evident. In particular, a modulation of the release over a period of 480 h is evident, and is also consistent with the obtained dynamic swelling data. In fact, even if the DEX_{40}-$PEG_{360}MA$ and DEX_{500}-$PEG_{360}MA$ gels reach the same swelling degree in terms of absolute q value, the time necessary to attain maximum swelling is deeply influenced by the molecular weight of the polymer. The entanglement of the polymer chains hinders the entrance of water, slowing down both the drug diffusion process and the matrix erosion.

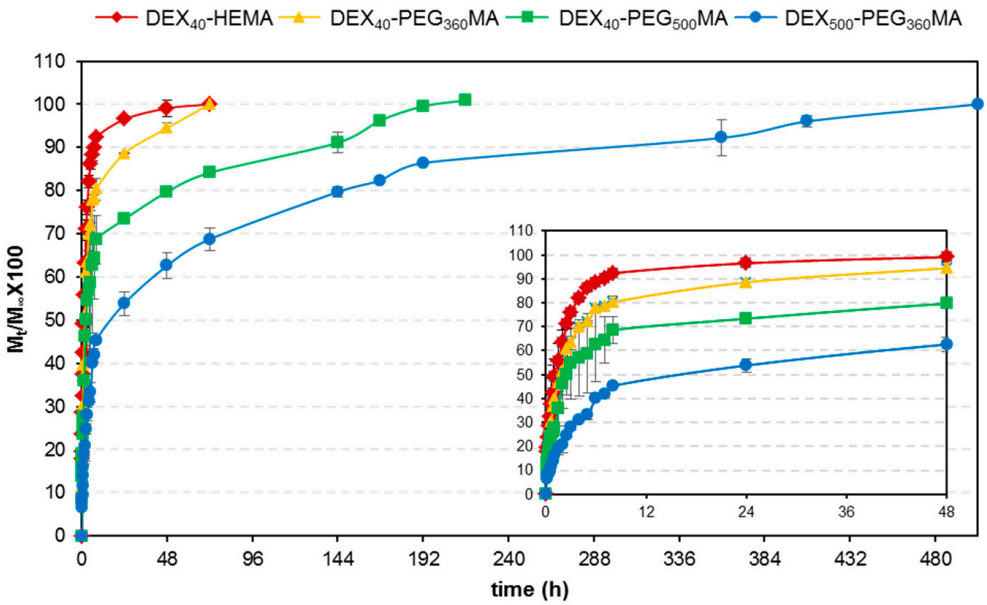

Figure 10. Release profiles of FITC-DEX from hydrogels fabricated with the different methacrylated DEX derivatives measured in PBS (pH 7.4) at 37.0 ± 0.5 °C. The insert represents an expanded region of the graph.

Globally, both the molecular weight of DEX as well as the length of the linker are able to modify the degradation rate of these new DEX polymers and consequently the release time of a macromolecule loaded inside the corresponding hydrogels. Therefore, both these parameters can be modulated and adjusted to opportunely tailor the release of the incorporated drug and in this way achieve specific therapeutic needs. However, the DEX_{500} derivative possesses more adequate rheological properties to develop injectable and in situ crosslinkable drug delivery systems. Finally, the different polymeric derivatives can be opportunely blended and this strategy can be adopted to obtain the most suitable drug delivery systems, conveniently designed to meet specific therapeutic needs. Therefore, these new biodegradable methacrylated dextrans appear to possess interesting and promising properties for the development of effective delivery systems of large bioactive molecules. Additionally, further investigation is needed to evaluate the applicability of these polymers under physiological conditions and, in particular, their biological safety, which represents a fundamental issue of every material with potential application in the biomedical or pharmaceutical field. However, evidence exists on the biocompatibility of several different methacrylated DEX derivatives [18,28], which may also allow us to presume a good safety profile for these new biodegradable methacrylated dextrans.

3. Conclusions

A series of biodegradable DEX derivatives was synthesized coupling methacrylated oxyethylene chains to the polymeric backbone through a carbonate ester bond. The oxyethylene chain length was able to affect the rheological properties of the corresponding photocrosslinked hydrogels, and was also able to modify the rate of water uptake, which is regulated by the balance between the hydrophilic and hydrophobic portions of the specific polymeric derivative. The longer the oxyethylene arm, the slower the swelling of the hydrogel. As a consequence of the slowing down of the entrance of water, the degradation rate decreases, and thus the release rate of a drug entrapped in the network. The rheological properties of the polymers as well as those of the corresponding hydrogels were also deeply affected by the molecular weight of the starting DEX. In particular, the viscosity of the polymer solution increased significantly when the molecular weight of the starting DEX was augmented. Anyway, the investigated polymer solution showed adequate injectability and, at the same time, was able to remain at the injection site without spreading. This

rheological behavior is due to the higher degree of polymer chain entanglement, which is also responsible for the reduced rate of water uptake and, consequently, decreased degradation rate of the network. These characteristics are able to influence the release profile of a large drug molecule loaded into the degradable polymeric matrices. Globally, both the molecular weight of the polymer as well as the length of the lateral arm can influence the biodegradability of these new hydrogels, and can therefore be modulated and adjusted to achieve defined drug release kinetics. An opportune choice of the molecular weight of the starting polymer as well as of the number of oxyethylene units of the linker, or the use of mixtures of different DEX derivatives can represent interesting strategies to easily control how large molecules are released, and tailor them to meet specific therapeutic needs.

4. Materials and Methods

4.1. Materials

All used reagents were of analytical grade. Dextran (DEX) from *Leuconostoc* ssp. (Mr 40,000, DEX_{40} and 500,000, DEX_{500}), hydroquinone mono-methyl ether, *N*,*N*′-carbonyldiimidazole (CDI), *N*-methyl-2-pyrrolidone, 4-dimethylaminopyridine (4-DMAP) were purchased from Fluka. Anhydrous dimethylsulfoxide (DMSO), DMSO-d6, anhydrous tetrahydrofuran (THF), ethanol (EtOH), 2-methoxyethanol, irgacure 2959, nicotinamide, fluorescein isothiocyanate-dextran (FITC-DEX, Mn 4000), hydroxyethyl methacrylate (HEMA), polyethylene glycol mono-methacrylate (Mn 360 and 500; PEG_{360}-MA and PEG_{500}-MA), D_2O, and dialysis membranes (cut-off 12,000–14,000 Da) were purchased from Sigma-Aldrich (Saint Louis, MO, USA).

4.2. Synthesis of Dextran Derivatives

The synthesis was carried out in two steps, according to the procedure already reported in the literature for this type of functionalization [29]. HEMA (0.29 g; 2 mmol) was dissolved in anhydrous THF (7 mL) under a nitrogen atmosphere and subsequently CDI (0.37 g; 2 mmol) was added and left to react for 16 h at room temperature. Then, hydroquinone mono-methyl ether (0.25 g) was added to the mixture and the solvent was evaporated under reduced pressure, obtaining HEMA-IC (hydroxyethyl methacrylate N-imidazoylcarbamate), which was employed without purification. In the second step, DEX (2.4 g) was dissolved in anhydrous DMSO (18 mL), then mixed with 4-DMAP (0.47 g) and HEMA-IC. The mixture was kept reacting for 24 h under magnetic stirring at room temperature and then EtOH (200 mL) was added dropwise to precipitate the polymer. The suspension was filtered and the recovered solid was dissolved in water (15 mL). The solution, having a pH about 10, was neutralized with 0.1 M HCl and submitted to exhaustive dialysis against distilled water. The solution was frozen and then freeze-dried by employing a LIO 5P freeze-dryer (5 Pascal, Milan, Italy) equipped with a vacuum pump Adixen (Annecy, France). After freeze-drying, the polymer was characterized by FTIR and NMR. FTIR spectra were recorded with a Perkin Elmer Spectrum-One spectrometer (Waltham, MA, USA) in the range of 4000–650 cm^{-1}. ^1H- and ^{13}C-NMR spectra were obtained with a Bruker Avance 400 spectrometer (Rheinstetten, Germany). Specifically, ^1H-NMR spectra were obtained in a mixture D_2O/DMSO-d6, while ^{13}C-NMR investigation was carried out in DMSO-d6. The degree of derivatization (DD, number of methacrylic groups every 100 repetitive units of DEX) was calculated on the basis of the ^1H-NMR spectrum using nicotinamide as the internal standard. The same synthetic procedure was employed for all the derivatives under study obtaining DEX_{40}-HEMA, DEX_{40}-PEG_{360}MA, DEX_{40}-PEG_{500}MA, DEX_{500}-PEG_{360}MA, and DEX_{500}-PEG_{500}MA, respectively. The derivatives from DEX_{500} were precipitated from the reaction mixture using 2-methoxyethanol instead of ethanol. A DD% of 5 ± 1 was achieved for all polymeric derivatives.

4.3. Preparation of Hydrogels

The hydrogels were prepared through UV irradiation performed with a G.R.E. 125W Helios Italquartz (Milan, Italy), equipped with a mercury vapor lamp. Aqueous solutions of the different methacrylated polymers (10% *w*/*v*) were mixed with irgacure 2959 dissolved in *N*-methyl-2-pyrrolidone (1% *w*/*v*) and bubbled with nitrogen, then they were photo-crosslinked for 10 min.

4.4. Rheological Measurements

Rheological experiments were performed with a rheometer TA Discovery HR 1 (TA Instruments, New Castle, DE, USA). Viscosity curves of the polymeric solutions were obtained with a cone-plate geometry (diameter of 40 mm, α 1.005°, gap 27 μm) by applying shear stresses in the range of 0.01–1 Pa. Moreover, photochemical hydrogels (thickness of 0.4 cm) were submitted to oscillatory frequency sweep analysis using a serrated plate–plate geometry in the range of 0.01–1 Hz and working in the linear viscoelastic region assessed through preliminary strain sweep studies.

All hydrogels were also submitted to dynamic mechanical analysis (DMA) in compression. The sample was placed between the upper and lower tool of the plate–plate measuring system of the instrument and subjected to a uniaxial load, moving the upper plate at the constant speed of 10 μm/s.

All the experiments were carried out at least in triplicate at the temperature of 37.0 ± 0.1 °C.

4.5. Swelling and Degradability Studies

The swelling degree (q) of the hydrogels was determined in phosphate buffer solution (PBS, pH 7.4, ionic strength I = 0.1). Precisely weighed aliquots of each hydrogel were immersed in PBS at 37.0 ± 0.5 °C and left to swell. At defined time intervals, the liquid in excess was removed and the samples were weighed. The swelling degree was expressed as:

$$q = W_s/W_d \quad (1)$$

where W_s and W_d are the weights of the swollen and the dry hydrogel, respectively. The process of swelling was monitored up to the complete degradation of all gels. Each experiment was carried out in triplicate and the mean value was reported as ± the standard deviation.

4.6. Release Studies

Drug loaded hydrogels were obtained by adding fluorescent dextran (FITC-DEX, 0.2 mg/mL) to the polymeric solution (10% *w*/*v*) prior to irradiation. Hydrogels loaded with FITC-DEX were put in 10 mL PBS (pH 7.4) under magnetic stirring (100 rpm) at 37.0 ± 0.5 °C. At pre-established time points, a sample of the release medium (0.25 mL) was withdrawn and replaced with the same amount of fresh buffer. Each sample was diluted (1:10) in distilled water and the release of FITC-DEX was monitored with a Perkin Elmer FL 6500 fluorescence spectrophotometer (Waltham, MA, USA). The amount of model molecule was determined measuring the fluorescence emitted at 520 nm, after excitation at 490 nm. All the experiments were carried out in triplicate and the results were reported as mean values ± the standard deviation.

Author Contributions: Conceptualization, L.D.M., P.P., and M.A.C.; Methodology, P.P., S.P., S.C., L.D.M., and M.A.C.; Validation, P.P., S.P., S.C., and M.A.C.; Formal analysis, P.P., S.P., S.C., L.D.M., and M.A.C.; Investigation, L.D.M., J.T., and C.B.; Resources, M.A.C.; Data curation, L.D.M., and P.P.; Writing—original draft preparation, L.D.M., M.A.C., and P.P.; Writing—review and editing, L.D.M., J.T., C.B., S.P., S.C., M.A.C., and P.P.; Visualization, L.D.M., and P.P.; Supervision, S.P., P.P., and M.A.C.; Project administration, L.D.M., P.P., and M.A.C.; Funding acquisition, M.A.C. All authors have read and agreed to the published version of the manuscript.

Funding: This research received financial support from Sapienza University of Rome.

Institutional Review Board Statement: Not applicable.

Informed Consent Statement: Not applicable.

Data Availability Statement: The data presented in this study are available on request to the corresponding author.

Conflicts of Interest: The authors declare no conflict of interest.

References

1. Jabobs, S.; Nair, A.B.; Shah, J.; Sreeharsha, N.; Gupta, S.; Shinu, P. Emerging role of hydrogels in drug delivery systems, tissue engineering and wound management. *Pharmaceutics* **2021**, *13*, 357.
2. Austin, M.J.; Rosales, A.M. Tunable biomaterials from synthetic, sequence controlled polymers. *Biomater. Sci.* **2019**, *7*, 490–505. [CrossRef] [PubMed]
3. Li, J.; Mooney, D.J. Designing hydrogels for controlled drug delivery. *Nat. Rev. Mater.* **2016**, *1*, 16071. [CrossRef] [PubMed]
4. Naahidi, S.; Jafari, M.; Logan, M.; Wang, Y.; Yuan, Y.; Bae, H.; Dixon, B.; Chen, P. Biocompatibility of hydrogel-based scaffolds for tissue engineering applications. *Biotechnol. Adv.* **2017**, *35*, 530–544. [CrossRef] [PubMed]
5. Li, Q.; Ning, Z.; Ren, J.; Liao, W. Structural design and physicochemical foundations of hydrogels for biomedical applications. *Curr. Med. Chem.* **2018**, *25*, 963–981. [CrossRef] [PubMed]
6. Rehman, W.U.; Asim, M.; Hussain, S.; Khan, S.A.; Khan, S.B. Hydrogel: A promising material in pharmaceutics. *Curr. Pharm. Des.* **2020**, *26*, 5892–5908. [CrossRef] [PubMed]
7. Sosnik, A.; Seremeta, K.P. Polymeric hydrogels as technology platform for drug delivery applications. *Gels* **2017**, *3*, 25. [CrossRef]
8. Raza, F.; Zafar, H.; Zhu, Y.; Ren, Y.; Ullah, A.; Ullah Khan, A.; He, X.; Han, H.; Aquib, M.; Boakye-Yiadom, K.O.; et al. A review on recent advances in stabilizing peptides/proteins upon fabrication in hydrogels from biodegradable polymers. *Pharmaceutics* **2018**, *10*, 16. [CrossRef]
9. Shoukat, H.; Buksh, K.; Noreen, S.; Pervaiz, F.; Maqbool, I. Hydrogels as potential drug-delivery systems: Network design and applications. *Ther. Deliv.* **2021**, *12*, 375–396. [CrossRef]
10. Mallicka, S.P.; Sumana, D.K.; Singhb, B.N.; Srivastavab, P.; Siddiquia, N.; Yellaa, V.R.; Madhualc, A.; Vemuria, P.K. Strategies toward development of biodegradable hydrogels for biomedical applications. *Polym. Plast. Tech. Mat.* **2020**, *59*, 911–927. [CrossRef]
11. Vermonden, T.; Censi, R.; Hennink, W.E. Hydrogels for protein delivery. *Chem. Rev.* **2012**, *112*, 2853–2888. [CrossRef]
12. Bae, K.H.; Kurisawa, M. Emerging hydrogel designs for controlled protein delivery. *Biomater. Sci.* **2016**, *4*, 1184–1192. [CrossRef]
13. Li, Y.; Yang, H.Y.; Lee, D.S. Advances in biodegradable and injectable hydrogels for biomedical applications. *J. Control. Release* **2021**, *330*, 151–160. [CrossRef]
14. Gao, F.; Jiao, C.; Yu, B.; Cong, H.; Shen, Y. Preparation and biomedical application of injectable hydrogels. *Mater. Chem. Front.* **2021**, *5*, 4912–4936. [CrossRef]
15. Fan, D.Y.; Tian, Y.; Liu, Z.J. Injectable hydrogels for localized cancer therapy. *Front. Chem.* **2019**, *7*, 675. [CrossRef]
16. Nguyen, Q.V.; Huynh, D.P.; Park, J.H.; Lee, D.S. Injectable polymeric hydrogels for the delivery of therapeutic agents: A review. *Eur. Polym. J.* **2015**, *72*, 602–619. [CrossRef]
17. Bae, K.H.; Wang, L.-S.; Kurisawa, M. Injectable biodegradable hydrogels: Progress and challenges. *J. Mater. Chem. B* **2013**, *1*, 5371–5388. [CrossRef]
18. Van Tomme, S.R.; Hennink, W.E. Biodegradable dextran hydrogels for protein delivery applications. *Expert Rev. Med. Dev.* **2007**, *4*, 147–164. [CrossRef] [PubMed]
19. Pacelli, S.; Paolicelli, P.; Casadei, M.A. New biodegradable dextran-based hydrogels for protein delivery: Synthesis and characterization. *Carbohydr. Polym.* **2015**, *126*, 208–214. [CrossRef] [PubMed]
20. Van Dijk-Wolthuis, W.N.E.; Kettenes-van den Bosch, J.J.; van der Kerk-van Hoof, A.; Hennink, W.E. Reaction of dextran with glycidyl methacrylate: an unexpected transesterification. *Macromolecules* **1997**, *30*, 3411–3413. [CrossRef]
21. Van Dijk-Wolthuis, W.N.E.; Franssen, O.; Talsma, H.; van Steenbergen, M.J.; Kettenes-van den Bosch, J.J.; Hennink, W.E. Synthesis, characterization, and polymerization of glycidyl methacrylate derivatized dextran. *Macromolecules* **1995**, *28*, 6317–6322. [CrossRef]
22. Lin-Gibson, S.; Bencherif, S.; Cooper, J.A.; Wetzel, S.J.; Antonucci, J.M.; Vogel, B.M.; Horkay, F.; Washburn, N.R. Synthesis and characterization of PEG dimethacrylates and their hydrogels. *Biomacromolecules* **2004**, *5*, 1280–1287. [CrossRef]
23. Pacelli, S.; Paolicelli, P.; Pepi, F.; Garzoli, S.; Polini, A.; Tita, B.; Vitalone, A.; Casadei, M.A. Gellan gum and polyethyleneglycol dimethacrylate double network hydrogels with improved mechanical properties. *J. Polym. Res.* **2014**, *21*, 409. [CrossRef]
24. Azri, A.; Giamarchi, P.; Grohens, Y.; Olier, R.; Privat, M. Polyethylene glycol aggregates in water formed through hydrophobic helical structures. *J. Colloid Interf. Sci.* **2012**, *379*, 14–19. [CrossRef]
25. Hammouda, B.; Ho, D.L.; Kline, S. Insight into clustering in poly(ethylene oxide) solutions. *Macromolecules* **2004**, *37*, 6932–6937. [CrossRef]
26. Chiang, W.H.; Lan, Y.J.; Huang, Y.-C.; Chen, Y.W.; Huang, Y.F.; Lin, S.C.; Chern, C.S.; Chiu, H.C. Multi-scaled polymersomes from self-assembly of octadecanol-modified dextrans. *Polymer* **2012**, *53*, 2233–2244. [CrossRef]
27. Van Dijk-Wolthuls, W.N.E.; Tsang, S.K.Y.; Kettenes-van den Bosch, J.J.; Hennink, W.E. A new class of polymerizable dextrans with hydrolyzable groups: Hydroxyethyl methacrylated dextran with and without oligolactate spacer. *Polymer* **1997**, *38*, 6235–6242. [CrossRef]

28. De Groot, C.J.; Van Luyn, M.J.; Van Dijk-Wolthuis, W.N.; Cadée, J.A.; Plantinga, J.A.; Den Otter, W.; Hennink, W.E. In vitro biocompatibility of biodegradable dextran-based hydrogels tested with human fibroblasts. *Biomaterials* **2001**, *22*, 1197–1203. [CrossRef]
29. De Jong, S.J.; De Smedt, S.C.; Demeester, J.; van Nostrum, C.F.; Kettenes-van den Bosch, J.J.; Hennink, W.E. Biodegradable hydrogels based on stereocomplex formation between lactic acid oligomers grafted to dextran. *J. Control. Release* **2001**, *72*, 47–56. [CrossRef]

Carbohydrate Polymers 296 (2022) 119916

Contents lists available at ScienceDirect

Carbohydrate Polymers

journal homepage: www.elsevier.com/locate/carbpol

Insights into the reaction of chondroitin sulfate with glycidyl methacrylate: 1D and 2D NMR investigation

Laura Di Muzio [a], Patrizia Paolicelli [a,*], Jordan Trilli [a], Stefania Petralito [a], Vito Cosimo Carriero [a], Chiara Brandelli [a], Mattia Spano [a], Anatoly Petrovich Sobolev [b], Luisa Mannina [a], Maria Antonietta Casadei [a]

[a] Department of Drug Chemistry and Technologies, "Sapienza" Università di Roma, Piazzale Aldo Moro 5, 00185 Rome, Italy
[b] Magnetic Resonance Laboratory "Annalaura Segre", Institute for Biological Systems, National Research Council, Via Salaria km 29.300, I-00015, Monterotondo, Rome, Italy

ARTICLE INFO

Keywords:
Chondroitin sulfate methacrylate
2D-NMR
Glycosaminoglycans
Transesterification
Epoxy ring-opening

ABSTRACT

Chondroitin sulfate methacrylate (CS-MA) is a semisynthetic biopolymer increasingly used for the fabrication of chemical hydrogels. In this study, the methacrylation reaction of native CS was carried out with glycidyl methacrylate in dimethyl sulfoxide and optimized to obtain tunable and reproducible methacrylation degrees in a short reaction time. The methacrylation reaction was deeply characterized by mono- and bi-dimensional (1D, 2D) NMR spectroscopy of CS-MA derivatives with different methacrylation degrees. In contrast to what previously reported in the literature, HSQC, HMBC and TOCSY analyses revealed that the methacrylation reaction proceeds via both epoxy ring-opening and transesterification, involving predominantly the primary hydroxyl groups of CS, while preserving sulfate and carboxyl groups of the biopolymer. These findings are of fundamental importance for appropriate and rational design of CS-MA-based biomaterials.

1. Introduction

Chondroitin sulfate (CS) is a sulfated linear polysaccharide composed of disaccharide units containing *N*-acetyl-D-galactosamine (GalNAc) and D-glucuronate (GlcA) residues, joined by β (1 → 4) glycosidic bonds (Sugahara et al., 2003; Volpi, 2006). CS belongs to the class of glycosaminoglycans (GAGs), natural long-chain polysaccharides, which are fundamental components of native extracellular matrix (ECM) with important structural and biological functions (Pomin & Mulloy, 2018). For this reason, over the years interest has progressively grown in GAGs as biomaterials for application in regenerative medicine and pharmaceuticals (Köwitsch et al., 2018; Neves et al., 2020; Scharnweber et al., 2015). Hyaluronic acid has been the most widely and extensively investigated GAG for the scope, however, CS has been receiving increasing attention. Depending on the nature of the disaccharide unit, the sulfation degree and the molecular weight, different types of CS are known (Volpi, 2009). Traditionally, there are two main structural categories of CS, namely chondroitin-4-sulfate (CS-A) and chondroitin-6-sulfate (CS-B), which consist of disaccharide units with a sulfate group in position 4 and 6 of GalNAc, respectively. Commercially available CS is a variously composed mixture of these two types, with low amounts of non-sulfated and disulfated disaccharide units (Volpi, 2007, 2019).

CS has attractive biological and pharmacological properties and, in addition, it is a safe, non-toxic and biocompatible material (Bang et al., 2018). For all these reasons, CS has been considered interesting for drug delivery and tissue engineering applications (Pal & Saha, 2019; Yang et al., 2020). Most of these applications require the production of semisynthetic derivatives of CS, including methacrylate derivatives (CS-MA), which have been proven to be suitable materials for tissue engineering (Li et al., 2003; Mei et al., 2021; Ouyang et al., 2020), also through innovative 3D bioprinting techniques (Costantini et al., 2016; Lafuente-Merchan et al., 2022; Wang et al., 2003). Despite the increasing interest in CS-MA, the procedure used to synthesize this polymer is still sub-optimal and the obtained products are not properly characterized. In many cases, neither the type nor the origin of the specific CS used for the synthesis are reported, while it is well known that the physical and chemical properties of this biopolymer are affected by its heterogeneous composition, which depends on the origin and tissue source (Volpi et al., 2021; Yang et al., 2020).

* Corresponding author at: Department of Drug Chemistry and Technologies, "Sapienza" University of Rome, Piazzale Aldo Moro 5, 00185 Rome, Italy.
E-mail address: patrizia.paolicelli@uniroma1.it (P. Paolicelli).

https://doi.org/10.1016/j.carbpol.2022.119916
Received 11 May 2022; Received in revised form 4 July 2022; Accepted 21 July 2022
Available online 1 August 2022

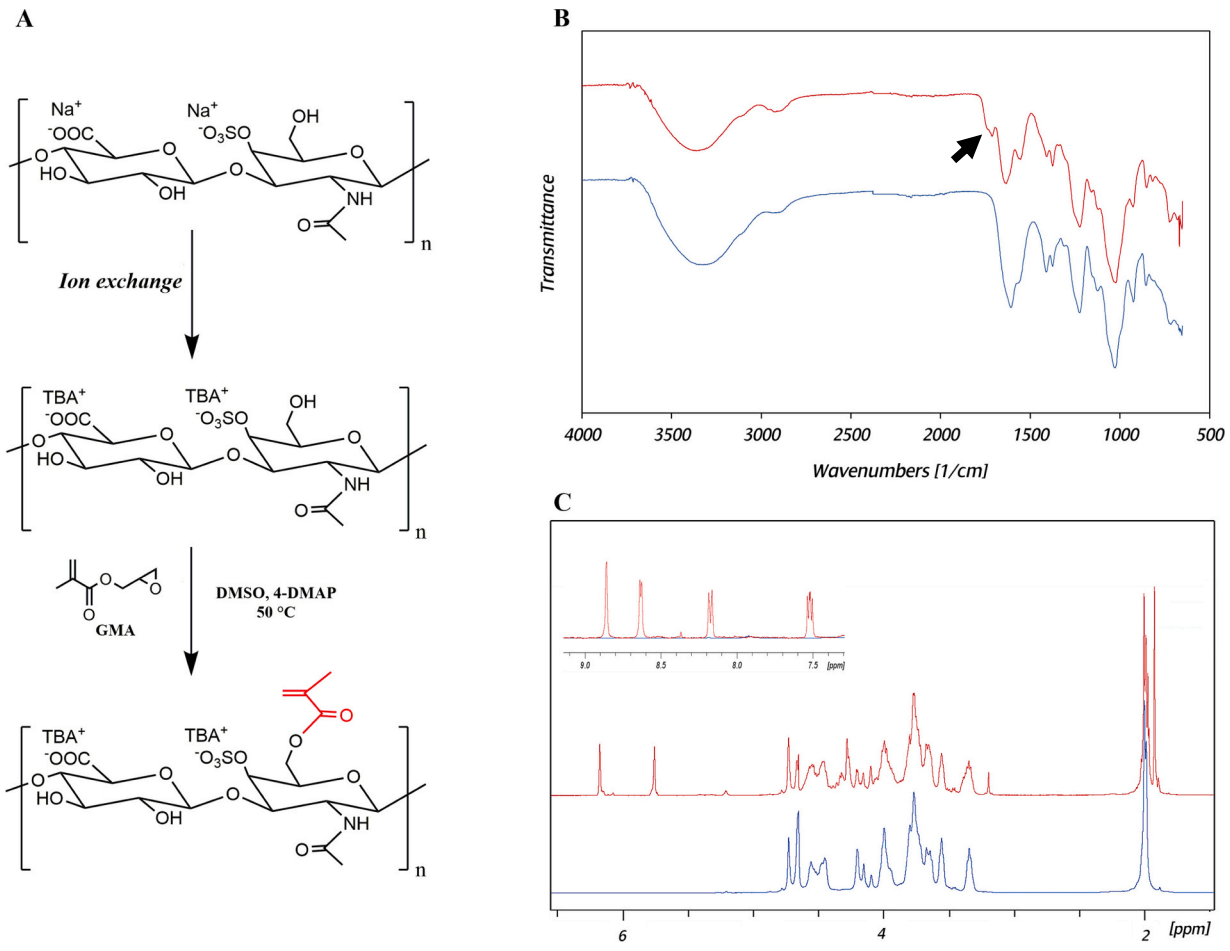

Fig. 1. (A) Scheme of the semisynthesis of CS-MA. (B) FT-IR spectra of CS_N (blue) and CS-MA (red). The arrow indicates the stretching vibration of carbonyl group of methacrylate ester ($\nu_{C=O}$ 1713 cm^{-1}). (C) ^1H NMR spectra of CS_N (blue) and CS-MA (red) recorded at 25 °C on a 400 MHz spectrometer. ^1H NMR spectrum of CS-MA shows peaks at 6.20 and 5.77 ppm of the vinyl protons of the methacrylate group, and a peak at 1.96 ppm, due to the methyl protons of the same group. The insert shows peaks of the internal standard (nicotinamide) used to calculate the DD% of CS-MA. (For interpretation of the references to colour in this figure legend, the reader is referred to the web version of this article.)

Table 1
Comparison between the DD% calculated according to the Eq.2 and Eq.4.

ED CS^-TBA^+	Mol ratio CS^-TBA^+:GMA:4-DMAP	DD%	
		Eq.2	Eq.4
1.8 ± 1	1:0.5:0.5	6 ± 1	3 ± 1
	1:1:1	12 ± 1	6 ± 1
	1:2:2	24 ± 1	12 ± 1
1.0 ± 1	1:0.5:0.5	n.d.	6 ± 1
	1:1:1	n.d.	12 ± 1
	1:2:2	n.d.	24 ± 1

CS methacrylation is commonly carried out in aqueous solution (Li et al., 2003). Both methacrylic anhydride (MAA) or glycidyl methacrylate (GMA) can be used for the synthesis, however the former is usually considered less efficient. Indeed, a large excess of MAA is needed to compensate for its hydrolysis and allow for obtaining adequate methacrylation degree of the polymer (Schuurmans et al., 2021). Whatever the reagent used, the reaction proceeds under heterogeneous-phase conditions, due to the poor water miscibility of both GMA and MAA. Because of these conditions, the methacrylation reaction results poorly efficient and the outcomes usually show low reproducibility, as already observed with other polymers, such as gelatin (Di Muzio et al., 2021). Recently, an alternative procedure has been reported for the synthesis of CS-MA based on the use of GMA and a polar aprotic solvent, namely dimethyl sulfoxide (Abbadessa et al., 2016). The proposed strategy appears very interesting as it allows to carry out the synthesis under homogeneous-phase conditions, even if long reaction times are required to achieve adequate derivatization degrees (DD%) of the polymer. For this reason, in this research work, the methacrylation reaction of CS-A with GMA was carefully investigated with the aim of optimizing the reaction parameters and achieve high DD% in a short time. Moreover, the possibility of synthesizing CS derivatives with controllable and reproducible methacrylation degrees and thus, with tunable physical and chemical properties, was evaluated. Finally, as the reaction environment and conditions may deeply influence the final outcome, bringing to CS-MA with different features and properties, the obtained derivatives were finely investigated by homonuclear and heteronuclear correlated 2D-NMR techniques, such as HSQC, HMBC and TOCSY.

2. Materials and methods

2.1. Materials

Chondroitin sulfate (CS_N) sodium salt from bovine trachea (70 % Type A, balanced with Type C), Dowex® 50WX4 hydrogen form resin (50–100 mesh), tetrabutylammonium bromide (TBAB), anhydrous dimethyl sulfoxide (DMSO), deuterium oxide (D_2O), dimethyl sulfoxide-d_6 (DMSO-d_6), glycidyl methacrylate (GMA), methacrylic anhydride (MAA), 4-(*N*,*N*-dimethylamino)pyridine (4-DMAP), triethylamine

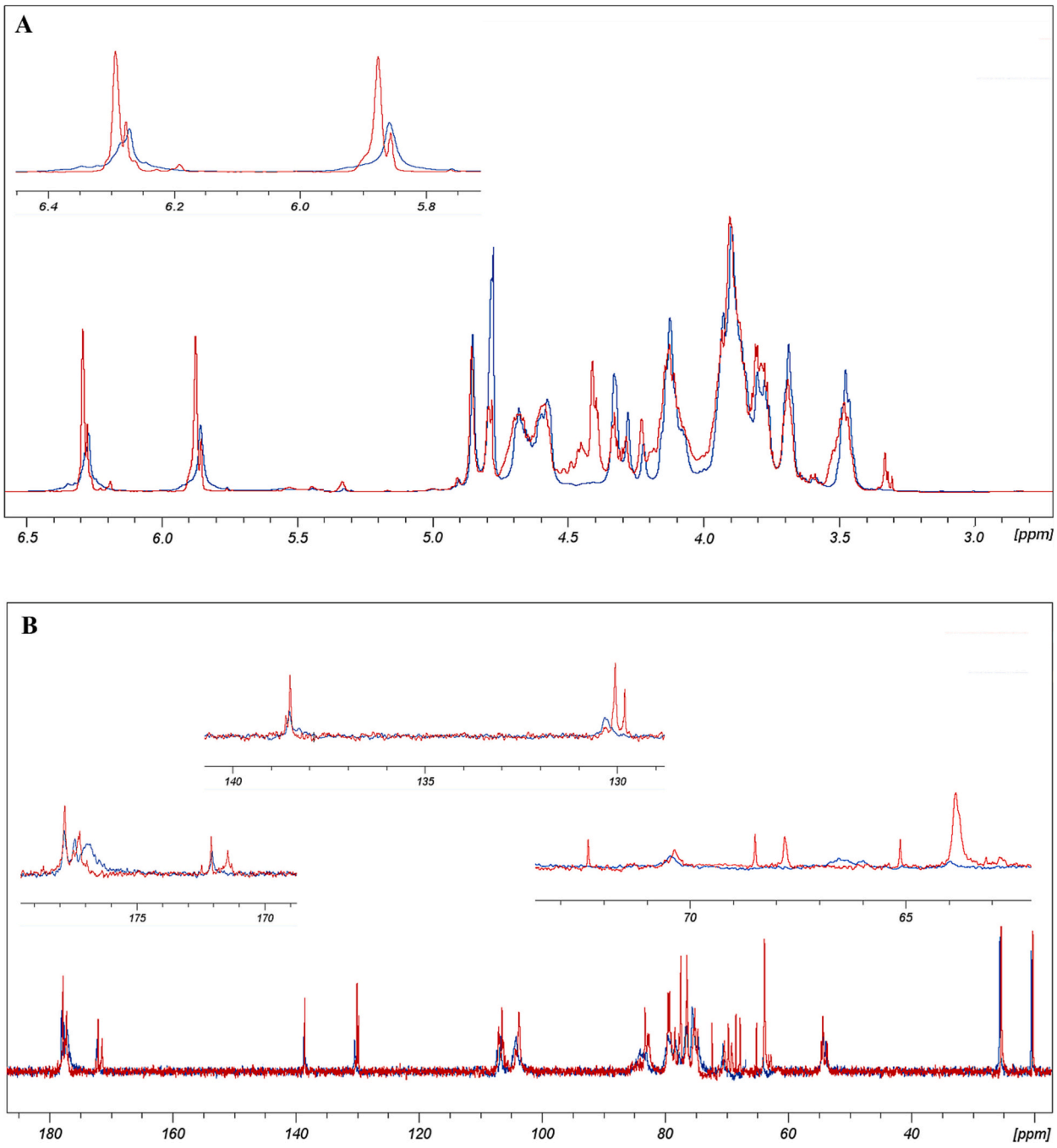

Fig. 2. (A) ^{1}H NMR spectra of CS-MA$_{MA}$ (blue) and CS-MA$_{GMA}$ (red). The insert shows the differences in the signals of the vinyl protons of CS-MA synthesized using MAA or GMA. (B) ^{13}C NMR spectra of CS-MA$_{MA}$ (blue) and CS-MA$_{GMA}$ (red). The region from 63 to 73 ppm, conveniently enlarged, shows signals of the glyceryl spacer of CS-MA$_{GMA}$. The region from 129 to 140 ppm, conveniently enlarged, shows signal of the vinyl carbons of CS-MA$_{GMA}$. The region from 169 to 179 ppm, conveniently enlarged, shows signal of the carbonyl carbons of CS-MA$_{GMA}$ deriving from the transesterification and epoxy ring-opening products. Both ^{1}H and ^{13}C NMR spectra were recorded at 36 °C on a 600 MHz spectrometer. (For interpretation of the references to colour in this figure legend, the reader is referred to the web version of this article.)

(TEA), dialysis membranes (cut-off 12–14 kDa) and nicotinamide (NIC) were obtained from Sigma-Aldrich (Darmstadt, Germany). Potassium dihydrogen phosphate (KH_2PO_4), sodium phosphate dibasic (Na_2HPO_4), sodium chloride (NaCl), sodium hydroxide (NaOH) and hydrochloric acid (HCl) were obtained from Carlo Erba Reagents (Milan, Italy).

All used reagents were of analytical grade.

2.2. Semisynthesis of chondroitin sulfate methacrylate (CS-MA)

2.2.1. Production of tetrabutylammonium salt of CS ($CS^{-}TBA^{+}$)

To increase the solubility in organic solvents, the sodium salt of CS$_N$ was converted in the TBA^{+} one through an ion-exchange process. To this end, Dowex® resin (10 ml) was flushed with 20 ml of TBAB aqueous solution (0.4 g/ml) and then washed with distilled water (100 ml) to remove the excess of salt. Next, 10 ml of an aqueous solution of CS$_N$ (1 g) was eluted through the resin and collected as $CS^{-}TBA^{+}$. Then, the polymer solution was frozen at −30 °C and freeze-dried. The solid was

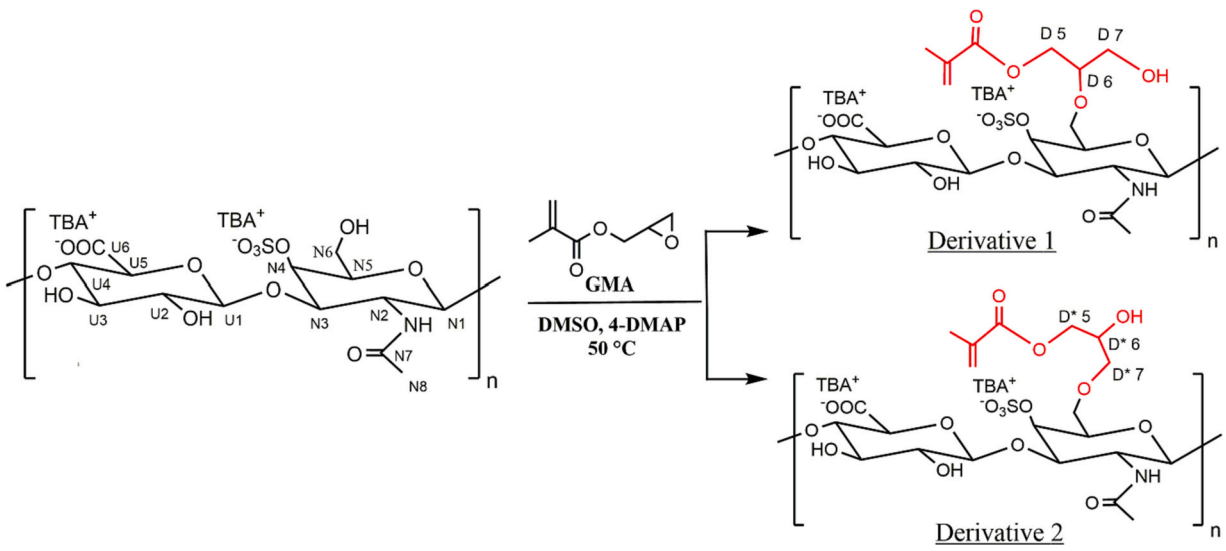

Fig. 3. Schematic illustration of the two possible derivatives obtained by opening of the GMA-epoxy ring.

dissolved in DMSO-d_6 and analysed by ^{1}H NMR at 25 °C, using a Bruker AC-400 spectrometer. The exchange degree (ED) of CS^-TBA^+ was expressed as the content of TBA^+ ions per disaccharide repeating unit of CS and was calculated according to the literature (Abbadessa et al., 2016), following Eq. (1).

$$ED = \frac{Average\ (I_{1.57}, I_{1.32})}{8} : \frac{I_{1.77}}{3} \quad (1)$$

$I_{1.57}$ and $I_{1.32}$ indicate the integrals of the signals corresponding to the eight chemically equivalent methylene protons of the four aliphatic chains of TBA^+ [$N^+(CH_2CH_2CH_2CH_3)_4$]. $I_{1.77}$ represents the integral of the methyl peak of GalNAc. Following the reported procedure, an ED of 1.0 ± 0.2 was obtained.

With the aim to double the ED of CS^-TBA^+, the above procedure was modified utilizing 20 ml of resin, 40 ml of TBAB solution and the same amount of CS_N. Following the modified procedure, an ED of 1.8 ± 0.2 was obtained.

2.2.2. Semisynthesis of CS-MA with GMA

CS-MA was synthesized according to the procedure reported by Abbadessa et al., 2016 with some modifications. CS^-TBA^+ (0.6 mmol of repeating units) was dissolved in anhydrous DMSO (8 ml) at 50 °C and, after complete dissolution, variable amounts of 4-DMAP and GMA were added and the mixture was allowed to react at 50 ± 1 °C under magnetic stirring and N_2 atmosphere for 24 h. In order to obtain CS-MA with different derivatization degrees (DD%), 3 different molar ratios CS^-TBA^+:4-DMAP:GMA were investigated, namely 1:0.5:0.5, 1:1:1 and 1:2:2.

After the reaction time, the mixtures were diluted with 25 ml of distilled water and the pH was adjusted to 5.5 using HCl 2 M. The products were extensively dialyzed first against 1 M NaCl for 2 days, then against distilled water for additional 2 days. Finally, the purified CS-MA was collected as sodium salt and freeze-dried.

2.2.3. Semisynthesis of CS-MA with MAA

CS^-TBA^+ (0.6 mmol of repeating units) was dissolved in anhydrous DMSO (8 ml) at 50 °C and after complete dissolution, TEA (270 μL; 1.8 mmol), 4-DMAP (0.22 g; 1.8 mmol) and MAA (176 μL; 1.8 mmol) were added to the polymer solution (molar ratio CS^-TBA^+:TEA:4-DMAP:MAA equal to 1:3:3:3). The mixture was allowed to react at 50 ± 1 °C under magnetic stirring and N_2 atmosphere for 48 h and, after the reaction time, it was treated and purified as described in Section 2.2.2. The obtained product was labelled $CS\text{-}MA_{MA}$.

2.3. Characterization of CS-MA

2.3.1. Fourier transform infrared spectroscopy (FTIR)

CS_N and CS-MA were analysed by ATR-FTIR spectroscopy. Attenuated total reflectance spectra were collected with a Spectrum-One Perkin Elmer® spectrophotometer equipped with a single-reflection diamond ATR accessory. Spectra were recorded in the range of 4000–650 cm^{-1}.

2.3.2. ^{1}H-Nuclear Magnetic Resonance (^{1}H NMR)

2.3.2.1. Determination of the DD% of CS-MA. In order to quantify the DD% of CS-MA, the polymer (10 mg) was dissolved in D_2O (0.7 ml), transferred in a 5 mm NMR tube and analysed by ^{1}H NMR at 25 °C, using a Bruker® AC-400 spectrometer. The DD% was defined as the number of methacrylate groups per 100 repeating units of the polymer and was determined according to Eq. (2) and (3).

$$DD\% = \frac{average\ (I_{6.20} I_{5.77})}{\frac{(I_{2.18-1.86} - 3)}{3}} \times 100 \quad (2)$$

$$DD\% = \frac{average\ (I_{6.20} I_{5.77})}{\frac{[I_{2.18-1.86} - 3\ average\ (I_{6.20} I_{5.77})]}{3}} \times 100 \quad (3)$$

where $I_{6.20}$ and $I_{5.77}$ represent the integrals of the vinyl protons and $I_{2.18–1.86}$ indicates the integral of the region where the broad signal at 1.96 ppm (methyl of methacrylate group) and the signal at 2.04 ppm (methyl of acetamide group) are partially overlapped. Alternatively, the DD% was calculated with an internal standard, using NIC for the scope. The samples were prepared by dissolving CS-MA (10 mg) in D_2O (0.5 ml) and adding 0.2 ml of NIC (1 mg/ml in D_2O). The mmol of methacrylate groups ($mmol_{MA}$) were quantified comparing the integrals of the vinyl protons of the methacrylate groups at 6.70 and 5.77 ppm with the integral of the NIC signal at 8.9 ppm. Then, the DD% was calculated using Eq. (4).

$$DD\% = \left(mmol_{MA} \times \frac{MW_a}{10} \right) 100 \quad (4)$$

where MW_a indicates the average molecular weight of the CS repeating unit, determined considering the percentage of methacrylate units with respect to the unmodified ones.

2.3.3. 1D and 2D NMR

Aliquots of CS-MA (20–30 mg) were dissolved in 0.7 ml of phosphate

Table 2
HSQC data of CS_N and CS_{GMA}.

GlcA unit	CS_N ^{13}C /^{1}H ppm	CS_{GMA} ^{13}C /^{1}H ppm	GalNAc unit	CS_N ^{13}C /^{1}H ppm	CS_{GMA} ^{13}C /^{1}H ppm
UC/UH-1; 4S*	106.4/ 4.51	106.4/ 4.51	NC/NH-1; 4S	103.6/ 4.62	103.7/ 4.62
UC/UH-1; 6S**	107.0/ 4.53	107.1/ 4.37	NC/NH-1; 6S	104.2/ 4.59	104.2/ 4.59
UC/UH-1; DES***	106.6/ 4.71	106.8/ 4.60	NC/NH-1; DES	103.4/ 4.59	103.7/ 4.59
UC/UH-2; 4S	75.2/ 3.41	75.2/ 3.41	NC/NH-2; 4S	54.3/ 4.06	54.4/ 4.06
UC/UH-2; 6S	75.2/ 3.41		NC/NH-2; 6S	53.7/ 4.05	53.8/ 4.08
UC/UH-2; DES			NC/NH-2; DES	54.3/ 4.00	54.4/ 3.99
UC/UH-3; 4S	76.5/ 3.62	75.5/ 3.62	NC/NH-3; 4S	78.4/ 4.06	78.5/ 4.05
UC/UH-3; 6S	76.5/ 3.62		NC/NH-3; 6S	82.9/ 3.88	82.9/ 3.87
UC/UH-3; DES			NC/NH-3; DES		
UC/UH-4; 4S	83.2/ 3.83	83.3/ 3.82	NC/NH-4; 4S	79.4/ 4.78	79.3/ 4.77
UC/UH-4; 6S	84.0/ 3.77	84.1/ 3.76	NC/NH-4; 6S	70.3/ 4.26	70.4/ 4.25
UC/UH-4; DES	84.5/ 3.80	84.6/ 3.80	NC/NH-4; DES	70.5/ 4.16	70.6/ 4.13
UC/UH-5; 4S	79.5/ 3.70	79.5/ 3.70	NC/NH-5; 4S	77.4/ 3.86	77.5/ 3.86
UC/UH-5; 6S	79.3/ 3.73	79.3/ 3.73	NC/NH-5; 6S	75.5/ 4.01	75.4/ 4.00
UC/UH-5; DES			NC/NH-5; DES	77.8/ 3.72	77.8/ 3.71
			NC/NH-5; D		79.7/ 4.04
			NC/NH-5; D*		76.3/ 4.12
			NC/NH-6; 4S	63.8/ 3.83	63.9/ 3.82
			NC/NH-6; 6S	70.4/ 4.21	70.4/ 4.25
			NC/NH-6; DES		
			NC/NH-6; D		63.4/ 3.83
			NC/NH-6; D*		62.8/ 3.90
			NC/NH-8	25.4/ 2.04	25.2/ 2.10

* Chondroitin-4-sulfate.
** Chondroitin-6-sulfate.
*** Chondroitin non-sulfate.

buffer in D_2O (100 mM, pH 7.4) and transferred in 5 mm NMR tubes. The buffer was prepared using anhydrous KH_2PO_4 (233.6 mg) e K_2HPO_4 (573.0 mg) in 50 mL D_2O. NMR spectra of the samples were recorded at 36 °C on a Bruker® AVANCE 600 NMR spectrometer operating at the proton frequency of 600.13 MHz and equipped with a Bruker multinuclear z-gradient inverse probe head, capable of producing gradients in the z-direction with a strength of 55 G cm^{-1}. ^{1}H spectra were acquired by co-adding 32 transients with a recycle delay of 5 s. The residual water signal was suppressed by using a solvent pre-saturation during recycle delay. The experiment was carried out by using 90° flip angle pulses of 10.0–12.0 μs, 16 K data points. ^{1}H—^{1}H Total Correlation Spectroscopy (TOCSY) spectra were registered in the States-TPPI phase-sensitive mode, with water presaturation during relaxation delay, a spectral width 6 kHz in both dimensions, a 2 s relaxation delay, an 80 ms mixing time, 2 K data points in f_2 and 512 increments in f_1. Zero filling in f_1 to 1 K real data points and unshifted sinusoidal window functions in both dimensions were applied before Fourier transformation. The ^{1}H—^{13}C gradient-selected Heteronuclear Single Quantum Coherence (HSQC) spectra were registered in the echo-antiecho phase-selective mode with the following parameters: 2.5 s relaxation delay, 14 μs 90° ^{13}C hard pulse and 74 μs for GARP ^{13}C decoupling, a coupling constant $^{1}J_{C-H}$ of 150 Hz, 6 and 24 kHz spectral widths in the proton and carbon dimensions respectively, 1 K data points in f_2 and 512 increments in f_1. Unshifted squared cosine window functions were applied in both dimensions before Fourier transformation. The ^{1}H—^{13}C Heteronuclear Multiple-Bond Correlation (HMBC) spectra were obtained with a 2.5 s relaxation delay, 14 μs 90° pulse for ^{13}C, 6 and 33 kHz spectral widths in the proton and carbon dimensions respectively, a delay for the evolution of long-range couplings of 80 ms, 1 K data points in f_2, 256 increments in f_1, linear prediction up to 512 points and zero filling in f_1 to 1 K real data points, processed with the use of unshifted squared cosine window functions in both dimensions. The $\{^{1}H\}^{13}C$ NMR spectra (proton–decoupled) were obtained by co-adding 10,000 transients with a recycle delay of 5 s, a 37.5 kHz spectral width, 64 K data points, a GARP pulse sequence for proton decoupling, and a ^{13}C pulse of 10 μs. The Bruker pulse sequence zgpg was used.

3. Results and discussion

3.1. Semisynthesis and characterization of CS-MA

The methacrylation of CS was carried out following the reaction scheme reported in Fig. 1A.

In the first step, CS_N was converted in its TBA^+ salt, in order to significantly increase polymer solubility in DMSO, the polar aprotic solvent used for the methacrylation reaction. ^{1}H-NMR of CS^-TBA^+ shows the signals at 3.16, 1.57, 1.32 and 0.94 ppm corresponding to the protons of the four aliphatic chains of TBA^+, confirming that Na^+ was effectively and quite completely replaced by TBA^+. Indeed, the ion-exchange procedure was carefully optimized to get CS^-TBA^+ with an ED of 1.8 ± 0.2, that approximately corresponds to two TBA^+ ions per each repeating unit.

The subsequent methacrylation reaction was carried out by fixing 3 different molar ratios CS^-TBA^+:4-DMAP:GMA, namely 1:0.5:0.5; 1:1:1 and 1:2:2, to evaluate the effect of this factor on the efficiency of the methacrylation reaction and obtain derivatives with different DD%. The successful derivatization of the polymer was first evaluated by FT-IR spectroscopy. As shown in Fig. 1B, the FT-IR spectrum of CS-MA shows a new band at 1713 cm^{-1}, which can be attributed to the characteristic stretching vibration of the carbonyl group ($\nu_{C=O}$) of methacrylate ester. Similar results were already described for CS-MA (Wang et al., 2003) and also reported for other methacrylate polymers, such as Dex-MA (Szafulera et al., 2018). The effective derivatization of CS was further confirmed by ^{1}H NMR. The spectrum (Fig. 1C) shows two distinctive peaks at 6.20 and 5.77 ppm, which can be attributed to the vinyl protons of the methacrylate group, and a peak at 1.96 ppm, due to the methyl protons of the same group. ^{1}H NMR spectrum was also used to quantify the DD% of CS-MA. Several methods were applied to calculate the DD%, trying to find the most reliable. First attempts were made considering the signal at 3.41 ppm due to the H2 proton of GlcA unit (Fajardo et al., 2013). However, accurate peak integration was impaired by partial signal overlapping. Therefore, other methods were evaluated. In particular, further attempts were made following Eq. 2 (Abbadessa et al., 2016). This method is based on the comparison of the integrals of the vinyl protons with the methyl protons of the GalNAc acetamide group at 2.04 ppm. However, this peak is partially overlapping the peak at 1.96 ppm (methyl of methacrylate group) and, for this reason, it cannot be properly integrated, neither with peak deconvolution. Even if Eq.2 attempts to consider this signal overlap, it can be properly applied only when the integrals of both vinyl protons show the value of 1, if not Eq.2 should be corrected in Eq.3. Anyway, in order to evaluate the accuracy of the DD% obtained by either Eq.2 or Eq.3, an internal standard (NIC), was used. ^{1}H NMR spectrum shows very clean signals in the range 7.00–9.00 ppm corresponding to the aromatic

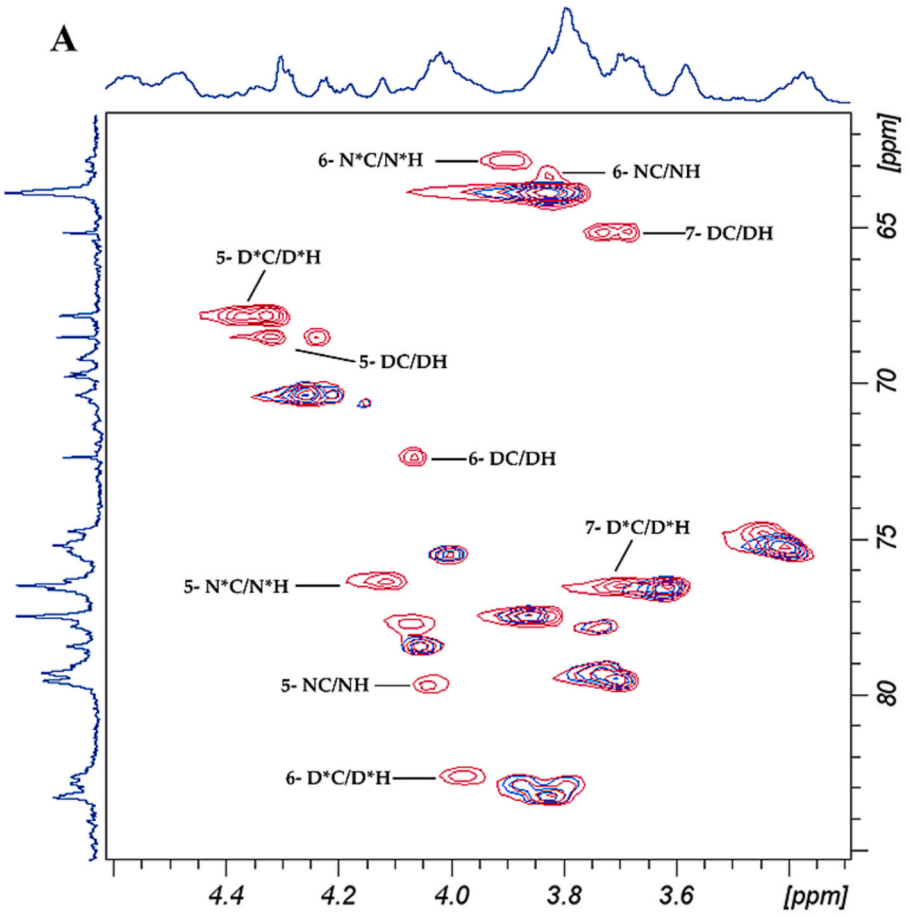

B

	$^{13}C/^{1}H$ - 5 (ppm)	$^{13}C/^{1}H$ - 6 (ppm)	$^{13}C/^{1}H$ - 7 (ppm)
Derivative 1 (D)	68.8/4.24-4.32	72.5/4.07	65.2/3.69-3.73
Derivative 2 (D*)	67.8/4.32-4.34	82.6/3.98	76.5/3.70-3.74

Fig. 4. (A) HSQC spectra of CS_N (blue) and CS-MA_{GMA} (red) recorded at 36 °C on a 600 MHz spectrometer. (B) HSQC data of the two ring-opening products of CS-MA_{GMA}. (For interpretation of the references to colour in this figure legend, the reader is referred to the web version of this article.)

protons of the pyridine ring of NIC (Fig. 1C). These peaks were utilised to quantify the DD% of CS-MA by applying Eq.4. Results obtained with the internal standard are reported in Table 1 in comparison with those achieved by following Eq.2. It can be observed a significant difference between the values. In particular, the DD% obtained applying Eq.2 results almost twice those estimated by the internal standard method.

The difference may be due to the partial overlap between the peaks of the methyl protons of the acetamide and methacrylate groups, as well as to the high difference in intensity between the peaks of the vinyl and methyl protons that hamper their precise integration. The discrepancy in the values is reduced when the DD% is calculated according to the more accurate Eq.3, instead of Eq.2, and using high-field NMR spectrometers (at least 600 MHz), which allow for better peak resolution. In any case, the use of an internal standard results more reliable and should be generally preferred to estimate the DD% values of CS-MA. The results reported in Table 1 show also a direct proportionality between the DD% and the molar feed ratio used in the synthesis. Therefore, the adopted experimental conditions allow a fine tuning of the methacrylation degree of CS-MA and allowed achieving a maximum DD% of 12 ± 1. Higher DD% were obtained using a $CS^{-}TBA^{+}$ with a lower ED. Considering the dimensions of the TBA cation, it may be supposed that its steric hindrance decreases CS reactivity. Indeed, the reactivity of the primary hydroxyl group of GalNAc unit could be influenced by the presence of the bulky TBA^{+} on the adjacent sulfate group.

Therefore, other reactions were carried out under the same conditions and using the same molar feed ratios, while employing a $CS^{-}TBA^{+}$ with an ED of 1.0 ± 0.2, which still allowed for adequate solubility of the polymer in DMSO. The ^{1}H NMR spectra show progressive increase in the intensity of the proton signals of the methacrylate group (Fig. S1).

The methacrylation reaction proceeds much more efficiently under these conditions allowing to achieve a doubling of the DD% (Table 1). While these results cannot be directly compared to the literature due to the different methods used to determine the DD%, it can be safely stated that the experimental set-up optimized in this work allows obtaining CS-MA derivatives with high, easily tunable and very reproducible methacrylation degrees in a short reaction time (24 h). Based on these results,

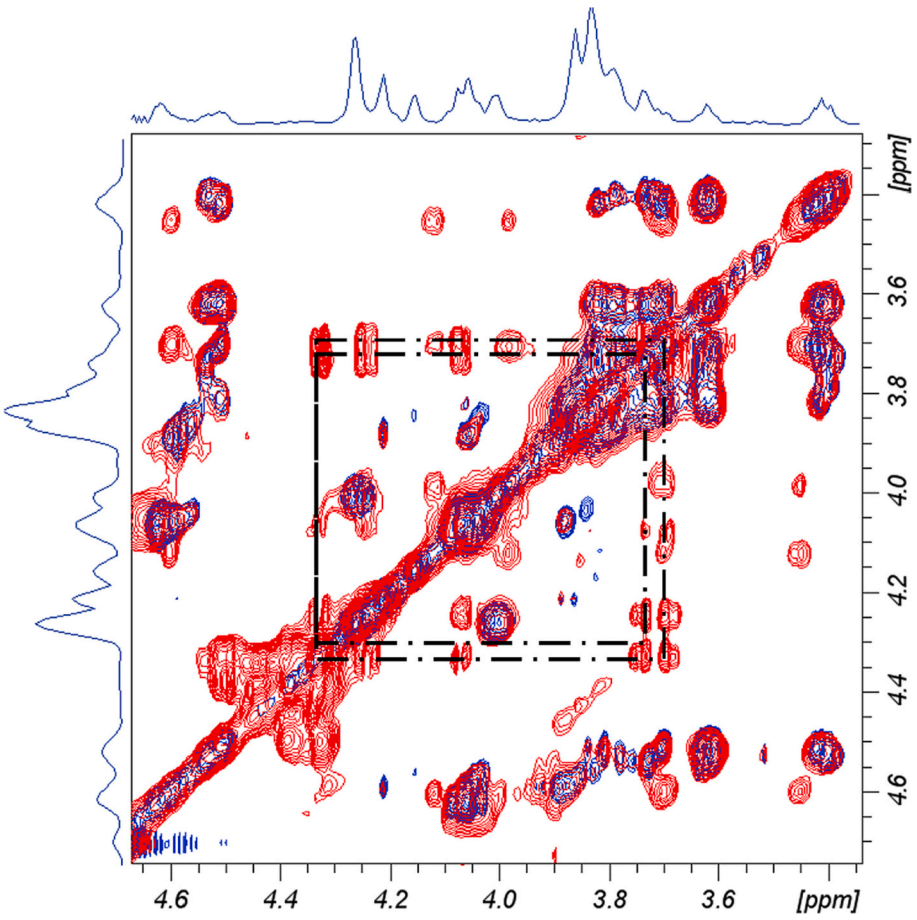

Fig. 5. TOCSY spectra of CS_N (blue) and CS-MA_{GMA} (red) recorded at 36 °C on a 600 MHz spectrometer. Spin systems correlations among DH-5, DH-6 and DH-7 and D*H-5, D*H-6 and D*H-7 of the two products deriving from the opening of the GMA-epoxy ring, are evidenced. (For interpretation of the references to colour in this figure legend, the reader is referred to the web version of this article.)

the DD% of CS-MA critically depends on the molar feed ratio of the reagents and the ED of $CS^{-}TBA^{+}$. Therefore, these parameters need to be finely adjusted, especially when high DD% must be achieved.

3.2. 1D and 2D NMR investigation of the reaction of CS with GMA

3.2.1. NMR characterization of the reaction products

The reaction of biopolymers with GMA is widely used to synthesize their methacrylate derivatives. It has been reported that the reaction with GMA may proceed via epoxy ring-opening or transesterification. When the reaction is carried out under heterogeneous-phase conditions, CS reacts with GMA via both mechanisms and the final outcome is deeply influenced by the pH value of the medium (Li et al., 2003). Indeed, in the initial stage of the reaction, the transesterification product results to be predominant. Later on, when the system pH begins to decrease due to the slow hydrolysis of the methacrylate ester and consequent formation of methacrylic acid, the ring-opening of the GMA-epoxy group is promoted. On the contrary, when the reaction is carried out under homogeneous-phase conditions, it has been reported that the CS methacrylation proceeds exclusively via transesterification (Abbadessa et al., 2016), in analogy with the findings already reported for dextran (van Dijk-Wolthuis et al., 1997). Anyway, it can be observed in the ^{1}H NMR spectra of CS-MA (Fig. 1C and S1) a broad signal in the range 4.25–4.40 ppm, which may suggest the presence of the glyceryl spacer of GMA. Such signal is also present, but not considered, in the ^{1}H NMR spectrum reported in the literature (Abbadessa et al., 2016).

Therefore, to unravel the mechanism of the CS methacrylation with GMA under homogeneous-phase conditions, CS-MA was deeper characterized by 1D and 2D NMR spectroscopy. To this end, a control reaction was carried out using MAA for CS methacrylation (CS-MA_{MA}), because it allows obtaining exclusively the esterification product. The reaction was carried out in anhydrous DMSO, but a large excess of MAA and longer time (48 h) were necessary to achieve a DD of at least 12 %, thus confirming the superiority of GMA for biopolymer methacrylation (Oudshoorn et al., 2007). CS-MA_{GMA} (DD% 24) and CS-MA_{MA} (DD% 12) were first analysed by ^{1}H NMR spectroscopy. The spectrum of CS-MA_{GMA} shows, in the area of vinyl protons, two distinct sets of signals (Fig. 2A). The peaks at 5.85 and 6.28 ppm can be observed in both CS-MA_{GMA} and CS-MA_{MA}, whereas the two further peaks at 5.88 and 6.30 ppm are completely absent in CS-MA_{MA}.

It can be reasonably assumed that these additional peaks and those in the range 4.25–4.50 ppm represent respectively the signals of the vinyl and methylene protons of the glyceryl spacer derived from GMA-epoxy ring opening. Similar findings were achieved with ^{13}C NMR spectroscopy. Indeed, CS-MA_{GMA} shows signals in the range 65–73 ppm, which are absent in CS-MA_{MA} (Fig. 2B). These peaks may represent the methylene carbons of the glyceryl spacer. Moreover, CS-MA_{GMA} spectrum reveals two different sets of signals in the region 138.0–130.0 ppm that can be attributed to the vinyl-carbon of the methacrylate group. The peaks at 130.5 and 138.1 ppm can be detected in both CS-MA_{GMA} and CS-MA_{MA} and can be then assigned to the vinyl-carbon of the CS-methacrylate ester. Consequently, the other signals in the same area may be attributed to the vinyl-carbons of the methacrylate groups originating from the epoxy ring-opening. Finally, CS-MA_{GMA} shows at least three different signals at approximately 172 ppm, while CS-MA_{MA} displays only one of them in the same region of the spectrum. These

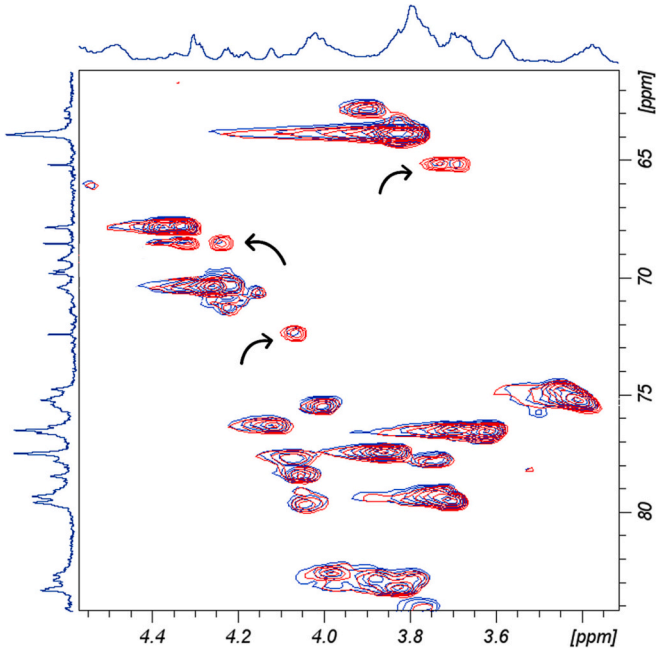

Fig. 6. HSQC spectra of CS-MA_{24} (red) and CS-MA_{12} (blue) recorded at 36 °C on a 600 MHz spectrometer. The arrows indicate the effect of the DD% of CS-MA on the intensity of the cross-peaks of DC/H-5, DC/H-6 and DC/H-7. (For interpretation of the references to colour in this figure legend, the reader is referred to the web version of this article.)

peaks may correspond to the carbonyl-carbons of the methacrylate groups and, similarly to the vinyl-carbons, can be attributed to both transesterification and ring-opening products. To confirm these assignments, vinyl- and carbonyl-carbons signals were further investigated by means of $^{1}H—^{13}C$ HMBC experiments. HMBC of CS-MA_{MA} reveals the correlations of the carbonyl-carbon at 172 ppm with the vinyl protons at 5.77 and 6.20 ppm and the methyl proton at 1.96 ppm. In addition, the spectrum shows a cross-peak between the latter proton and the vinyl-carbon at 138 ppm (Fig. S2). These signals are also present in the HMBC of CS-MA_{GMA}, definitely confirming the presence of the transesterification product. Based on these results, it can be safely confirmed that the methacrylation reaction of CS with GMA in DMSO proceeds via both transesterification and epoxy ring-opening.

Hence, the reaction outcome was further examined by $^{1}H—^{13}C$ HSQC and $^{1}H—^{1}H$ TOCSY NMR to specifically investigate the regioselectivity of the reaction. As known, nucleophiles can attack the epoxy ring of GMA in two different positions, thus generating two different derivatives, as reported in Fig. 3.

Preliminary studies were carried out on CS_N to identify and fully characterize its structure. The complete cross-peaks assignment of the HSQC spectrum of CS_N is reported in Table 2.

Compared to CS_N, the HSQC spectrum of CS-MA_{GMA} evidenced new correlation peaks (Fig. 4A). These cross-peaks were finely identified and attributed to the methine/methylene groups generated by the reaction of CS-hydroxyl groups with the GMA-epoxy ring (Fig. 4B).

In detail, it is possible to identify the correlations between carbons and protons 5-DC/DH, 6-DC/DH-and 7-DC/DH of derivative 1 (Fig. 3), and also the cross-peaks corresponding to D*C/H-5, D*C/H-6 and D*C/H-7 of derivative 2 (Shaw et al., 2006; van Dijk-Wolthuis et al., 1995).

The assignment based on HSQC spectra was confirmed by TOCSY experiments, which allowed identifying the homonuclear spin system correlations between the methine/methylene protons of the two ring-opening products of CS-MA_{GMA}. TOCSY spectrum exhibits the spin system correlations between DH-5, DH-6 and DH-7, definitely confirming that these protons belong to the same molecular framework (Fig. 5). The spectrum also reveals the correlations between D*H-5, D*H-6 and D*H-7, even if less evident. The methylene protons of the two products show, as expected, very similar chemical shifts, which cause their partial overlapping. Some signals due to desulfated CS-MA can also be observed. More in detail, it can be observed a spin system correlation between protons at 4.59, 3.99, 4.13 and 3.71 ppm. These signals correspond respectively to N1, N2, N4 and N5 protons and derive from the cleavage of the sulfate at C4 position of GalNAc unit (Mucci et al., 2000). This observation agrees with the results reported in the literature, where a DMSO/MeOH mixture was used for regioselective desulfation of CS in this position (Han et al., 2018). Data reported in Table 2 show that partial desulfation is already present in CS_N. Following the methacrylation procedure, a slight increase in the desulfation degree of the biopolymer was observed, which can be roughly estimated from ^{1}H NMR spectra to be in the order of 20 %. The occurrence of desulfation during the methacrylation of CS is a frequently ignored issue, whereas it would deserve special attention, since it is reported in the literature that some biological activities of CS are closely related to the sulfation pattern (Gama et al., 2006; Malliappan et al., 2022).

Globally, the assignment carried out by HSQC analysis resulted to be correct and the presence of the two products deriving from the nucleophilic attack on the two different positions of the GMA-epoxy ring can be definitively confirmed. Furthermore, the HSQC spectrum of CS-MA_{GMA} allowed identifying new cross-peaks at 79.72/4.04; 63.35/3.83; 76.32/4.12 and 62.79/3.90 ppm (Fig. 4). Analysing these chemical shifts, it can be supposed that these signals come from N5 and N6 of CS_N, according to the substituent effect expected with the derivatization in position 6. Thus, these cross-peaks presumably correspond to N5/N6 of the derivative 1 and N*5/N*6 of the derivative 2, respectively. The assignment was validated by TOCSY analysis (Fig. 5), which allowed to identify the homonuclear spin system correlations between NH-5/NH-6 (4.04/3.83 ppm) and N*H-5/N*H-6 (4.11/3.90 ppm) protons. HSQC spectra of CS-MA_{GMA} and CS-MA_{MA} (Fig. S3) also enable the detection of NC-5/NH-5 cross-peak (77.71/4.07 ppm) belonging to the transesterification product at position 6. Conversely, the N6 signal of the transesterification product was not detected. Likely, this signal is overlapped with the high intense cross-peaks of the GalNAc unit of CS_N. Consequently, in agreement with the results previously reported in the literature (Abbadessa et al., 2016), it can be reasonably confirmed that under the adopted synthetic conditions, the methacrylation reaction involves predominantly the primary hydroxyl groups of CS. On the contrary, when the reaction is carried out under heterogeneous liquid-liquid phase conditions, the methacrylation involves the sulfate and carboxyl groups of the biopolymer (Li et al., 2003). This difference can be explained considering the different properties of the two solvents used (DMSO and H_2O), but also by the presence of TBA cations. The steric hindrance of TBA^{+} on the sulfate and carboxyl groups of CS_N may significantly decrease their reactivity, thus directing the reaction towards the primary hydroxyl groups of the polymer.

3.2.2. *Effect of the methacrylation degree on the reaction outcome*

The reaction outcome was also investigated for all the other CS-MA derivatives, having DD% 12 (CS-MA_{12}) and 6 (CS-MA_6). For this purpose, the HSQC spectrum of CS-MA_{24} was carefully compared with those of CS-MA_{12} and CS-MA_6. The signals assignment of CS-MA_{12} and CS-MA_6 does not show any significant difference. On the other hand, the HSQC spectra of CS-MA_{12} and CS-MA_6 revealed a different intensity of the signals corresponding to the methine/methylene protons of the two products derived from the epoxy ring-opening. Indeed, while the cross-peaks corresponding to D*C/H-5, D*C/H-6 and D*C/H-7 are clearly identified, those from DC/H-5, DC/H-6 and DC/H-7 show very low intensity in CS-MA_{12} (Fig. 6) and are completely absent in CS-MA_6 (data not shown).

Based on the experimental results, it can be confirmed, as expected, that nucleophilic attack on the less sterically hindered position of the epoxy ring is preferred. Therefore, the use of low amounts of GMA leads to the preferential formation of one of the two possible ring-opening

products.

3.3. Conclusions

The methacrylation reaction of CS was carefully optimized to achieve tunable and reproducible methacrylation degrees in short reaction times. The use of GMA showed superior reactivity compared to MAA and should be preferred when CS-MA with high DD% needs to be synthesized. More specifically, when the methacrylation reaction is carried out under homogeneous-phase conditions in DMSO, the DD% critically depends on the molar feed ratio of the repeating unit of the polymer, the methacrylate reagent and catalyst used, as well as on the extent of CS exchange with the bulky TBA^+. Therefore, these parameters need to be finely adjusted to achieve CS-MA with the desired methacrylation rate. Accurate evaluation of the DD% of CS-MA required the use of an internal standard associated with ^1H NMR spectroscopy. Furthermore, 1D and 2D NMR experiments evidenced that the reaction proceeds via both transesterification and opening of GMA-epoxy ring. These analyses also showed that in DMSO GMA reacts predominantly with primary hydroxyl groups of CS, whereas the same reaction carried out in water brings to the prevalent substitution of carboxyl and sulfate groups. Therefore, the reaction environment deeply influences the final outcome, bringing to CS-MA derivatives with different features and properties. These findings are of fundamental importance for the proper and rational design of CS-MA-based biomaterials. Indeed, whether the specific application envisaged for CS-MA requires free carboxyl and sulfate groups, then the methacrylation reaction of CS needs to be carried out under homogeneous-phase conditions.

Supplementary data to this article can be found online at https://doi.org/10.1016/j.carbpol.2022.119916.

CRediT authorship contribution statement

Laura Di Muzio: Writing – original draft, Data curation, Investigation, Writing – review & editing, Visualization, Formal analysis, Conceptualization, Methodology. **Patrizia Paolicelli:** Project administration, Writing – original draft, Writing – review & editing, Conceptualization, Methodology, Visualization. **Jordan Trilli:** Writing – review & editing, Formal analysis. **Stefania Petralito:** Writing – review & editing, Methodology, Formal analysis. **Vito Cosimo Carriero:** Writing – review & editing, Formal analysis. **Chiara Brandelli:** Writing – review & editing, Formal analysis. **Mattia Spano:** Data curation, Writing – review & editing, Formal analysis. **Anatoly Petrovich Sobolev:** Data curation, Investigation, Resources, Writing – review & editing, Formal analysis, Methodology. **Luisa Mannina:** Supervision, Writing – review & editing. **Maria Antonietta Casadei:** Resources, Supervision, Writing – review & editing, Conceptualization.

Declaration of competing interest

The authors declare that they have no known competing financial interests or personal relationships that could have appeared to influence the work reported in this paper.

Data availability

Data will be made available on request.

Acknowledgements

University project funds

References

Abbadessa, A., Blokzijl, M. M., Mouser, V. H. M., Marica, P., Malda, J., Hennink, W. E., & Vermonden, T. (2016). A thermo-responsive and photo-polymerizable chondroitin sulfate-based hydrogel for 3D printing applications. *Carbohydrate Polymers, 149*, 163–174.

Bang, S., Jung, U.-W., & Noh, I. (2018). Synthesis and biocompatibility characterizations of in situ chondroitin sulfate-gelatin hydrogel for tissue engineering. *Tissue Engineering and Regenerative Medicine, 15*(1), 25–35.

Costantini, M., Idaszek, J., Szöke, K., Jaroszewicz, J., Dentini, M., Barbetta, A., Brinchmann, J. E., & Święszkowski, W. (2016). 3D bioprinting of BM-MSCs-loaded ECM biomimetic hydrogels for in vitro neocartilage formation. *Biofabrication, 8*(3), 35002.

Di Muzio, L., Cienzo, F., Paolicelli, P., Petralito, S., Garzoli, S., Brandelli, C., Trilli, J., & Antonietta Casadei, M. (2021). A convenient strategy to synthesize highly tunable gelatin methacryloyl with very low gelation temperature. *European Polymer Journal, 154*, Article 110538.

van Dijk-Wolthuis, W. N. E., Franssen, O., Talsma, H., Van Steenbergen, M. J., Kettenes-Van Den Bosch, J. J., & Hennink, W. E. (1995). Synthesis, characterization, and polymerization of glycidyl methacrylate derivatized dextran. *Macromolecules, 28*(18), 6317–6322.

van Dijk-Wolthuis, W. N. E., Kettenes-van den Bosch, J. J., van der Kerk-van Hoof, A., & Hennink, W. E. (1997). Reaction of dextran with glycidyl methacrylate: An unexpected transesterification. *Macromolecules, 30*(11), 3411–3413.

Fajardo, A. R., Fávaro, S. L., Rubira, A. F., & Muniz, E. C. (2013). Dual-network hydrogels based on chemically and physically crosslinked chitosan/chondroitin sulfate. *Reactive and Functional Polymers, 73*(12), 1662–1671.

Gama, C. I., Tully, S. E., Sotogaku, N., Clark, P. M., Rawat, M., Vaidehi, N., Goddard, W. A., Nishi, A., & Hsieh-Wilson, L. C. (2006). Sulfation patterns of glycosaminoglycans encode molecular recognition and activity. *Nature Chemical Biology, 2*(9), 467–473.

Han, W., Li, Q., Lv, Y., Wang, Q. C., & Zhao, X. (2018). Preparation and structural characterization of regioselective 4-O/6-O-desulfated chondroitin sulfate. *Carbohydrate Research, 460*, 8–13.

Köwitsch, A., Zhou, G., & Groth, T. (2018). Medical application of glycosaminoglycans: A review. *Journal of Tissue Engineering and Regenerative Medicine, 12*(1), e23–e41.

Lafuente-Merchan, M., Ruiz-Alonso, S., Zabala, A., Gálvez-Martín, P., Marchal, J. A., Vázquez-Lasa, B., … Pedraz, J. L. (2022). Chondroitin and dermatan sulfate bioinks for 3D bioprinting and cartilage regeneration. *Macromolecular Bioscience*, 2100435.

Li, Q., Wang, D., & Elisseeff, J. H. (2003). Heterogeneous-phase reaction of glycidyl methacrylate and chondroitin sulfate: Mechanism of ring-opening−transesterification competition. *Macromolecules, 36*(7), 2556–2562.

Malliappan, S. P., Yetisgin, A. A., Sahin, S. B., Demir, E., & Cetinel, S. (2022). Bone tissue engineering: Anionic polysaccharides as promising scaffolds. *Carbohydrate Polymers, 283*.

Mei, Q., Rao, J., Bei, H. P., Liu, Y., & Zhao, X. (2021). 3D bioprinting photo-crosslinkable hydrogels for bone and cartilage repair. *International Journal of Bioprinting, 7*(3), 37–53.

Mucci, A., Schenetti, L., & Volpi, N. (2000). 1H and 13C nuclear magnetic resonance identification and characterization of components of chondroitin sulfates of various origin. *Carbohydrate Polymers, 41*(1), 37–45.

Neves, M. I., Araújo, M., Moroni, L., da Silva, R. M. P., & Barrias, C. C. (2020). Glycosaminoglycan-inspired biomaterials for the development of bioactive hydrogel networks. *Molecules, 25*(4), 978.

Oudshoorn, M. H. M., Rissmann, R., Bouwstra, J. A., & Hennink, W. E. (2007). Synthesis of methacrylated hyaluronic acid with tailored degree of substitution. *Polymer, 48*(7), 1915–1920.

Ouyang, L., Armstrong, J. P. K., Lin, Y., Wojciechowski, J. P., Lee-Reeves, C., Hachim, D., Zhou, K., Burdick, J. A., & Stevens, M. M. (2020). Expanding and optimizing 3D bioprinting capabilities using complementary network bioinks. *Science Advances, 6*(38).

Pal, D., & Saha, S. (2019). Chondroitin: A natural biomarker with immense biomedical applications. *RSC Advances, 9*(48), 28061–28077.

Pomin, V. H., & Mulloy, B. (2018). *Glycosaminoglycans and proteoglycans*. Multidisciplinary Digital Publishing Institute.

Scharnweber, D., Hübner, L., Rother, S., Hempel, U., Anderegg, U., Samsonov, S. A., Pisabarro, M. T., Hofbauer, L., Schnabelrauch, M., & Franz, S. (2015). Glycosaminoglycan derivatives: Promising candidates for the design of functional biomaterials. *Journal of Materials Science: Materials in Medicine, 26*(9), 232.

Schuurmans, C. C. L., Mihajlovic, M., Hiemstra, C., Ito, K., Hennink, W. E., & Vermonden, T. (2021). Hyaluronic acid and chondroitin sulfate (meth)acrylate-based hydrogels for tissue engineering: Synthesis, characteristics and pre-clinical evaluation. *Biomaterials, 268*, Article 120602.

Shaw, S. E., Russo, T., Solomon, D. H., & Qiao, G. G. (2006). An alternative pathway for the hydrolysis of epoxy ester compounds. *Polymer, 47*(25), 8247–8252.

Sugahara, K., Mikami, T., Uyama, T., Mizuguchi, S., Nomura, K., & Kitagawa, H. (2003). Recent advances in the structural biology of chondroitin sulfate and dermatan sulfate. *Current Opinion in Structural Biology, 13*(5), 612–620.

Szafulera, K., Wach, R. A., Olejnik, A. K., Rosiak, J. M., & Ulański, P. (2018). Radiation synthesis of biocompatible hydrogels of dextran methacrylate. *Radiation Physics and Chemistry, 142*, 115–120.

Volpi, N. (2006). *Chondroitin sulfate : Structure, role and pharmacological activity* ((1st ed.)). Elsevier.

Volpi, N. (2007). Analytical aspects of pharmaceutical grade chondroitin sulfates. *Journal of Pharmaceutical Sciences, 96*(12), 3168–3180.

Volpi, N. (2009). Quality of different chondroitin sulfate preparations in relation to their therapeutic activity. *Journal of Pharmacy and Pharmacology, 61*(10), 1271–1280.

Volpi, N. (2019). Chondroitin sulfate safety and quality. *Molecules, 24*(8), 1447.

Volpi, N., Galeotti, F., Maccari, F., Capitani, F., & Mantovani, V. (2021). Structural definition of terrestrial chondroitin sulfate of various origin and repeatability of the

production process. *Journal of Pharmaceutical and Biomedical Analysis, 195*, Article 113826.

Wang, L.-F., Shen, S.-S., & Lu, S.-C. (2003). Synthesis and characterization of chondroitin sulfate–methacrylate hydrogels. *Carbohydrate Polymers, 52*(4), 389–396.

Yang, J., Shen, M., Wen, H., Luo, Y., Huang, R., Rong, L., & Xie, J. (2020). Recent advance in delivery system and tissue engineering applications of chondroitin sulfate. *Carbohydrate Polymers, 230*, Article 115650.